BETTER SHIPS, BLUE OCEANS

Propeller design review, second design

Assessment of performance during propulsion and regeneration

Report No. : 32992-2-POW
Date : July 2023
Version : 1.0
Final Report

Propeller design review, second design

Assessment of performance during propulsion and regeneration

MARIN order No. : 32992
MARIN Project Manager : John Huisman

Number of pages : 121

Ordered by : DYKSTRA NAVAL ARCHITECTS
Kruithuisstraat 21
1018 WJ AMSTERDAM

Order document : Email dated 26 April 2024,
Quotation “230328 Quotation 32992 SHIPS_POW_v3.0.pdf”
Reference : Project ZERO

Reported by : ir. T.J. Huisman
Reviewed by : dr. ir. E.J. Foeth

Version	Date	Version description
0.1	20-06-2023	Draft Report
0.2	27-06-2023	Final draft report, updated contents for regeneration
0.3	04-07-2023	Final draft report, update after client review

MANAGEMENT SUMMARY

Dykstra Naval Architects commissioned MARIN to study the two updated thrusters for the sailing yacht ZERO. The objective was to determine both the propulsive performance and the performance during power regeneration.

Propeller manufacturer Hundested provided the updated propeller designs via Dykstra. The propellers were largely based on the proposal for optimized propellers as given in MARIN report No. 32992-1-POW. Dykstra also provided the updated designs of the thrusters. The goal of this project was to assess the performance of both thrusters and propellers in both propulsion and regeneration mode according to the operational scenarios as provided by Dykstra.

CFD computations were performed using RANS-BEM to obtain the wake fields of the ship and thrusters both in regeneration and propulsion. For propulsion the wake field was determined with feathered front propeller. Separate CFD computations were also performed using RANS-BEM on both thrusters to determine the open water characteristics, both in propulsion and regeneration mode.

Polynomials as function of propeller pitch and advance coefficient for both propulsion and regeneration mode were determined for both thrusters. These polynomials can be integrated into the performance prediction programs.

Using the polynomials, based on the usage scenarios, operational conditions were determined in terms of propeller pitch and propeller rotational speed for both propulsion and regeneration.

Using computational tools MARIN analysed the performance of the propeller designs in terms of powering, regeneration and cavitation behaviour.

In propulsion, the efficiency, cavitation behaviour and hull excitation was improved considerably compared to the first geometries, up to 10% reduction in required power.

In regeneration, the efficiency of the units was improved as well. The regeneration efficiency at 16 knots was improved such that 5% less drag would be encountered at 250 kW regeneration compared to the earlier geometry.

However, the total regeneration efficiency was improved less than expected due to a less favourable interaction of flow from the front propeller with the aft propeller. The cavitation behaviour was also not as good as expected from the new geometries, but regarded to be suitable for project ZERO.

CONTENTS PAGE

1 INTRODUCTION

By email, 24 March 2023, Dykstra Naval Architects (Dykstra), requested MARIN to evaluate the updated thrusters and propellers for project ZERO. The first geometries have been reported in MARIN report No. 32992-1-POW. By email, 26 April 2023, Dykstra commissioned MARIN according to quotation 230328 Quotation 32992 SHIPS_POW_v3.0.

Hundested provided via Dykstra the updated designs of the propellers. Dykstra provided the updated designs of the thrusters for evaluation and design checks by MARIN.

The goal was again to assess the performance of both propellers in propulsion and regeneration modes. The following subsections describe the required scope of work to achieve this goal.

1.1 Open water characteristics

Using the RANS-BEM approach, open water characteristics of the units and the propellers were computed for both the first and third quadrant of operation. The computations provide the thruster resistance and propeller torque and thrust. The pressure distributions and flow characteristics on the thruster bodies were studied.

1.2 Wake field computations

The wake field of the ship at the location of both thrusters is required, which may include the boundary layer of the ship, and for the aft thruster the wake from the keel and front thruster. It was chosen to redo these computations in view of possible changes in propeller-thruster-hull interaction due to the update in the propeller and thruster geometry. In propulsion mode the front propeller is feathered. In MARIN report No. 32992-1-POW the front propeller was also evaluated in propulsion. In view of the low mechanical efficiency for low power, this was left out of the scope of the current work.

MARIN computed the effective wake fields to capture the effect of the front propeller on the aft propeller in both propulsion and regeneration mode.

The computations also give the difference between the open water performance and the in-behind performance of the thrusters. Nominal computations (without working propellers) of the ship were also done, to investigate the propulsion factors of wake fraction and thrust deduction.

For all calculations a double-body CFD approach was used for simplicity. DYKSTRA provided the resistance characteristics of the ship, which were used for the predictions on propulsive performance.

1.3 Analysis and assessment of operational performance

The propeller design evaluation involves a study into the feasibility of the propeller designs provided by Hundested, by calculations and comparison to MARIN's database and MARIN's experience. For each condition MARIN advised the client regarding:

- Propeller performance in terms of thrust (or drag) and torque.
- Cavitation characteristics and cavitation noise (if any), both in terms of sheet cavitation and tip vortex cavitation, and the risk of cavitation erosion.
- Hull-pressure excitation.
- Cavitation-inception speed and characteristics.

2 DESIGN INPUT

2.1 Geometry

The thrusters were included in the 3D model of the ship as shown in Figure 2-1. The propellers were supplied separately after a small update to the fillet geometry.

Table 2-1: Summary of supplied input files.

3D model of the ship, including propellers	24-00 Lines plan 3D Lns 087 Keel05 Rudd05 Thr03.3dm
Front propeller	5444v2 forward.stp
Aft propeller	8455v2 aft.stp
Scenarios and ship resistance	Operational scenarios for prop optimization.pdf

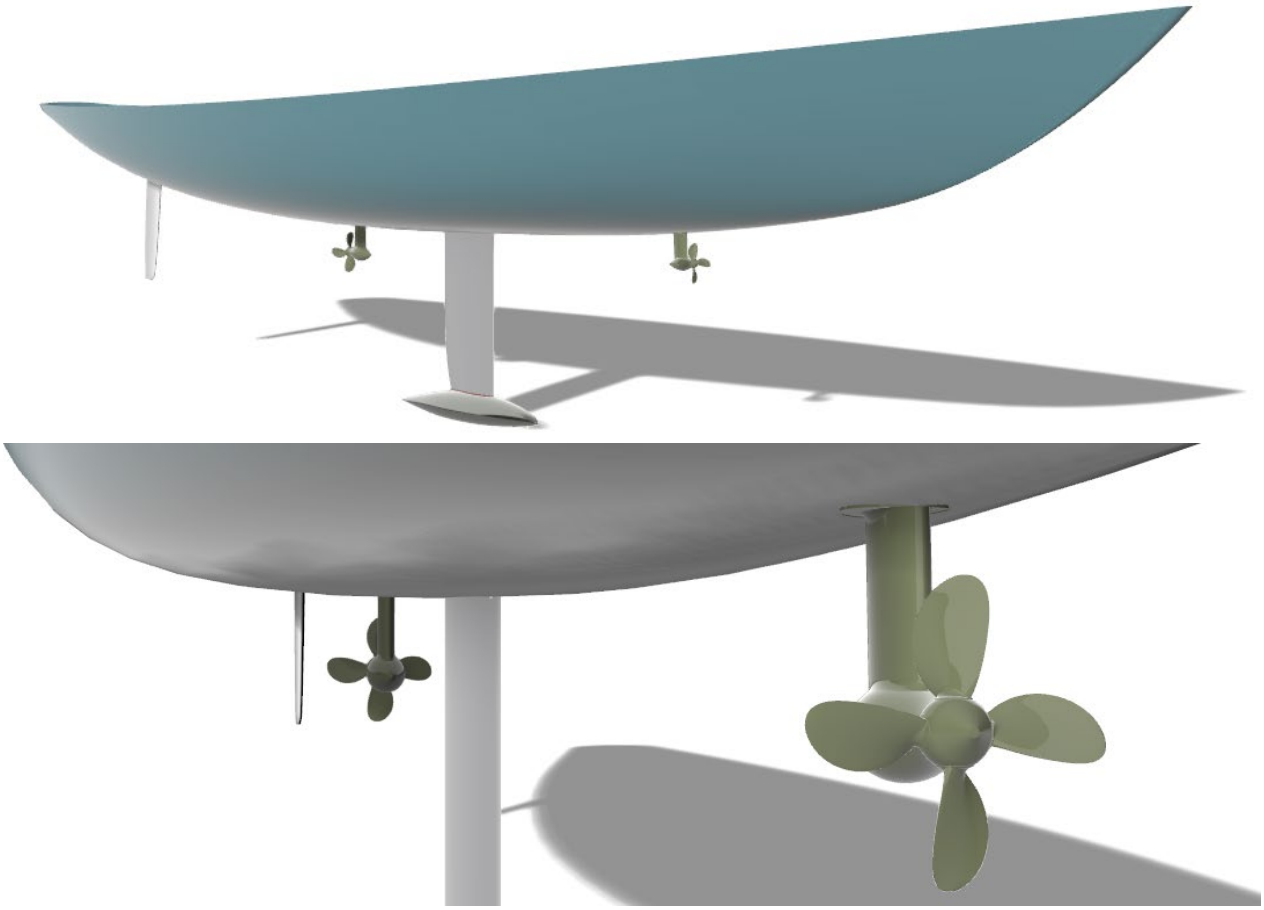

Figure 2-1: Renderings of yacht ZERO with HUNDESTED thrusters front and aft.

The new propellers were largely based on the proposal for optimized propellers as given in MARIN report No. 32992-1-POW. The largest changes were made to the skew and rake distributions.

The thruster geometries were updated significantly. The strut is now shaped with a NACA profile, as shown in Figure 2-2. The aft thruster has the lowest resistance in propulsion mode, while the front thruster has the lowest resistance in regeneration mode.

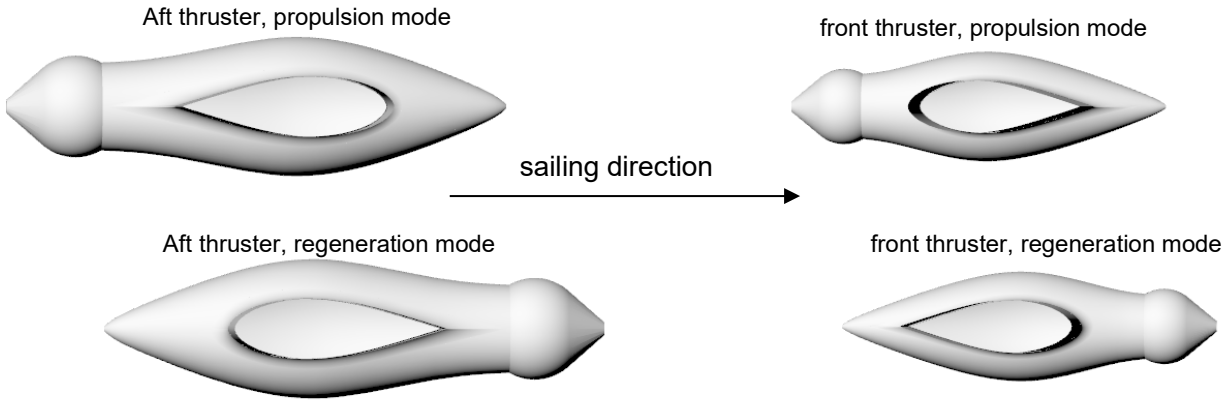

Figure 2-2: Orientation and modes of the new thruster geometries

2.2 Operational scenarios

Operational scenarios were provided by Dykstra, which were not changed compared to the previous study as reported in MARIN report No. 32992-1-POW. The ship is powered by sails and propellers which can be used in different combinations.

CHARTER MODE

1. Maximum regeneration with both props at 16 knots ship speed with an expected total power generation of 250 kW.
2. Intermediate speed motoring for short stretches, propelled by the aft propeller at a ship speed of 12 knots.

CROSSING / DELIVERY MODE

3. Regeneration mode with both props active at 14 knots ship speed with expected total power generation of 125 kW.
4. Light regeneration of 20 kW at a ship speed of 10 knots. It is to be investigated whether the aft propeller should be featured or lightly regenerating. At ship speeds over 10 knots, the aft propeller would probably be used for regeneration as well.
5. Free sailing with both propellers feathered at a ship speed of 8 knots.
6. Motor sailing on the aft propeller, front propeller either feathered or lightly driven to reduce drag. The ship speed is 10 knots and the total propulsion power is 50 kW.
7. Economic motoring for maximum range (no wind) on the aft propeller, with the front propeller either feathered or lightly driven to reduce drag. Ship speed is 8 knots, at an approximate power of 100 kW.

OTHER REQUIREMENTS

8. Maximum power on both propellers in bollard pull condition in order to sail away from a lee-shore.

Two more scenarios were provided by Dykstra. However, during discussions it was agreed to leave the analyses for those two scenarios out of the scope of work.

9. Manoeuvring, using the thrusters sideways.
10. Crash stop (by changing pitch).

2.3 Hull resistance

The following information regarding the hull resistance was provided by Dykstra:

Vs [kts]	Resistance [kN]	Windage at zero true wind speed [kN]	Total [kN]
6	7.55	0.69	8.2
8	11.6	1.23	12.8
10	18.8	1.92	20.7
12	29.5	2.77	32.3
14	44.0	3.76	47.8
16	71.5	4.92	76.4

Drag additions for rudder and various small items were added already by DYKSTRA.

3 COMPUTATIONAL METHODS

3.1 REFRESCO

MARIN performed simulations with the RANS solver ReFRESCO, see www.refresco.org . It solves the incompressible viscous flows based on the Reynolds-Averaged Navier-Stokes equations. Double-body simulations are used converging the simulation until the flow features and forces stabilise. The results are presented in the form of pressure coefficient, the friction coefficient ratio on the hull surface, the velocity and headloss in the flow.
The pressure coefficient is defined as:

$$C_p = \frac{P - P_{hs}}{\frac{1}{2} * \rho * V_s^2}$$

With:
P = pressure in [Pa]
P_{hs} = hydrostatic pressure in [Pa]
ρ = water density in [kg/m^3],
V_s = ship speed in [m/s]

The friction coefficient ratio is defined as:

$$C_{f,ratio} = \frac{C_f}{C_{f,ref}}$$

With C_f, the local skin friction coefficient, defined by:

$$C_f = \frac{\tau}{\frac{1}{2} * \rho * V_s^2}$$

Where τ is the shear stress, in [Pa]. The reference flat-plate skin friction coefficient $C_{f,ref}$ is defined by:

$$C_{f,ref} = 0.37 \times \log_{10}(R_{e,l})^{2.584}$$

Where $R_{e,l}$ is the local Reynolds number:

$$R_{e,l} = \frac{\rho V_s \Delta_x}{\mu}$$

With Δ_x the distance from the bow to the local point in [m] and μ the water viscosity in [kg.s/m].

The 3D flow features are presented using slices of normalised X velocity, head loss and X vorticity. Regions of reversed flow are given as well (regions were the flow follows the ship). The headloss gives a clear impression of the energy loss in the wake of the ship and is defined as follows:

$$H_l = 1 - \left(\left(\frac{\|\vec{V}\|}{V_s} \right)^2 + C_p \right)$$

The normalised X Velocity is defined as follows:

$$u = \frac{V_x}{V_s}$$

Where V_x is the X velocity component in [m/s]

The X Vorticity is defined as follows:

$$\omega_x = \Omega_x \times \frac{L_{pp}}{V_s}$$

Where Ω_x is the X component of the vorticity vector.

3.2 PROCAL

Propeller computations were done with PROCAL, a boundary element method (BEM) which computes the inviscid flow around the propeller within the ship's wake field. The calculations give the behind efficiency, the pressure distribution and the extent and dynamics of the sheet cavitation developing on the propeller blades. PROCAL has been developed by MARIN within the Cooperative Research Ships (CRS) framework. The primary input for a PROCAL computation is an operational condition in terms of speed, rotation rate and required thrust.

Although the tip vortex is not computed in PROCAL, separate models are used to compute the strength of the tip vortex used to determine inception and noise. The Empirical cavitating Tip Vortex (ETV) model is used which is an engineering model developed at MARIN.

PROCAL can be used to predict the cavitation inception buckets for sheet-cavitation and tip-vortex cavitation for both pressure-side and suction-side cavitation. A range of propeller loading coefficients is computed with PROCAL providing the pressure distributions on the propeller blade, while the ETV model provides an estimate of the cavitation inception of the tip vortices, which are usually the dominant types of cavitation in terms of inception speed.

PROCAL was used with a computational mesh including the actual hub shape. PROCAL takes the effective wake field from the RANS-BEM coupling, described further in Section 3.3, such that the flow including the suction effect of the propellers is included.

The results are presented using the normalised pressure coefficient CPN and cavitation inception number σ_N, which are defined as:

$$\mathrm{CPN} = \frac{p - (p_a + \rho g h_s)}{\frac{1}{2}\rho n^2 D^2} \qquad \sigma_N = -\frac{p_v - (p_a + \rho g h_s)}{\frac{1}{2}\rho n^2 D^2}$$

with p pressure, p_a the atmospheric pressure, $\rho g h_s$ the hydrostatic pressure at the shaft depth, p_v the vapour pressure, ρ water density, n rotational speed and D the propeller diameter. Using this definition, CPN can directly be compared with the cavitation number σ_N in the calculations. If -CPN equals or exceeds σ_N (p equals or exceeds p_v), then inception of cavitation occurs and the cavitation extent is computed.

The results in terms of propulsion are reported in terms of the advance coefficient J, thrust coefficient K_T and torque coefficient K_Q, as further provided in the appendices.

For power regeneration, the results are presented as function the hydrodynamic pitch angle β which is defined as

$$\beta = \arctan\frac{V}{0.7\pi n D}$$

The propeller thrust and torque, are made non-dimensional by the relative resultant velocity at 0.7R radius and defined as,

$$V_r = \sqrt{V^2 + (0.7\pi n D)^2}$$

The propeller thrust loading coefficient is defined as:

$$C_T = \frac{T}{(\frac{1}{2}\rho V_r^2)\ \frac{\pi}{4}D^2}$$

The propeller torque loading coefficient is defined as:

$$C_Q = \frac{Q}{(\frac{1}{2}\rho V_r^2)\ \frac{\pi}{4}D^3}$$

The regeneration efficiency is defined as

$$\eta_{regen} = \frac{P}{VT} = \frac{C_Q}{C_T}\frac{2}{0.7\tan(\beta)}$$

Finally, the power coefficient is defined as

$$C_P = \frac{P}{P_{flow}} = \frac{2C_Q\left(1+\frac{1}{(\tan\beta)^2}\right)}{0.7\tan\beta}$$

with propeller power $P = 2\pi nQ$ and flow power $P_{flow} = \frac{1}{2}\rho V^3\frac{\pi}{4}D^2$

3.3 RANS-BEM

In RANS-BEM the flow around the thruster housing is calculated by means of RANS, while the flow around both propellers is calculated by means of the boundary element method (BEM) PROCAL. Doing so, the mutual interaction between the hull, thruster and propeller is calculated. In the RANS simulations the action of the propeller is represented by force fields that follow from PROCAL calculation of the propeller. The PROCAL calculation requires the effective inflow to the propeller. These effective wake fields follow from the total velocity field according to RANS minus the propeller induced velocities according to a previous PROCAL calculation. This iterative process is repeated until converged.

The effective wake methodology ensures that the inflow is similar as compared to full RANS computations with sliding interface with the propeller is fully modelled in a viscous flow simulation but at a greatly reduced computational cost. Although details of interaction of tip vortices is not captured, the mean flow which governs the propeller performance is computed sufficiently accurately.

This method is successfully validated with RANS-RANS sliding interface computations and model tests. The RANS-BEM approach is attractive in terms of cost and computational effort compared to a sliding interface approach.

4 RESULTS AND DISCUSSION

4.1 Open water computations

CFD computations using RANS-BEM were performed for a set of 20 conditions for both the aft and front thruster in open water to determine the open water characteristics in terms of thrust and torque as function of advance ratio. The resistance of the thruster and the effective inflow in the propeller follow from the RANS computation, while the propeller thrust and torque are computed by the BEM computation with PROCAL.

4.1.1 Propulsion polynomial

For the analysis of the scenarios a reduced factorial polynomial was created based on PROCAL computations at different J value and different pitch settings. The set of 20 RANS-BEM computations was analysed, which was further used to compute a set of 600 PROCAL computations for both the front and aft propeller at different J value and different pitch settings. A MARIN correlation allowance was used to correct the thruster force from CFD to account for bolts, anodes, gaps, roughness and other factors; this allowance may be somewhat conservative.

The polynomials are presented on page T1. Both the unit thrust coefficient K_{T_u} and the propeller thrust coefficient K_{T_p} are provided as well as the power coefficient K_Q. The thruster performance K_{T_u} is visualised in Figure 4-1 for both the front and aft unit. For the front unit in a P07/D range of 0.5 to 1.9 and for the aft unit in a P07/D range of 0.5 to 1.8 with steps of 0.1.

The aft unit clearly has higher efficiency, especially in higher pitch operation. This is predominantly due to the more favourable orientation of the strut of the unit (refer to Figure 2-2).

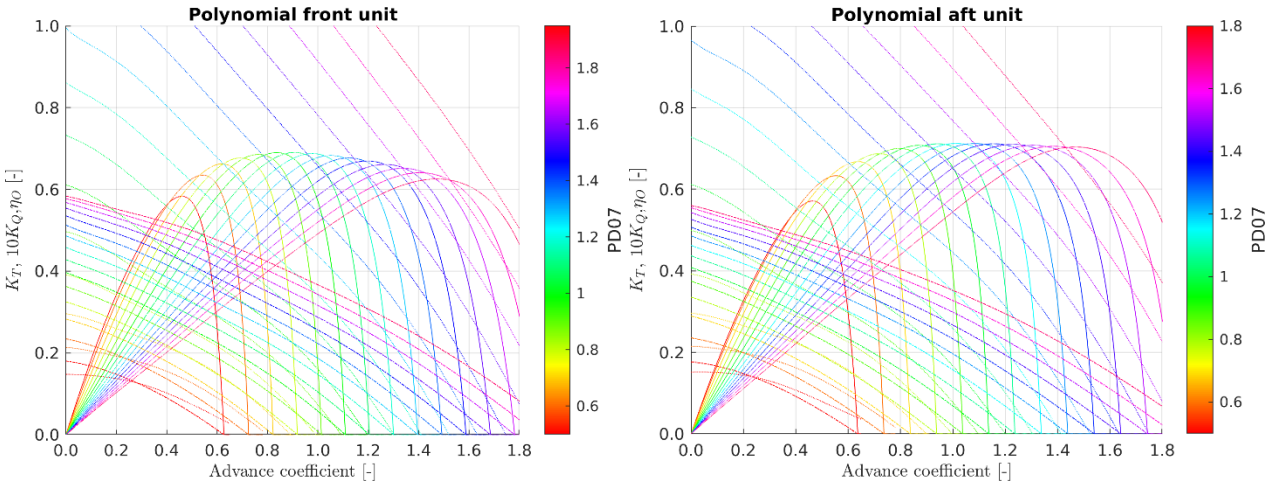

Figure 4-1: Polynomial description of the open water performance of the thruster.

4.1.2 Regeneration polynomial

The Hundested propellers were also extensively computed with RANS-BEM and PROCAL in the third quadrant for a range of beta and pitch; that is, with the thrusters reversed (rotated 180 degrees) and the propellers rotating in the other direction . A reduced factorial polynomial was made for both the front and aft unit, as given in the table on page T2. The polynomial was optimised to capture the peak efficiency and peak CP correctly and is intended to be used for that area of operational only. This polynomial should be evaluated for beta in radians (minus pi). For pitch the polynomial is valid between $P_{0.7}/D = 0.5$ and $P_{0.7}/D = 2.5$.

Both the unit thrust and the propeller thrust are provided. Figure 4-2 provides a visualisation of the polynomial for the unit thrust and torque loading coefficient as function of propeller pitch, in steps of 0.05 deg. For low pitch and high beta the polynomial is observed to become wavy, but this is outside the intended range only and does not affect the analyses.

The corresponding efficiency and CP are plotted in Figure 4-3. There are differences between the front and aft unit, both due to the propeller design, the design pitch, but more importantly the resistance of the thruster body and strut. Relatively, the strut for the front unit features lower resistance, due to the more favourable orientation of the NACA profile of the strut in regeneration mode.

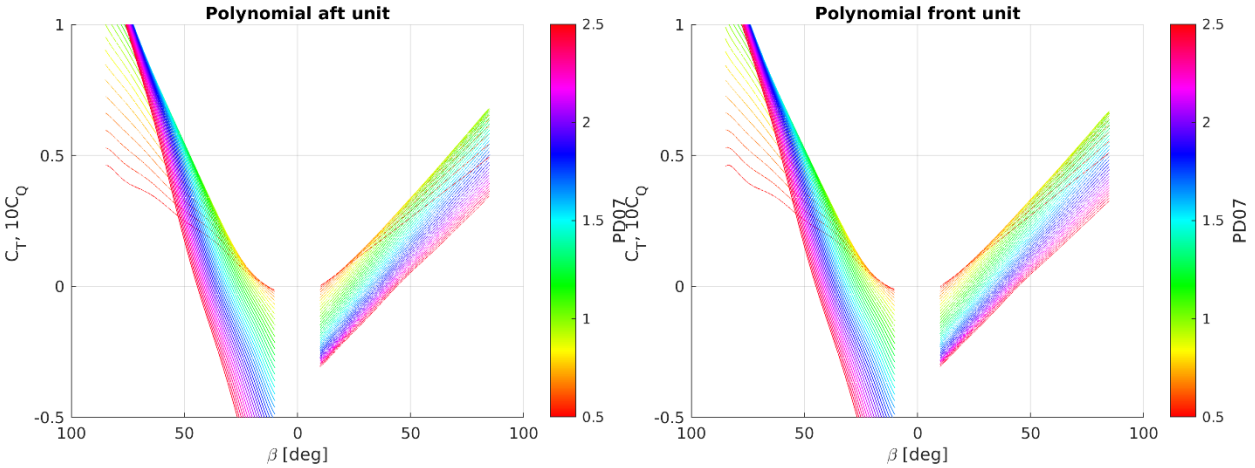

Figure 4-2: Polynomial of C_T and C_Q for the aft and front unit.

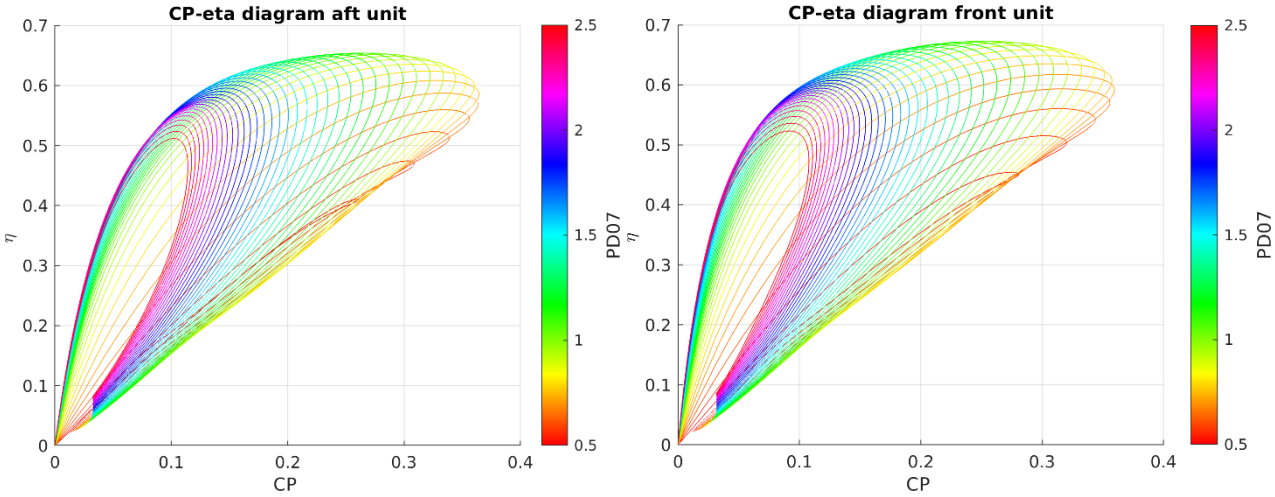

Figure 4-3: Polynomial presentation of the regeneration power and efficiency for the aft and front unit.

4.2 CFD computations in behind

Two CFD computations were performed using the RANS-BEM approach:

1. 12 knots, front propeller feathered, as shown in Figure 4-4 and on pages F1 through F8.
2. 16 knots, both propellers regenerating, as shown in Figure 4-7 and on pages F9 through F15.

The following subsections provide more information on the CFD computations.

4.2.1 12 knots propulsion

Figure 4-4 shows the axial velocity profiles Vx. The ships sails at 12 knots, represented by Vx = 1.0. The boundary layer of the ship is becoming visible near the aft part of the hull. The feathered propeller decelerates the flow somewhat. The aft propeller produces the thrust which is required to propel the ship. This gives high velocity flow behind the aft propeller.

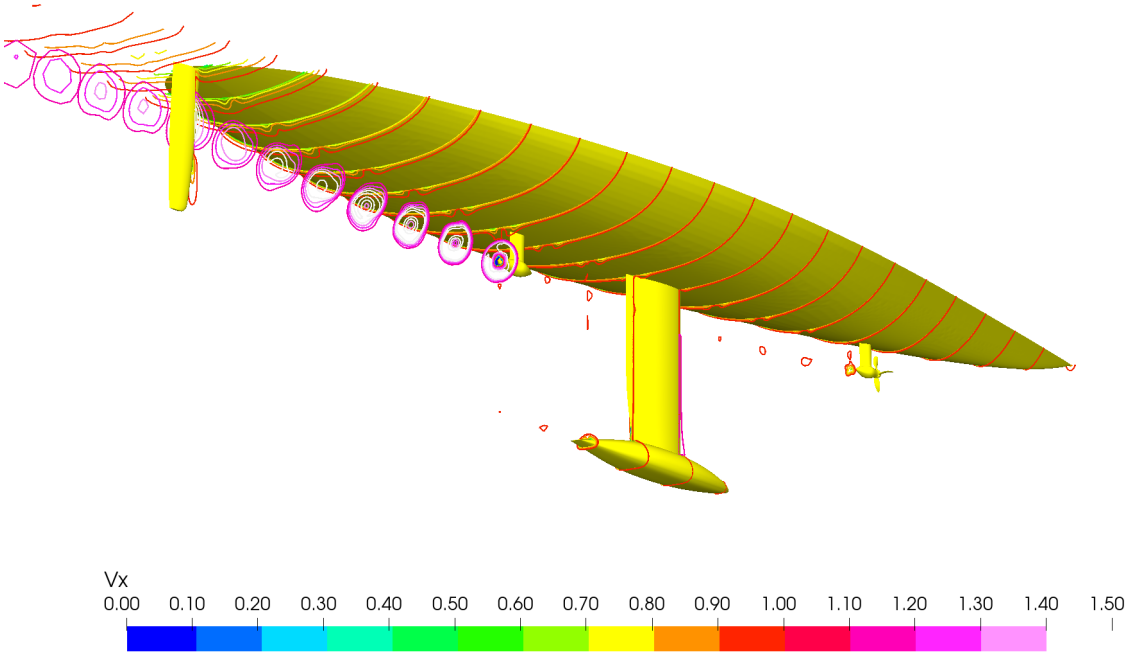

Figure 4-4: Velocity profiles at 12 knots with working aft and feathered front propeller.

The flow separation on both units is visualised in Figure 4-5. The colour scale on the surface represents the pressure level. The dark red / gray colour is a visualization of the flow separation at one time instance.

The flow separation is very limited on the aft unit, but on the front unit with feathered propeller, there is quite some flow separation present, both on the lower radii of the propeller blade as well as on the portside of the strut. The flow separation on the unit is most probably initiated by the disturbed flow from the feathered propeller. It is recommended to study the best feathering position both in angle of the blades and pitch angles during commissioning.

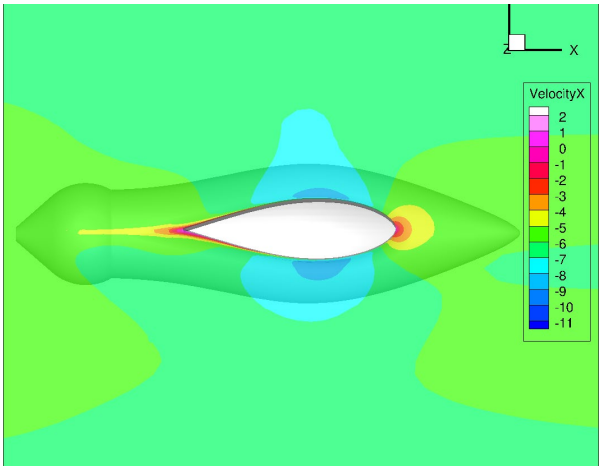

Velocity distribution, aft thruster, propulsion

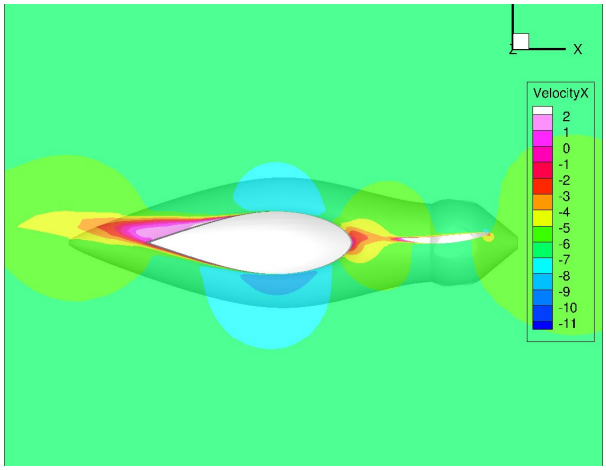

Velocity distribution, front thruster, feathered.

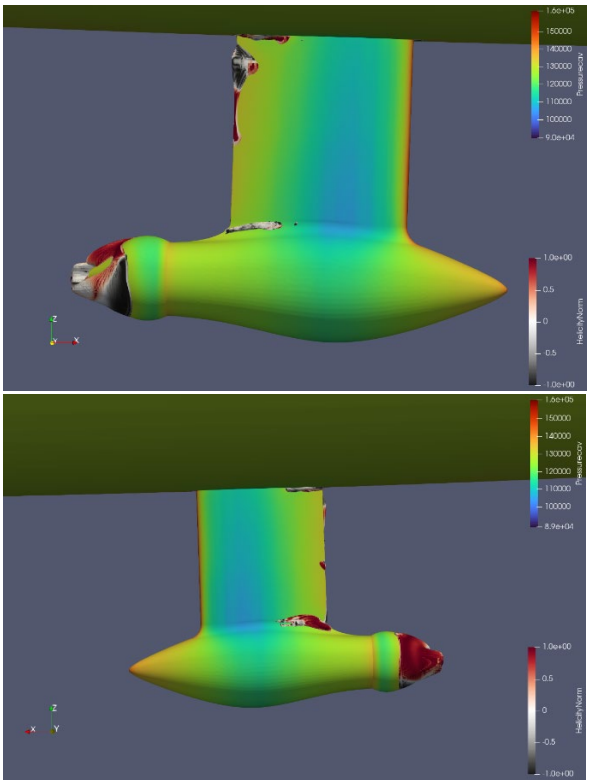

Pressure distribution and flow separation, aft thruster, propulsion.

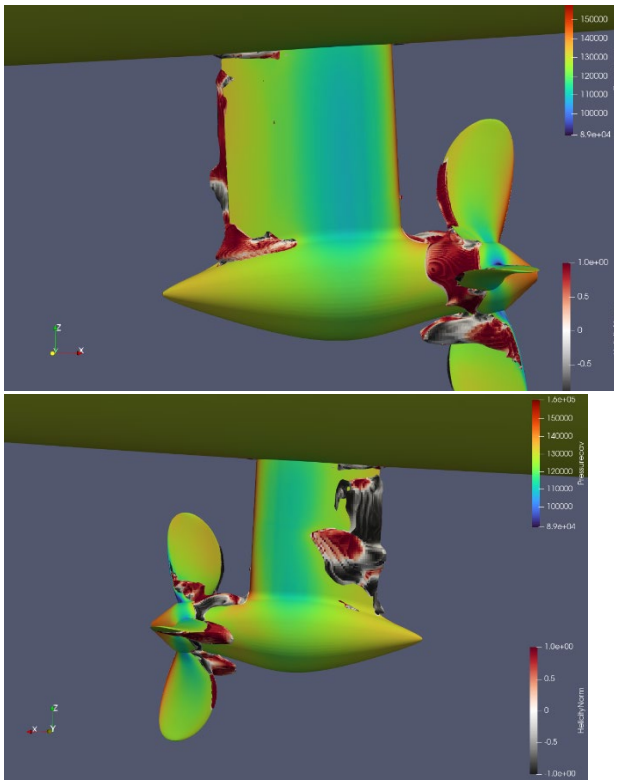

Pressure distribution and flow separation, front thruster, feathered.

Figure 4-5: Velocity, pressure distribution and reversed flow in propulsion at 12 knots

The wake field of the flow encountered by the aft propeller is given in Figure 4-6. The influence of the strut of the thruster is clearly visible in top position. The influence of the ship, keel and feathered front propeller is limited, such that the wake field is relatively clean and undisturbed.

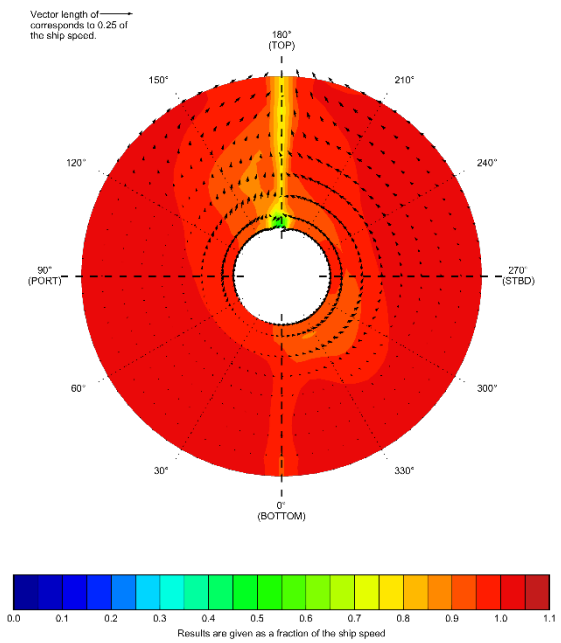

Time averaged wake field for the aft propeller, feathered front propeller

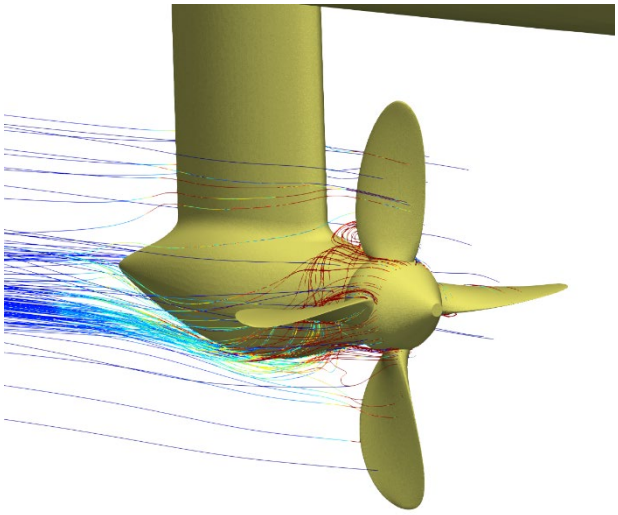

Velocity streamlines around the feathered front propeller

Figure 4-6: Wake field of the aft propeller at 12 knots ship speed

4.2.2 16 knots regeneration

Figure 4-7 shows the headloss (as defined in Section 3.1) during regeneration for the first geometry and updated geometry.

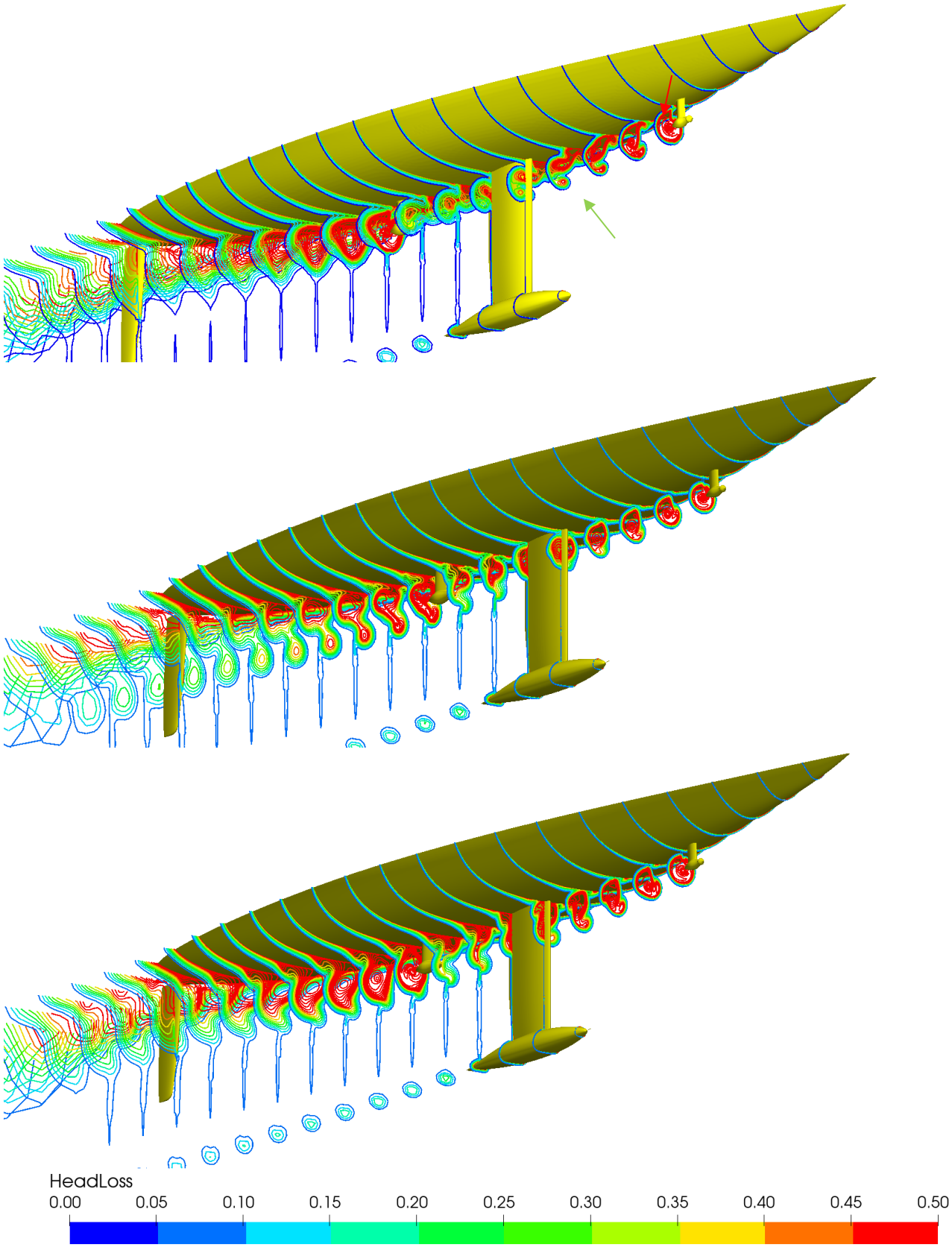

Figure 4-7: Headloss due to the regenerating propellers. Top: previous geometry, middle: first iteration, bottom: max regeneration

The headloss gives a clear impression of the energy loss in the wake of the ship, with in blue low energy loss and in red high energy loss. The energy loss directly behind the propellers is obvious.

For the initial geometry, as reported in MARIN report No. 32922-1-POW, the flow from the front propeller is advected into the boundary layer of the ship (red arrow) and mixes with the high velocity surrounding flow (green arrow). The remaining low energy flow from the front propeller stays close to the ship and passes the aft propeller only in the top region.

However, for the updated geometry, as shown in the middle and bottom of Figure 4-7, the jet from the front propeller is much more stable. There is no disturbing effect from the flow separation on the strut of the unit. In a first iteration with assumed pitch and rpm such that 250 kW would be obtained, there was hardly any interaction with the boundary layer of the ship and much less mixing with the surrounding flow. The expected power was hence not generated by the propellers at the specified pitch and rotation rate. Therefore, a second computation was done in which the front propeller was fully loaded for maximum regeneration. Somewhat more interaction with the boundary layer is observed, and a slightly better flow into the aft propeller.

The updated geometry features a less favourable inflow into the aft propeller compared to the initial geometry, with both lower average velocity and more variation over the blade positions. Especially at the 150 degree (in the sign convention of the wake plots) position, the flow velocity is lower, which makes the propeller more sensitive to pressure-side cavitation than anticipated in the earlier work.

In regeneration mode, the front propeller encounters - apart from an upstream effect of stagnation from the strut – a clean inflow. The wakefields are shown in Figure 4-8.

The wake into the aft propeller originates from a complex flow process involving mixing of the slipstream of the front propeller with low velocities and the surrounding higher velocity flow. All kind of vortices are present, which makes this a highly unsteady process. This leads to variations in the velocity distributions which the aft propeller encounters, as shown by Figure 4-9. The wake for the aft propeller was averaged over the last 25 evaluations.

Considering the individual evaluations, power absorption variations up to 10% are computed due to the variation in the wake field. . It is recommended to take this into account for the controllers and engine settings. Also, the drag varies. This may be lead to velocity variations, depending on the eigenfrequencies. Note that this is the worst-case scenario in which the ship encounters no drift. In practise the slipstream from the front propeller may likely pass the aft propeller and then these variations would not occur.

The aft and front propeller rotate in opposite directions to recover some of the rotational energy from the wake of the front propeller by the aft propeller. However, in the current situation, without drift and heel, the rotation of the flow from the front propeller is already largely removed by the interaction with the keel.

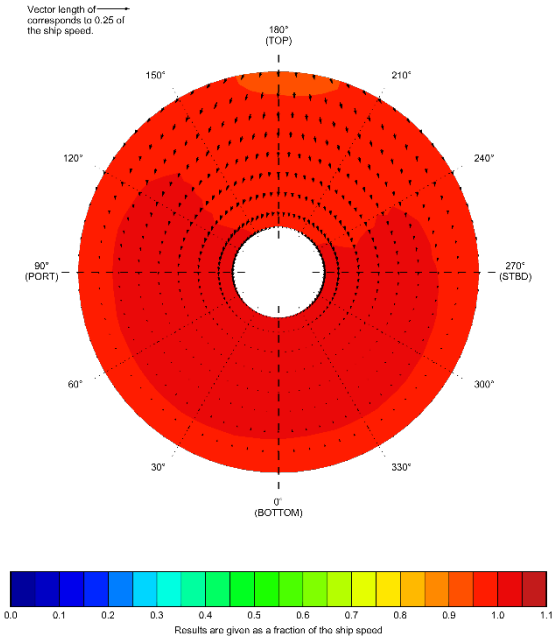

New geometry, wake for front propeller

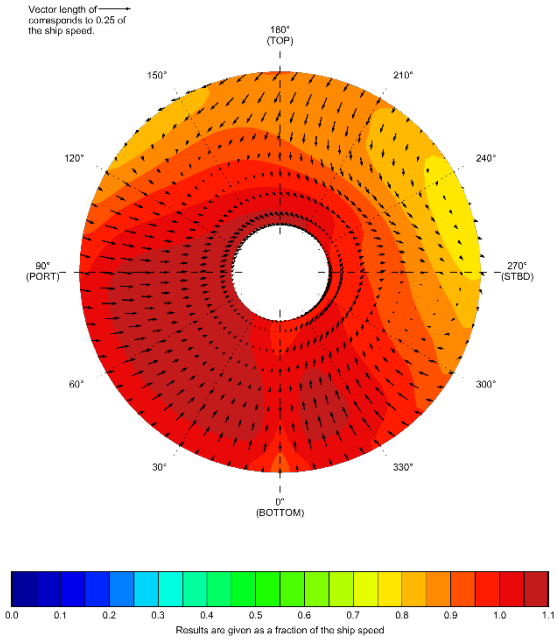

Previous geometry, wake for the aft propeller

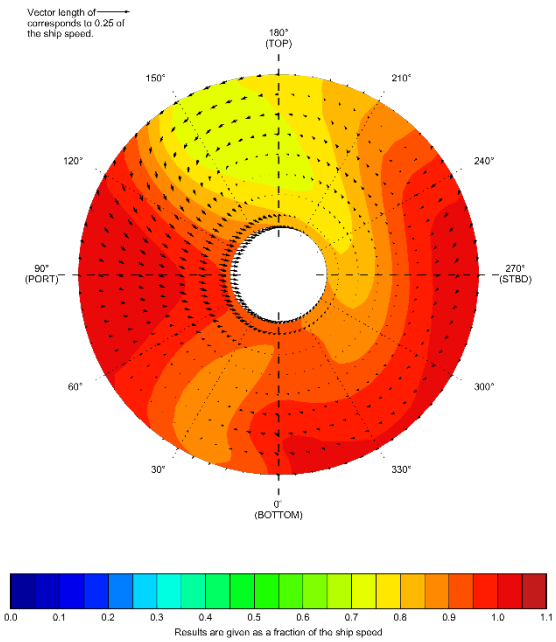

New geometry, wake for aft propeller, iteration 1

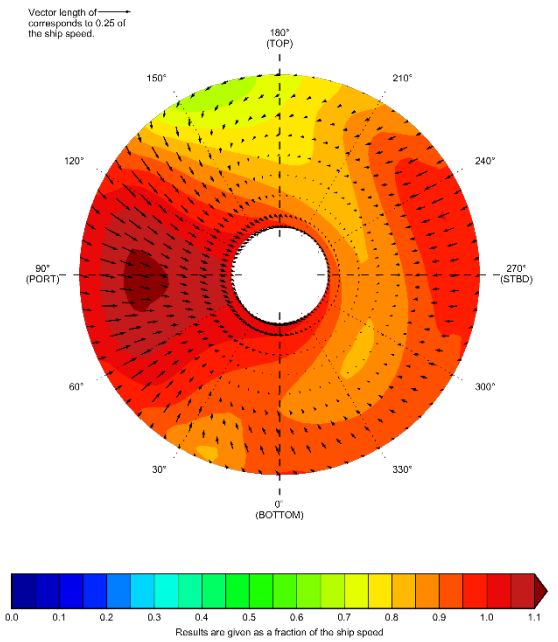

New geometry, wake for aft propeller, max regeneration of front propeller

Figure 4-8: Wake field of the aft and front propeller at 16 knots ship speed in regeneration mode.

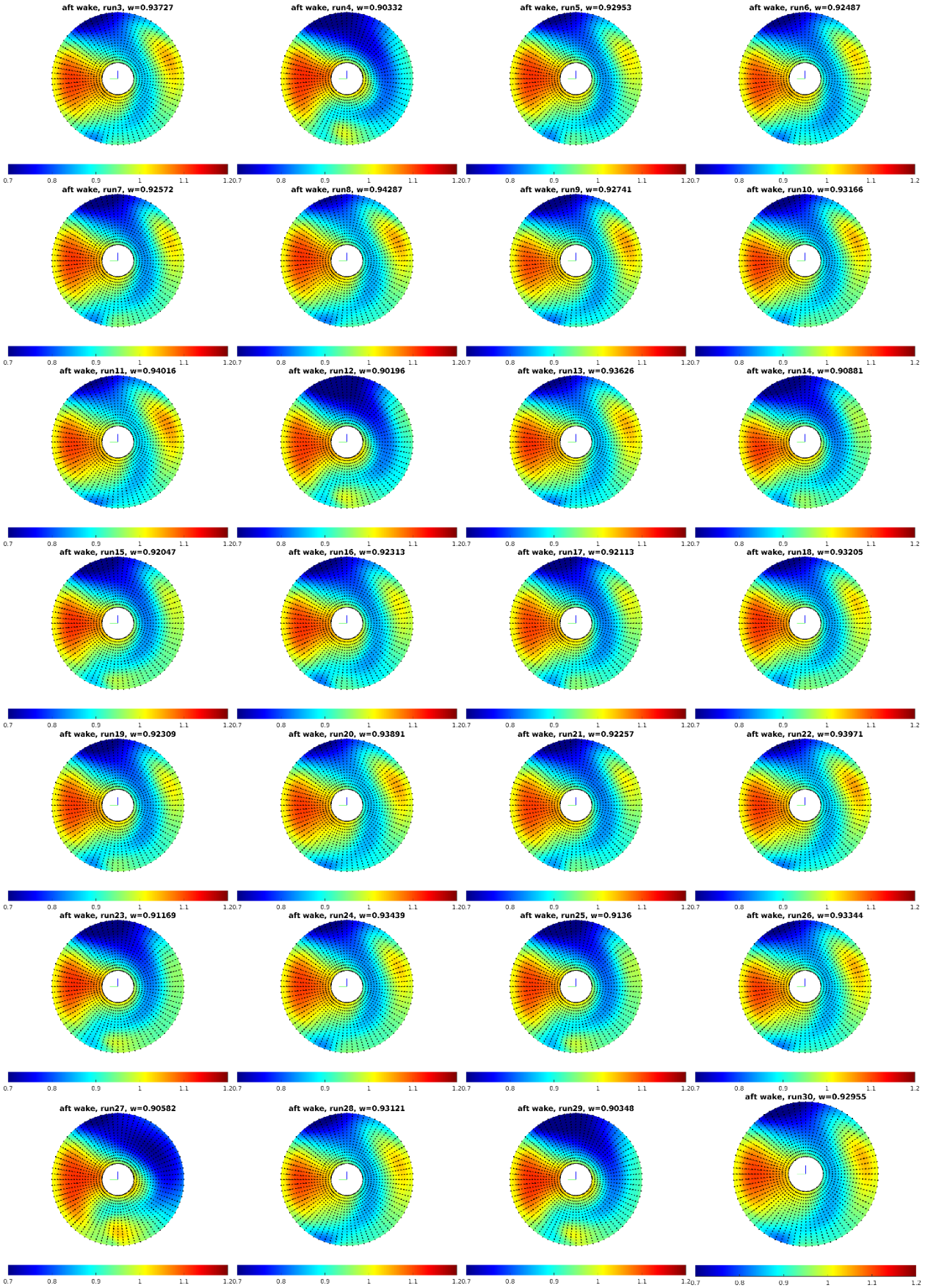

Figure 4-9: Evaluations of the wake field of the aft propeller in regeneration mode.

Two attempts were made to improve the interaction of the front propeller with the aft propeller. The first by setting the tilt angle of the front unit to zero, and the second by decreasing the clearance between the hull and the front propeller to 15% of the diameter. The tilt angle does not have any improvement, while the clearance does have a small effect on the wake field. This was however considered not worth the additional risk on inboard noise and vibrations.

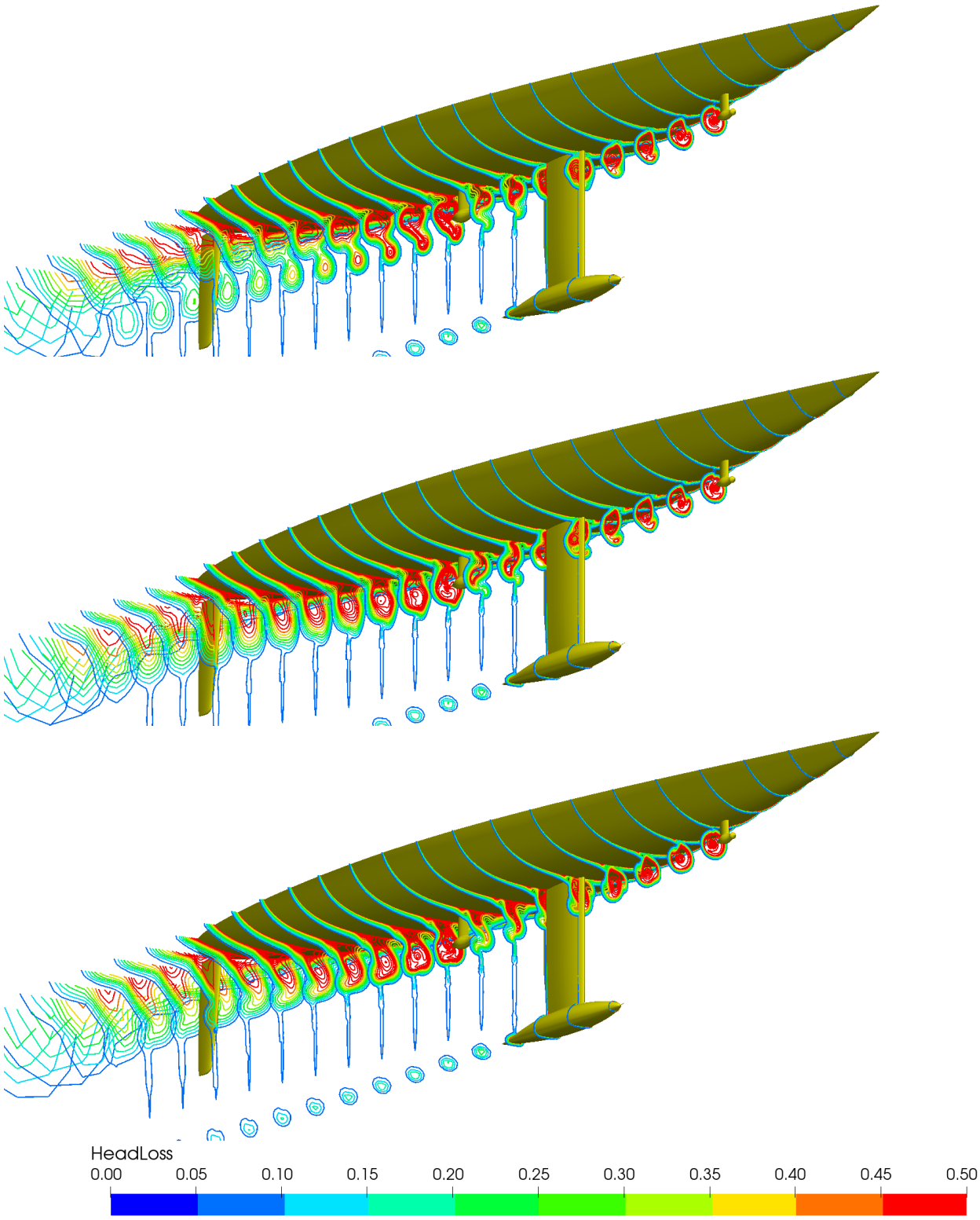

Figure 4-10: Headloss during regeneration for original (top), tilt modified (middle) and clearance modified (bottom) geometry.

4.3 Propeller analysis, feathered

The trailing edge forward with the pod in regeneration mode would be the best option for feathering, as shown in MARIN report No. 32992-1-POW.
The new propeller geometries were evaluated with the trailing edge forward, with the pod oriented such that the NACA profile of the strut is oriented favourably in the flow. For the front unit this is the regeneration mode and for the aft unit the propulsion mode (refer to Figure 2-2).

At the neutral angle of 91 degrees, the drag D_F for both propellers is similar, and can be estimated by:

$$D_F = \frac{8.4 * D^2 * V^2}{1000} \; [kN]$$

in which D [m] the propeller diameter and V the ship speed [m/s].

The feathered drag of the new propeller geometries is larger compared to the first geometries, due to the higher camber and larger pitch variation.

In addition to the drag of the feathered propeller, the drag of the aft and front unit can be estimated by $0.038V^2$ and $0.024V^2$ respectively. Corrections for roughness and mechanical parts and anodes have been added.

In scenario 5, the ship is powered by the wind at 8 knots ship speed, both propellers are feathered. The total drag of the feathered units is about 1.6 kN.

4.4 Propeller analysis, propulsion

Three scenarios deal with the propulsion of the ship:
- Scenario 2. Intermediate speed motoring for short stretches at 12 knots.
- Scenario 6. Motor sailing on the aft propeller at 10 knots, with total power P_D = 50 kW.
- Scenario 7. Economic motoring at 8 knots.

Using the provided resistance of the ship, the results from the CFD computations (see Section 4.1) and the polynomial speed-power predictions were done based on K_T/J^2 identity. The results are given in Table 4-1. The relative rotative efficiency is assumed to be one.

The thrust deduction of the ship (THD ship) was evaluated by comparing a nominal computation (a computation without working propellers) to a computation with working propellers, both including the geometry of the units. The CFD computations show that the added resistance due to the working of the propellers is net zero; there is an exchange in the pressure contribution and friction contribution to the total resistance but the effect on the resistance on the resistance of the unit only is zero

The first geometry had much more interaction with the ship mainly via an increase in the frictional resistance. In terms of thrust deduction the new geometry shows a clear improvement.

The wake fraction is also zero. The influence of the feathered propeller and the wake of the keel is compensated by overspeed (i.e., displacement effect) due to the shape of the hull.

It was agreed with Dykstra to leave a lightly driven front propeller out of the scope of work. Hence, Table 4-1 provides the results for a feathered front propeller only.

Table 4-1: Powering prediction for different propulsion scenarios.

		feathered front propeller			
		motoring	motor sailing	economic motoring	
P07/D aft	@0.7R	0.915	1.430	0.945	pitch aft
VS	KNOTS	12.00	10.00	8.00	ship speed
Rship	kN	32.3	5.9*	12.8	resistance of the ship
Rfeather	kN	1.4	1.0	0.6	drag of the feathered front propeller and unit
THD ship	kN	0.0	0.0	0.0	Added resistance in propulsion due to working propellers.
THDF aft, unit only	1-R/TH	0.00	0.00	0.00	thrust deduction aft, unit only
WT aft		0.00	0.00	0.00	wake fraction aft
ETA-Rs		1.0	1.0	1.0	relative rotative efficiency
N aft	RPM	367.0	170.7	232.6	rotation speed aft propeller
PD	kW	312.5	50.0	81.8	delivered power (to the aft propeller)
TH aft	kN	33.7	6.9	13.4	thrust of the aft unit
TH front	kN	-1.4	-1.0	-0.6	thrust (or drag) of the front unit
TH	kN	32.3	5.9	12.8	total thrust on the ship (including drag from the front unit)
THp aft	kN	34.8	7.5	13.9	thrust of the aft propeller
THp front	kN	-0.5	-0.3	-0.2	drag of the feathered front propeller
KQs aft		0.0279	0.0444	0.0287	
KTs aft		0.173	0.164	0.172	
KTp aft		0.179	0.179	0.178	
CTp aft		0.975	0.288	0.874	
SIGN aft		2.98	13.77	7.41	cavitation number aft
ETA-O aft		0.665	0.710	0.675	
R_total (Rship + R_feather + THD ship)		33.7	6.9	13.4	
ETA-D total (from Rship*V/PD)		0.638	0.611	0.644	ETA-D is about the ship, what does it cost to propel the ship with resistance Rship
ETA_H aft		1.000	1.000	1.000	Hull efficiency
ETA_feathered (1-Rfeather/TH aft)		0.959	0.860	0.954	Feathering efficiency. What is lost due to the feathering compared to the total thrust (from the aft unit)
ETA_D aft		0.665	0.710	0.675	ETA_R * ETA_H * ETA_O
ETA_D total (from efficiencies)		0.638	0.611	0.644	ETA_D aft * ETA_feathered

**Additional thrust of the propeller. The remainder of the ship resistance is provided by wind propulsion using the sails*

The pitch and rotational speed of the aft propeller were optimized for minimum required propulsive power. In the motor sailing scenario, the thrust of the aft unit was optimized for a power consumption of 50 kW.

Compared to the results presented in MARIN report No. 32992-1-POW, the efficiencies have improved significantly with about 10%, both due to the improved propeller-thrust-hull interaction, thruster design and propeller design. The new geometries require PD = 312.5 kW to propel the ship at 12 knots, while the first geometry required

The aft propeller was analysed again with PROCAL in the conditions as shown in Table 4-1. The results are presented in the following subsections.

4.4.1 Pressure distributions

Contour plots are provided by Figure 4-11 at the blade position - zero degrees is top position - in which the lowest pressures occur on the blades. The pressure coefficient CPN is visualised, ranging from high pressure in red, to low pressure in dark blue where -CPN equals the cavitation number σ_N. Pressure below the vapour pressure, or CPN lower than σ_N, is indicated in magenta, in which area cavitation will be formed and then spread over the blade.

For the 12 knots condition the figures on pages F16 through F21 provide the contour plots for all blade angles.

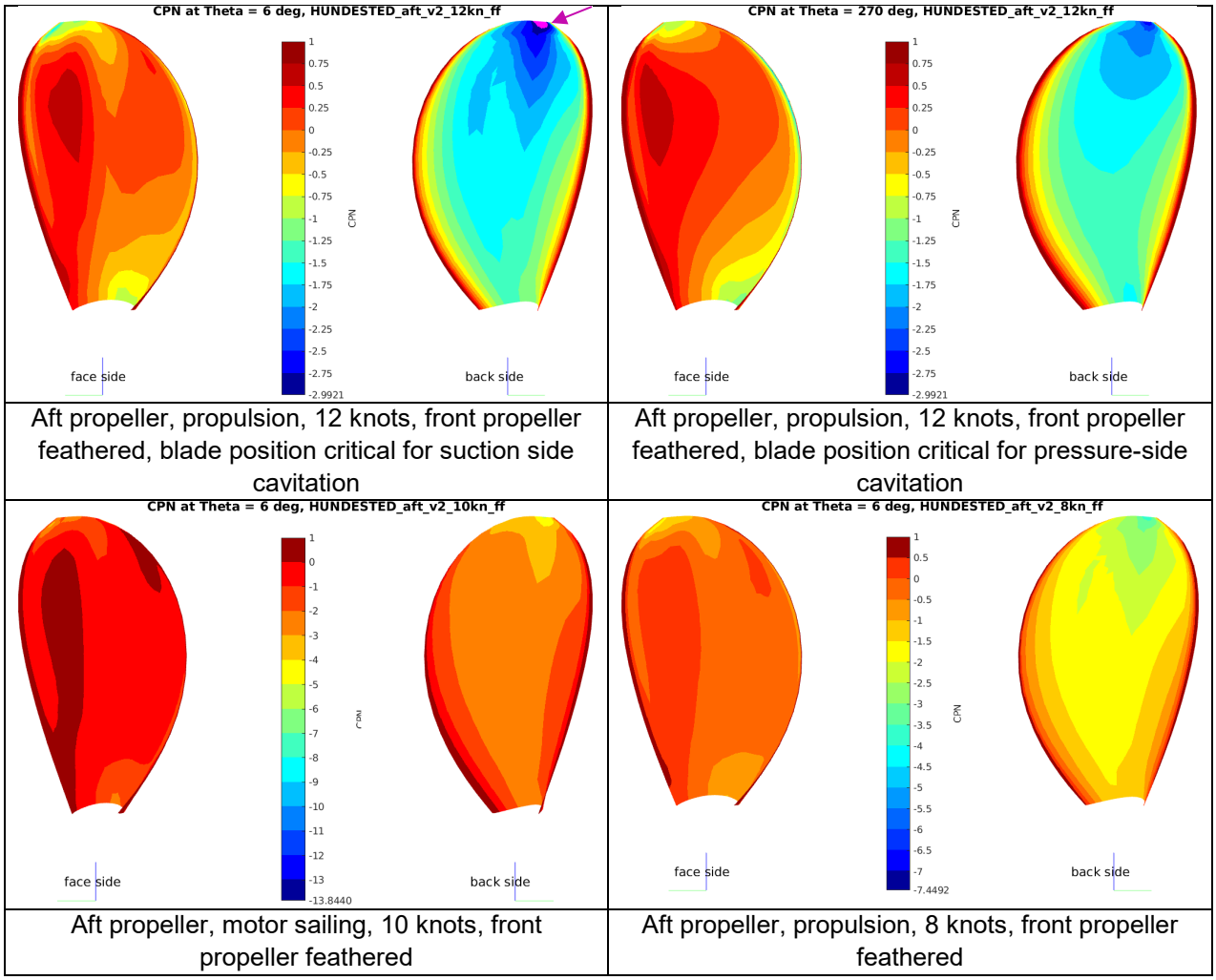

Aft propeller, propulsion, 12 knots, front propeller feathered, blade position critical for suction side cavitation

Aft propeller, propulsion, 12 knots, front propeller feathered, blade position critical for pressure-side cavitation

Aft propeller, motor sailing, 10 knots, front propeller feathered

Aft propeller, propulsion, 8 knots, front propeller feathered

Figure 4-11: Pressure contours for the aft propeller (non-cavitating computation).

As shown, only the 12 knots condition show a small spot of pressure below the vapour pressure at the tip (see magenta arrow). This will lead to cavitation, which could nicely merge with the tip-vortex cavitation. Cavitation computations are provided in Section 4.4.3. There is sufficient margin against cavitation at the leading edge, near the root and at the mid chord of the blade..

The minimum pressures as function of propeller radius are provided in Figure 4-12. This figure indicates that cavitation is predicted near the tip for the 12 knots condition only. At 12 knots, the margin against pressure side cavitation is relatively small, but sufficient. The 10 knots and 8 knots condition are free of cavitation.

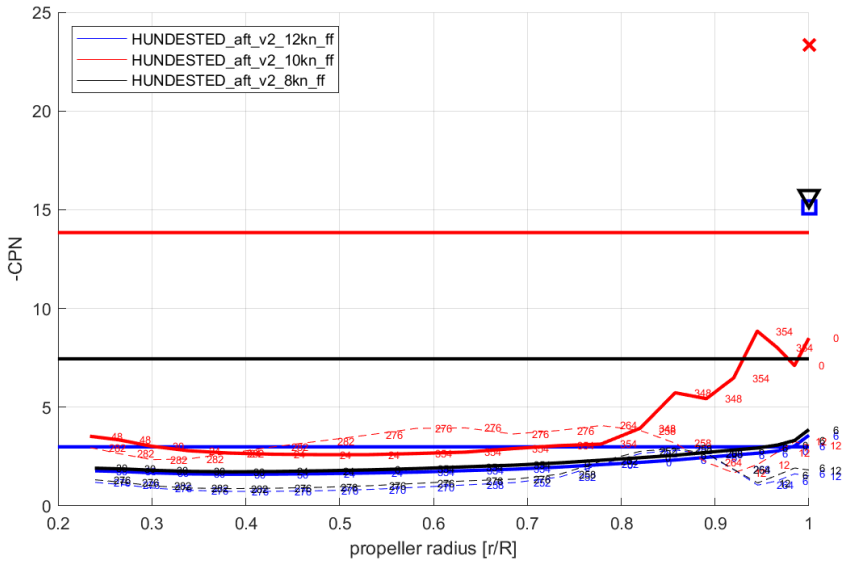

Figure 4-12: Minimum pressure coefficient as function of propeller radius for the aft propeller. The horizontal lines indicate the cavitation inception limit. The solid lines represent the suction-side pressure-peak and the dashed lines the pressure-side pressure-peak. The markers give the pressure coefficient of the core of the tip vortex.

4.4.2 Cavitation inception

In terms of cavitation-inception characteristics, Figure 4-13 provides the cavitation inception lines for the aft propeller. For sheet cavitation, the inception is determined on the propeller within the interval of the specified propeller radii as given in the title of the plots.

The operational points are provided by the small cross markers. Additionally, for the 12 knots condition (with feathered front propeller for the aft propeller), the operational curve (σ_N, K_T) as function of ship speed is also given.

The two sets of lines per condition indicate pressure side cavitation with low pressure in terms of CPN at low K_T and suction side cavitation with low pressure in terms of CPN at high K_T. The cavitation bucket is the area between both lines. The numbers near the inception lines provide the angle in degrees in which the pressure is critical with 0 degrees the top position.

The pressure coefficient -CPN occurring on the propeller can directly be compared with the cavitation number σ_N. Cavitation occurs when –CPN > σ_N, i.e., if the cavitation inception lines would be above the operational points.

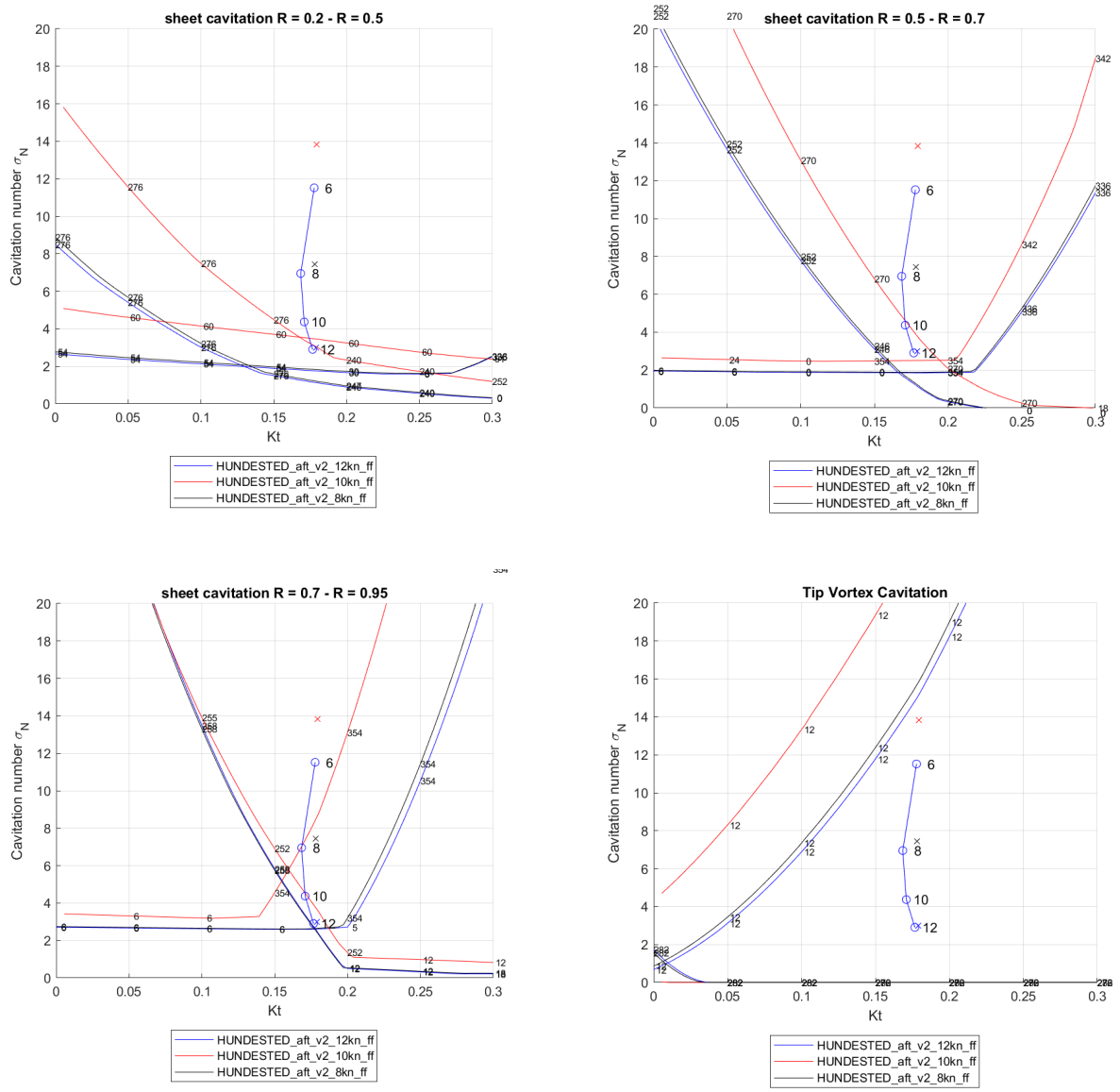

Figure 4-13: Computed sheet cavitation inception diagrams for the aft propeller.

The differences in the inception curves are dominated by the pitch setting in each condition. Therefore, the inception lines of the 8 and 12 knots conditions are very similar. The cavitation bucket becomes smaller with increasing pitch, but the operational point is also at lower rpm which positions the operational point higher in the diagram.

Tip vortex cavitation is the first occurring form of cavitation. The propeller is well-balanced between suction-side and pressure-side cavitation.

4.4.3 Cavitation behaviour

Figure 4-14 provides sketches of the cavitation behaviour which are obtained from cavitation computations. In black the contour of the cavitation and propeller is given. Only in 12 knots, there is a tiny amount of cavitation in the tip, which would merge with the tip vortex. The 12 knots condition is also shown on figure page F22 for multiple blade angles during the rotation in the wake field.

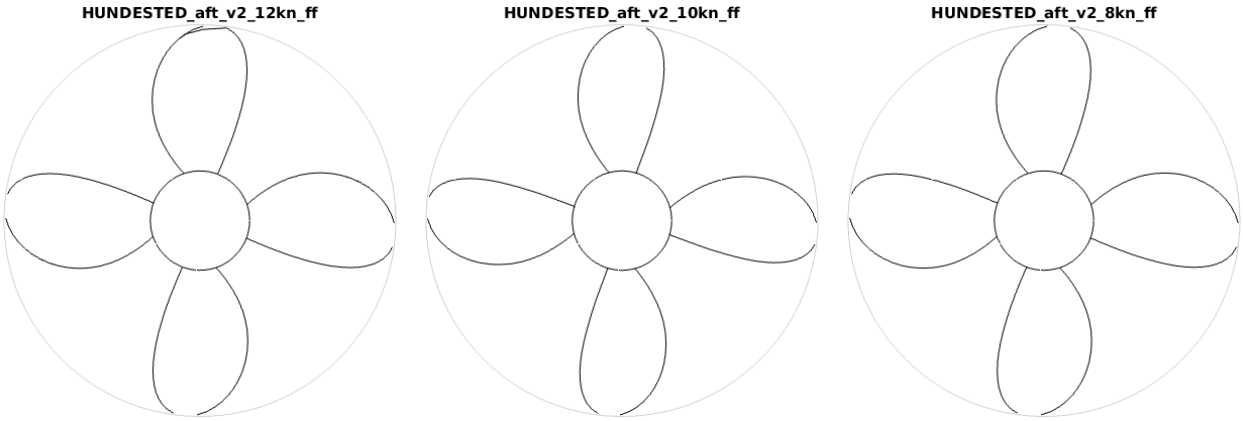

Aft propeller, 12 knots propulsion, feathered front propeller

Aft propeller, 10 knots motor sailing, feathered front propeller

Aft propeller, 8 knots propulsion, feathered front propeller

Figure 4-14: Computed cavitation behaviour of the aft propeller in propulsion

4.4.4 Underwater radiated noise

The estimate of the total underwater radiated noise is provided by Figure 4-15. For reference, the level of the DNV Quiet 11 knots notation is presented. The noise of the tip vortex is dominant. As shown, the current propeller only just exceeds this level at 12 knots.

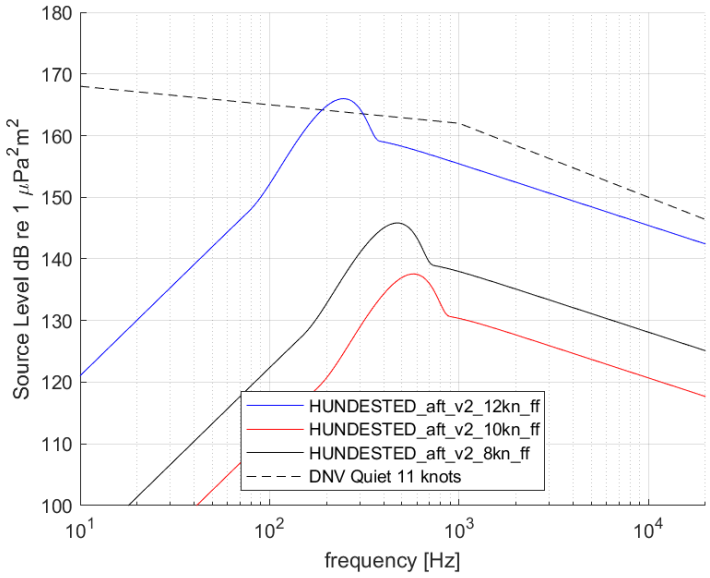

Figure 4-15: Underwater radiated noise predictions for the aft propeller in propulsion with front propeller feathered

4.4.5 Radial loading distribution

The distribution of the radial loading distribution—circulation—over the propeller radius is given in Figure 4-16. The circulation at the tip is the main driver of the strength of the tip vortex and ensuing underwater radiated noise.

The solid line indicates the mean circulation, while the cross-marked and square-marked lines indicate the maximum and minimum circulation in the wake field, respectively. From an analysis of the MARIN ETV model it is concluded that a silent propeller would have a mean circulation of around 0.03 at r/R = 0.95 to meet the DNV Quiet notation at top speed as well. As shown, the mean circulation for 12 knots near the tip exceeds this value, but not by much.

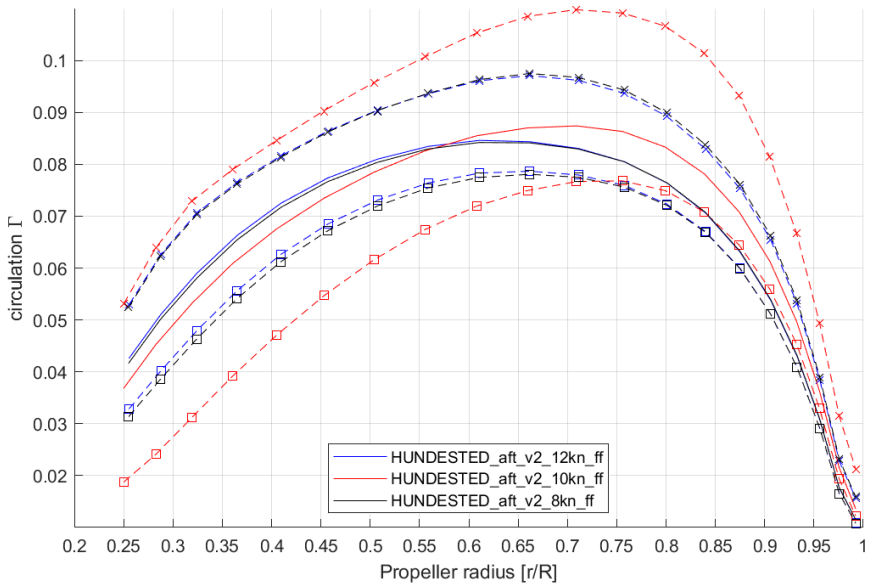

Figure 4-16: Radial distribution of the circulation for the aft propeller

4.4.6 Hull pressure excitation

Figure 4-17 gives the results of the computations on hull pressure fluctuations as induced by the propeller and the cavitation on the propeller. For reference, a level of 1.0 kPa is commonly regarded as the upper limit for yachts, although some yards require 0.75 kPa as a maximum. At 12 knots these criteria are exceeded. Nonetheless, the hull pressure level is dominated by the non-cavitating part which only occurs first blade harmonic for which the ship structure is probably stiffened enough in view of the construction required for the thruster.

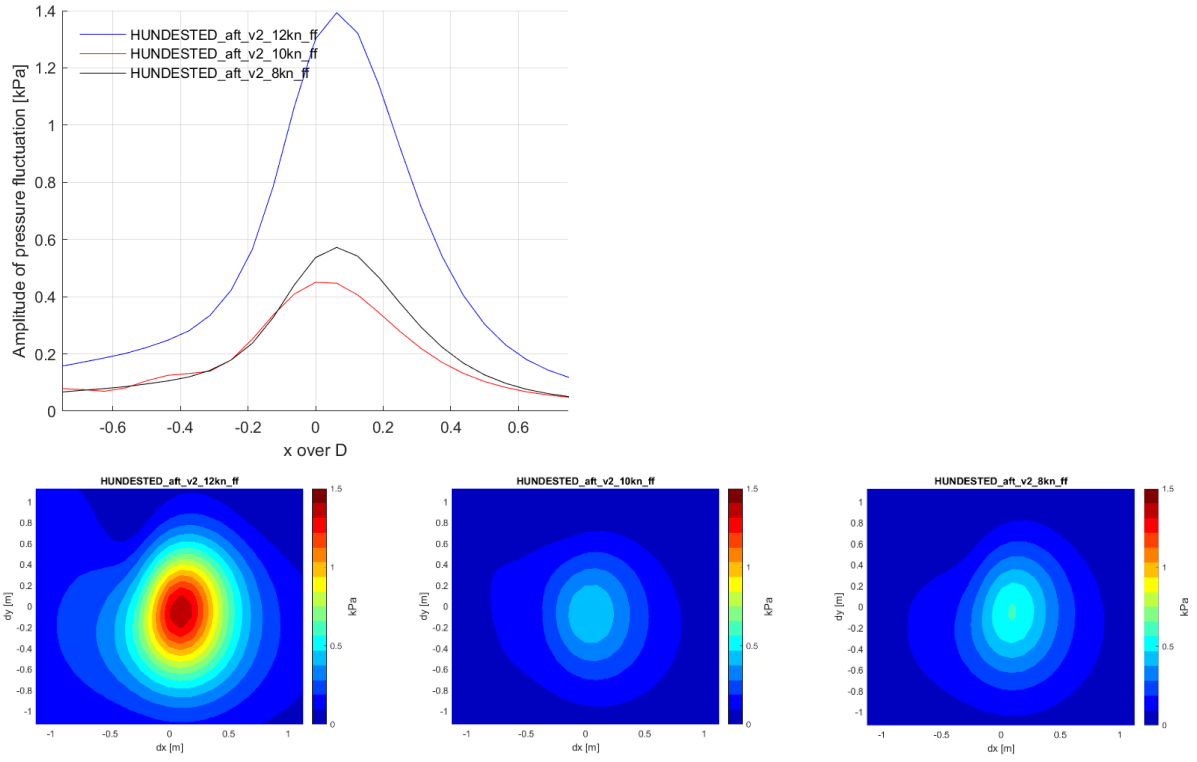

Figure 4-17: Computation of propeller-induced hull pressure fluctuation at the first blade harmonic frequency for the aft propeller

4.4.7 Thrust variation

The dimensionless blade and shaft forces are reported in Figure 4-18 for the aft propeller. The blade forces act on the CPP mechanism, while the shaft forces excite the unit and its foundation. The force variations are normal for a thruster.

At 10 knots motor sailing, the pitch setting of the blade is large and the rotation rate is relatively low. This gives higher variations in the angle of attack and hence somewhat higher blade force amplitudes than at lower pitch settings.

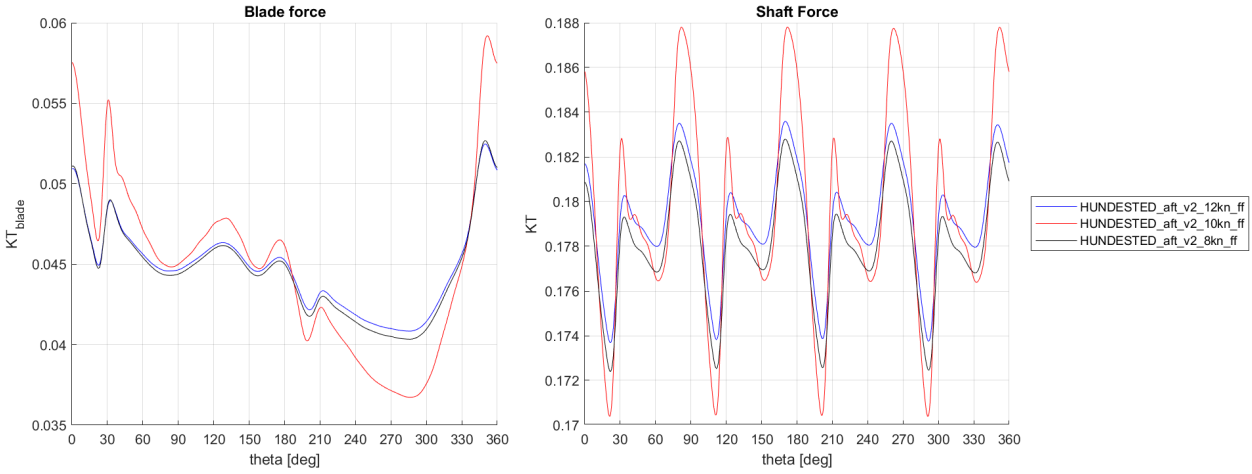

Figure 4-18: Blade and shaft forces for the aft propeller.

4.4.8 Summary of propulsion performance

The current computations show that the aft propeller behaves well in propulsion and is regarded as a suitable propeller for project ZERO.

In comparison to the results for the first set of HUNDESTED propellers, the new set of thrusters improve quite significantly on both on efficiency, cavitation behaviour and hull excitation. The improvement originates from a better propeller-pod-hull interaction, lower thruster resistance and improved propeller efficiency.

4.5 Propeller analysis, regeneration

For regeneration the propellers were analysed in three scenarios:

- Scenario 1. Max regeneration at 16 knots, 250 kW
- Scenario 3. 14 knots, 125 kW
- Scenario 4. Front propeller only at 10 knots, 20 kW

Using the polynomial, Table 4-2 summarises the performance data of both propellers in each of the three scenarios. The pitch and rpm of both propeller were optimised such that the efficiency of the combination of both propellers is optimal. It is assumed that the sails deliver sufficient thrust to maintain the ship speed.

Note that the assumption is being made that the wake fraction of the aft propeller is constant for the maximum efficiency at 16.0 knots, the 14.0 knots and 10.0 knots conditions, despite the varying load on the front propeller.

The wake fraction of the new front propeller is slightly different compared to the first geometry. At highly loaded regeneration, the flow velocity at the outer radii of the new propeller is larger. The flow velocity increases around the stagnation point of the propeller, part of which higher flow velocity is utilized by the propeller itself.

In view of probable leeway and heel of the ship, the probability is not large that the slipstream of the front propeller interacts as negatively (refer to Section 4.2.2) with the aft propeller. Therefore, the data can be regarded on the conservative side and the assumption of equal wake fraction for the different conditions is considered to be appropriate.

In terms of thrust deduction, both the thrust deduction of the units and the thrust deduction on the ship are provided. The thrust deduction of the units is zero; the units have similar resistance in open water as below the ship. This kind of interaction with the ship is hence much more favourable compared to the first geometry as report in MARIN report No. 32992-1-POW.

In comparison with the results as presented in MARIN report No. 32992-1-POW, there is seemingly hardly improvement at 16 knots, 250 kW regeneration, when regarding the efficiency behind the ship as reported previously. This is due to the less favourable interaction of the front propeller with the aft propeller. The more favourable thrust deduction was however not taken into account in this comparison.

	V aft [m/s]	TH units [kN]	ETA behind
First geometry	8.01	-50.7	0.599
Second geometry	7.53	-50.5	0.601

If the thrust deduction of the total ship is properly taken into account, the following comparison can be made:

	V aft [m/s]	TH units + THD ship [kN]	ETA total behind
First geometry	8.01	-50.7 – 4.0 = -54.7	0.555
Second geometry	7.53	-50.5 – 1.4 = -51.9	0.585

This shows that the new geometry is – overall - about 5% more efficient compared to the first geometry. The THD ship is the additional resistance of the ship due to the regenerating propellers, which disturb the pressure field around the ship and influence the frictional resistance on the ship. The new geometries have better hull interaction in this respect.

Table 4-2: Performance data during regeneration.

		250 kW	*max PD*	*max ETA*	*125 kW*	*20 kW*	*20 kW*
V	**KNOTS**	**16.0**	**16.0**	**16.0**	**14.0**	**10.0**	**10.0**
PD front	@0.7R	0.799	0.704	0.979	0.956	1.273	1.035
PD aft	@0.7R	0.853	0.732	1.189	1.121	2.219	feathered
w front		-0.010	-0.015	0.000	0.000	0.000	0.000
w aft		0.085	0.073	0.100	0.100	0.100	
thdf front, unit only		0.00	0.00	0.00	0.00	0.00	0.00
thdf aft, unit only		0.00	0.00	0.00	0.00	0.00	0.00
VA front	m/s	8.31	8.35	8.23	7.20	5.14	5.14
VA aft	m/s	7.53	7.63	7.41	6.48	4.63	
VR front	m/s	18.41	18.80	17.56	15.45	9.78	10.81
VR aft	m/s	16.39	17.10	14.29	12.89	6.54	
beta front	rad	0.468	0.461	0.488	0.485	0.554	0.496
beta aft	rad	0.478	0.463	0.545	0.527	0.787	
CTu front		-0.1118	-0.1197	-0.0911	-0.0938	-0.0736	-0.0852
CQ front		-0.1253	-0.1234	-0.1135	-0.1156	-0.1043	-0.1086
CTp front		-0.1034	-0.1118	-0.0813	-0.0841	-0.0608	-0.0749
CP front		0.347	0.359	0.278	0.289	0.174	0.253
ETA front		0.633	0.593	0.671	0.668	0.655	0.673
ETAp front		0.684	0.635	0.752	0.745	0.793	0.766
CTu aft		-0.1173	-0.1251	-0.0957	-0.0978	-0.0722	
CQ aft		-0.1327	-0.1267	-0.1323	-0.1301	-0.1225	
CTp aft		-0.1064	-0.1151	-0.0807	-0.0837	-0.0439	
CP aft		0.347	0.365	0.232	0.253	0.070	
ETA aft		0.625	0.580	0.651	0.654	0.483	
ETAp aft		0.688	0.631	0.772	0.764	0.795	
TH front	kN	-22.0	-24.5	-16.3	-13.0	-4.1	-5.7
THp front	kN	-20.3	-22.9	-14.5	-11.7	-3.4	-5.0
-PD front	kW	115.7	121.6	90.1	62.6	13.8	20.0
THu aft	kN	-28.5	-33.2	-17.7	-14.7	-2.8	-1.5
THp aft	kN	-25.9	-30.5	-14.9	-12.6	-1.7	-0.5
-PD aft	kW	134.3	146.8	85.4	62.4	6.3	
-PD	kW	250.0	268.5	175.5	125.0	20.0	20.0
PD front / PD		0.463	0.453	0.513	0.501	0.688	1.000
PD aft / PD		0.537	0.547	0.487	0.499	0.312	0.000
THu	kN	-50.5	-57.7	-34.0	-27.7	-6.9	-7.2
N front	RPM	373.6	382.8	352.8	310.9	189.1	216.2
N aft	RPM	264.7	278.3	222.2	202.7	83.9	
KT front		-0.247	-0.265	-0.198	-0.204	-0.160	-0.182
KT aft		-0.256	-0.273	-0.210	-0.213	-0.167	
SIGMA_N front		4.46	4.24	5.00	6.44	17.39	13.31
SIGMA_N aft		5.73	5.18	8.13	9.76	56.94	
ETA front behind		0.639	0.602	0.671	0.668	0.655	0.680
ETA aft behind		0.572	0.538	0.586	0.588	0.435	
ETA behind		0.601	0.565	0.626	0.626	0.565	0.538
CP front behind		0.358	0.376	0.278	0.289	0.174	0.253
CP aft behind		0.266	0.290	0.169	0.184	0.051	
THD ship	kN	1.4	1.5	1.0	0.8	0.3	0.1
TH total behind	kN	-51.9	-59.2	-35.0	-28.5	-7.2	-7.3
ETA total behind		0.585	0.551	0.609	0.608	0.542	0.534

Additionally, if leeway is supposed such that the aft propeller encounters the 16 knots flow, the following comparison is made, assuming that the hull-interaction at zero drift is still representative. This shows an efficiency improvement of about 12%.

	V aft [m/s]	TH units + THD ship [kN]	ETA total behind
First geometry	8.23	-53.2	0.571
Second geometry	8.23	-47.5	0.640

In addition to the three conditions as already provided, the optimal power share and corresponding pitch and rotation rates were wider investigated, primarily to check the behaviour of the polynomials. Figure 4-19 shows for a ship speed of 16.0 knots the performance as function of power regeneration, optimised for the total efficiency of the front and aft propeller combined.

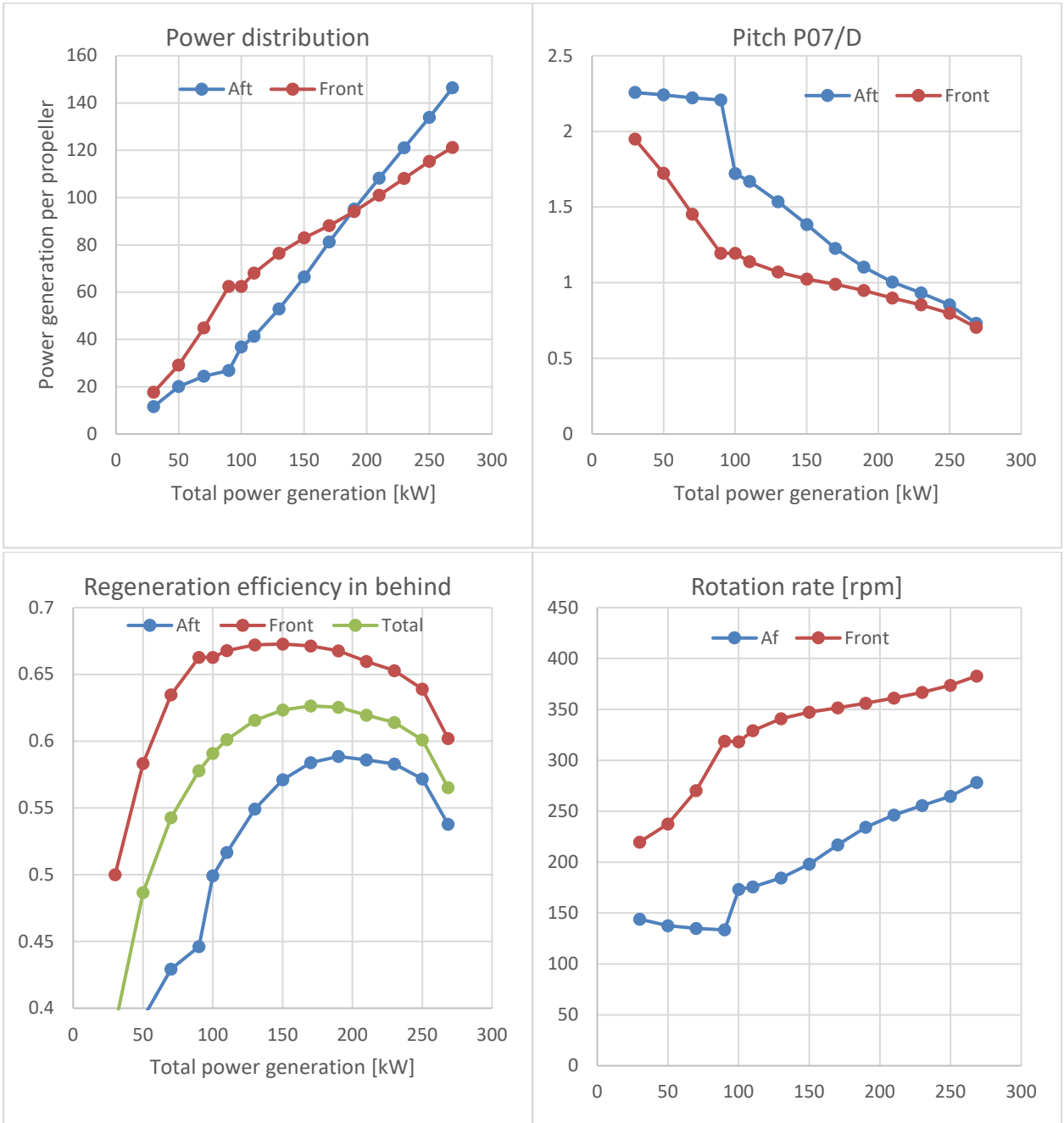

Figure 4-19: Relations between power share and corresponding pitch and rotation rates at 16.0 knots ship speed.

At low power generation the front propeller takes most of the share due to its higher efficiency via its favourable wake fraction and thruster design. For higher power generation, the aft propeller comes into play to deliver the requested total power as efficiently as possible.

Finally, Figure 4-20 shows the CP-ETA diagrams for the aft and front propeller of the first and second geometry, when regenerating 250 kW at 16 knots. The black dots connect the operational point. Both propellers are required to work at a higher CP to cope with the updated operational point. The front propeller takes more power share than before, while the aft propeller sees lower velocity which is compensated to some point by operating at higher CP.

As also shown, the optimized propellers are capable to operate at higher efficiency at higher CP. The maximum efficiency at lower CP is not improved as significantly compared to higher CP.

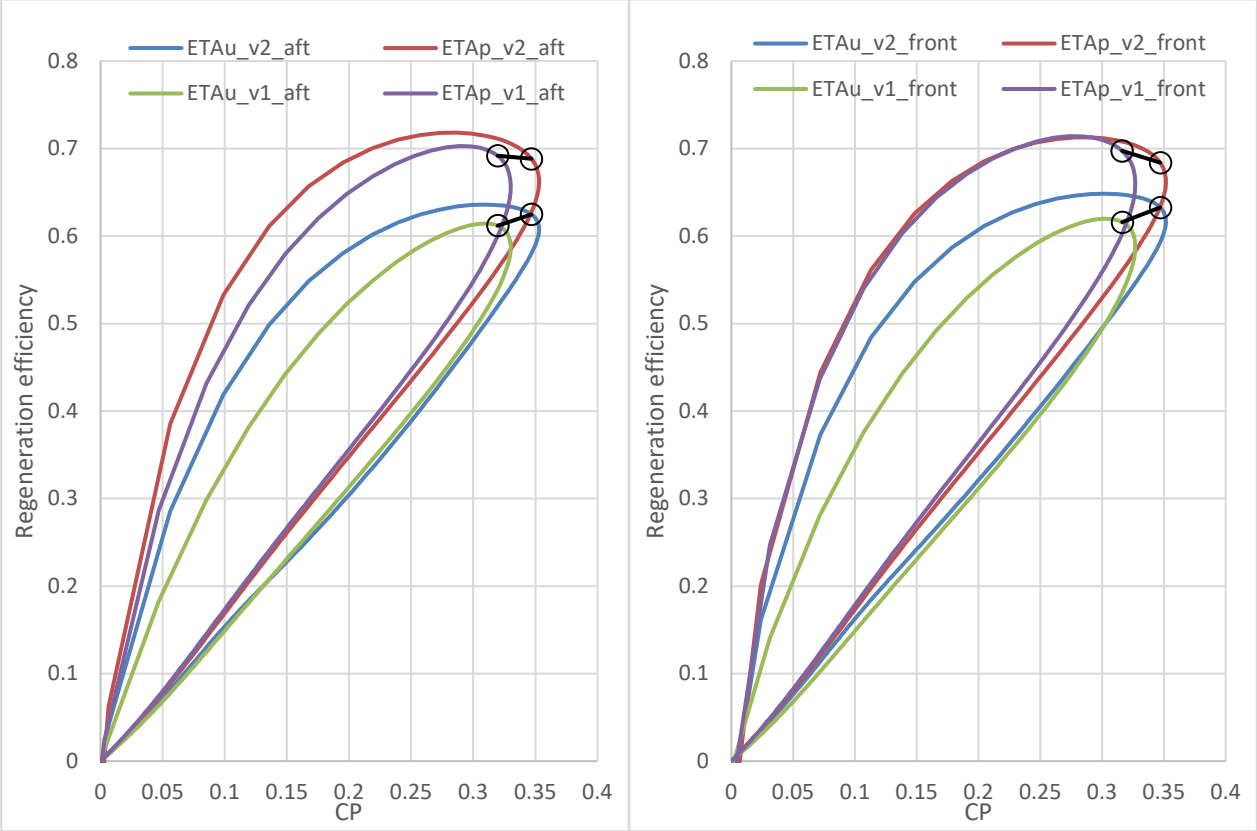

Figure 4-20: Comparison between the first geometry and second geometry at 250 kW regeneration for the aft unit. The black dots connect the operational point.

PROCAL was used again for further computations to analyse the cavitation behaviour of the propellers in the conditions as provided in Table 4-2.

4.5.1 Pressure distributions

Contour plots are provided by Figure 4-21 and Figure 4-22. The pressure coefficient CPN is visualised, ranging from high pressure in red, to low pressure in dark blue where –CPN equals the cavitation number σ_N. Pressure below the vapour pressure, or CPN lower than σ_N, is indicated in magenta.

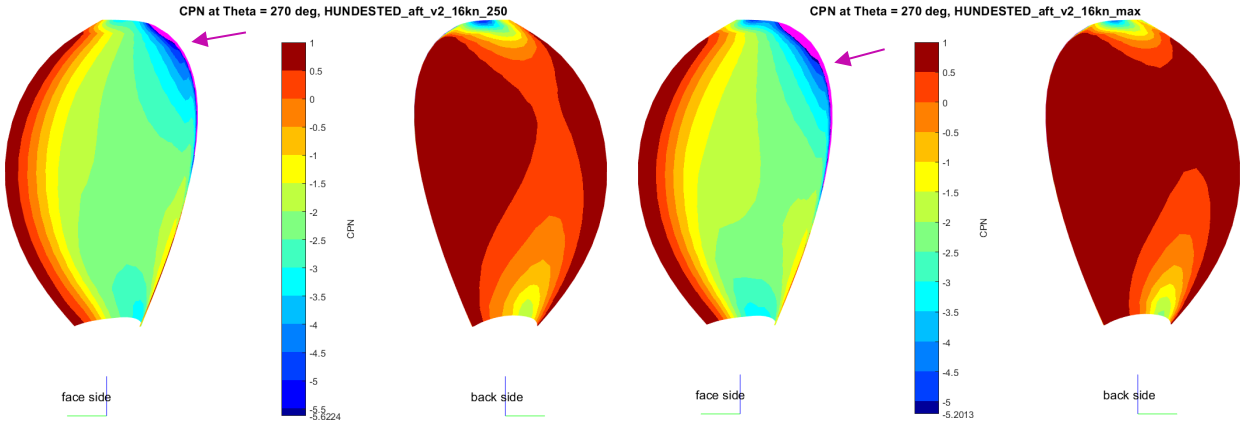

Aft propeller, 16 knots, 250 kW regeneration

Aft propeller, 16 knots, maximum regeneration

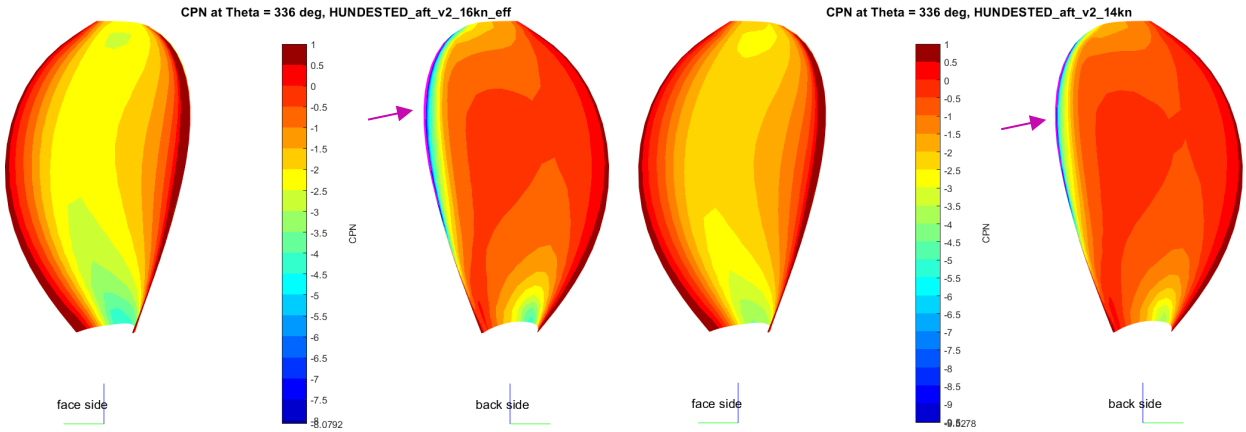

Aft propeller, 16 knots, most efficient regeneration

Aft propeller, 14 knots, 125 kW regeneration

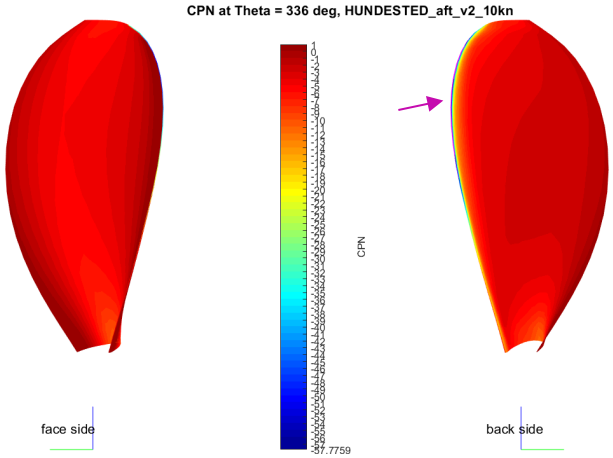

Aft propeller, 10 knots, 20 kW regeneration

Figure 4-21: Pressure contours for the aft propeller during regeneration (non-cavitating computation).

For the aft propeller, all conditions show pressures below the vapour pressure along the upper part of the leading edge. At 16 knots 250 kW and maximum regeneration, there is low pressure on suction side, while at the condition at 16 knots with most efficient regeneration, the 14 knots condition and the 10 knots condition, there is a pressure peak on pressure-side.

For the front propeller, at 16 knots 250 kW and maximum regeneration, there is a band of low pressure at suction side – the face side in regeneration - along the leading edge, as indicated by the arrows.

Cavitation computations are provided in Section 4.5.3. At the root and mid chord of the blade, there is sufficient margin against cavitation.

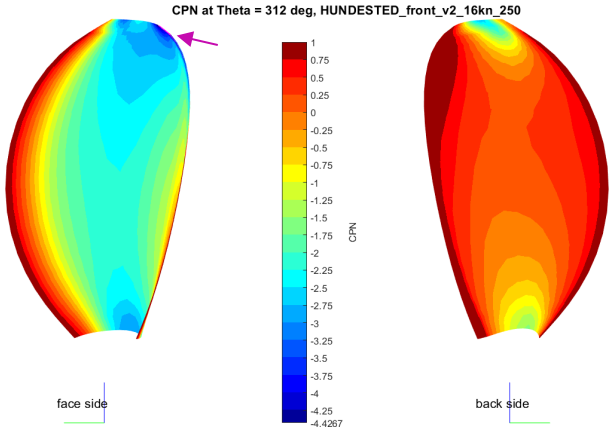

Front propeller, 16 knots, 250 kW regeneration mode

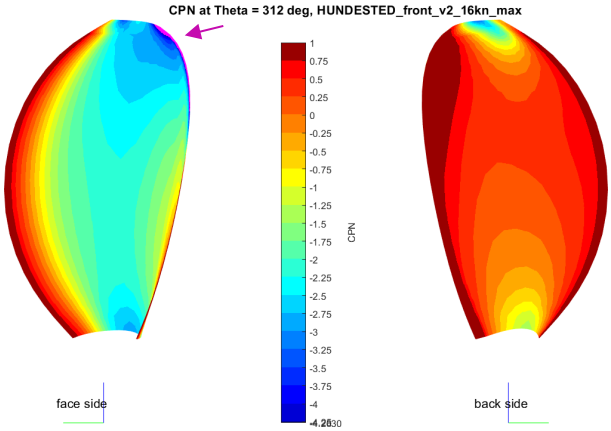

Front propeller, 16 knots, maximum regeneration mode

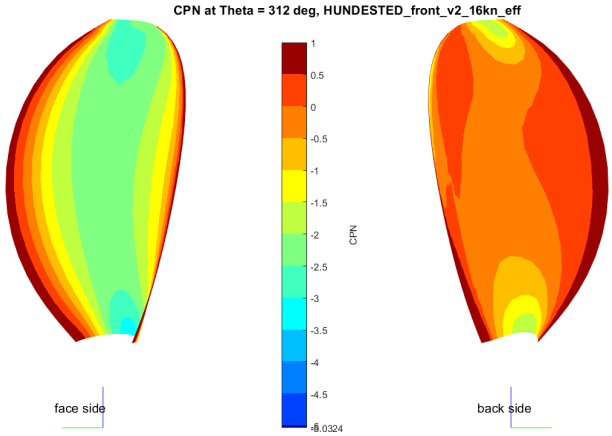

Front propeller, 16 knots, most efficient regeneration mode

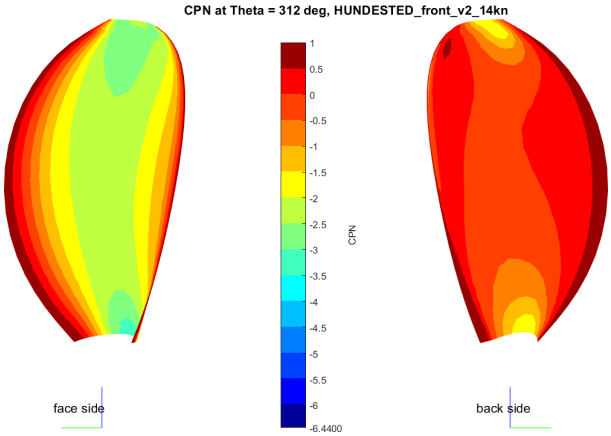

Front propeller, 14 knots, 125 kW regeneration mode

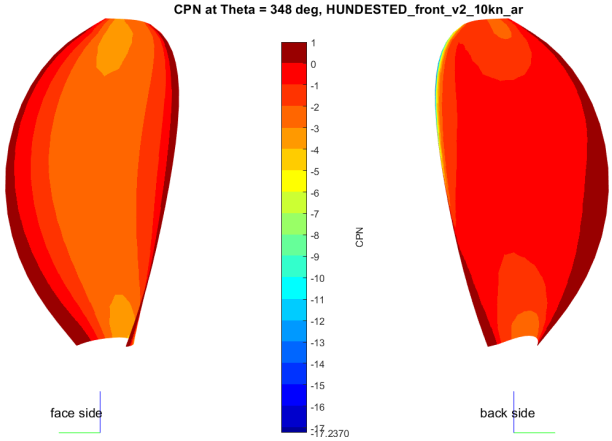

Front propeller, 10 knots, 20 kW regeneration mode, aft propeller regenerating as well

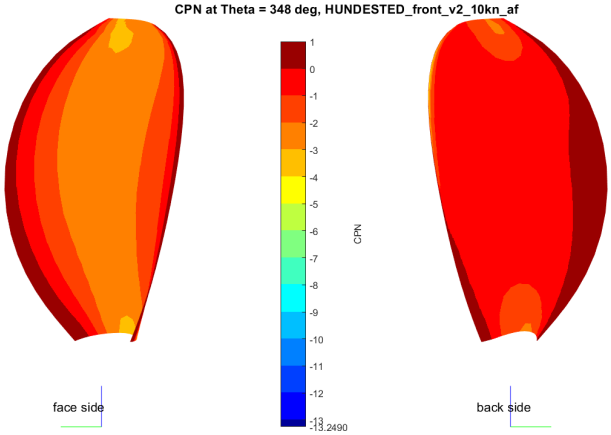

Front propeller, 10 knots, 20 kW regeneration mode, aft propeller feathered

Figure 4-22: Pressure contours for the front propeller during regeneration (non-cavitating computation).

For the 16 knots condition in 250 kW regeneration mode, the figures on pages F23 through F34 and F35 through F40 provide the contour plots for all blade angles for the aft and front propeller, respectively. As an alternative presentation, the minimum pressures as function of propeller radius are provided in Figure 4-12. The bold lines provide pressure-side and the dashed line indicate suction side.

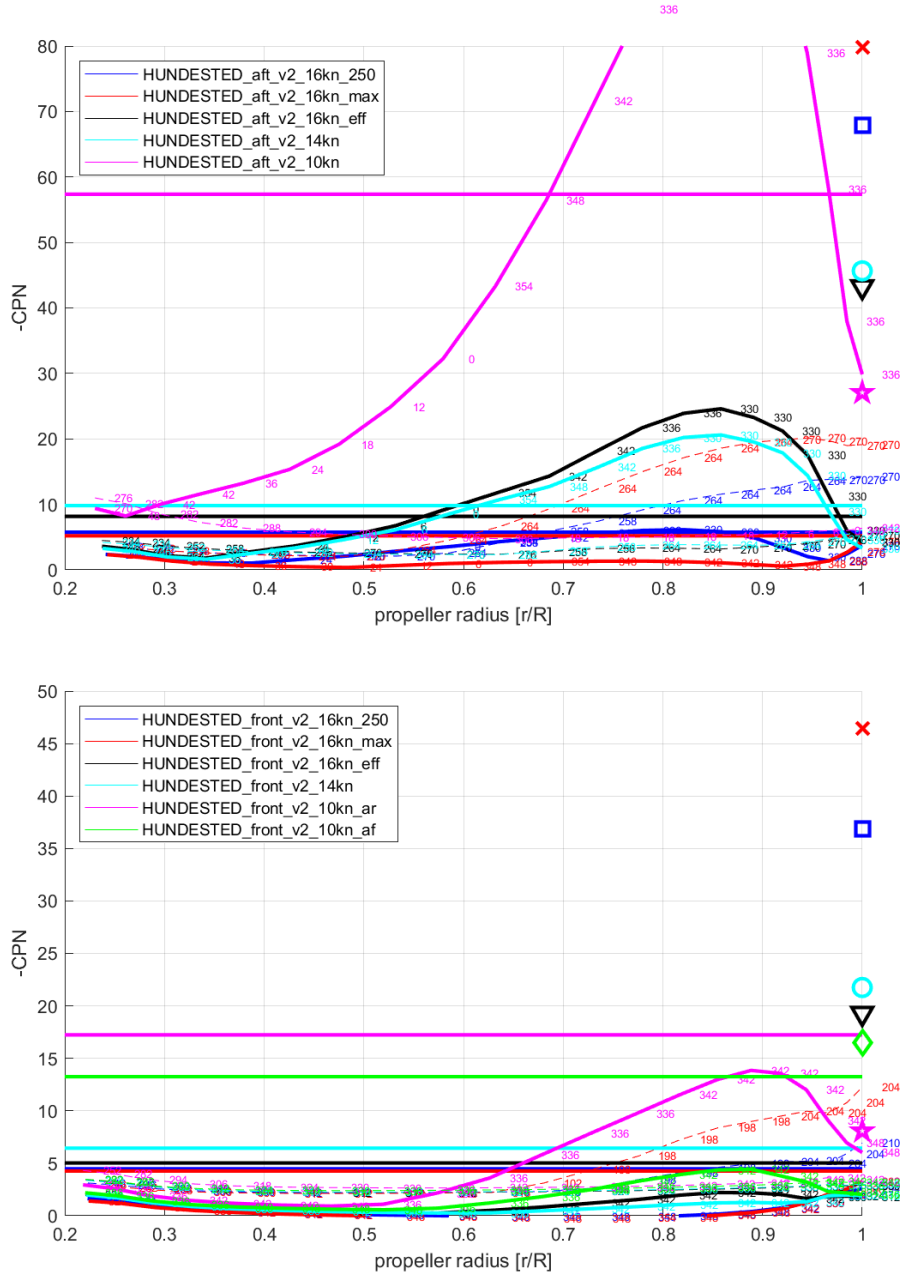

Figure 4-23: Minimum pressure coefficient as function of propeller radius for the aft propeller (top) and front propeller (bottom) during regeneration. The horizontal lines indicate the cavitation inception limit. The solid lines represent the suction-side back-side pressure-peak and the dashed lines the face-side pressure-peak. The markers give the pressure coefficient of the core of the tip vortex.

4.5.2 Cavitation inception

Figure 4-24 and Figure 4-25 provide the cavitation inception lines for the aft and front propeller, respectively. For sheet cavitation, inception is determined on the propeller within the interval of the specified propeller radii as given in the title of the plots.

The operational points are provided by the small cross markers. The two sets of lines per condition indicate face cavitation - in regeneration this is the suction-side - with low pressure in terms of CPN at low K_T and back cavitation - in regeneration this is the pressure-side - with low pressure in terms of CPN at high K_T. The numbers near the inception lines provide the angle in degrees in which the pressure is critical with 0 degrees the top position.

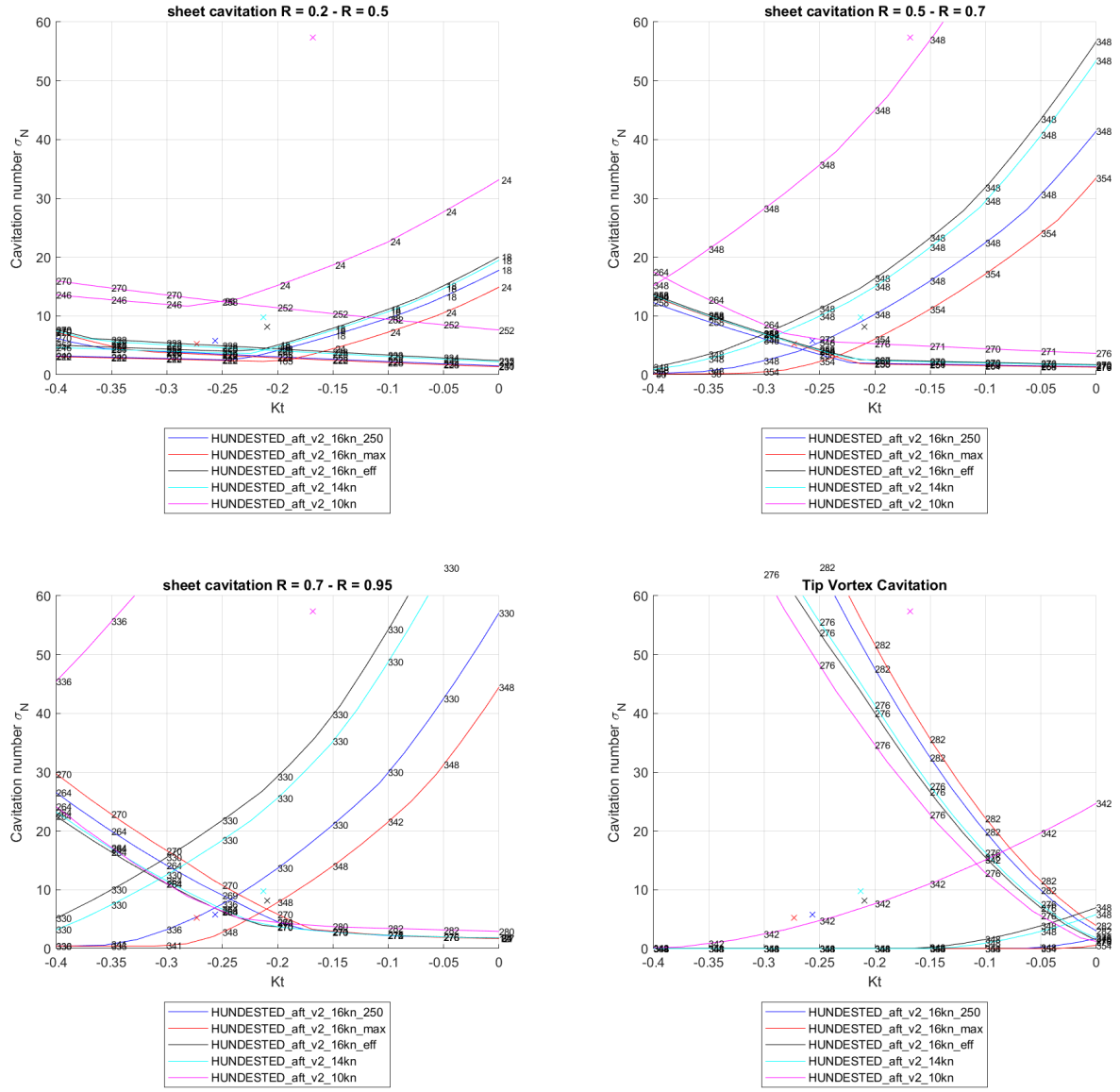

Figure 4-24: Computed sheet cavitation inception diagrams for the aft propeller during regeneration.

The differences in the inception curves are dominated by the pitch setting in each condition. Therefore, some inception lines are very similar due to their similarity in pitch setting. As shown, the cavitation bucket becomes narrower with increasing pitch, but the margin is still sufficient since the operational point is also at lower rpm and thus higher in the diagram.

At 250 kW, 16 knots, the aft propeller is properly balanced between suction side and pressure side cavitation. However, at 14 knots pressure-side cavitation becomes dominant. The reason is twofold. First, the wake field is significantly more challenging compared to the wake field from the first geometry. The propeller would be free of pressure side cavitation in the earlier wake field. Second, the aft propeller becomes less loaded for optimum efficiency due to the higher wake fraction compared to the first geometry.

Due to the higher loading than expected based on the results of the previous iteration as reported in MARIN report No. 32992-1-POW, the front propeller has suction side cavitation at 16 knots, 250 kW. Nonetheless, the propeller is still reasonably well-balanced for suction-side and pressure-side cavitation in all conditions.

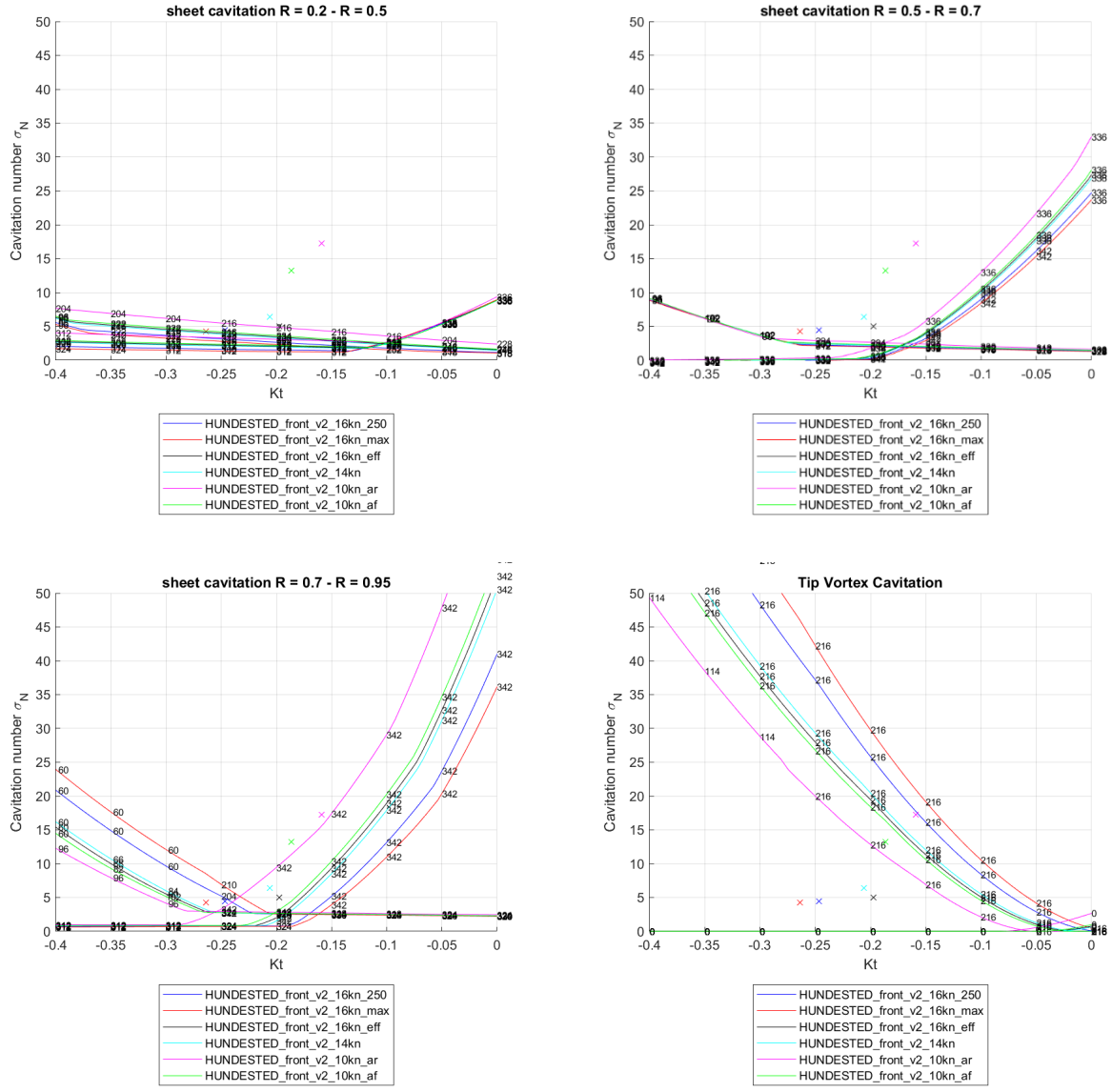

Figure 4-25: Computed sheet cavitation inception diagrams for the front propeller during regeneration.

4.5.3 Cavitation behaviour

Figure 4-26 and Figure 4-27 and provide sketches of the cavitation behaviour which are obtained from cavitation computations. In black the contour of the cavitation and propeller is given. In regeneration, suction side cavitation occurs on the face side which is presented in purple. Pressure-side cavitation occurs on the back side, and is shown in red. The 16 knots conditions are also shown on figure pages F41 through F44 for multiple angles in the wake field.

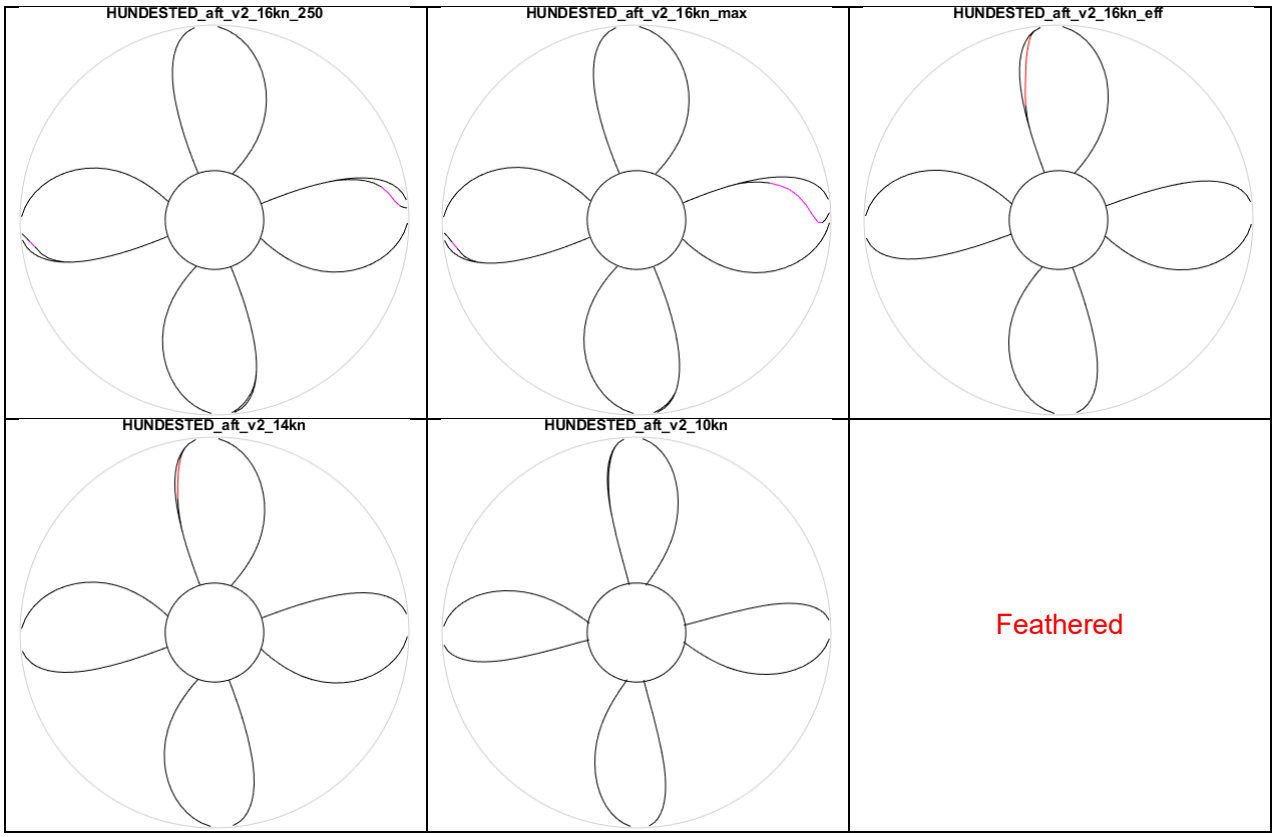

Figure 4-26: Computed cavitation behaviour of the aft propeller during regeneration.

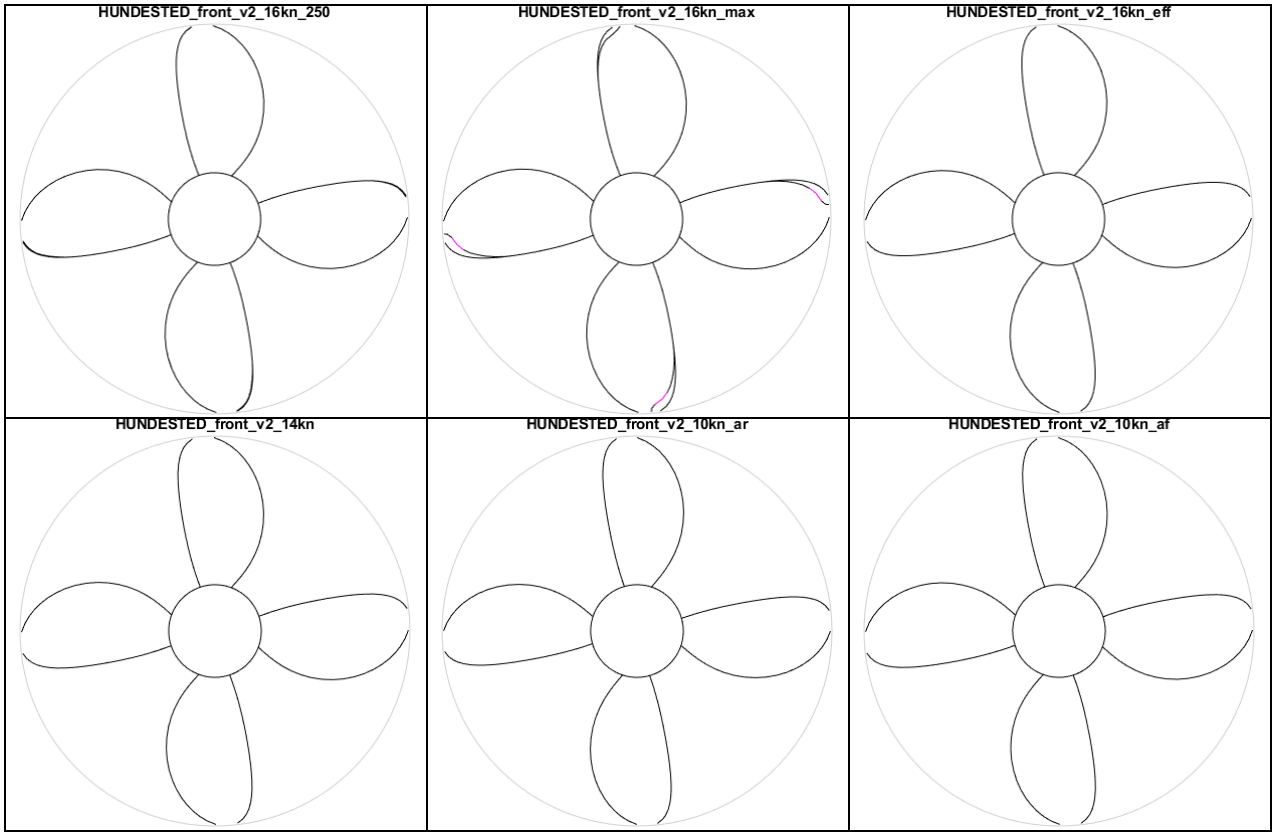

Figure 4-27: Computed cavitation behaviour of the front propeller during regeneration.

Sheet cavitation occurs at 16 knots 250 kW regeneration and maximum regeneration on the suction side (face side of propeller during regeneration), on both the front and aft propeller. For all considered conditions, the cavitation behaves stable and probably non-erosive, thereby providing robustness for variations in the conditions during sailing.

The front propeller is free of cavitation for 16 knots most efficient regeneration and the lower ship speeds. The aft propeller, however, features a narrow strip of pressure side cavitation. The pressure side cavitation has non-erosive character due to its sufficiently high aspect ratio and relatively long existence during the rotation.

4.5.4 Underwater radiated noise

The estimate of the total underwater radiated noise is provided by Figure 4-28. The levels for 10 and 14 knots (almost) coincide on a base level. Although sheet cavitation is present in the 16 knots condition for 250 kW and max power regeneration, the noise of the tip vortex is dominant. For reference, the level of the DNV Quiet 11 knots notation is presented. As shown, the current propellers only exceed this level at 16 knots while regenerating at high power. The front and aft propeller have similar levels, although the aft propeller clearly dominates the front propeller, due to its unfavourable inflow.

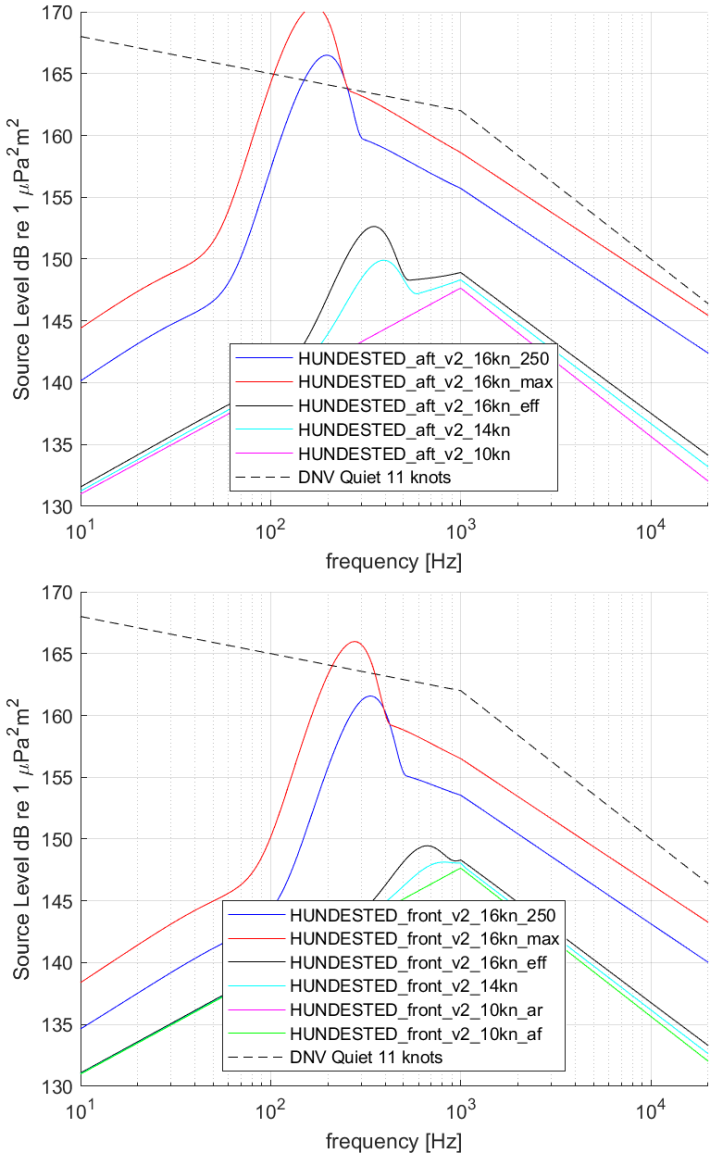

Figure 4-28: Underwater radiated noise predictions for the aft propeller (top) and front propeller (bottom) during regeneration.

4.5.5 Radial loading distribution

The distribution of the radial loading distribution—circulation—over the propeller radius is given in Figure 4-29 and Figure 4-30. The circulation at the tip is the main driver of the strength of the tip vortex and ensuing underwater radiated noise.

The solid line indicates the mean circulation, while the cross-marked and square-marked lines indicate the maximum and minimum circulation in the wake field, respectively.

Compared to the figures shown in MARIN report No. 32992-1-POW, the circulation of especially the aft propeller has much larger amplitudes through the wakefield, due to the less uniform wake distribution.

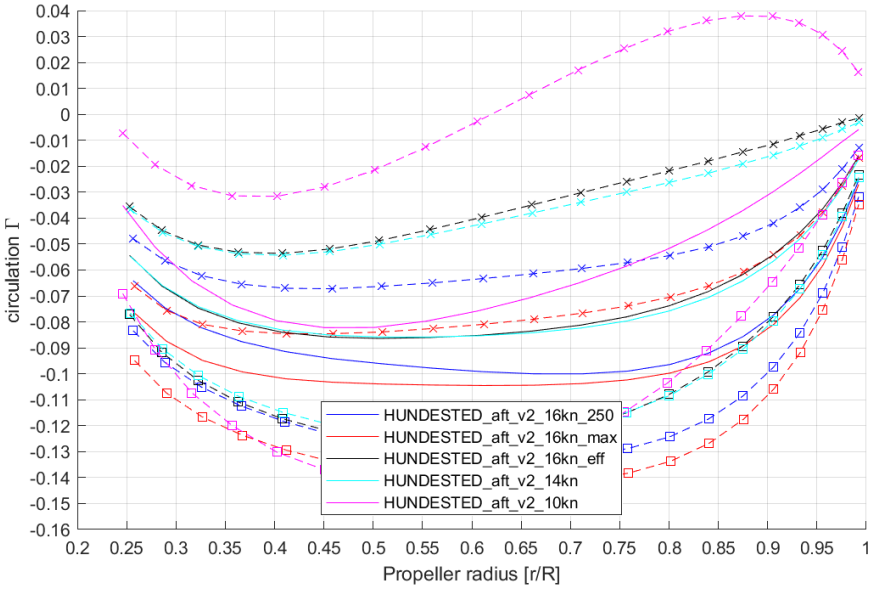

Figure 4-29: Radial distribution of the circulation for the aft propeller in regeneration.

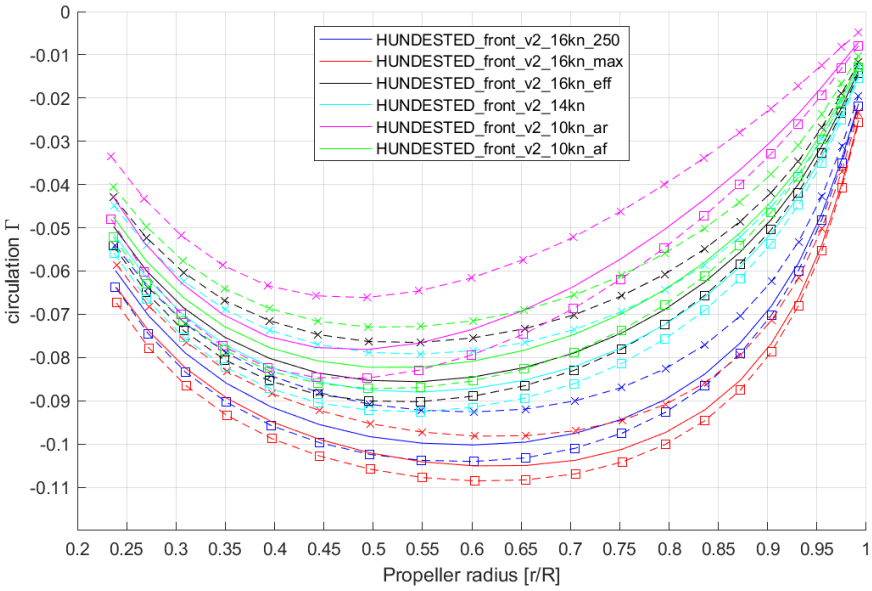

Figure 4-30: Radial distribution of the circulation for the front propeller in regeneration.

4.5.6 Hull pressure excitation

Figure 4-31 gives the results of the computations on hull pressure fluctuations as induced by the propeller and the cavitation on the propeller. The hull pressure fluctuations do not give rise to concerns on propeller induced vibrations.

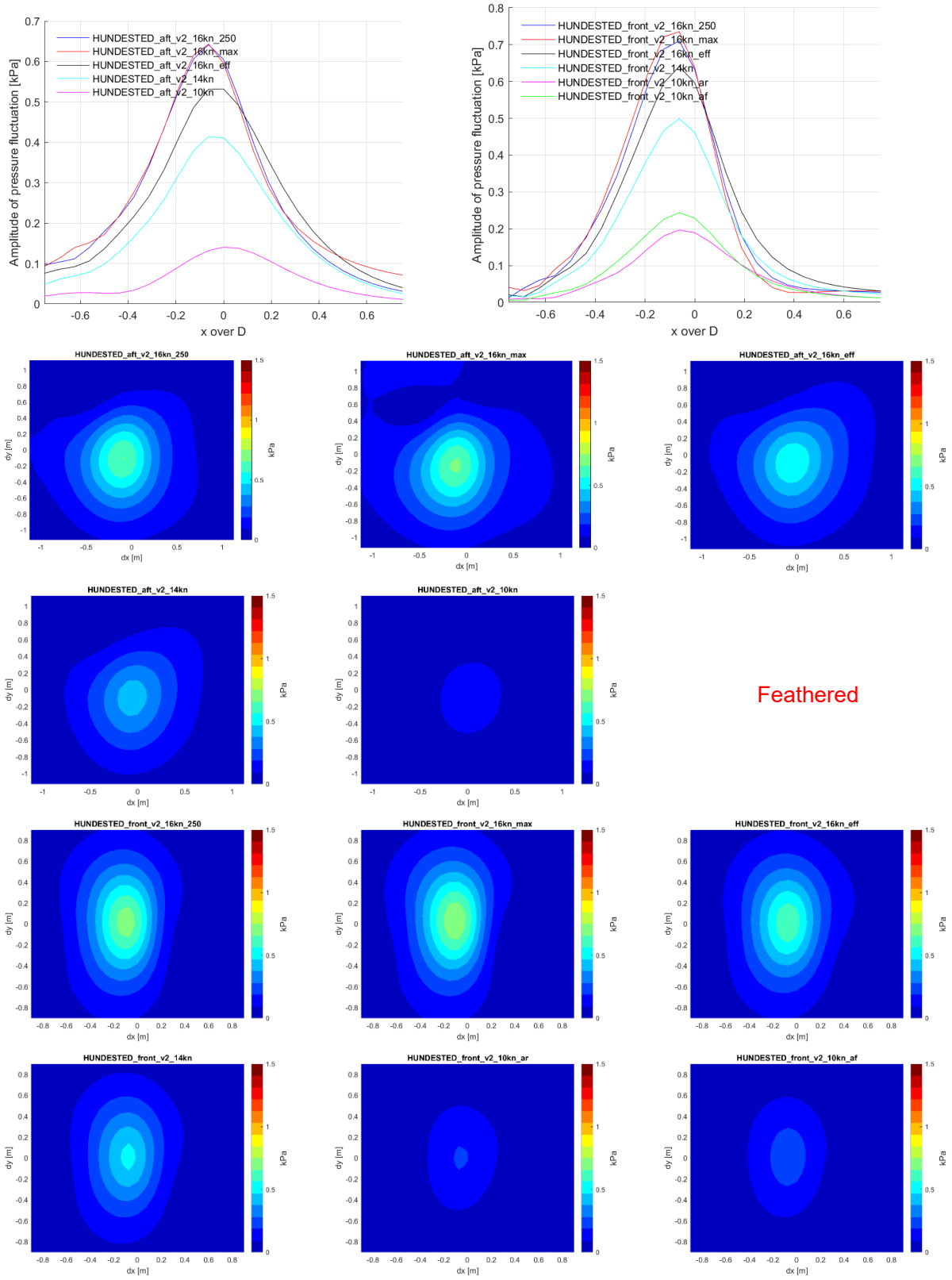

Figure 4-31: Computation of propeller-induced hull pressure fluctuation at the first blade harmonic frequency for both propellers in regeneration.

4.5.7 Thrust variation

The dimensionless blade and shaft forces are reported in Figure 4-32 and Figure 4-33 for the aft and front propeller, respectively. The wake from the aft propeller is more complicated which gives also some quite large variations in the blade force. The shaft force variation, is also quite present. Nonetheless, there are no indications for any issues due to thrust variations in that sense.

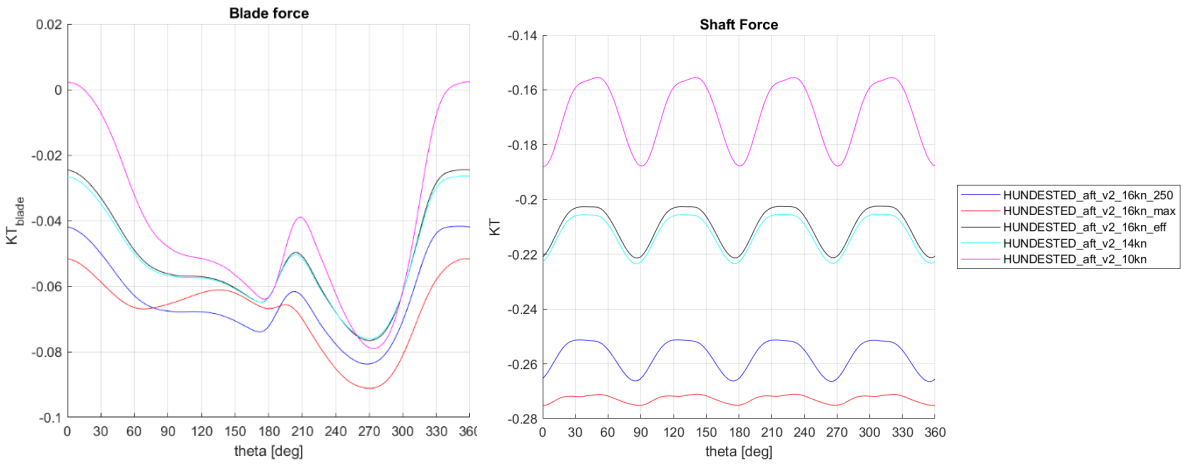

Figure 4-32: Blade and shaft forces for the aft propeller.

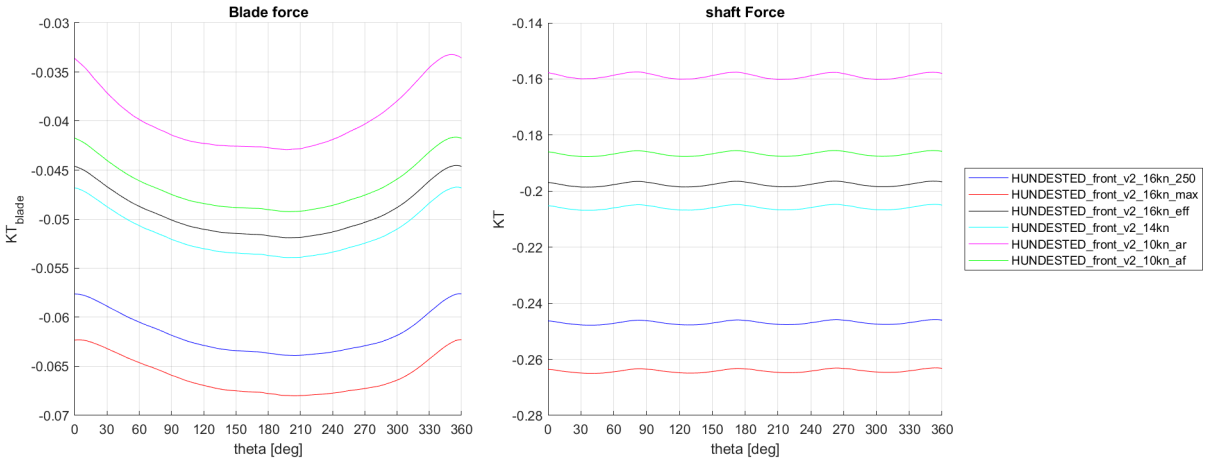

Figure 4-33: Blade and shaft forces for the front propeller.

4.5.8 Summary of regeneration performance

At 250 kW, 16 knots, the aft propeller is properly balanced between suction side and pressure side cavitation. However, at 14 knots pressure-side cavitation becomes dominant. The reason is twofold. The aft propeller becomes lower loaded for optimum efficiency due to the higher wake fraction. Second, the wake field is significantly more challenging compared to the earlier wake field as reported in MARIN report No. 32992-1-POW. It was checked that the pressure-side cavitation was absent in the wake distribution from the previous geometry.

Due to the higher loading than expected based on the results of the previous iteration as reported in MARIN report No. 32992-1-POW, the front propeller has suction side cavitation at 16 knots, 250 kW and above. Nonetheless, the propeller is still reasonably well-balanced for suction-side and pressure-side cavitation in all conditions.

The improvements compared to the previous geometry in regeneration are not as large as expected due to the unfavourable inflow in the aft propeller. Nonetheless, both propellers are regarded as suitable for project ZERO.

Another iteration step could focus on a slightly better rebalance of the cavitation, but large improvements can probably only be obtained at the cost of efficiency and increased hull pressure fluctuations.

4.6 Propeller analysis, other requirements, bollard pull

Scenarios 8 to 10 deal with bollard pull, manoeuvring and crash stop, of which the bollard pull is the most relevant scenario in terms of propeller design. If the bollard pull is successful, other manoeuvring conditions are usually no problem. The crash stop is very dependent on the ship mass and other aspects and is usually tackled in a simulation using standard B-series data, which is outside the scope of the current propeller design review.

In bollard pull it is assumed that the propeller will absorb maximum power of 400 kW and 300 kW at the maximum rotation rate of 400 rpm and 500 rpm for the aft and front propeller, respectively . Using the polynomials, this gives a pitch $P_{0.7}/D$ of 0.677 and 0.730, and a bollard pull of 60.8 kN and 41.6 kN for the aft and front propeller respectively, assuming a commonly used thrust deduction factor of 0.05.

Cavitation during bollard pull is usually very stable and not critical in terms of erosion. Too much cavitation could lead to thrust breakdown, from which the propellers do not suffer with ample margin.

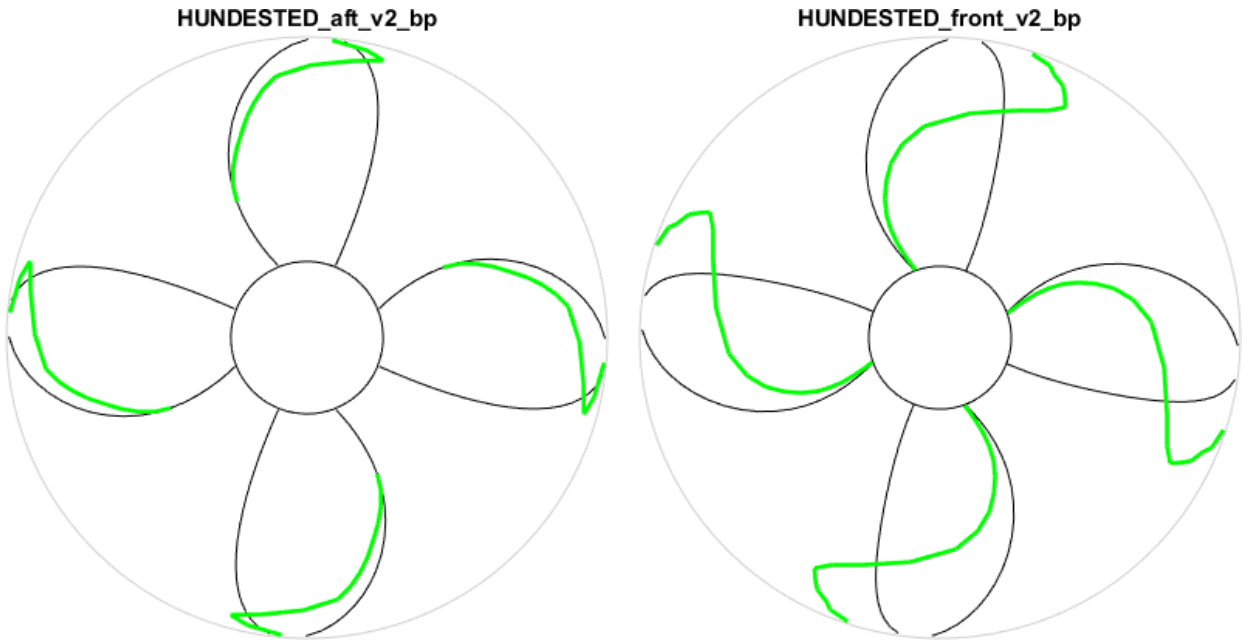

Figure 4-34: Cavitation extent during bollard pull at maximum power, maximum rotation rate.

5 CONCLUSIONS AND RECOMMENDATIONS

The updated geometry of the thrusters and propellers were analysed, similarly as was done in MARIN report No. 32992-1-POW.

CFD computations were performed using RANS-BEM to obtain the wake field of the ship and thrusters both in regeneration and propulsion mode. In propulsion the wake field was determined with feathered front propeller.

CFD computations were performed using RANS-BEM on both thrusters to determine the open water characteristics, both in propulsion and regeneration mode. Polynomials as function of propeller pitch and advance coefficient for both propulsion and regeneration were determined, for both the front and aft thruster. These polynomials can be integrated in the performance prediction programs. Using the polynomials, based on the usage scenarios, operational conditions were determined in terms of propeller pitch and propeller rotational speed for both propulsion and regeneration.

Using computational tools MARIN analysed the performance of the propeller designs in terms of powering, regeneration and cavitation behaviour.

- In propulsion, the efficiency, cavitation behaviour and hull excitation was improved considerably, up to 10% reduction of required power.

- In regeneration, the efficiency of the units was improved as well. The regeneration efficiency at 16 knots was improved such that 5% less drag would be encountered at 250 kW regeneration compared to the earlier geometry. However, the total regeneration efficiency was improved less than expected due to a less favourable interaction of flow from the front propeller with the aft propeller. The cavitation behaviour was also not as good as expected from the new geometries, but regarded to be suitable for project ZERO.

The conclusions and recommendations do not supersede the more detailed comments made in the report.

Wageningen, July 2023
MARITIME RESEARCH INSTITUTE NETHERLANDS

Ir. G. Gaillarde
Head of Ships Department

TABLES

powers		aft			front		
Pitch	J	Ktu	Ktp	Kq	Ktu	Ktp	Kq
P07/D							
0	0	-0.0263	-0.1427	0.0219	0.0529	-0.0834	-0.0254
1	0	-0.2783	0.4647	-0.1065	-0.7933	0.0521	0.2485
2	0	3.0851	1.2556	0.2276	4.0819	2.0635	-0.8077
3	0	-4.9914	-2.6580	-0.0794	-5.5386	-3.0468	1.4286
4	0	3.8400	2.2354	-0.0289	3.6129	1.9329	-1.1856
5	0	-1.4439	-0.8778	0.0352	-1.1482	-0.5622	0.4786
6	0	0.2114	0.1312	-0.0088	0.1405	0.0583	-0.0757
0	1	-1.3042	-0.3743	-0.5160	-1.6959	-0.9522	-0.3653
1	1	9.7242	4.1116	3.9200	12.1032	8.2737	2.6198
2	1	-28.3855	-15.3095	-11.6229	-32.8915	-25.6739	-7.3663
3	1	39.9507	24.4947	17.2594	42.6674	36.2013	10.5166
4	1	-29.8705	-19.8569	-13.6033	-29.0584	-26.2059	-8.1098
5	1	11.3807	7.9487	5.3866	9.9921	9.4524	3.1762
6	1	-1.7296	-1.2409	-0.8415	-1.3595	-1.3380	-0.4936
0	2	4.0228	0.7282	0.7509	4.7210	1.5549	0.7095
1	2	-32.4834	-11.6714	-7.8776	-36.1536	-19.3537	-7.0344
2	2	92.5885	46.2163	30.7789	98.0536	71.0244	27.2080
3	2	-134.7130	-85.9702	-58.5075	-135.3625	-121.4918	-52.0877
4	2	108.6986	81.9462	55.5621	103.3069	107.0333	50.1975
5	2	-45.3505	-37.5413	-25.1042	-40.5211	-46.0350	-23.0584
6	2	7.5081	6.5001	4.3130	6.2482	7.5593	4.0236
0	3	-2.0642	0.6165	1.1334	-2.6178	1.1585	1.0841
1	3	16.8080	-11.4771	-7.6540	20.2394	-15.2322	-8.5295
2	3	-50.0848	23.1447	12.2986	-55.3118	19.2636	15.5081
3	3	81.2497	8.2414	13.0903	85.8415	31.1189	8.3549
4	3	-87.4197	-58.0979	-40.1451	-88.7292	-84.1214	-38.1046
5	3	49.0058	45.1760	26.8039	46.5662	57.0021	27.4358
6	3	-10.1402	-10.1773	-5.6353	-8.8106	-11.9690	-6.0450
0	4	0.3156	5.5461	0.5035	0.0905	6.6699	1.0637
1	4	-0.9402	-2.4615	3.8437	-2.4531	6.6865	3.6127
2	4	-0.5310	-45.3510	-34.4358	-5.0514	-71.5111	-36.8787
3	4	31.3740	101.7603	50.6700	38.2544	123.2026	58.7488
4	4	-21.1675	-52.5132	-17.6229	-17.4670	-55.1321	-24.7058
5	4	-5.7548	-3.4381	-4.0507	-8.6324	-7.1381	-2.8076
6	4	4.1758	4.8455	2.2692	3.9258	5.7563	2.5786
0	5	-0.1674	-7.3964	-1.5387	0.7916	-11.8634	-2.4559
1	5	-2.4929	31.7259	15.6806	4.2815	39.6764	18.0355
2	5	-30.9663	-62.3746	-13.9573	-35.7737	-60.1268	-20.9197
3	5	12.5959	-0.7265	-16.0158	-1.8001	-14.7462	-11.3104
4	5	19.1640	36.9978	16.8237	26.3389	46.9557	18.5446
5	5	-8.2355	-11.8402	-3.9234	-7.5609	-13.3785	-5.2637
0	6	1.6399	-0.8166	-2.3701	-1.4027	0.7052	-2.0549
1	6	19.2946	10.9112	-4.8993	16.9498	3.6706	-2.7898
2	6	2.0165	35.0187	21.2828	20.3181	47.0565	21.0817
3	6	-25.3368	-45.0396	-12.2352	-30.9039	-52.3285	-16.3142
4	6	8.7601	11.5733	2.0578	6.7647	12.1799	3.9423
0	7	-5.4393	-2.3010	2.4681	-3.1127	-1.3777	1.7618
1	7	-7.5684	-20.0086	-7.1203	-16.0471	-22.7707	-7.8438
2	7	16.8735	22.2840	1.5076	16.2998	24.1149	4.5238
3	7	-4.8631	-4.8365	0.2017	-2.1880	-4.4032	-1.0950
0	8	3.0629	4.4966	0.4017	4.0112	4.7083	0.7794
1	8	-4.8923	-4.2961	1.2863	-2.8013	-4.3644	0.2553
2	8	1.0165	0.3471	-0.4038	-0.5321	-0.1106	0.0369
0	9	0.2639	-0.1013	-0.3023	-0.2612	-0.1299	-0.2024
1	9	0.1084	0.2932	0.0238	0.4364	0.4474	-0.0271
0	10	-0.0367	-0.0362	0.0205	-0.0426	-0.0554	0.0198

POLYNOMIAL FOR THE PERFORMANCE OF THE AFT AND FRONT UNIT IN PROPULSION AS FUNCTION OF PITCH AND ADVANCE COEFFICIENT

powers		aft			front		
Pitch	Beta - π	Ctu	Ctp	10Cq	Ctu	Ctp	10Cq
P07/D	[rad]						
0	0	0.0493	0.4229	-0.7479	1.4768	0.2541	0.1266
0	1	5.4073	-2.2701	1.4766	-11.7302	-1.0276	-6.7656
0	2	-89.3998	-21.1260	28.9592	6.1579	-24.1093	67.5842
0	3	472.5503	153.5159	-225.3887	165.8064	158.2057	-354.2276
0	4	-1334.8617	-486.5606	721.8400	-711.5592	-489.4089	1063.4819
0	5	2315.1126	918.5813	-1337.2261	1474.5329	909.7421	-2004.8901
0	6	-2572.5803	-1106.5612	1572.4962	-1818.5207	-1080.7719	2454.7575
0	7	1810.5588	857.4463	-1166.3414	1380.1168	826.4711	-1915.7596
0	8	-761.7662	-414.2868	508.8941	-621.5496	-394.2000	896.7402
0	9	167.8934	113.7423	-111.9817	148.3667	106.8193	-222.2239
0	10	-13.6751	-13.5533	8.2081	-13.7716	-12.5532	21.2578
1	0	-3.3742	-3.1531	4.9205	-6.8455	-2.2983	1.7471
1	1	41.0493	34.9563	-36.8817	73.2281	28.9461	-13.0568
1	2	-112.3422	-86.8299	122.4960	-256.6606	-72.4141	52.7246
1	3	137.9033	131.6320	-173.9204	501.9122	105.4200	-85.0301
1	4	-66.3305	-138.5251	161.4002	-615.1581	-91.9173	143.6264
1	5	-57.7047	92.2812	-185.3751	481.7590	28.6092	-266.3447
1	6	211.6385	-21.6162	102.0950	-171.2486	34.4252	194.1375
1	7	-265.0263	-12.1922	83.1282	-61.4875	-42.4240	51.9764
1	8	149.6465	8.9179	-109.3994	78.2204	18.2281	-114.5604
1	9	-31.4212	-1.7226	30.4855	-19.7540	-2.9966	34.3192
2	0	5.0766	5.4670	-8.3072	8.7878	3.7810	-3.3474
2	1	-67.8171	-62.4582	61.6368	-95.8264	-51.7733	26.0443
2	2	176.3024	141.2724	-182.6603	289.6595	120.3799	-78.5270
2	3	-177.5314	-162.2441	177.6667	-441.3438	-143.8502	16.9039
2	4	78.6958	132.2214	48.8371	404.9496	122.2563	187.8992
2	5	-113.3921	-98.3132	-57.4075	-312.2799	-91.5526	-115.4548
2	6	190.4251	51.8449	-156.8874	231.0026	47.2995	-167.3507
2	7	-125.1204	-14.8954	164.7293	-112.9970	-13.3974	187.0033
2	8	28.1335	2.0190	-43.1677	22.6948	1.8678	-49.8655
3	0	-4.5385	-5.4526	6.4238	-6.2795	-3.7778	2.5715
3	1	61.8708	59.8145	-53.7424	70.4939	49.7514	-28.7674
3	2	-164.7616	-129.7848	174.2222	-197.1917	-109.8226	110.3122
3	3	155.8388	114.5369	-235.9974	246.2995	97.5164	-150.7798
3	4	4.9179	-42.8875	41.1121	-121.7302	-36.8986	-27.9841
3	5	-102.2304	10.6733	163.5740	-13.4813	10.2042	207.2794
3	6	66.2673	-3.6967	-129.8043	34.0328	-3.7091	-150.5657
3	7	-14.0356	0.2685	29.3679	-8.5796	0.2254	34.0834
4	0	2.1811	2.9242	-2.4852	2.4415	2.0675	-0.8476
4	1	-30.1790	-31.4665	21.5934	-28.8904	-26.6633	12.0498
4	2	83.9541	69.5846	-69.8087	78.2833	60.1422	-48.6970
4	3	-97.4992	-59.4487	122.1667	-98.0390	-51.2202	100.8910
4	4	53.8693	17.5135	-106.6935	63.3478	14.2954	-99.1808
4	5	-16.1541	-0.7004	45.2314	-21.3253	-0.2549	46.3177
4	6	2.6474	0.2489	-7.5769	2.8610	0.2504	-8.5587
5	0	-0.5302	-0.7727	0.5210	-0.4879	-0.5557	0.1679
5	1	7.2113	8.3178	-4.1694	6.0295	7.2121	-2.3428
5	2	-18.4811	-18.7640	8.8584	-14.2862	-16.7230	5.0588
5	3	17.3556	16.1490	-9.4411	13.5196	14.4992	-5.3795
5	4	-5.5009	-4.6637	4.0882	-5.2431	-4.0893	1.9753
5	5	0.1684	0.0151	-0.4525	0.7291	-0.0476	0.0299
6	0	0.0624	0.0789	-0.0729	0.0486	0.0572	-0.0462
6	1	-0.8121	-0.8612	0.6300	-0.6168	-0.7624	0.5411
6	2	2.0704	1.9638	-1.3429	1.3923	1.7990	-1.2540
6	3	-1.8976	-1.6912	1.2427	-1.1386	-1.5767	1.2219
6	4	0.5595	0.4850	-0.3990	0.2931	0.4564	-0.4147

POLYNOMIAL FOR THE PERFORMANCE OF THE AFT AND FRONT UNIT IN REGENERATION AS FUNCTION OF PITCH AND BETA.

FIGURES

SHIP ID	:	C2352A	Draught Fore (Tf)	:	1.924 m
Water depth	:	infinite	Draught Aft (Ta)	:	1.924 m
Thrust coeff	:	-ct-	Dyn. sinkage	:	0.000 m
Scale	:	1	Dyn trim	:	0.00 deg
Turb model	:	K_OMEGA (SST_2003)	Speed	:	12.00 kn

12 KNOTS, MOTORING, FRONT PROPELLER FEATHERED

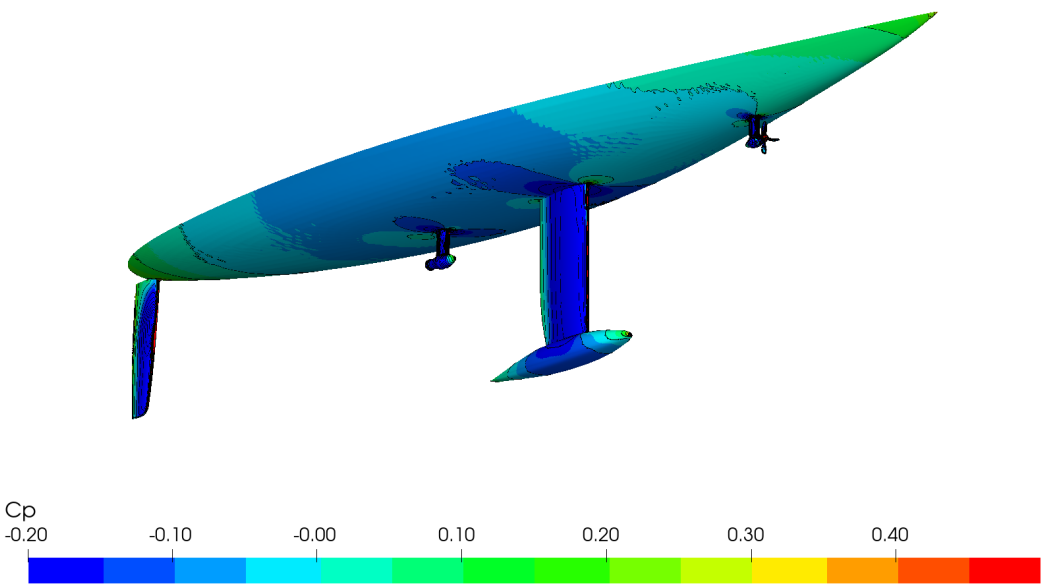

Dynamic pressure coefficient distribution on the hull, oblique underwater view from the bow

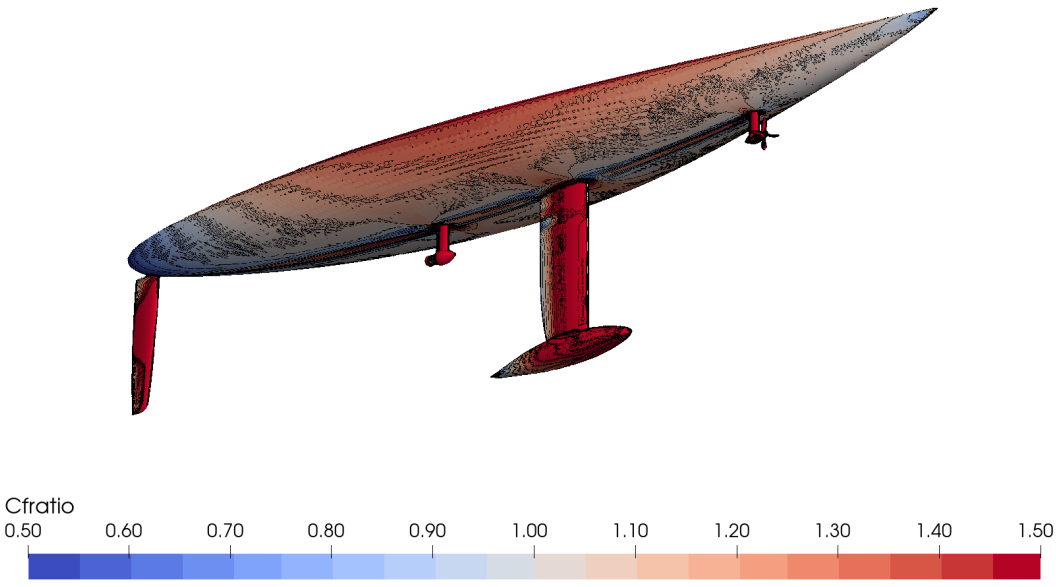

Local skin friction to flat plate friction ratio, oblique underwater view from the bow

SHIP ID	:	C2352A	Draught Fore (Tf)	:	1.924 m
Water depth	:	infinite	Draught Aft (Ta)	:	1.924 m
Thrust coeff	:	-ct-	Dyn. sinkage	:	0.000 m
Scale	:	1	Dyn trim	:	0.00 deg
Turb model	:	K_OMEGA (SST_2003)	Speed	:	12.00 kn

12 KNOTS, MOTORING, FRONT PROPELLER FEATHERED

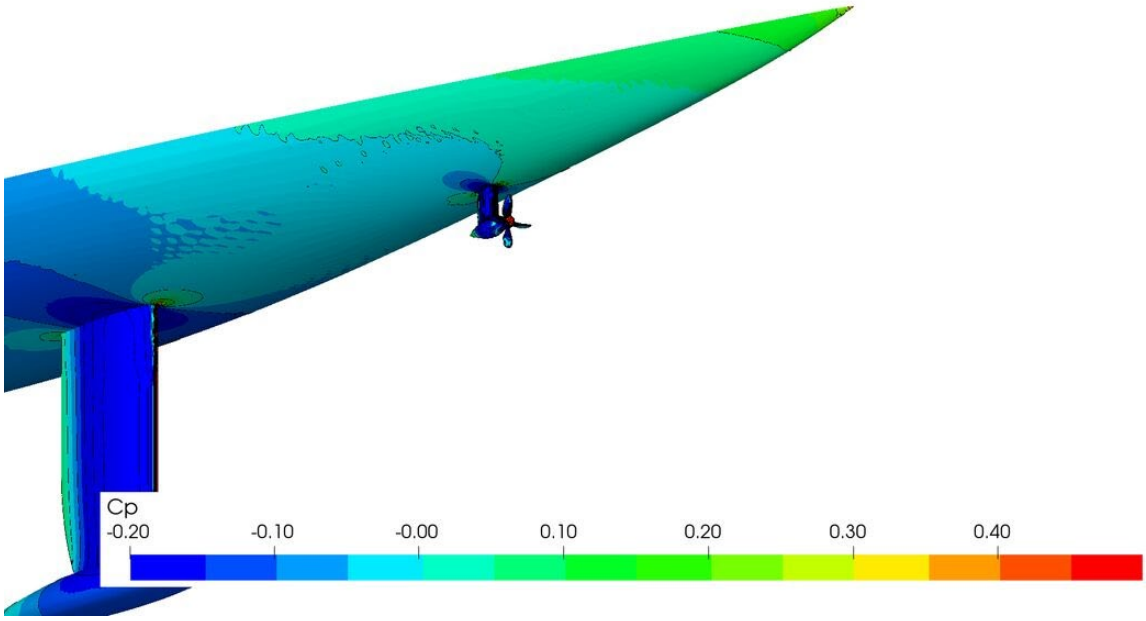

Dynamic pressure coefficient distribution on the hull, oblique underwater view on the bow

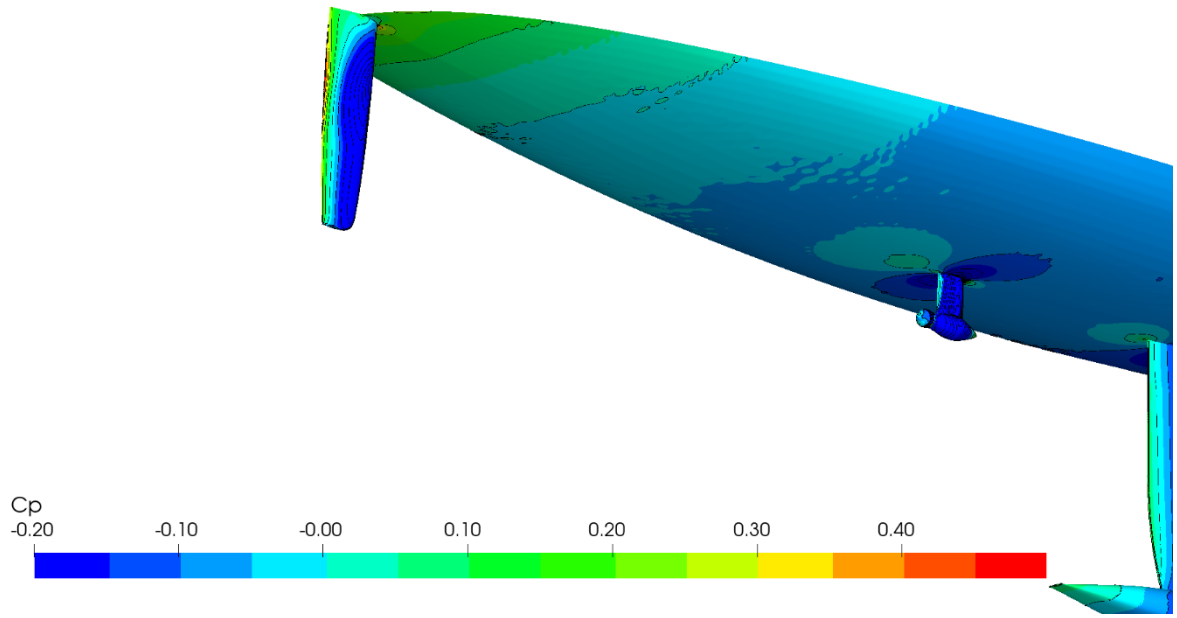

Dynamic pressure coefficient distribution on the hull, oblique underwater view on the stern

SHIP ID	:	C2352A	Draught Fore (Tf)	:	1.924 m
Water depth	:	infinite	Draught Aft (Ta)	:	1.924 m
Thrust coeff	:	-ct-	Dyn. sinkage	:	0.000 m
Scale	:	1	Dyn trim	:	0.00 deg
Turb model	:	K_OMEGA (SST_2003)	Speed	:	12.00 kn

12 KNOTS, MOTORING, FRONT PROPELLER FEATHERED

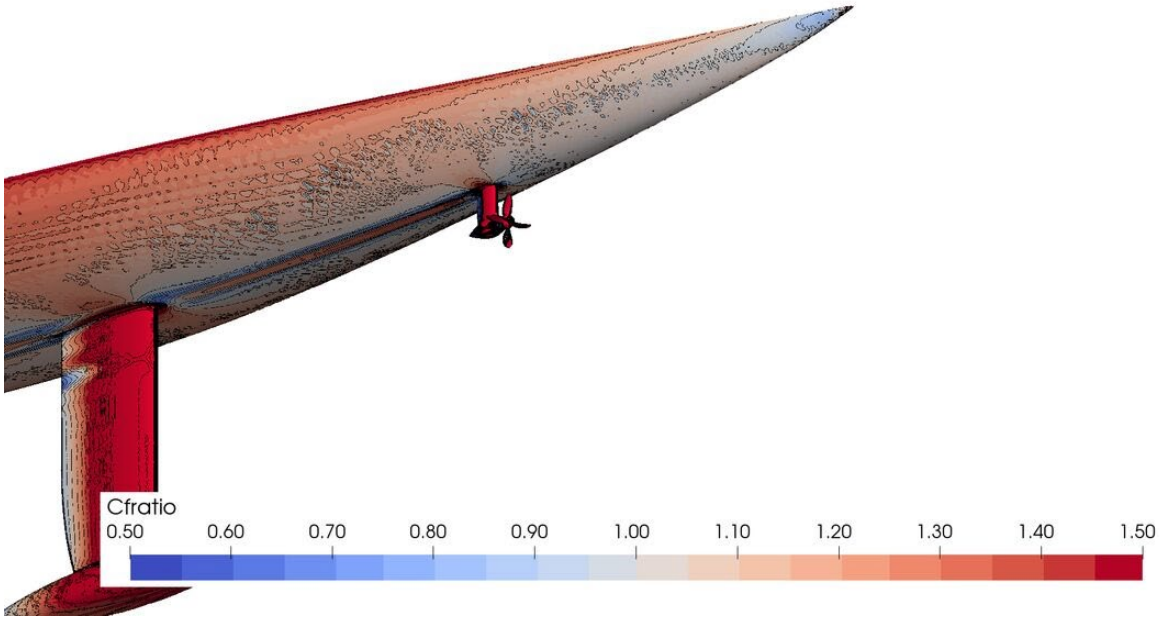

Local skin friction to flat plate friction ratio, oblique underwater view on the bow

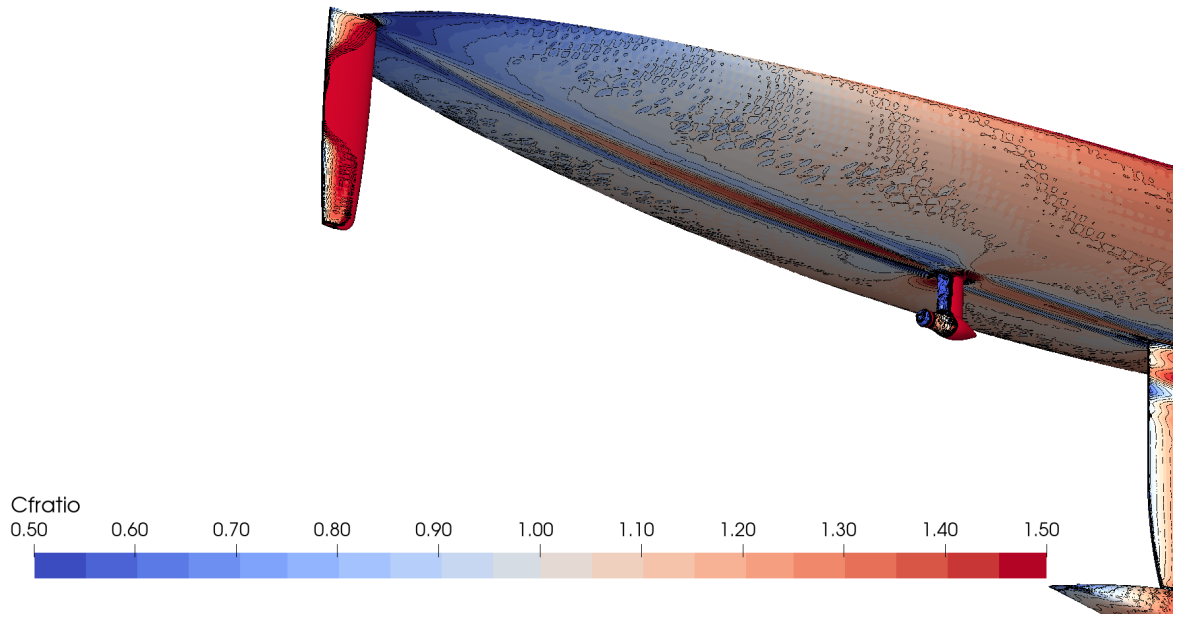

Local skin friction to flat plate friction ratio, oblique underwater view on the stern

SHIP ID	:	C2352A	Draught Fore (Tf)	:	1.924 m
Water depth	:	infinite	Draught Aft (Ta)	:	1.924 m
Thrust coeff	:	-ct-	Dyn. sinkage	:	0.000 m
Scale	:	1	Dyn trim	:	0.00 deg
Turb model	:	K_OMEGA (SST_2003)	Speed	:	12.00 kn

12 KNOTS, MOTORING, FRONT PROPELLER FEATHERED

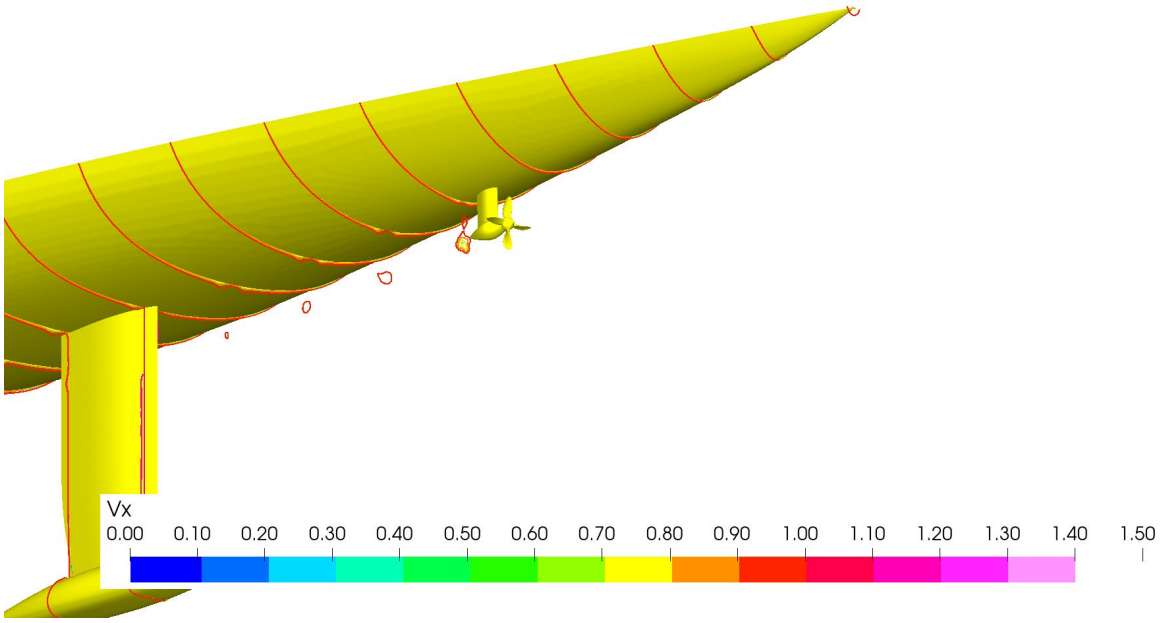

Slices of axial velocity, oblique underwater view on the bow

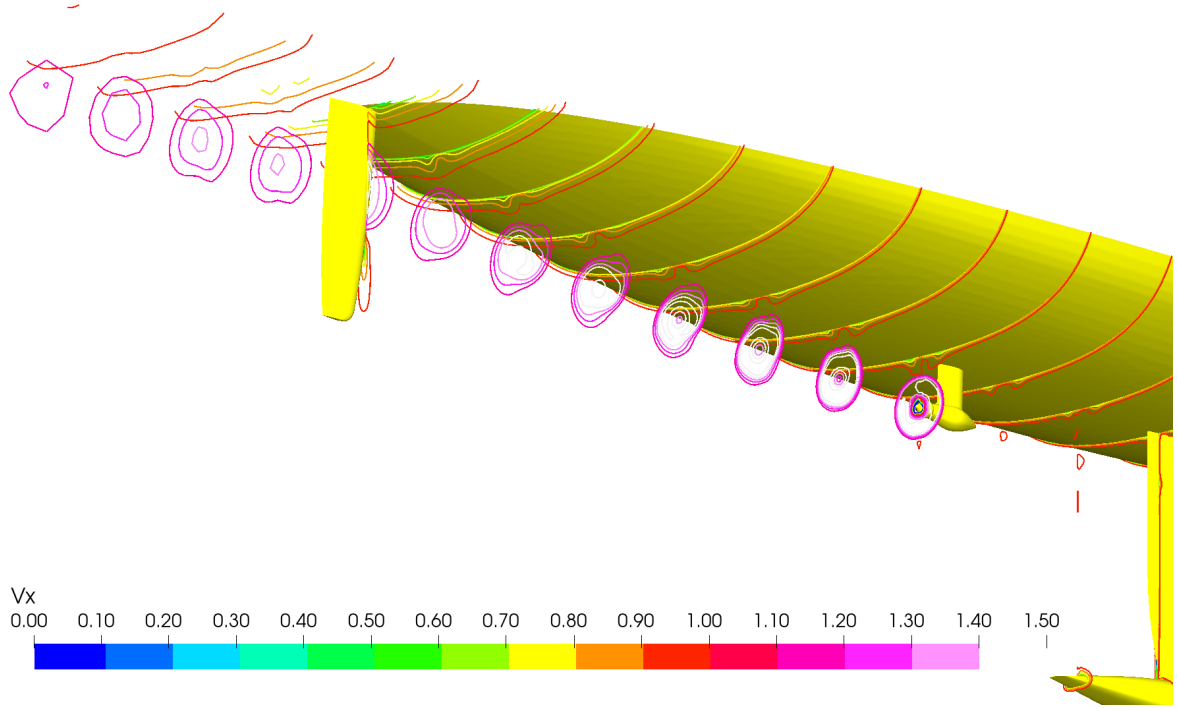

Slices of axial velocity, oblique underwater view on the stern

SHIP ID	:	C2352A	Draught Fore (Tf)	:	1.924 m
Water depth	:	infinite	Draught Aft (Ta)	:	1.924 m
Thrust coeff	:	-ct-	Dyn. sinkage	:	0.000 m
Scale	:	1	Dyn trim	:	0.00 deg
Turb model	:	K_OMEGA (SST_2003)	Speed	:	12.00 kn

12 KNOTS, MOTORING, FRONT PROPELLER FEATHERED

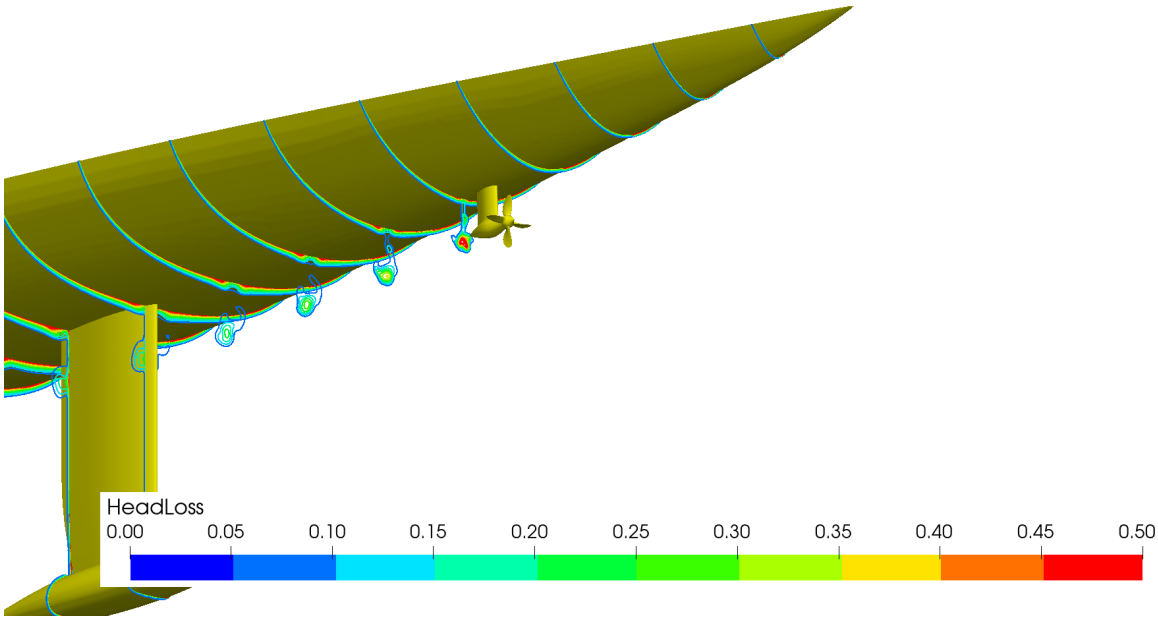

Slices of head loss, oblique underwater view on the bow

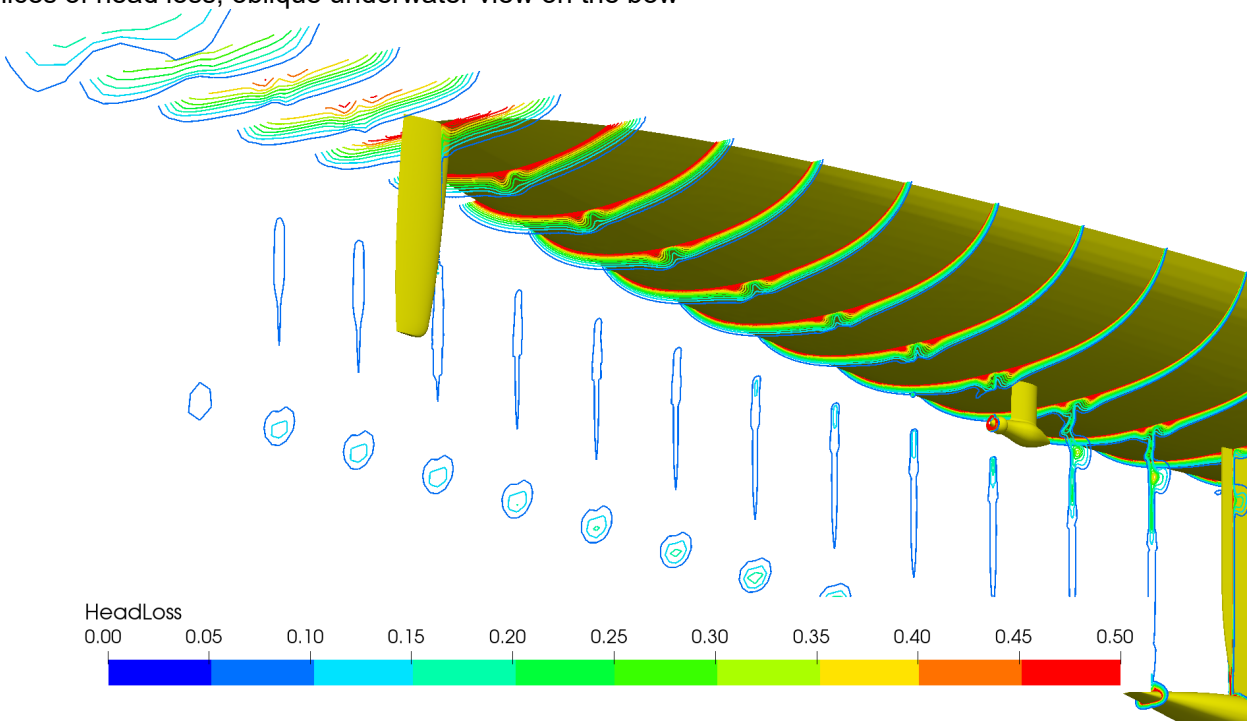

Slices of head loss, oblique underwater view on the stern

SHIP ID	:	C2352A	Draught Fore (Tf)	:	1.924 m
Water depth	:	infinite	Draught Aft (Ta)	:	1.924 m
Thrust coeff	:	-ct-	Dyn. sinkage	:	0.000 m
Scale	:	1	Dyn trim	:	0.00 deg
Turb model	:	K_OMEGA (SST_2003)	Speed	:	12.00 kn

12 KNOTS, MOTORING, FRONT PROPELLER FEATHERED

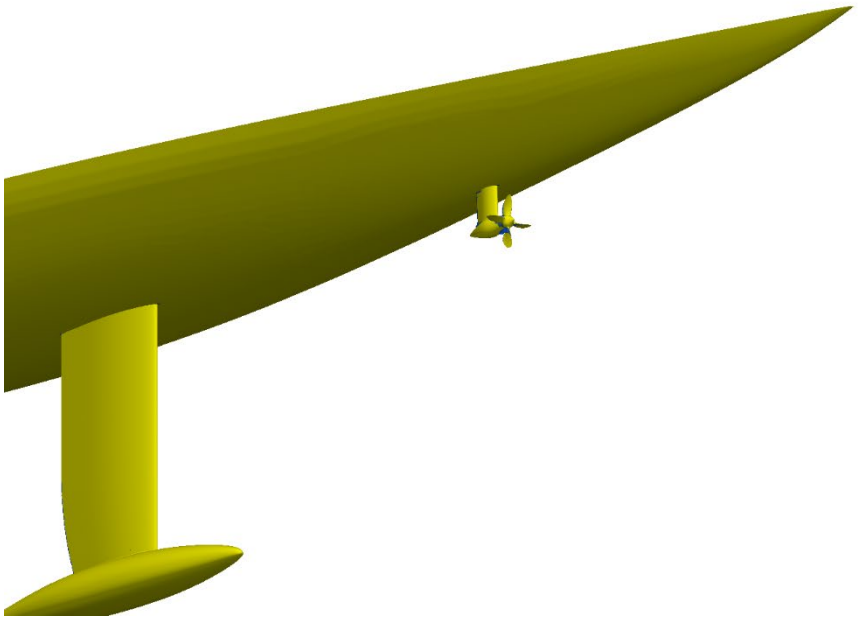

Reversed flow regions, oblique underwater view on the bow

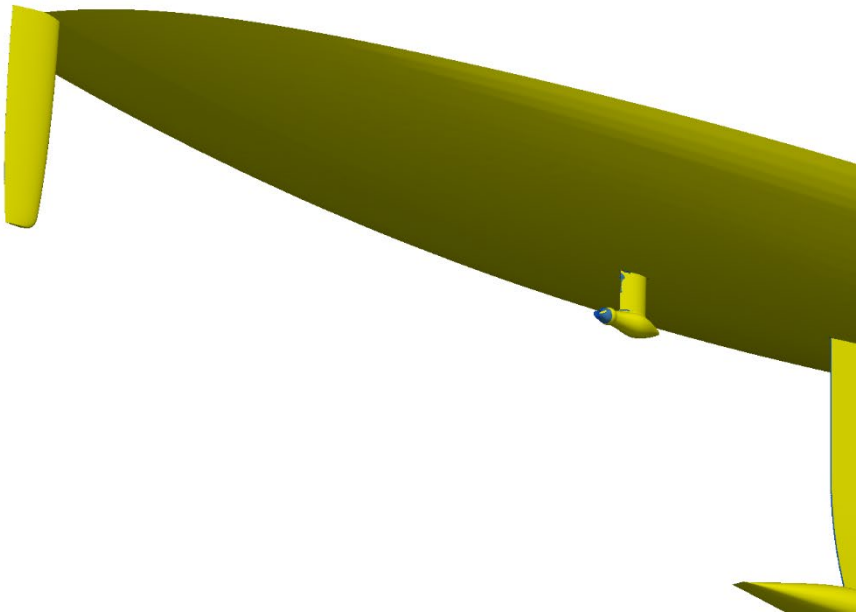

Reversed flow regions, oblique underwater view on the stern

SHIP ID	:	C2352A	Draught Fore (Tf)	:	1.924 m
Water depth	:	infinite	Draught Aft (Ta)	:	1.924 m
Thrust coeff	:	-ct-	Dyn. sinkage	:	0.000 m
Scale	:	1	Dyn trim	:	0.00 deg
Turb model	:	K_OMEGA (SST_2003)	Speed	:	12.00 kn

12 KNOTS, MOTORING, FRONT PROPELLER FEATHERED

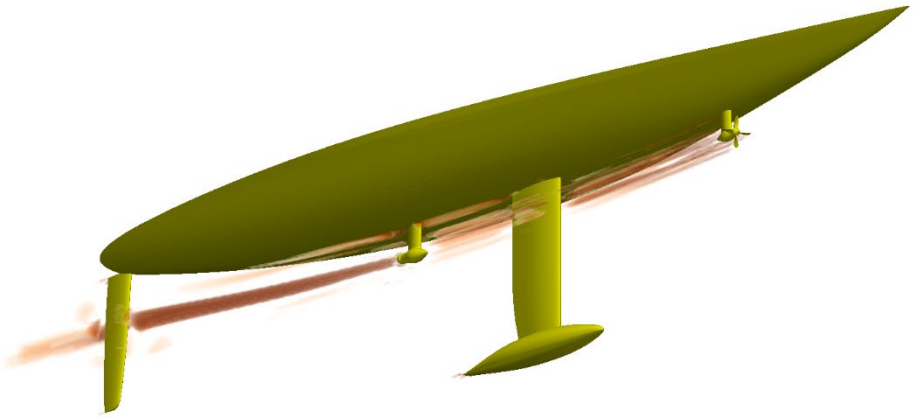

Vortices, oblique underwater view on the bow

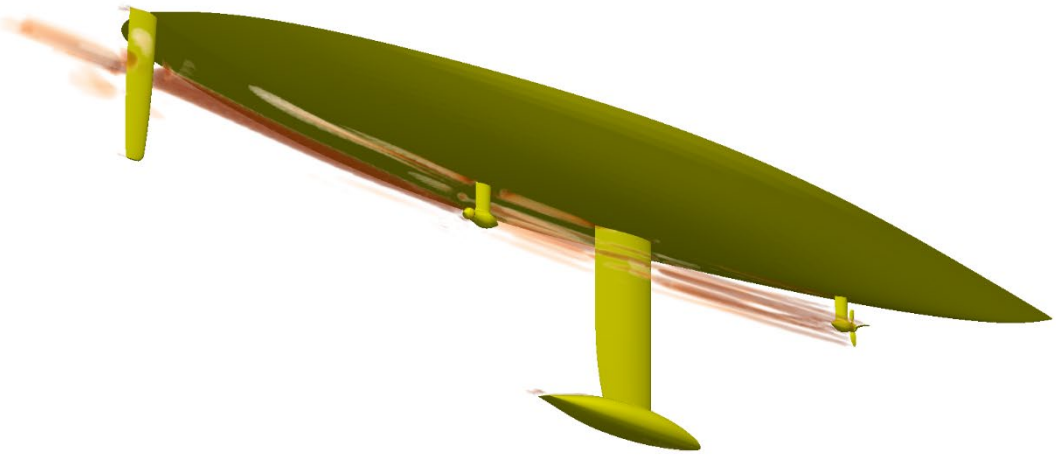

Vortices, oblique underwater view on the stern

SHIP ID	:	C2352A	Draught Fore (Tf)	:	1.924 m
Water depth	:	infinite	Draught Aft (Ta)	:	1.924 m
Thrust coeff	:	-ct-	Dyn. sinkage	:	0.000 m
Scale	:	1	Dyn trim	:	0.00 deg
Turb model	:	K_OMEGA (SST_2003)	Speed	:	12.00 kn

12 KNOTS, MOTORING, FRONT PROPELLER FEATHERED

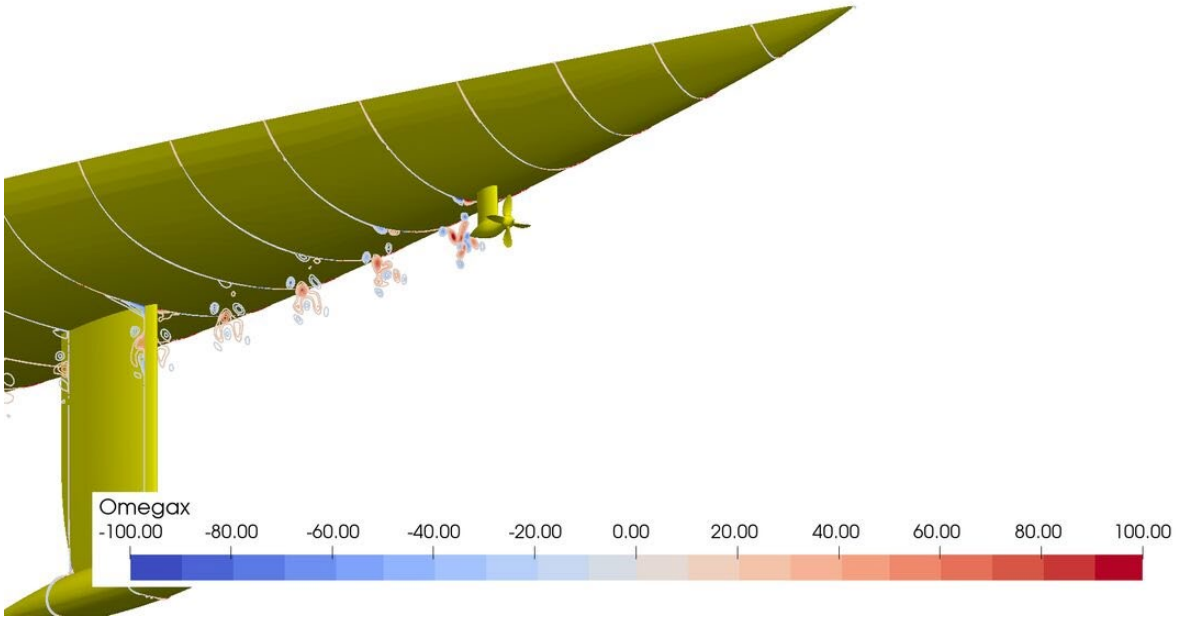

Slices of axial vorticity, oblique underwater view on the bow

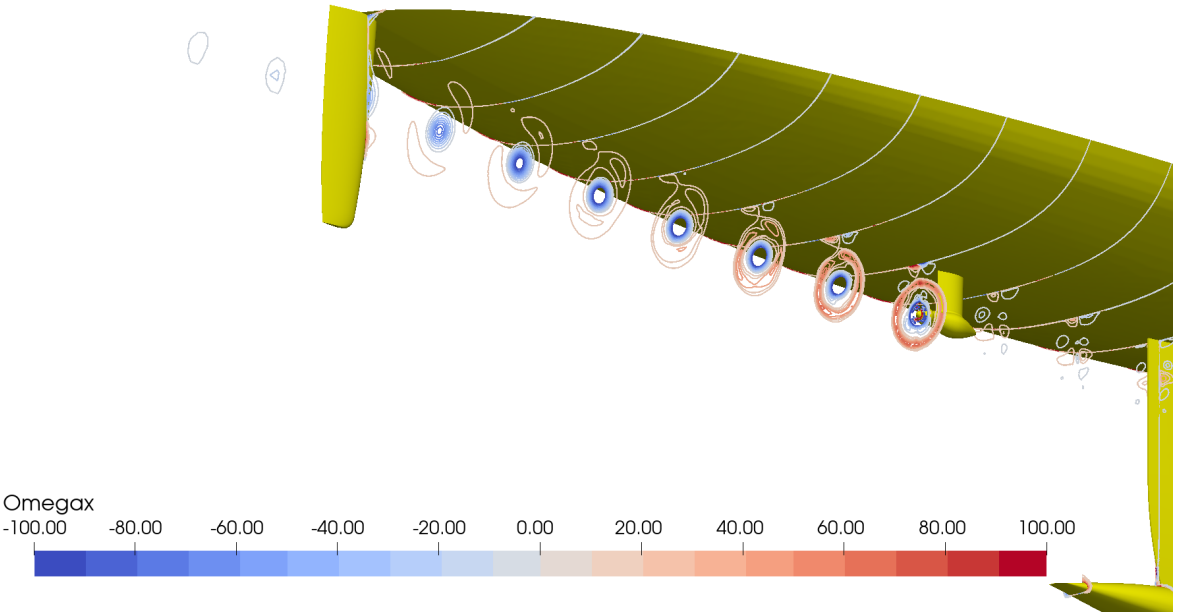

Slices of axial vorticity, oblique underwater view on the stern

SHIP ID	:	C2352	Draught Fore (Tf)	:	1.924 m
Water depth	:	infinite	Draught Aft (Ta)	:	1.924 m
Thrust coeff	:	-ct-	Dyn. sinkage	:	0.000 m
Scale	:	1	Dyn trim	:	0.00 deg
Turb model	:	K_OMEGA (SST_2003)	Speed	:	16.00 kn

16 KNOTS, REGENERATING WITH BOTH PROPELLERS

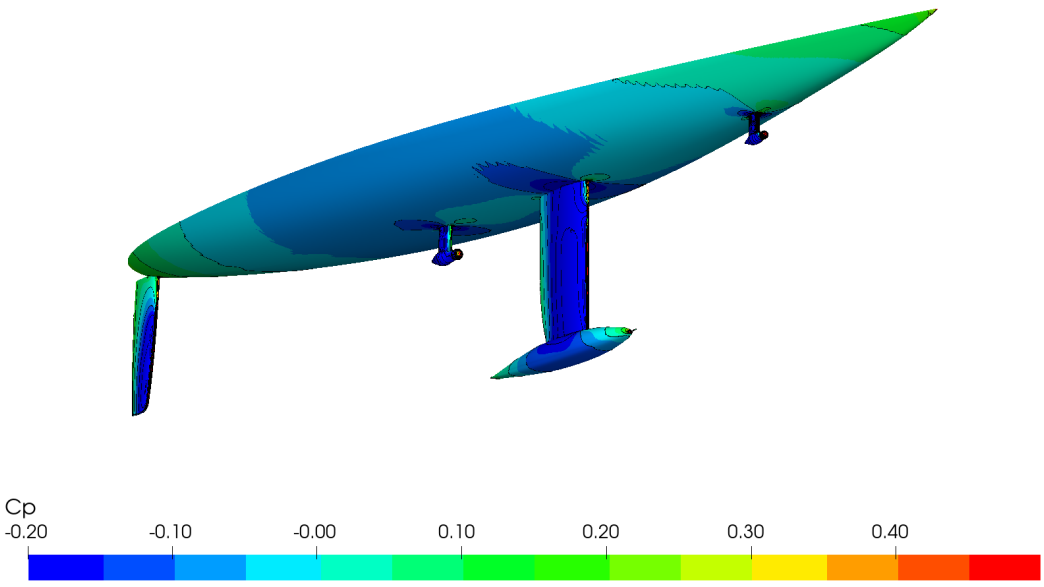

Dynamic pressure coefficient distribution on the hull, oblique underwater view from the bow

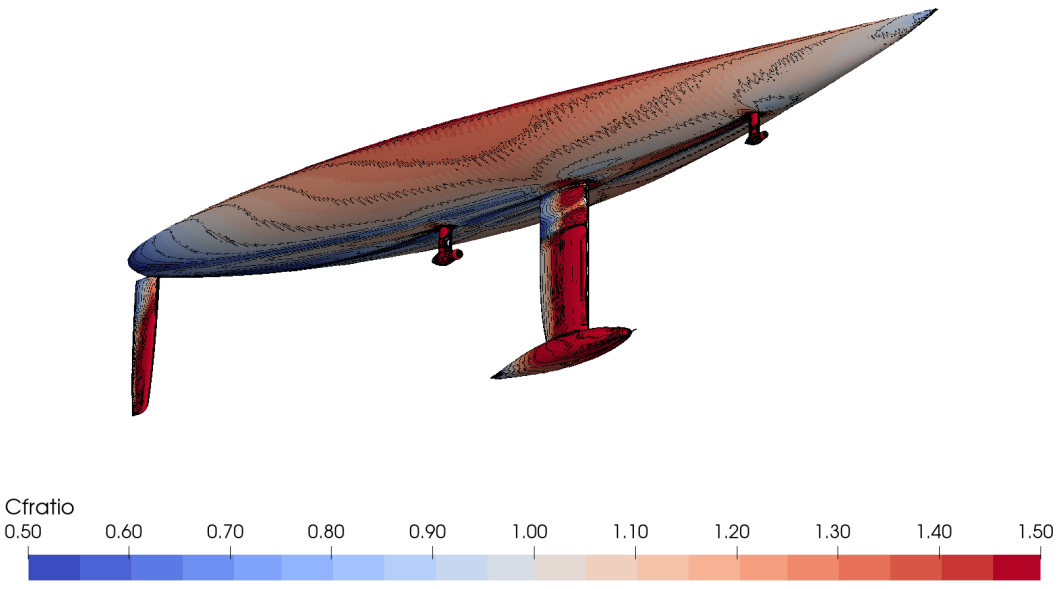

Local skin friction to flat plate friction ratio, oblique underwater view from the bow

SHIP ID	:	C2352	Draught Fore (Tf)	:	1.924 m
Water depth	:	infinite	Draught Aft (Ta)	:	1.924 m
Thrust coeff	:	-ct-	Dyn. sinkage	:	0.000 m
Scale	:	1	Dyn trim	:	0.00 deg
Turb model	:	K_OMEGA (SST_2003)	Speed	:	16.00 kn

16 KNOTS, REGENERATING WITH BOTH PROPELLERS

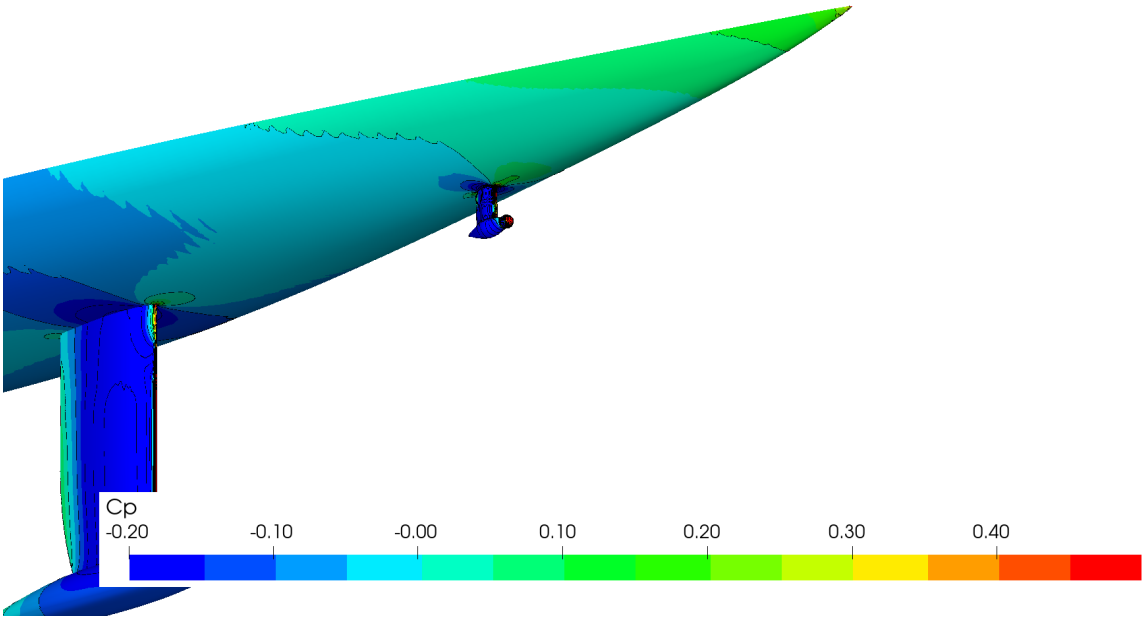

Dynamic pressure coefficient distribution on the hull, oblique underwater view on the bow

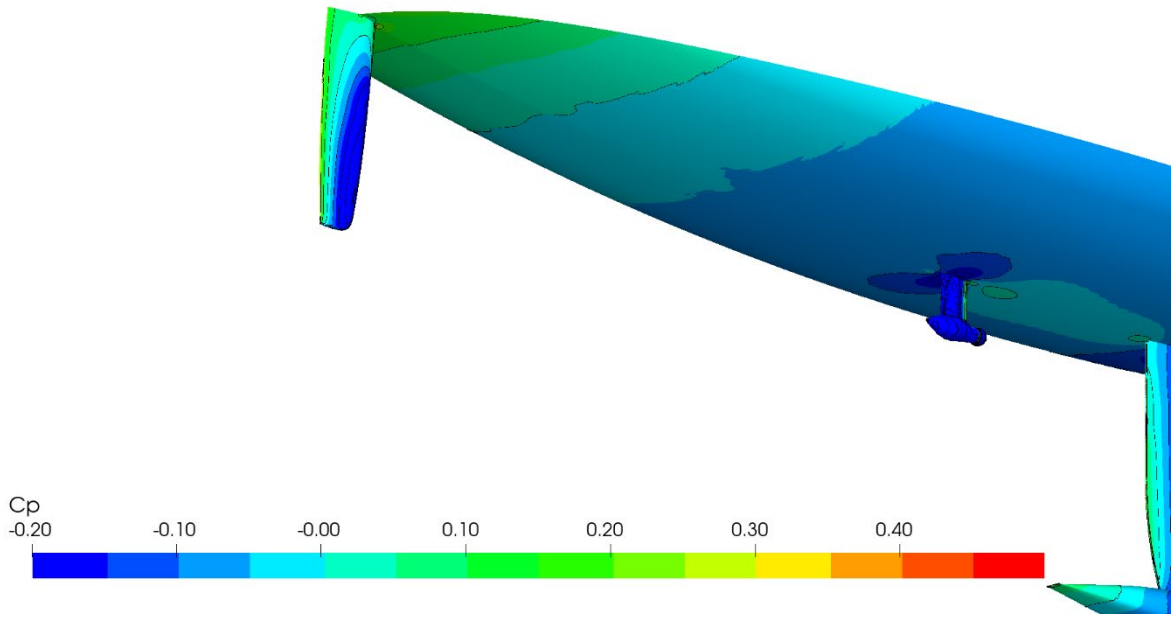

Dynamic pressure coefficient distribution on the hull, oblique underwater view on the stern

SHIP ID	:	C2352	Draught Fore (Tf)	:	1.924 m
Water depth	:	infinite	Draught Aft (Ta)	:	1.924 m
Thrust coeff	:	-ct-	Dyn. sinkage	:	0.000 m
Scale	:	1	Dyn trim	:	0.00 deg
Turb model	:	K_OMEGA (SST_2003)	Speed	:	16.00 kn

16 KNOTS, REGENERATING WITH BOTH PROPELLERS

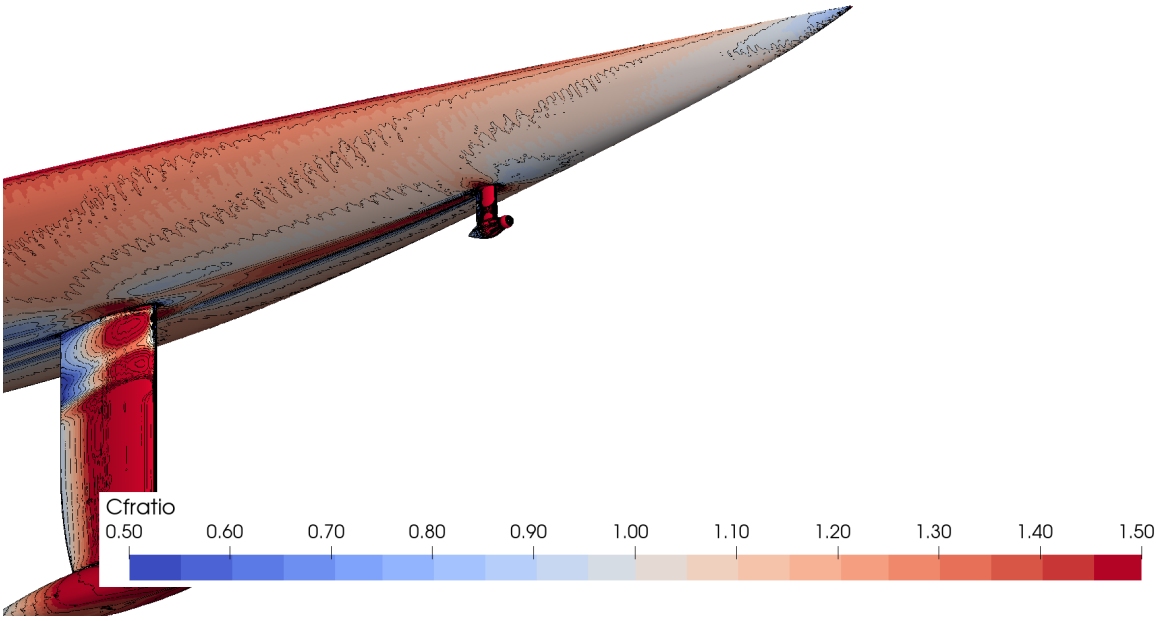

Local skin friction to flat plate friction ratio, oblique underwater view on the bow

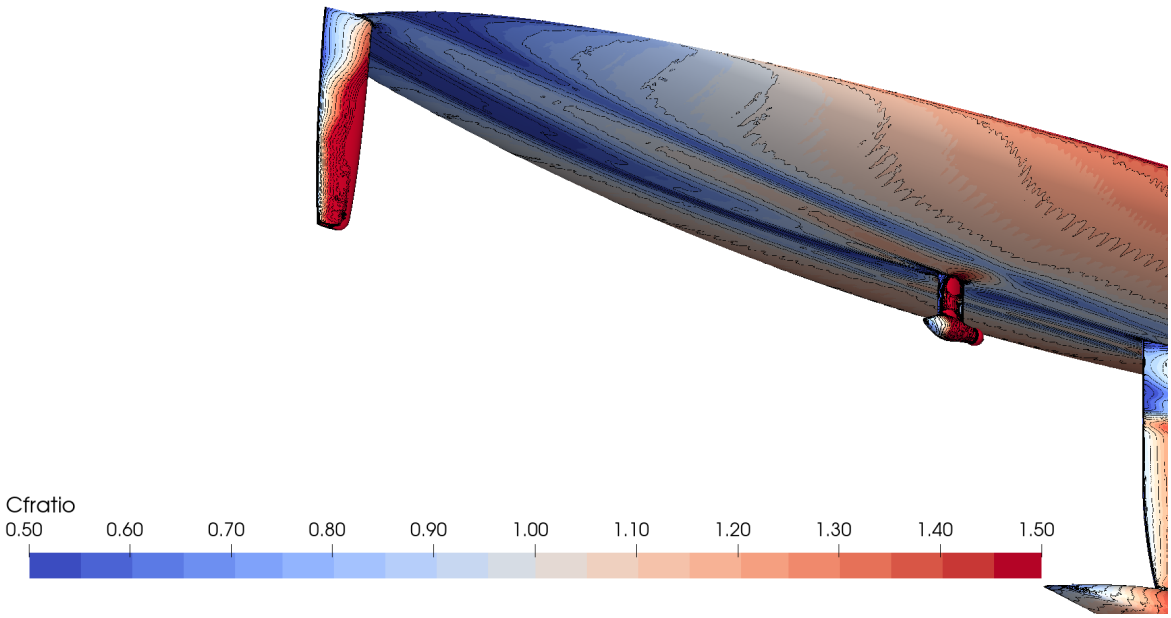

Local skin friction to flat plate friction ratio, oblique underwater view on the stern

SHIP ID	:	C2352	Draught Fore (Tf)	:	1.924 m
Water depth	:	infinite	Draught Aft (Ta)	:	1.924 m
Thrust coeff	:	-ct-	Dyn. sinkage	:	0.000 m
Scale	:	1	Dyn trim	:	0.00 deg
Turb model	:	K_OMEGA (SST_2003)	Speed	:	16.00 kn

16 KNOTS, REGENERATING WITH BOTH PROPELLERS

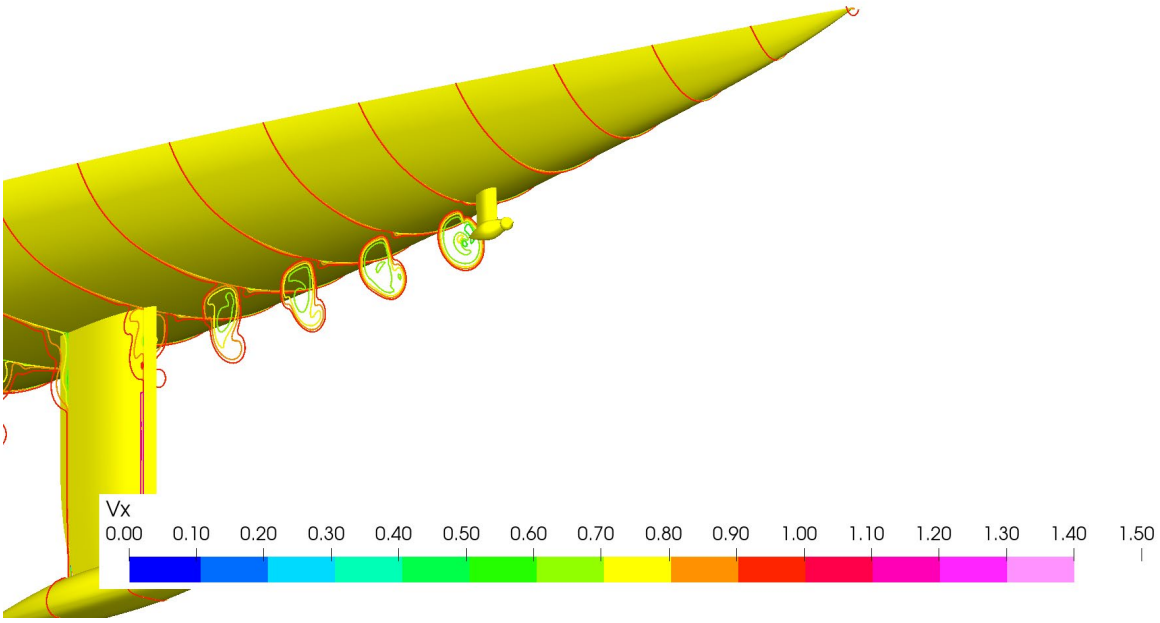

Slices of axial velocity, oblique underwater view on the bow

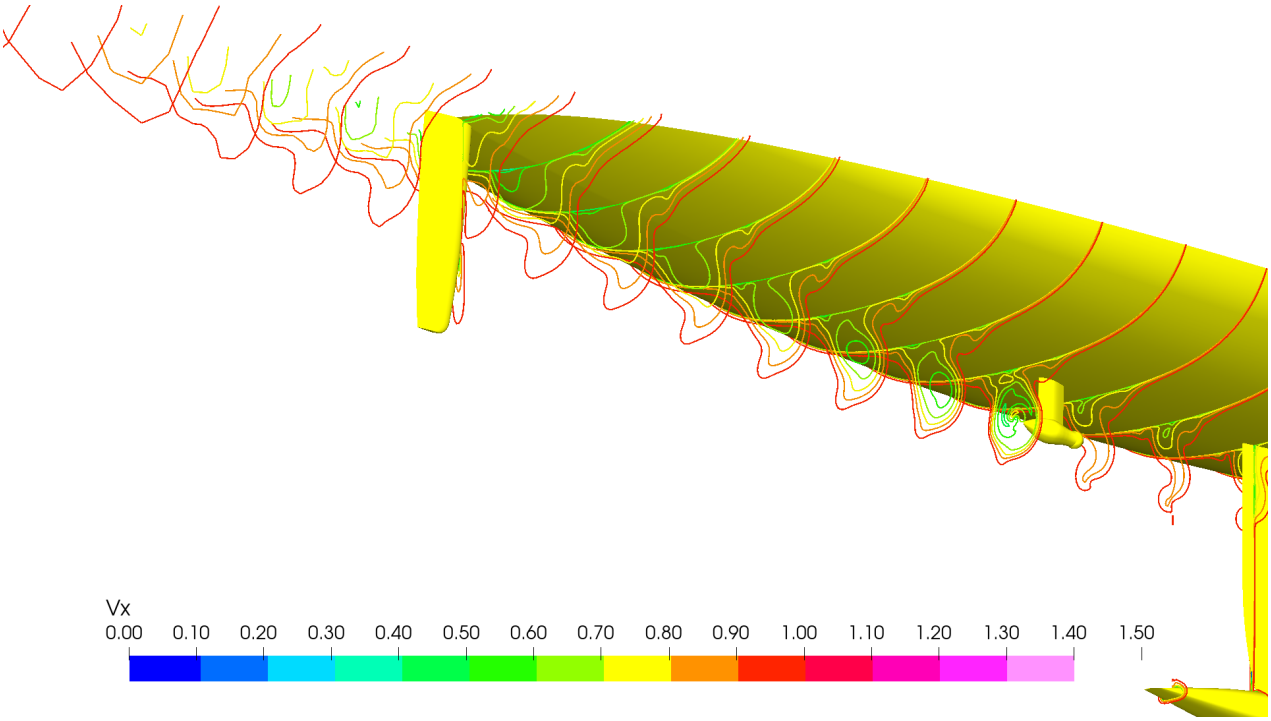

Slices of axial velocity, oblique underwater view on the stern

SHIP ID	:	C2352	Draught Fore (Tf)	:	1.924 m
Water depth	:	infinite	Draught Aft (Ta)	:	1.924 m
Thrust coeff	:	-ct-	Dyn. sinkage	:	0.000 m
Scale	:	1	Dyn trim	:	0.00 deg
Turb model	:	K_OMEGA (SST_2003)	Speed	:	16.00 kn

16 KNOTS, REGENERATING WITH BOTH PROPELLERS

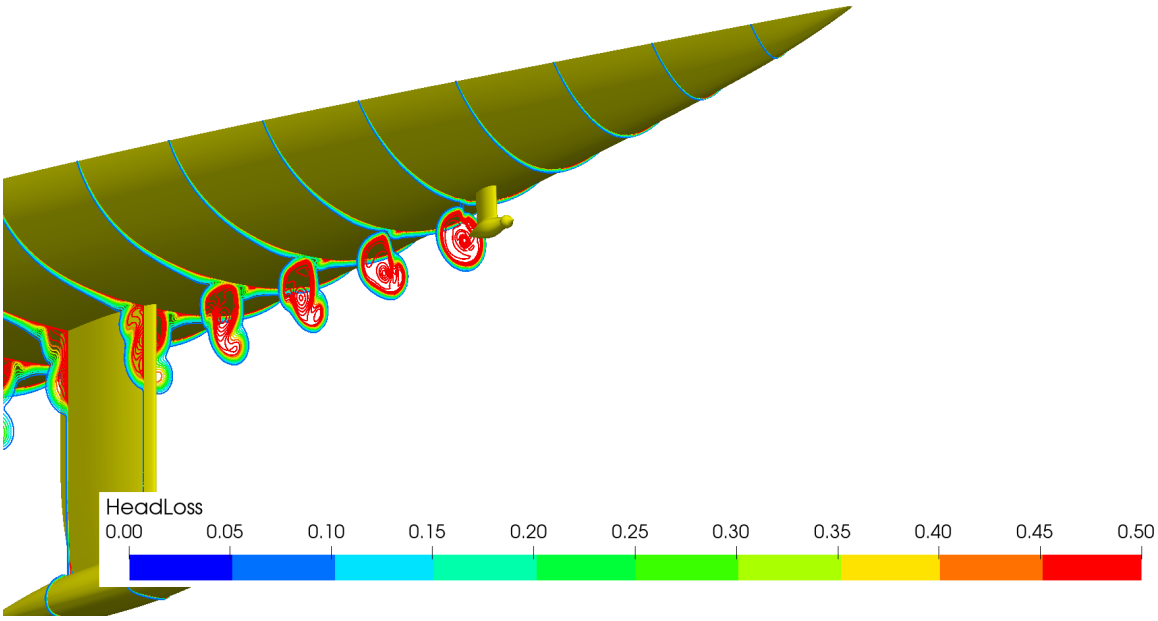

Slices of head loss, oblique underwater view on the bow

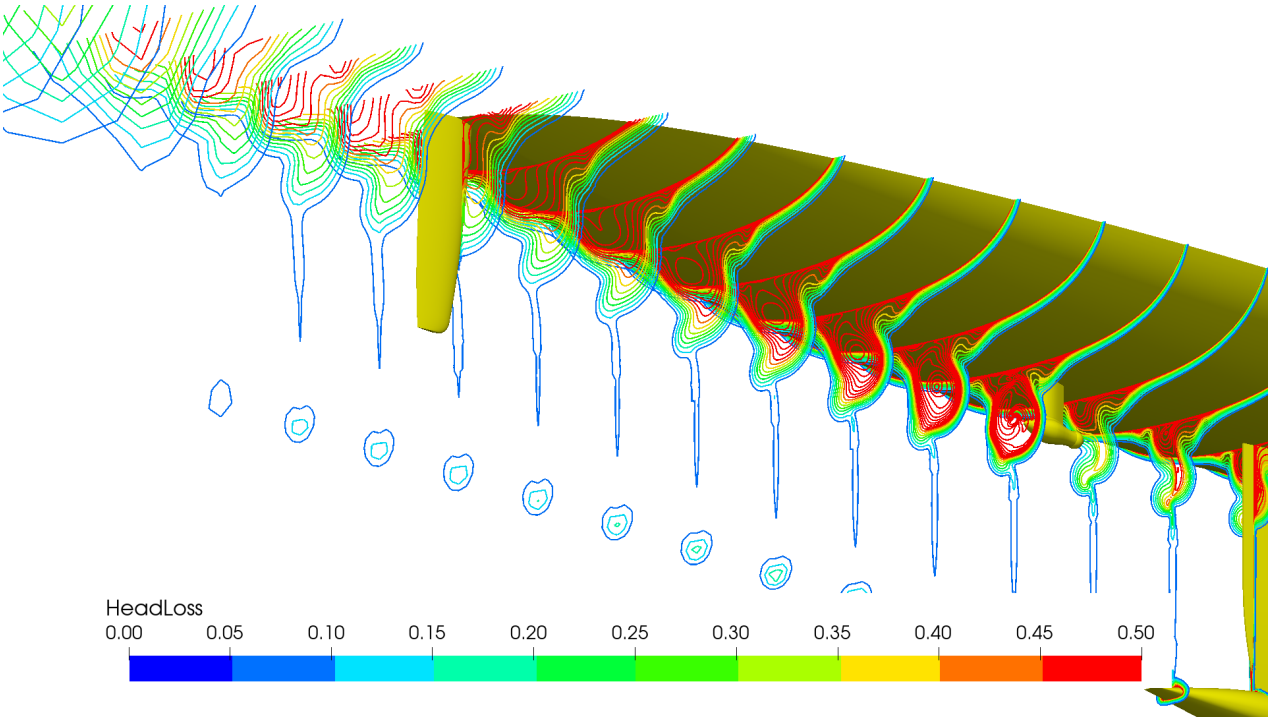

Slices of head loss, oblique underwater view on the stern

SHIP ID	:	C2352	Draught Fore (Tf)	:	1.924 m
Water depth	:	infinite	Draught Aft (Ta)	:	1.924 m
Thrust coeff	:	-ct-	Dyn. sinkage	:	0.000 m
Scale	:	1	Dyn trim	:	0.00 deg
Turb model	:	K_OMEGA (SST_2003)	Speed	:	16.00 kn

16 KNOTS, REGENERATING WITH BOTH PROPELLERS

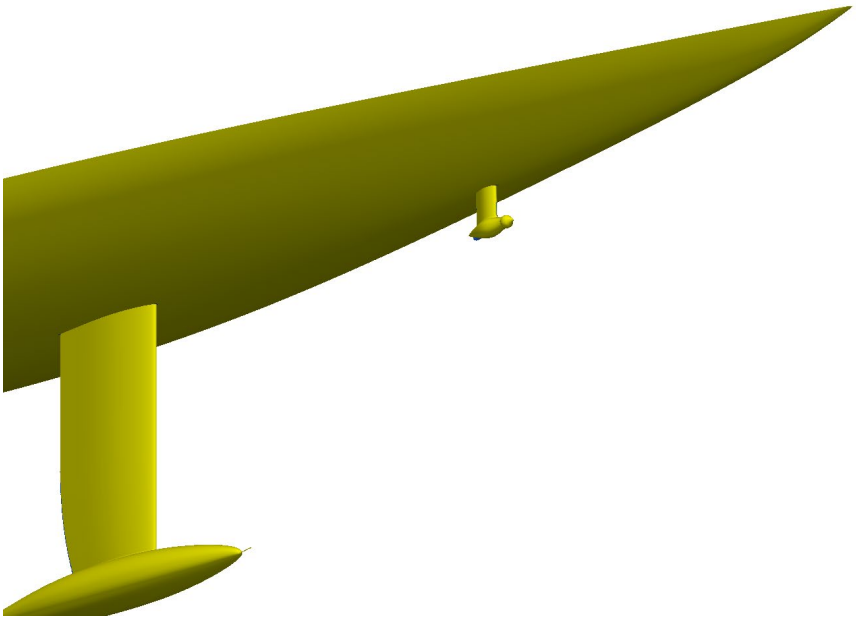

Reversed flow regions, oblique underwater view on the bow

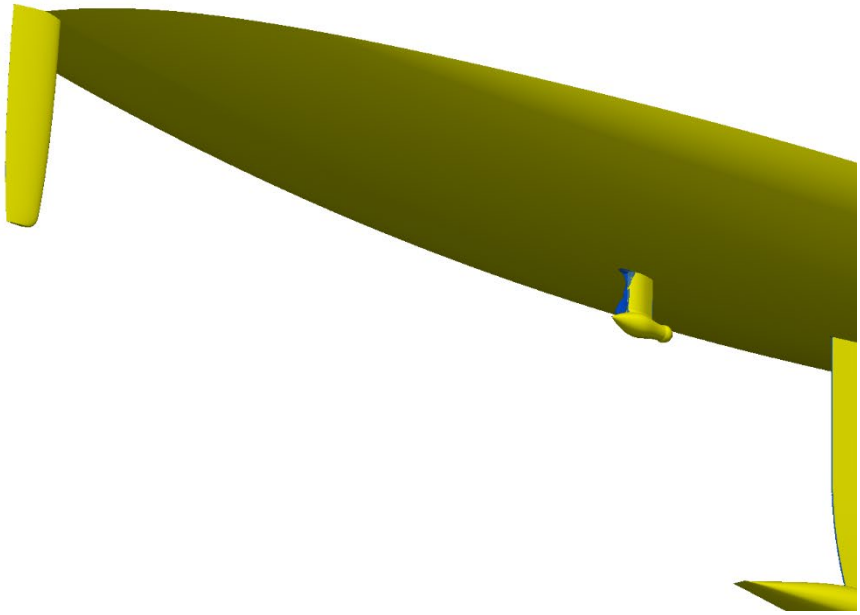

Reversed flow regions, oblique underwater view on the stern

SHIP ID	:	C2352	Draught Fore (Tf)	:	1.924 m
Water depth	:	infinite	Draught Aft (Ta)	:	1.924 m
Thrust coeff	:	-ct-	Dyn. sinkage	:	0.000 m
Scale	:	1	Dyn trim	:	0.00 deg
Turb model	:	K_OMEGA (SST_2003)	Speed	:	16.00 kn

16 KNOTS, REGENERATING WITH BOTH PROPELLERS

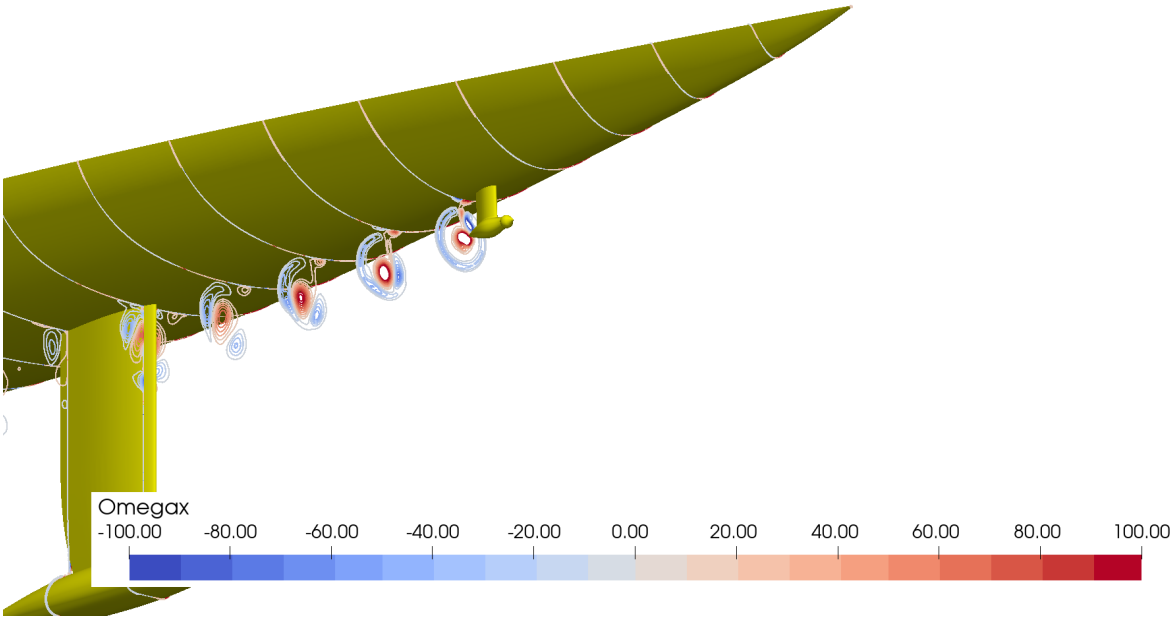

Slices of axial vorticity, oblique underwater view on the bow

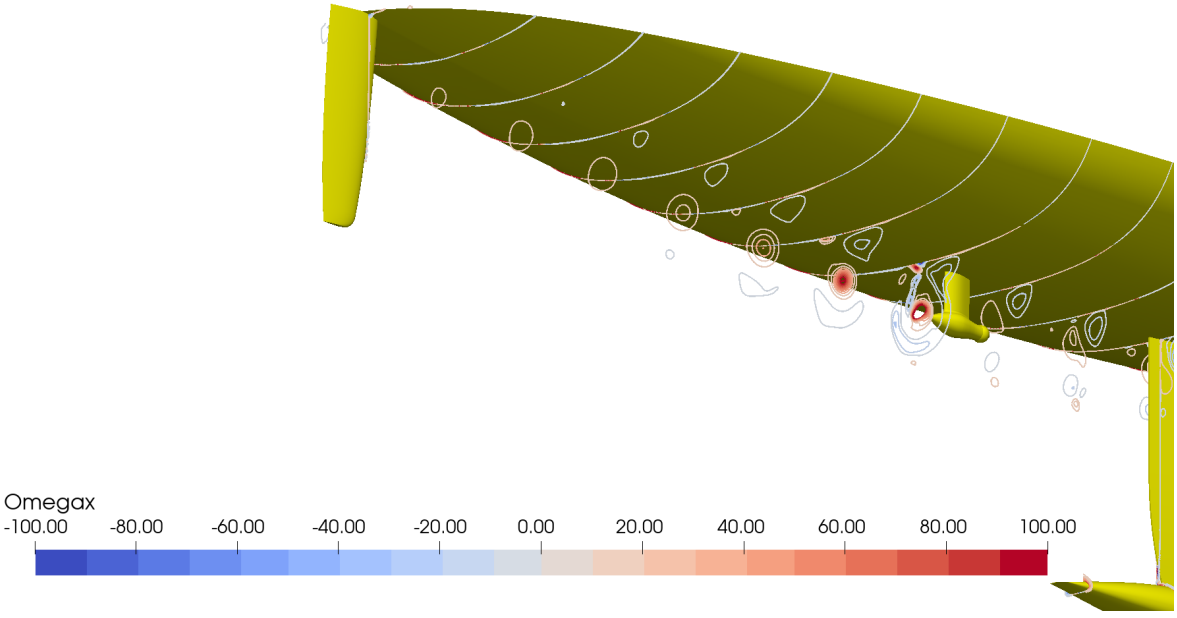

Slices of axial vorticity, oblique underwater view on the stern

PRESSURE CONTOURS ON THE AFT PROPELLER AT 12.00 KNOTS

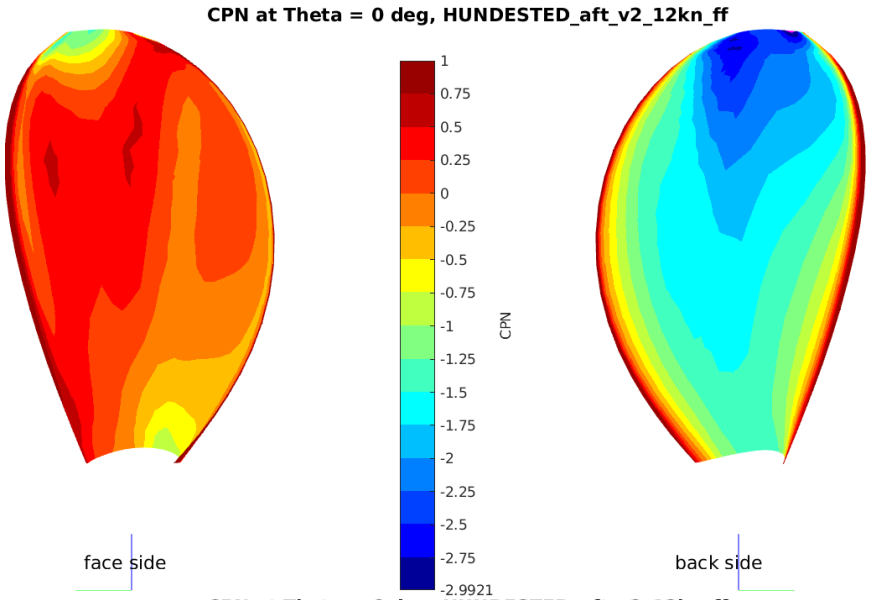

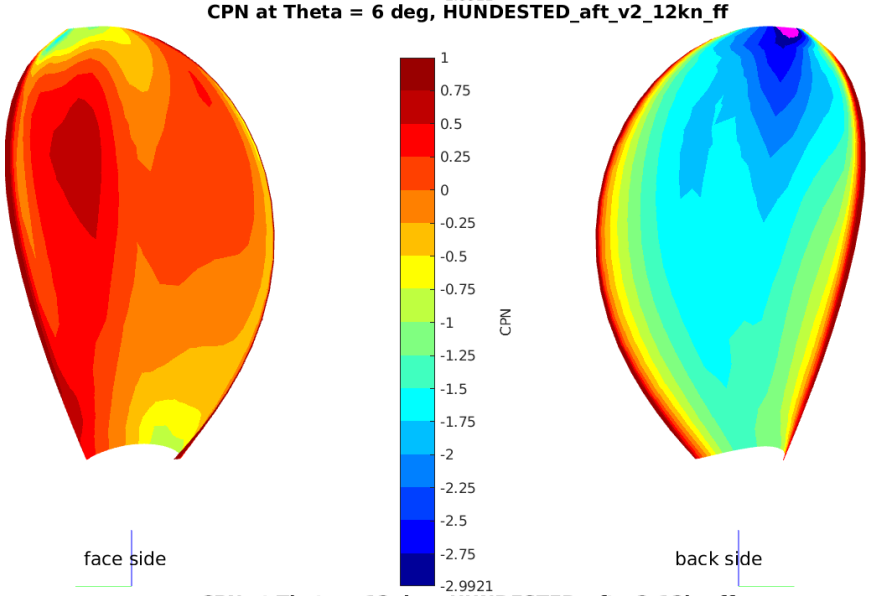

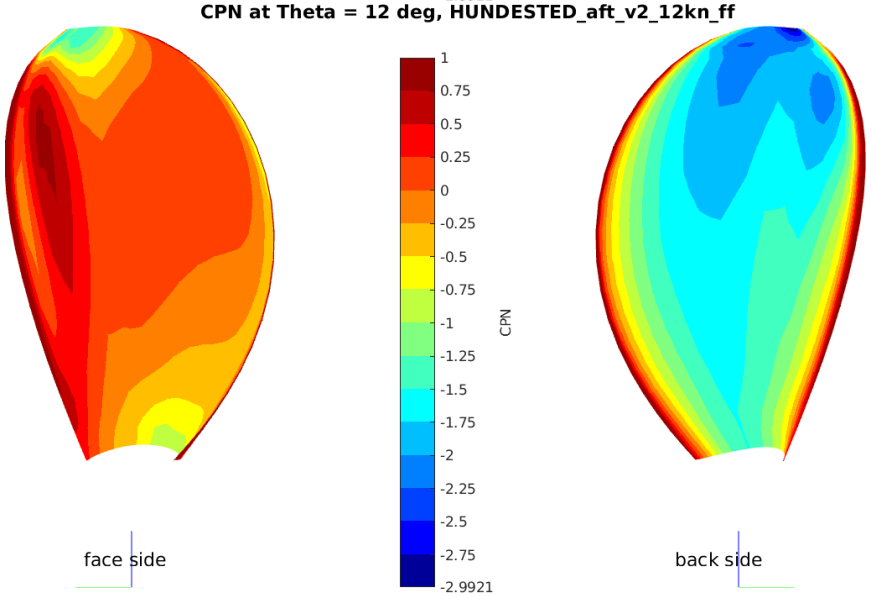

CPN at Theta = 30 deg, HUNDESTED_aft_v2_12kn_ff

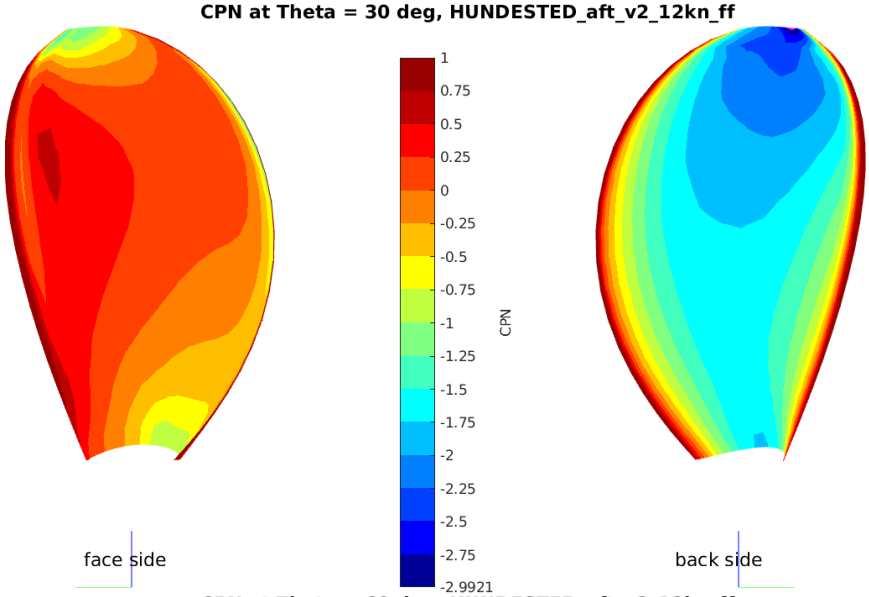

CPN at Theta = 60 deg, HUNDESTED_aft_v2_12kn_ff

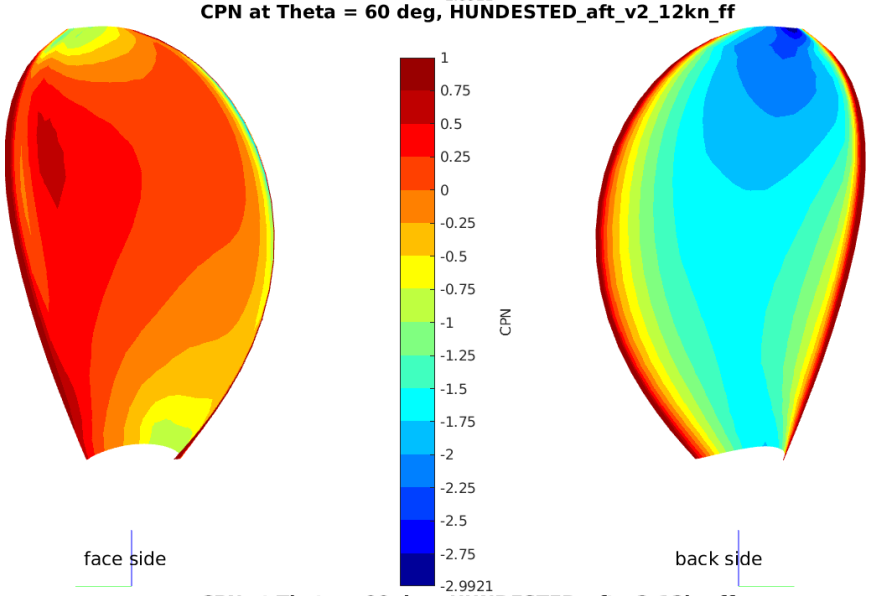

CPN at Theta = 90 deg, HUNDESTED_aft_v2_12kn_ff

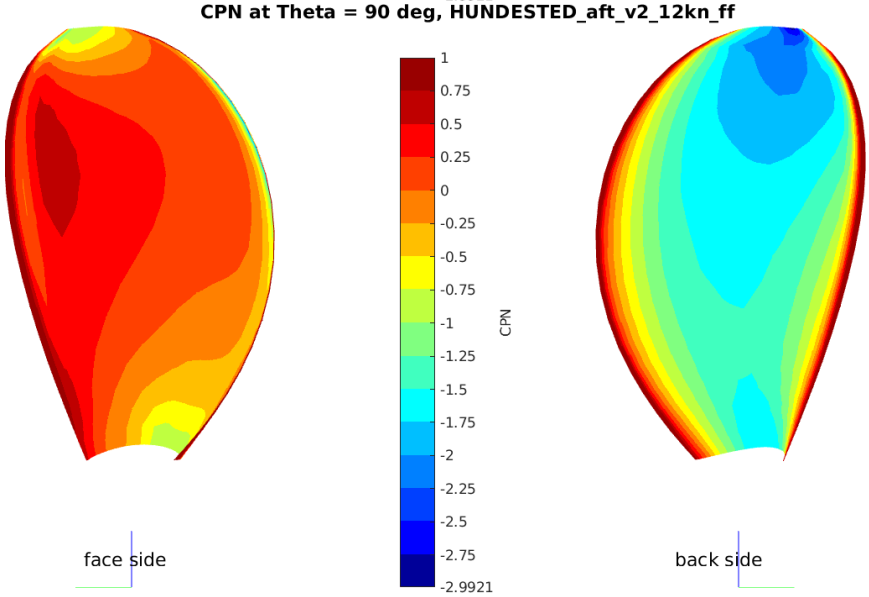

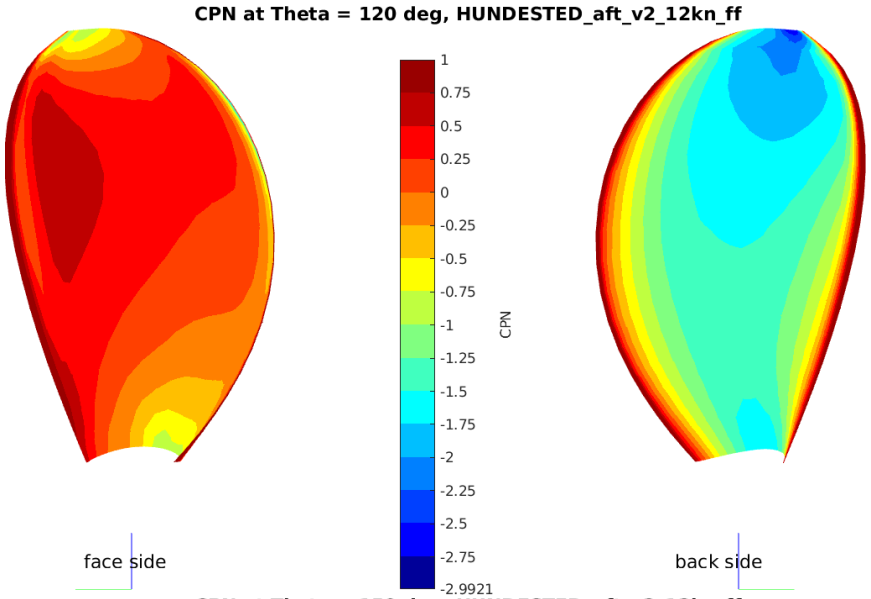
CPN at Theta = 120 deg, HUNDESTED_aft_v2_12kn_ff
1
0.75
0.5
0.25
0
-0.25
-0.5
-0.75
-1
-1.25
-1.5
-1.75
-2
-2.25
-2.5
-2.75
-2.9921
CPN
face side
back side

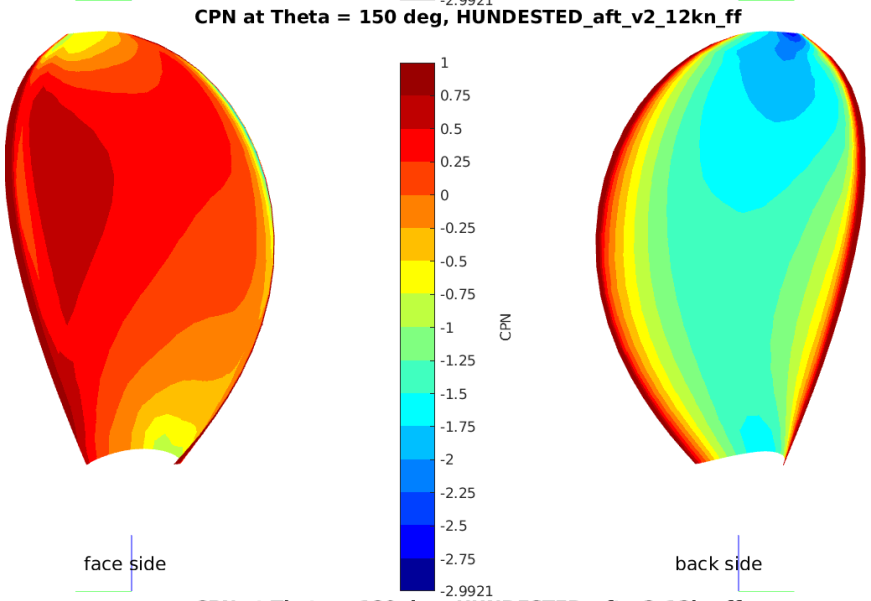
CPN at Theta = 150 deg, HUNDESTED_aft_v2_12kn_ff
1
0.75
0.5
0.25
0
-0.25
-0.5
-0.75
-1
-1.25
-1.5
-1.75
-2
-2.25
-2.5
-2.75
-2.9921
CPN
face side
back side

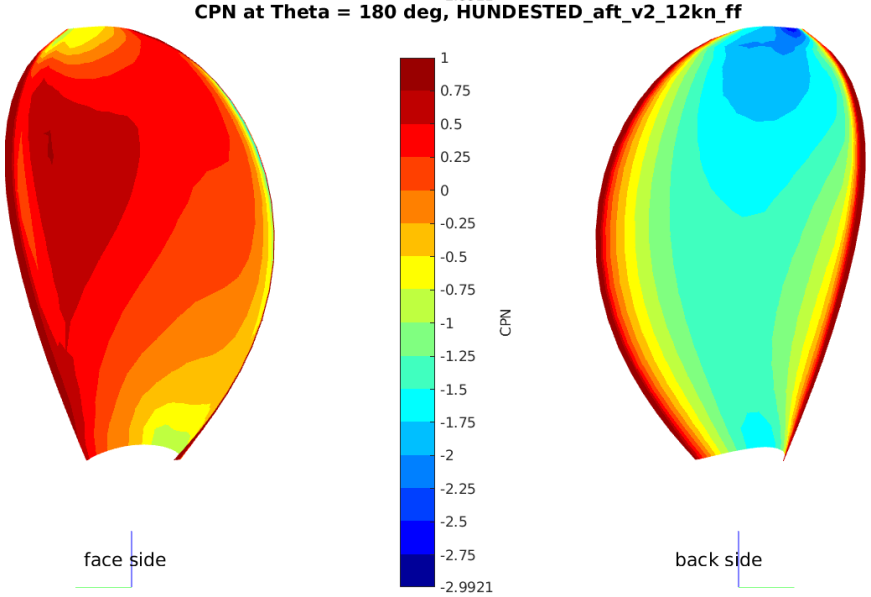
CPN at Theta = 180 deg, HUNDESTED_aft_v2_12kn_ff
1
0.75
0.5
0.25
0
-0.25
-0.5
-0.75
-1
-1.25
-1.5
-1.75
-2
-2.25
-2.5
-2.75
-2.9921
CPN
face side
back side

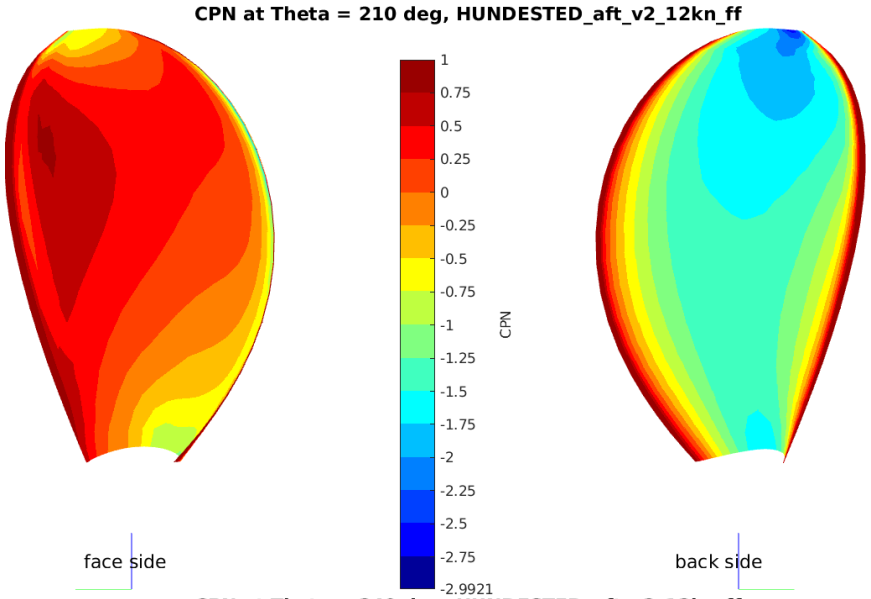
CPN at Theta = 210 deg, HUNDESTED_aft_v2_12kn_ff
1
0.75
0.5
0.25
0
-0.25
-0.5
-0.75
-1
-1.25
-1.5
-1.75
-2
-2.25
-2.5
-2.75
-2.9921
CPN
face side
back side

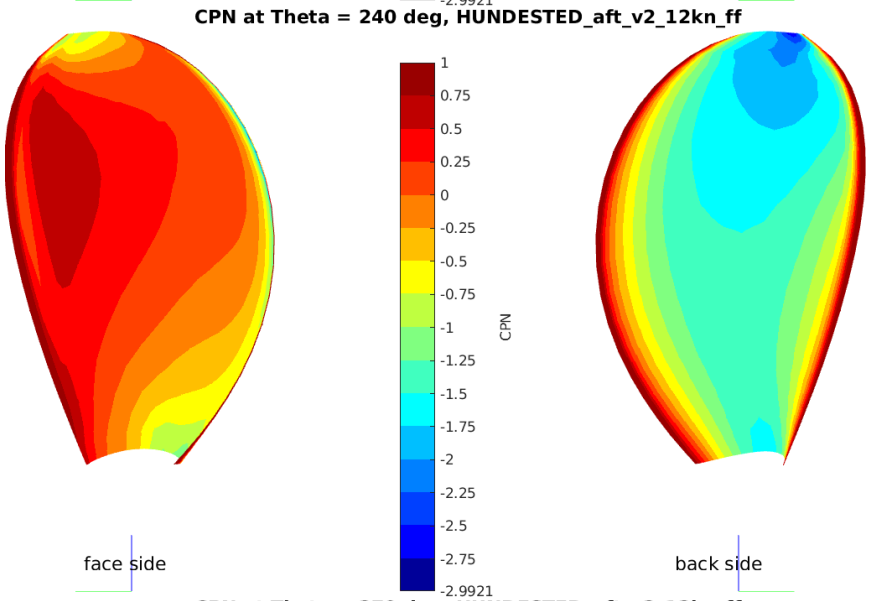
CPN at Theta = 240 deg, HUNDESTED_aft_v2_12kn_ff
1
0.75
0.5
0.25
0
-0.25
-0.5
-0.75
-1
-1.25
-1.5
-1.75
-2
-2.25
-2.5
-2.75
-2.9921
CPN
face side
back side

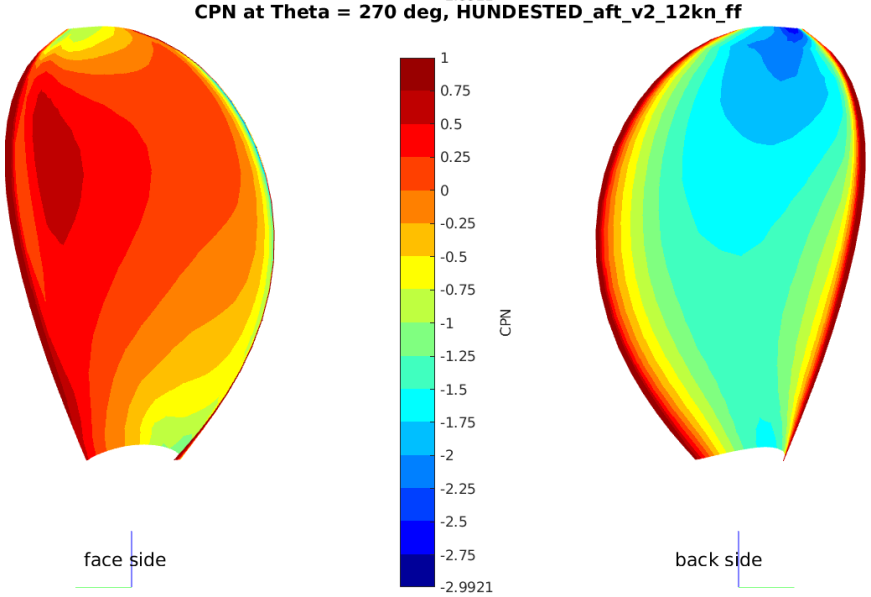
CPN at Theta = 270 deg, HUNDESTED_aft_v2_12kn_ff
1
0.75
0.5
0.25
0
-0.25
-0.5
-0.75
-1
-1.25
-1.5
-1.75
-2
-2.25
-2.5
-2.75
-2.9921
CPN
face side
back side

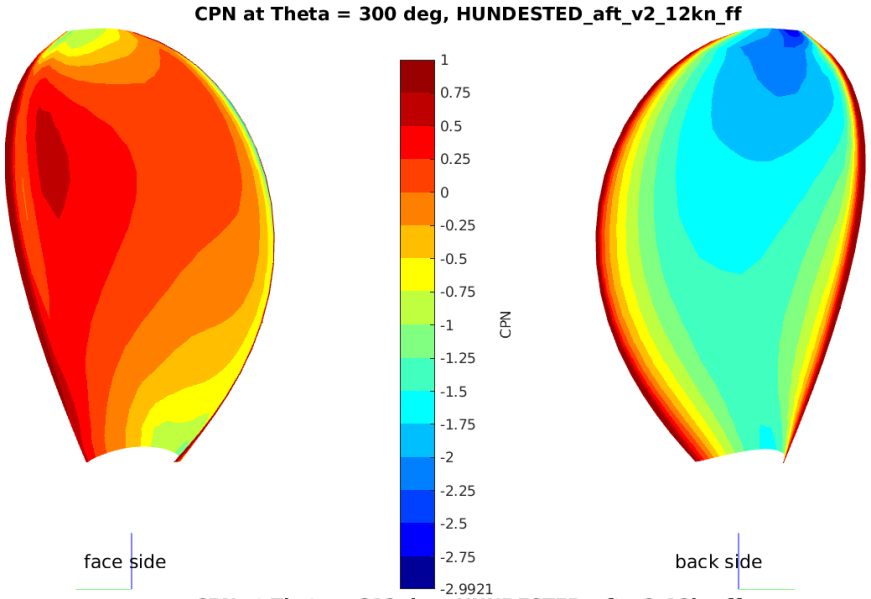
CPN at Theta = 300 deg, HUNDESTED_aft_v2_12kn_ff
1
0.75
0.5
0.25
0
-0.25
-0.5
-0.75
-1
-1.25
-1.5
-1.75
-2
-2.25
-2.5
-2.75
-2.9921
CPN
face side
back side

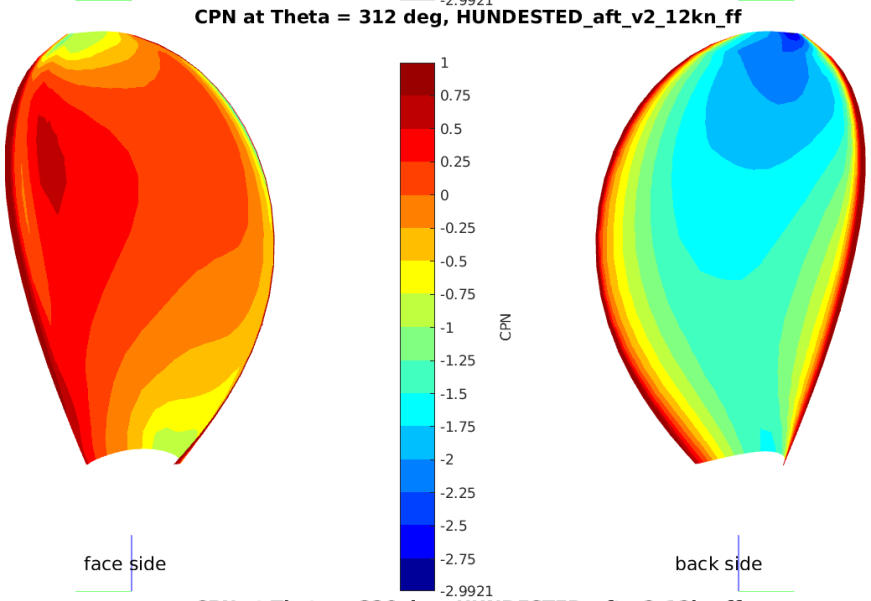
CPN at Theta = 312 deg, HUNDESTED_aft_v2_12kn_ff
1
0.75
0.5
0.25
0
-0.25
-0.5
-0.75
-1
-1.25
-1.5
-1.75
-2
-2.25
-2.5
-2.75
-2.9921
CPN
face side
back side

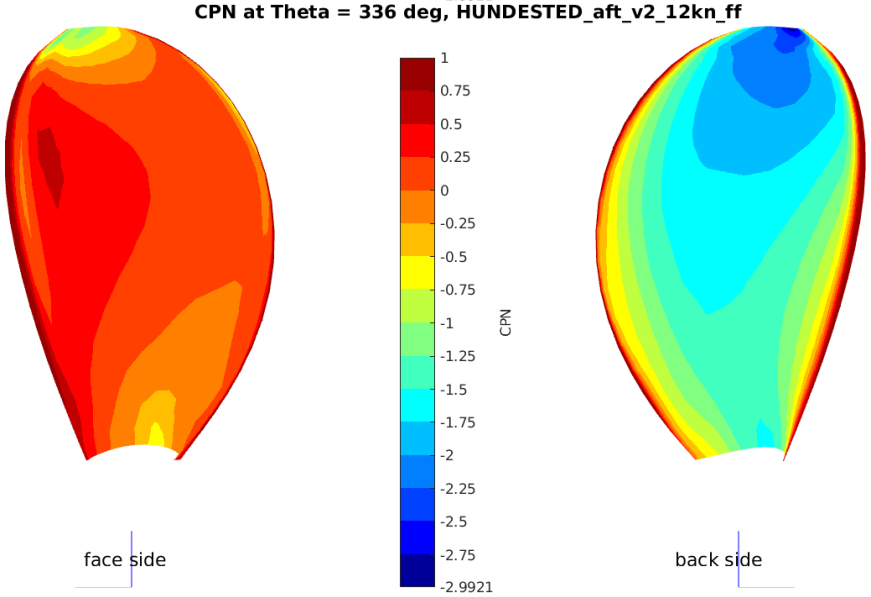
CPN at Theta = 336 deg, HUNDESTED_aft_v2_12kn_ff
1
0.75
0.5
0.25
0
-0.25
-0.5
-0.75
-1
-1.25
-1.5
-1.75
-2
-2.25
-2.5
-2.75
-2.9921
CPN
face side
back side

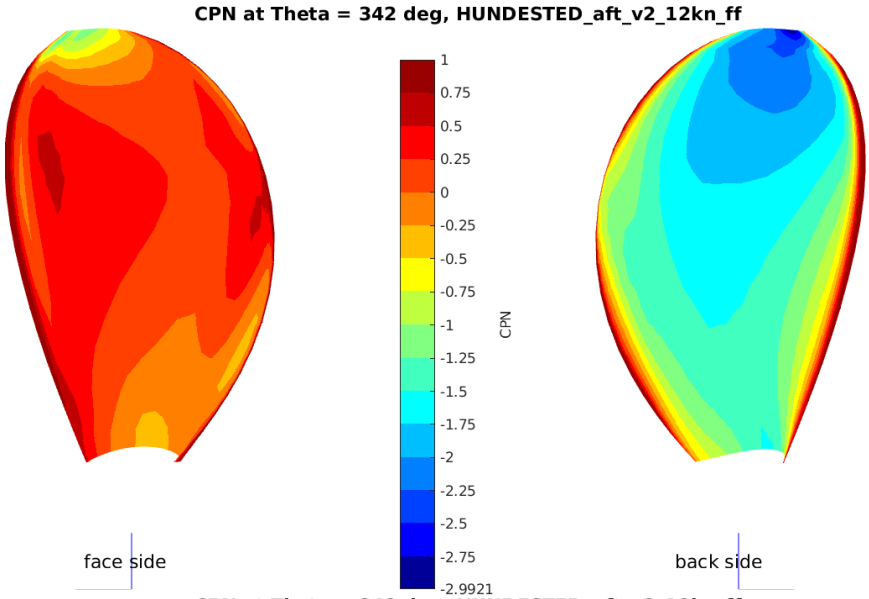

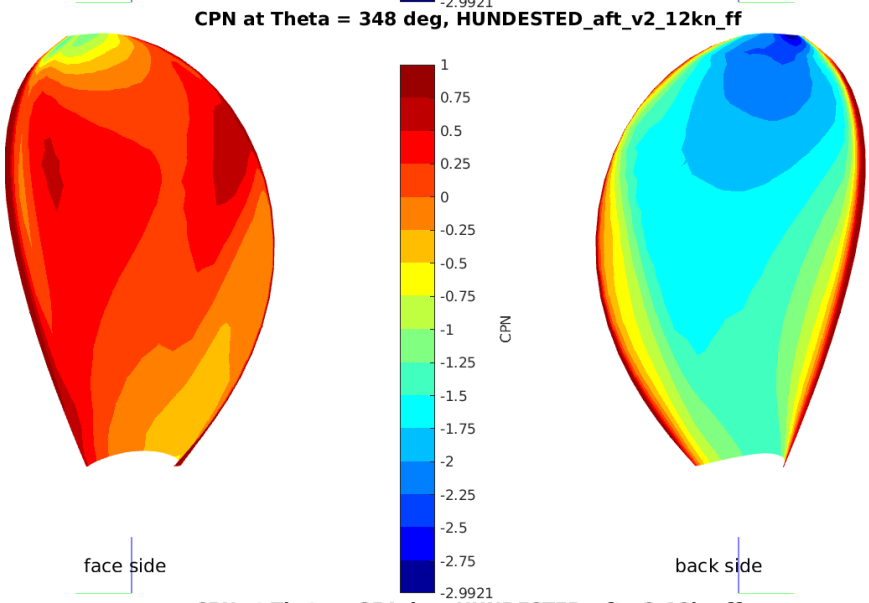

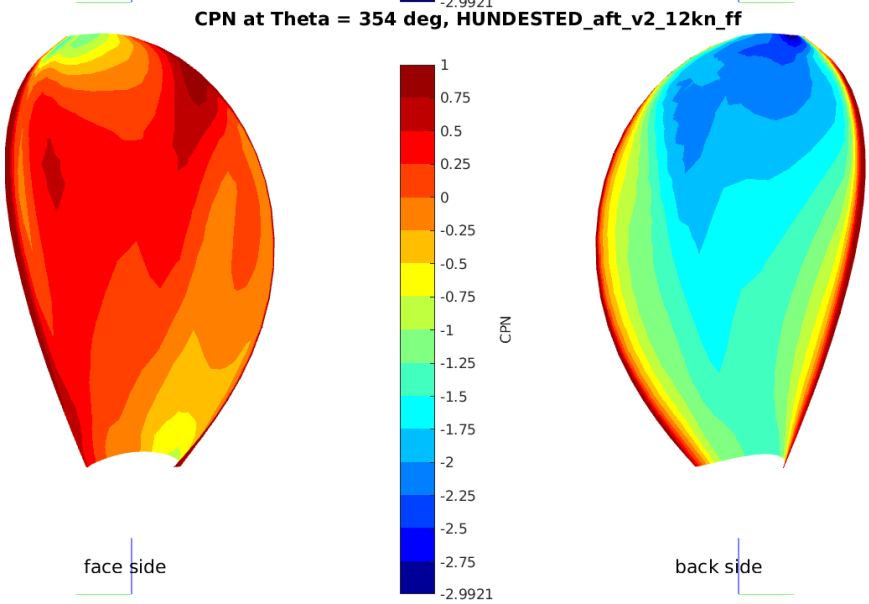

PRESSURE CONTOURS ON THE AFT PROPELLER AT 12.00 KNOTS

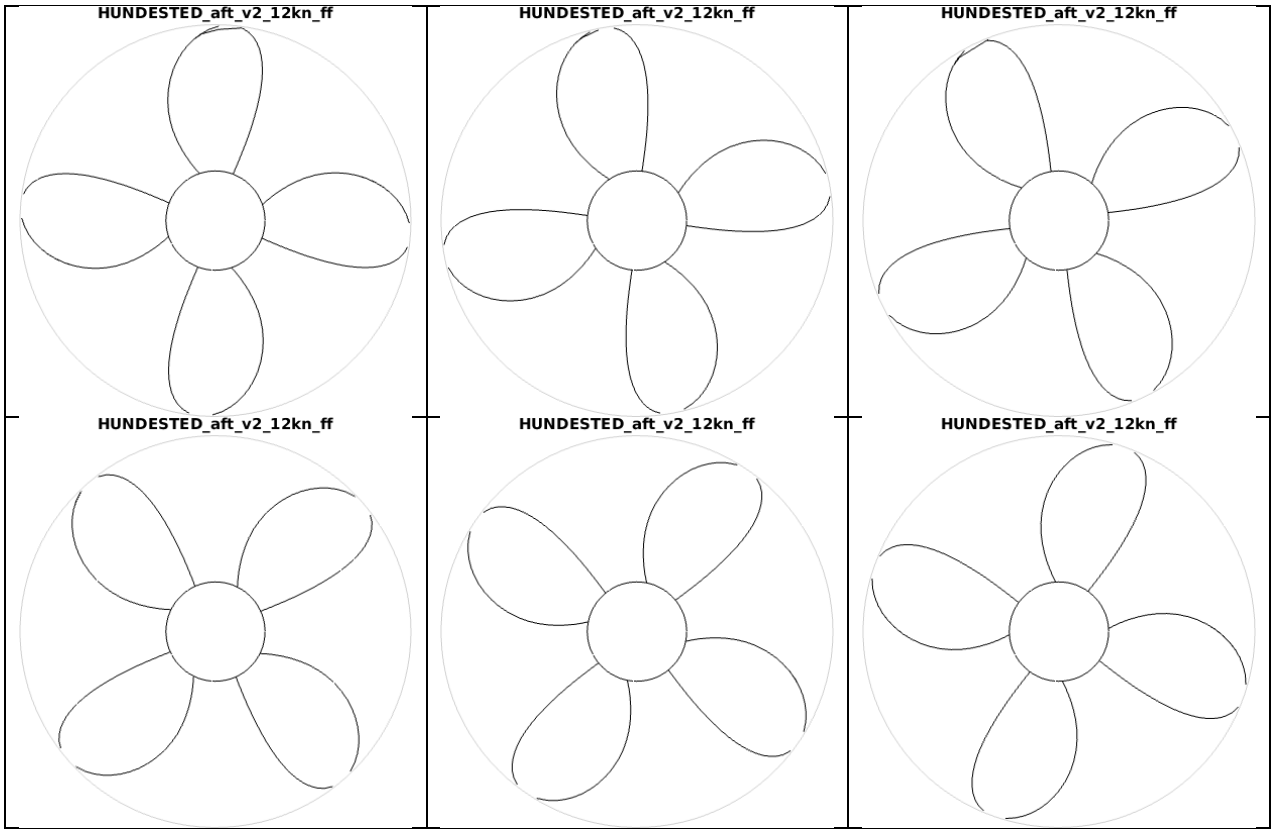

CAVITATION BEHAVIOUR OF AFT PROPELLER, WITH FRONT PROPELLER FEATHERED DURING PROPULSION AT 12 KNOTS

PRESSURE CONTOURS ON THE AFT PROPELLER AT 16 KNOTS, REGENERATING 250 KW MODE

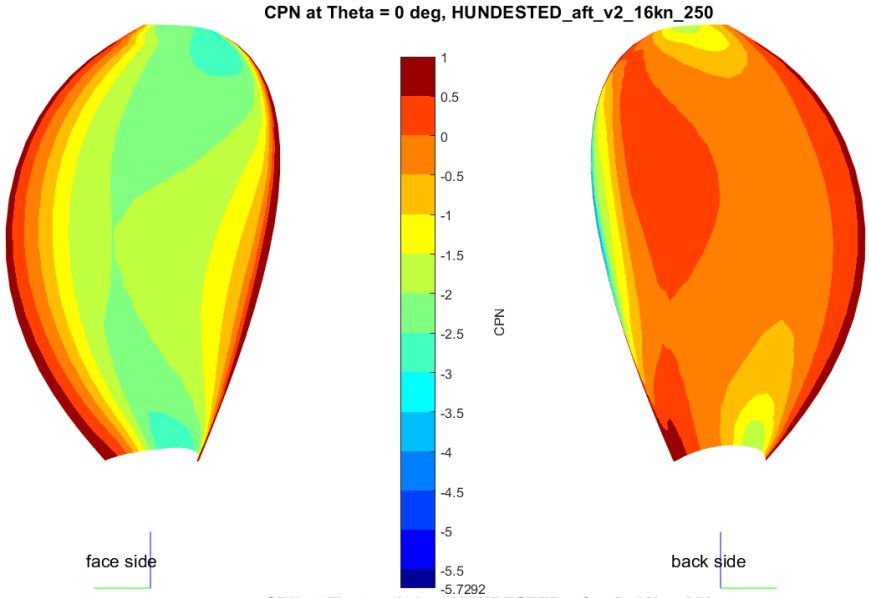

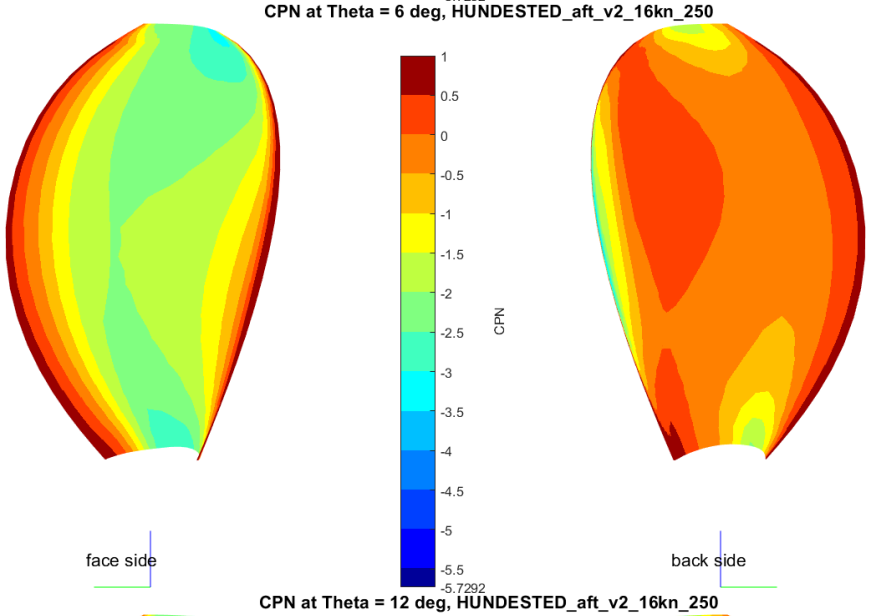

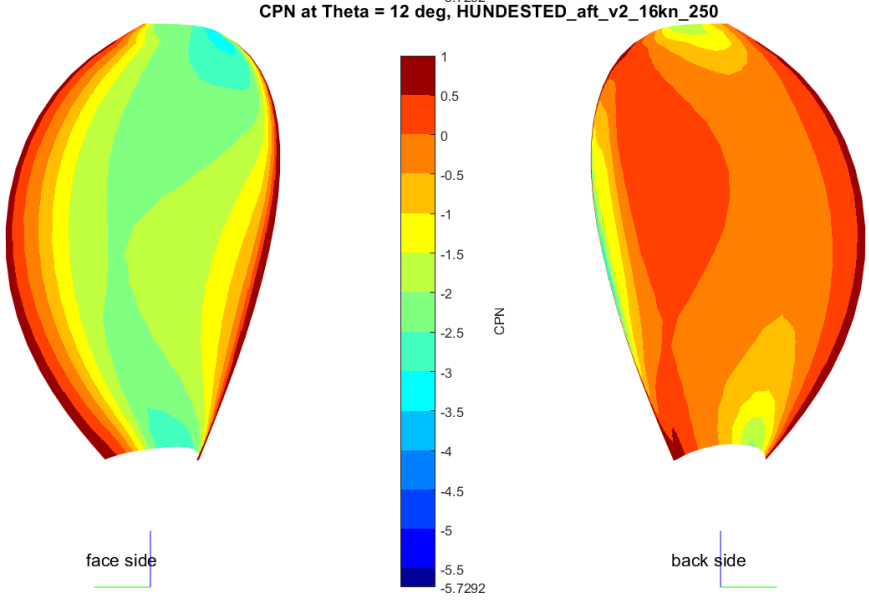

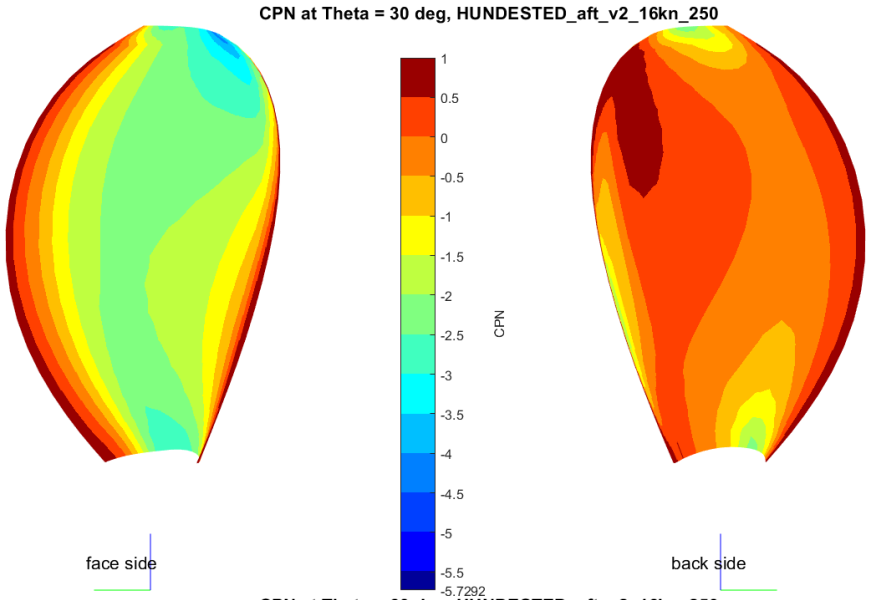
CPN at Theta = 30 deg, HUNDESTED_aft_v2_16kn_250
1
0.5
0
-0.5
-1
-1.5
-2
-2.5
-3
-3.5
-4
-4.5
-5
-5.5
-5.7292
CPN
face side
back side

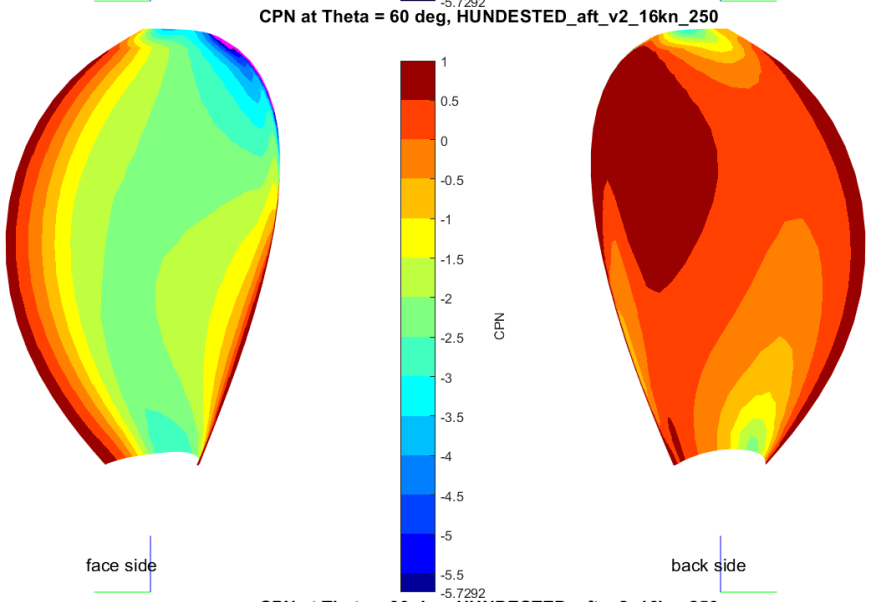
CPN at Theta = 60 deg, HUNDESTED_aft_v2_16kn_250
1
0.5
0
-0.5
-1
-1.5
-2
-2.5
-3
-3.5
-4
-4.5
-5
-5.5
-5.7292
CPN
face side
back side

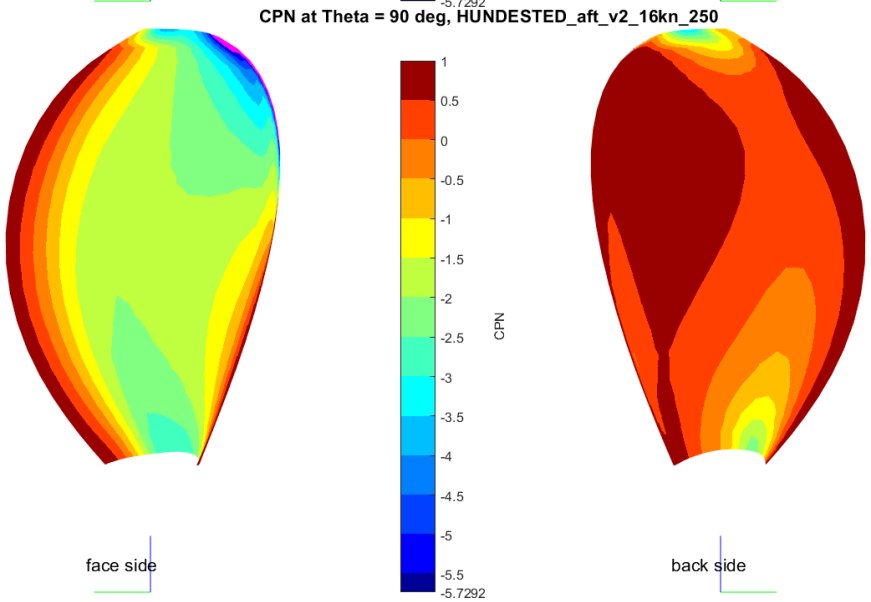
CPN at Theta = 90 deg, HUNDESTED_aft_v2_16kn_250
1
0.5
0
-0.5
-1
-1.5
-2
-2.5
-3
-3.5
-4
-4.5
-5
-5.5
-5.7292
CPN
face side
back side

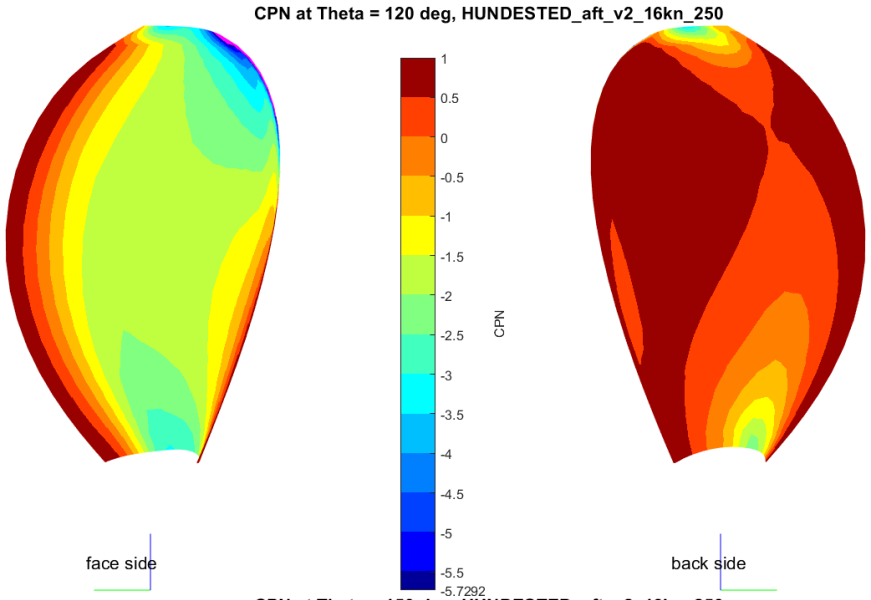
CPN at Theta = 120 deg, HUNDESTED_aft_v2_16kn_250
1
0.5
0
-0.5
-1
-1.5
-2
-2.5
-3
-3.5
-4
-4.5
-5
-5.5
-5.7292
CPN
face side
back side

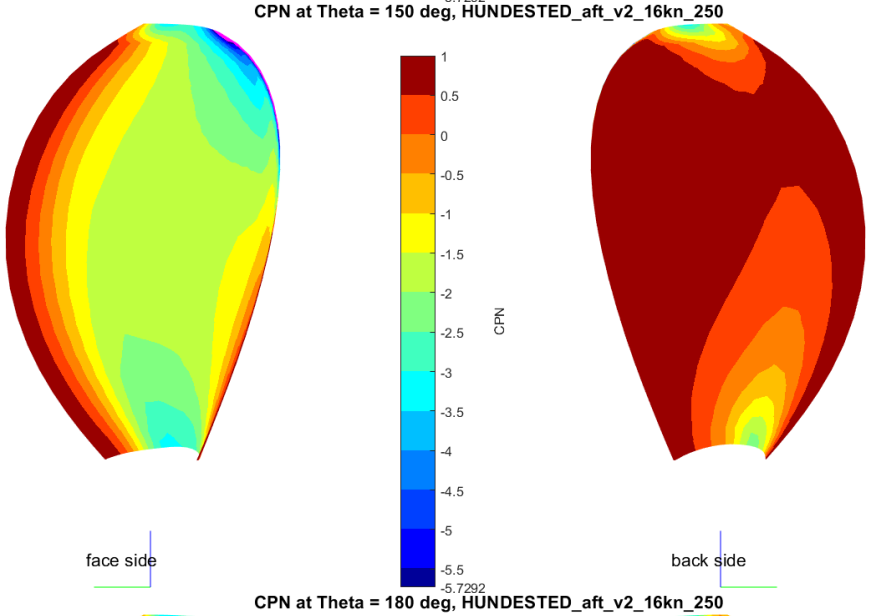
CPN at Theta = 150 deg, HUNDESTED_aft_v2_16kn_250
1
0.5
0
-0.5
-1
-1.5
-2
-2.5
-3
-3.5
-4
-4.5
-5
-5.5
-5.7292
CPN
face side
back side

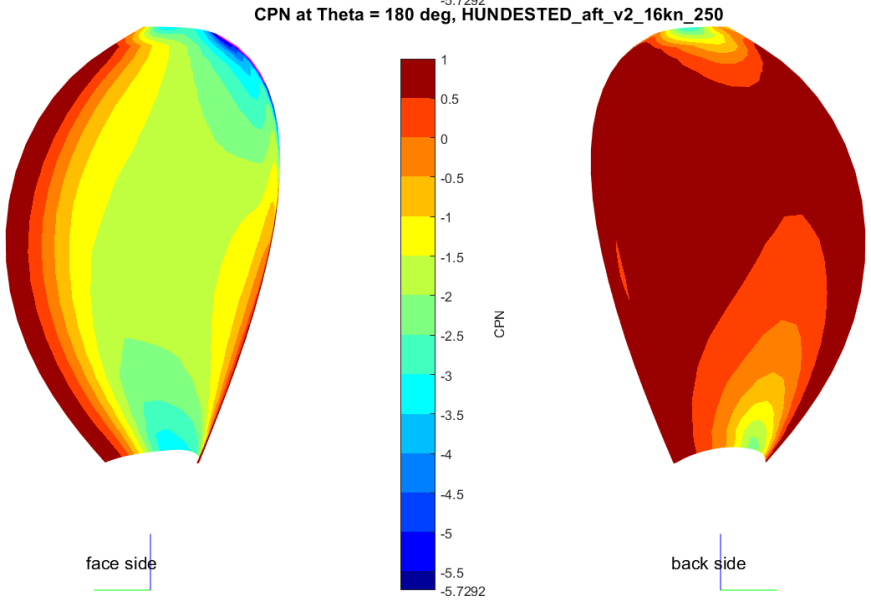
CPN at Theta = 180 deg, HUNDESTED_aft_v2_16kn_250
1
0.5
0
-0.5
-1
-1.5
-2
-2.5
-3
-3.5
-4
-4.5
-5
-5.5
-5.7292
CPN
face side
back side

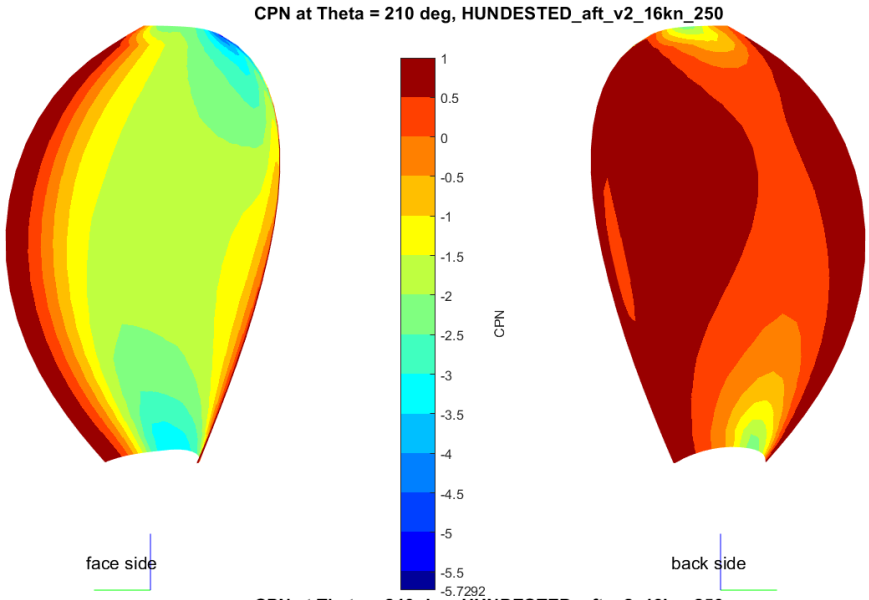
CPN at Theta = 210 deg, HUNDESTED_aft_v2_16kn_250
1
0.5
0
-0.5
-1
-1.5
-2
-2.5
-3
-3.5
-4
-4.5
-5
-5.5
-5.7292
CPN
face side
back side

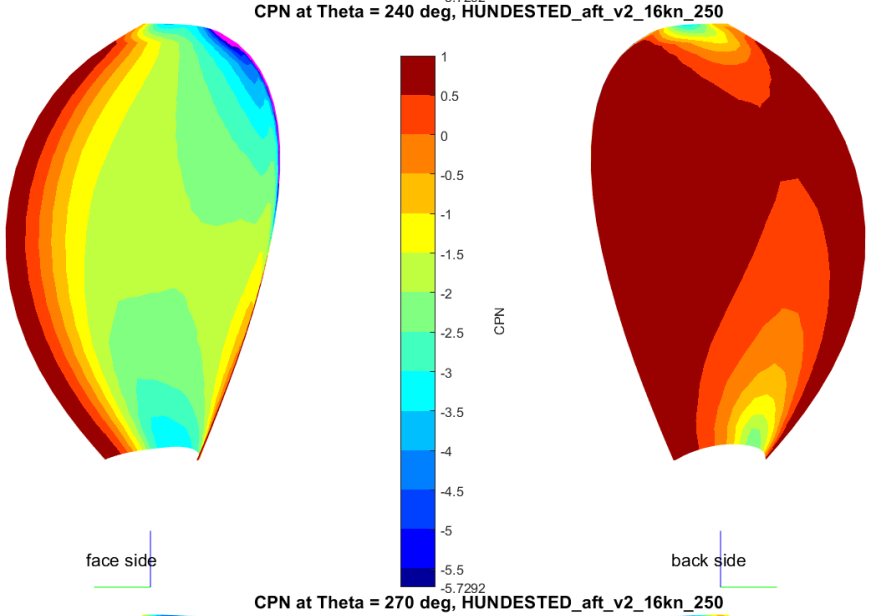
CPN at Theta = 240 deg, HUNDESTED_aft_v2_16kn_250
1
0.5
0
-0.5
-1
-1.5
-2
-2.5
-3
-3.5
-4
-4.5
-5
-5.5
-5.7292
CPN
face side
back side

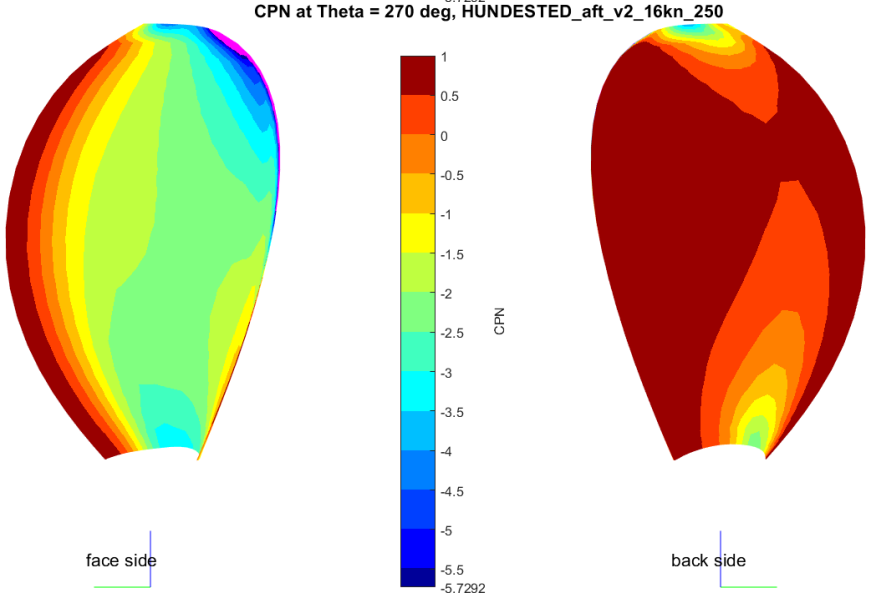
CPN at Theta = 270 deg, HUNDESTED_aft_v2_16kn_250
1
0.5
0
-0.5
-1
-1.5
-2
-2.5
-3
-3.5
-4
-4.5
-5
-5.5
-5.7292
CPN
face side
back side

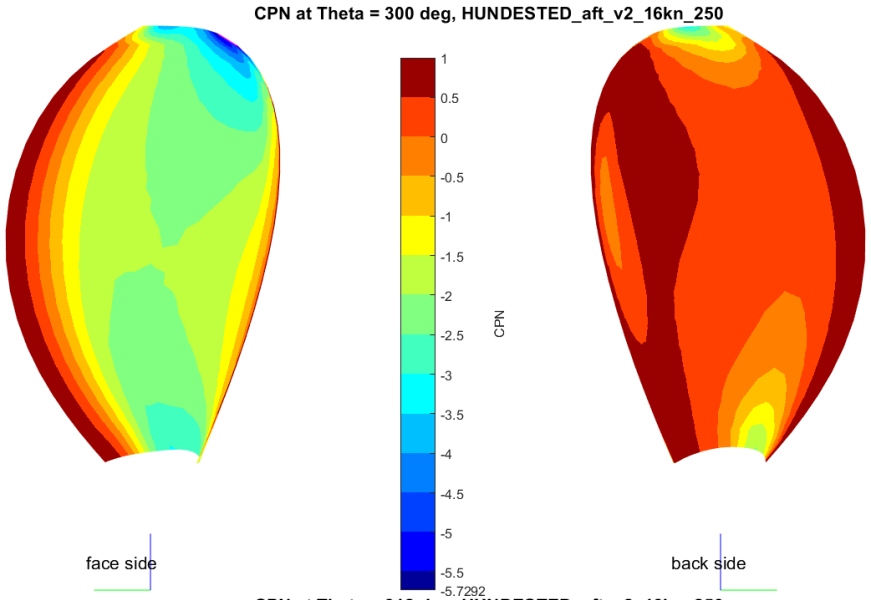
CPN at Theta = 300 deg, HUNDESTED_aft_v2_16kn_250
1
0.5
0
-0.5
-1
-1.5
-2
-2.5
-3
-3.5
-4
-4.5
-5
-5.5
-5.7292
CPN
face side
back side

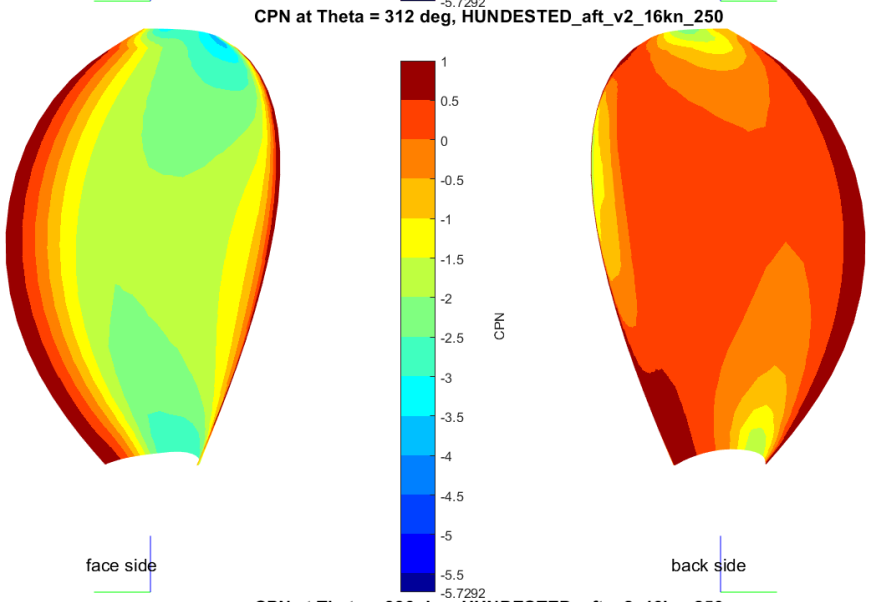
CPN at Theta = 312 deg, HUNDESTED_aft_v2_16kn_250
1
0.5
0
-0.5
-1
-1.5
-2
-2.5
-3
-3.5
-4
-4.5
-5
-5.5
-5.7292
CPN
face side
back side

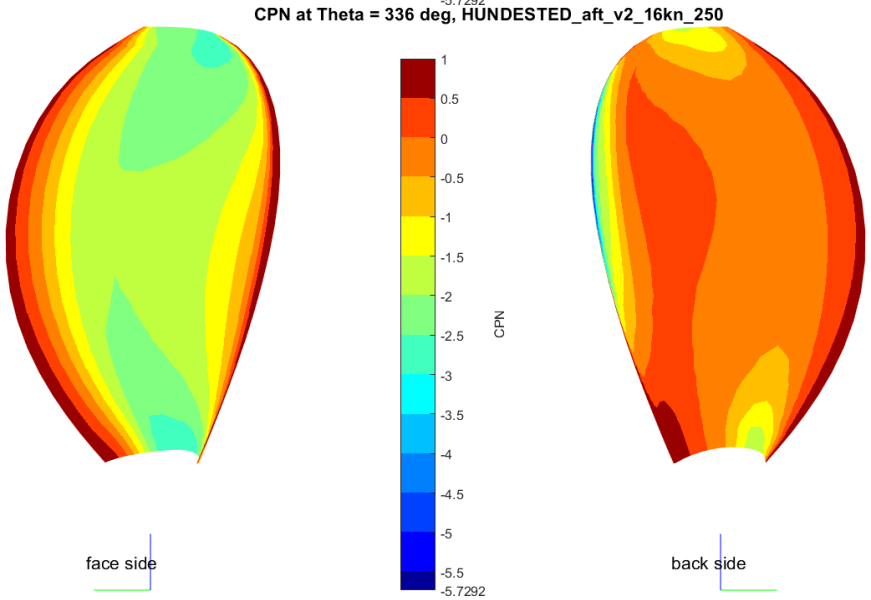
CPN at Theta = 336 deg, HUNDESTED_aft_v2_16kn_250
1
0.5
0
-0.5
-1
-1.5
-2
-2.5
-3
-3.5
-4
-4.5
-5
-5.5
-5.7292
CPN
face side
back side

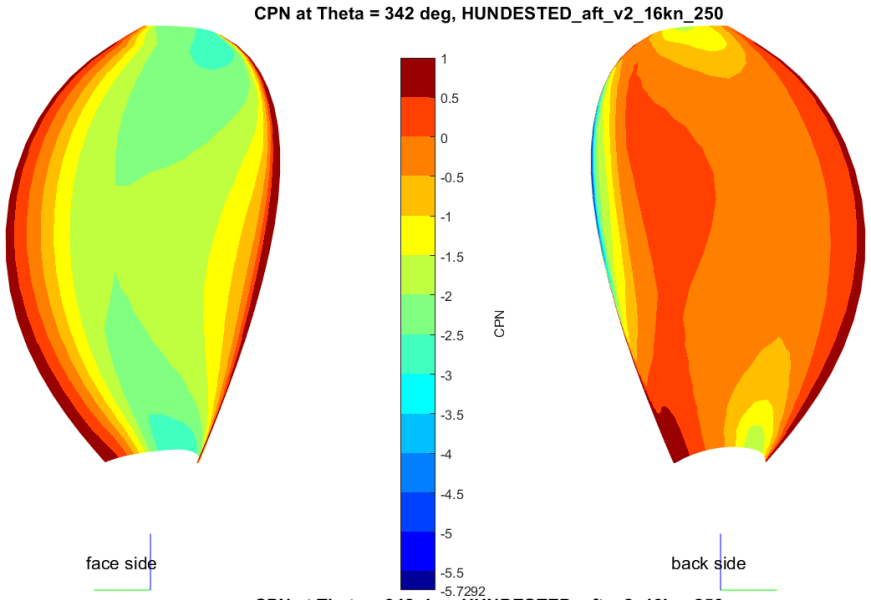

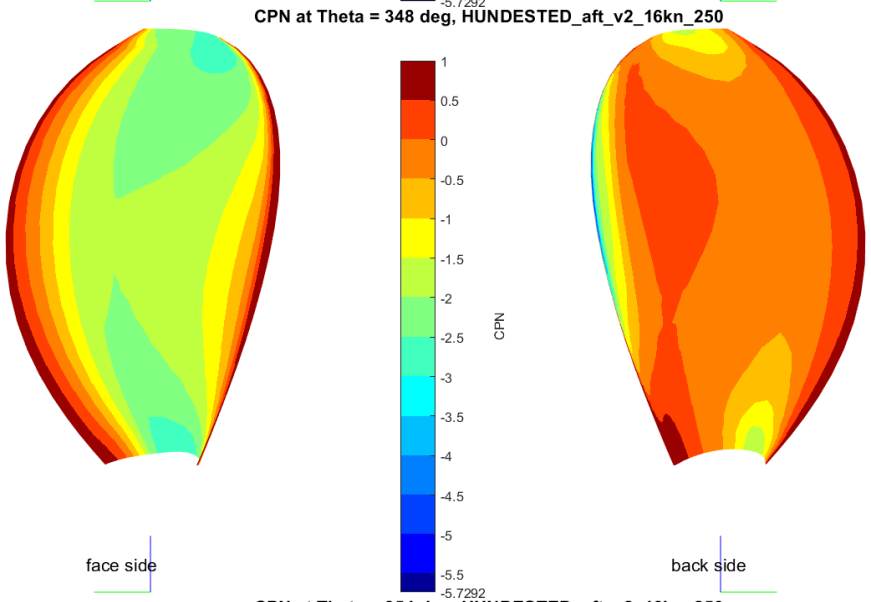

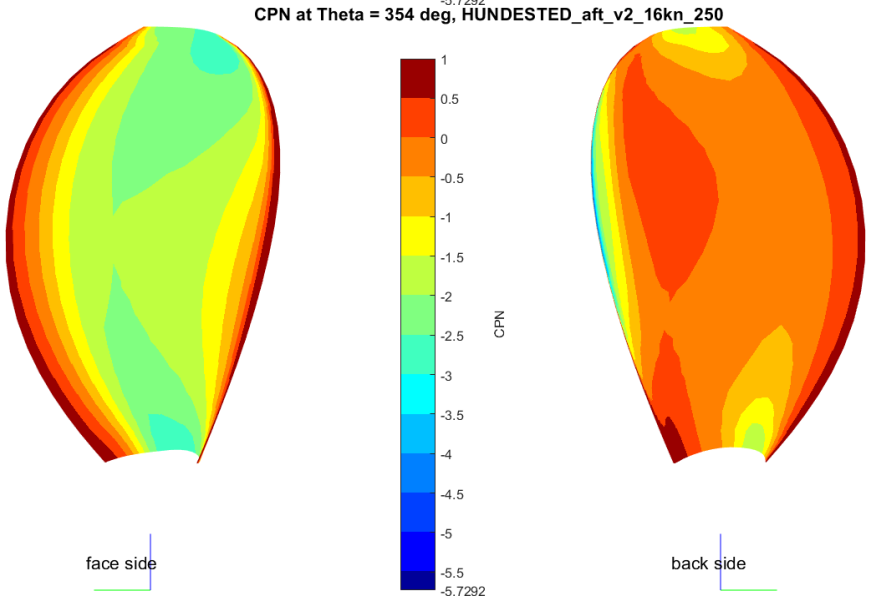

PRESSURE CONTOURS ON THE AFT PROPELLER AT 16 KNOTS, REGENERATING 250 KW MODE

PRESSURE CONTOURS ON THE AFT PROPELLER AT 14 KNOTS, REGENERATING 125 KW MODE

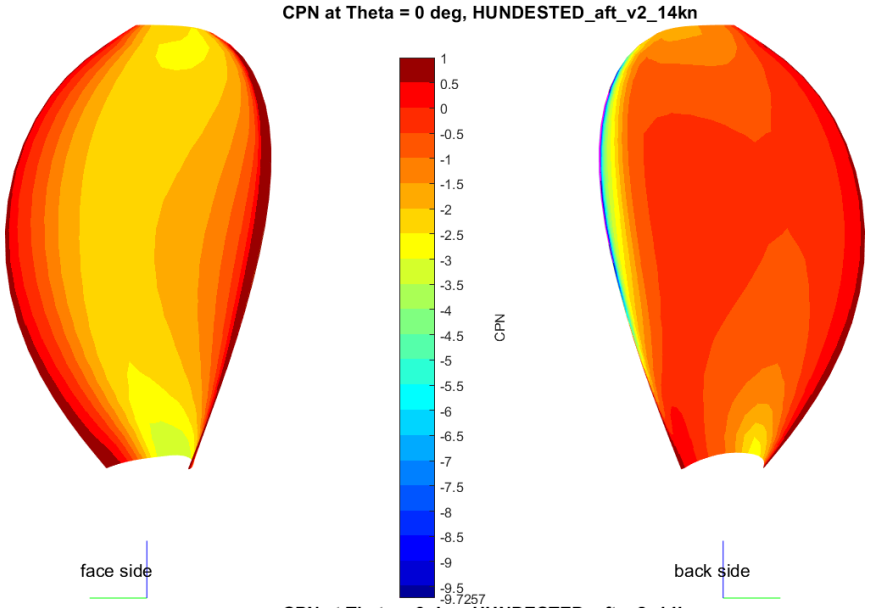

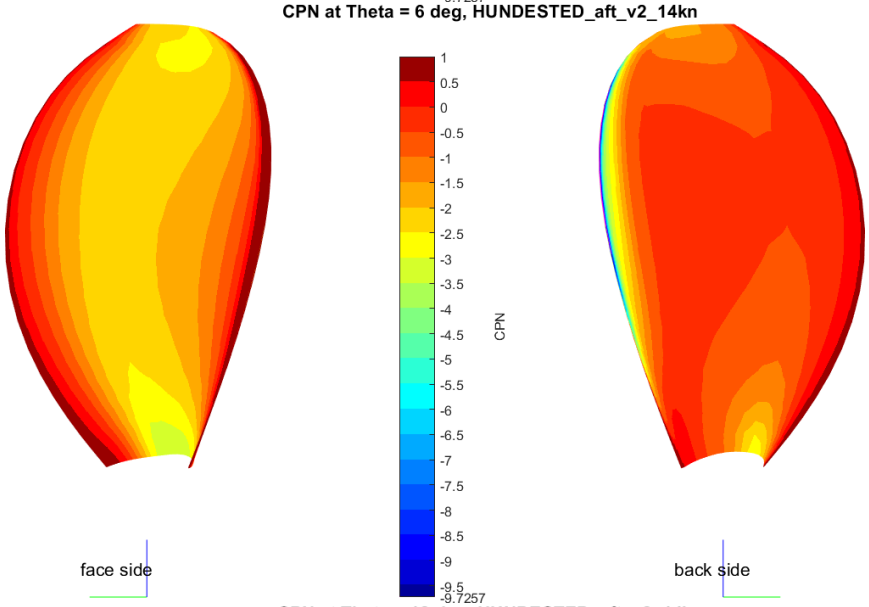

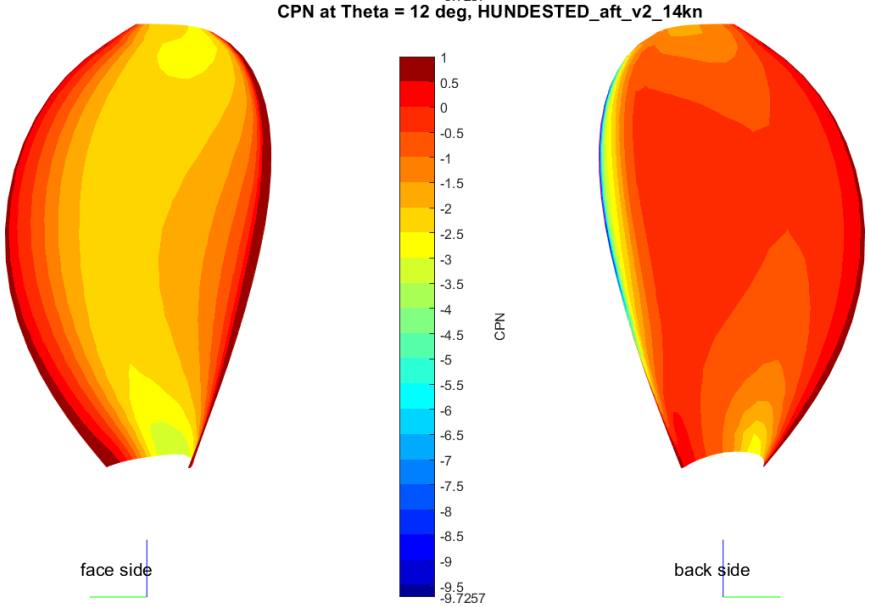

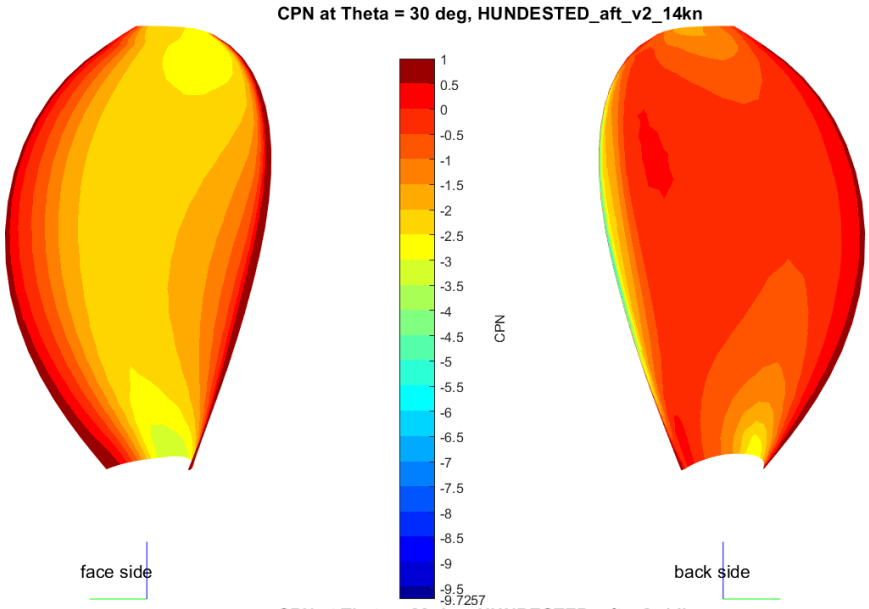
CPN at Theta = 30 deg, HUNDESTED_aft_v2_14kn
1
0.5
0
-0.5
-1
-1.5
-2
-2.5
-3
-3.5
-4
-4.5
-5
-5.5
-6
-6.5
-7
-7.5
-8
-8.5
-9
-9.5
-9.7257
CPN
face side
back side

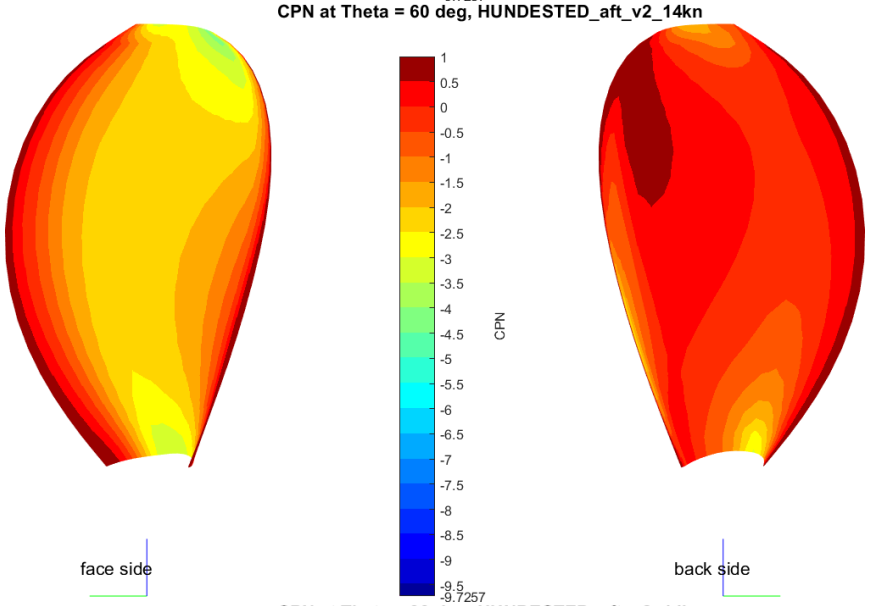
CPN at Theta = 60 deg, HUNDESTED_aft_v2_14kn
1
0.5
0
-0.5
-1
-1.5
-2
-2.5
-3
-3.5
-4
-4.5
-5
-5.5
-6
-6.5
-7
-7.5
-8
-8.5
-9
-9.5
-9.7257
CPN
face side
back side

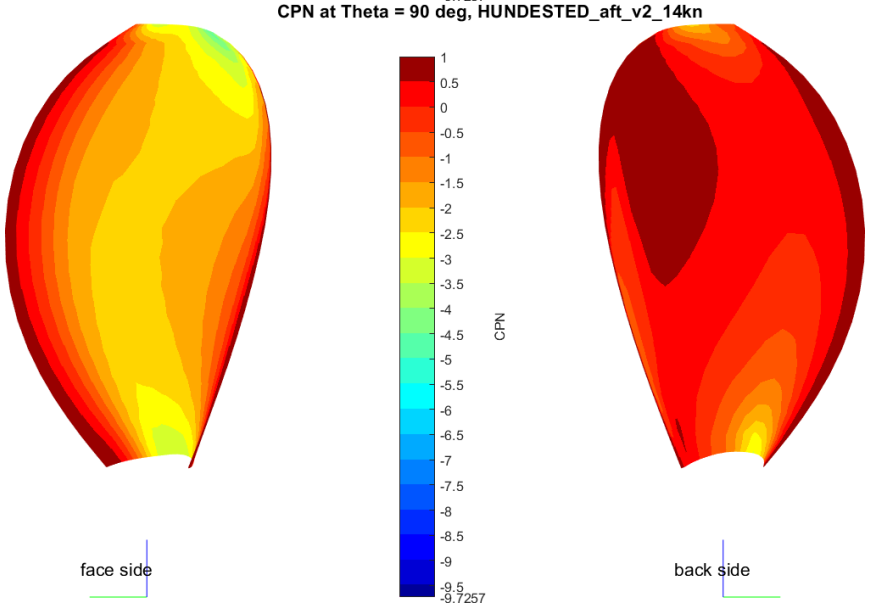
CPN at Theta = 90 deg, HUNDESTED_aft_v2_14kn
1
0.5
0
-0.5
-1
-1.5
-2
-2.5
-3
-3.5
-4
-4.5
-5
-5.5
-6
-6.5
-7
-7.5
-8
-8.5
-9
-9.5
-9.7257
CPN
face side
back side

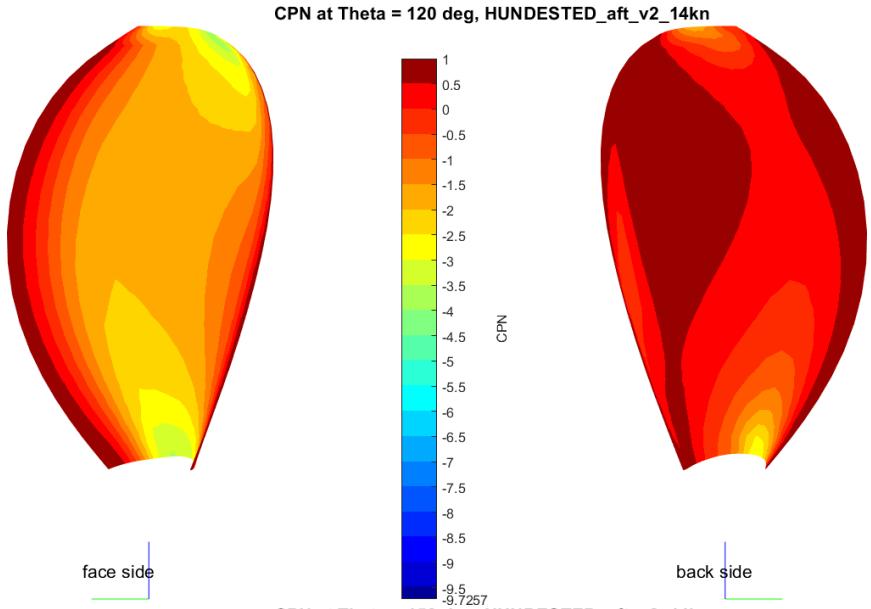
CPN at Theta = 120 deg, HUNDESTED_aft_v2_14kn
face side
back side
CPN
1
0.5
0
-0.5
-1
-1.5
-2
-2.5
-3
-3.5
-4
-4.5
-5
-5.5
-6
-6.5
-7
-7.5
-8
-8.5
-9
-9.5
-9.7257

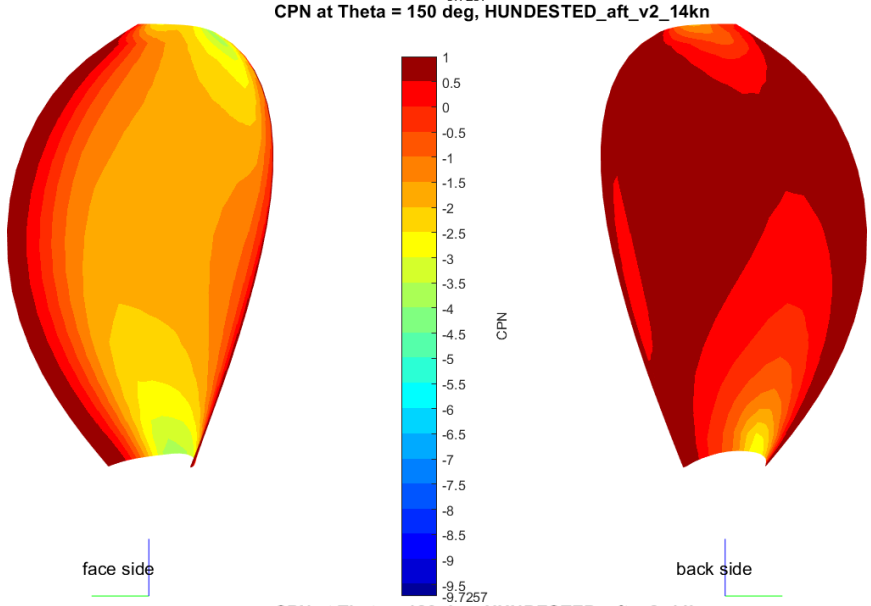
CPN at Theta = 150 deg, HUNDESTED_aft_v2_14kn
face side
back side
CPN
1
0.5
0
-0.5
-1
-1.5
-2
-2.5
-3
-3.5
-4
-4.5
-5
-5.5
-6
-6.5
-7
-7.5
-8
-8.5
-9
-9.5
-9.7257

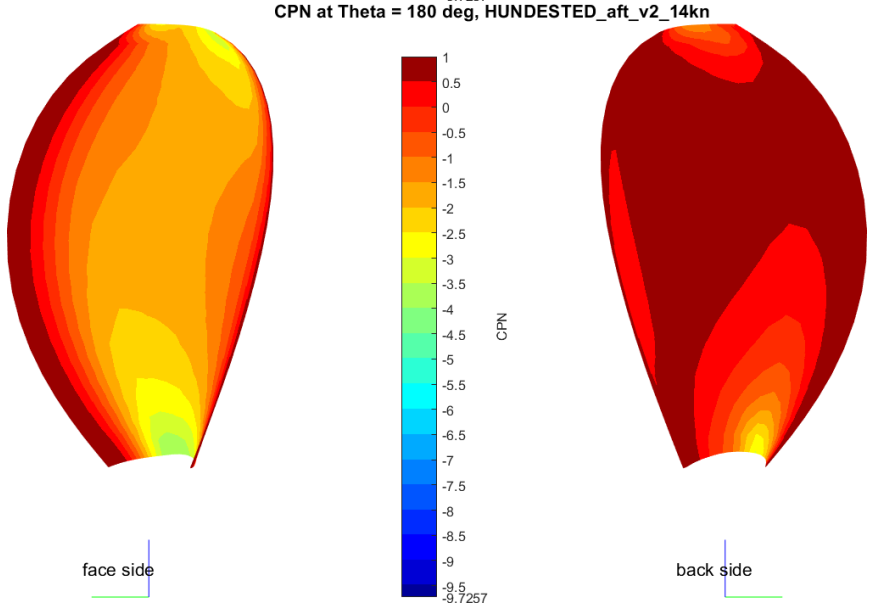
CPN at Theta = 180 deg, HUNDESTED_aft_v2_14kn
face side
back side
CPN
1
0.5
0
-0.5
-1
-1.5
-2
-2.5
-3
-3.5
-4
-4.5
-5
-5.5
-6
-6.5
-7
-7.5
-8
-8.5
-9
-9.5
-9.7257

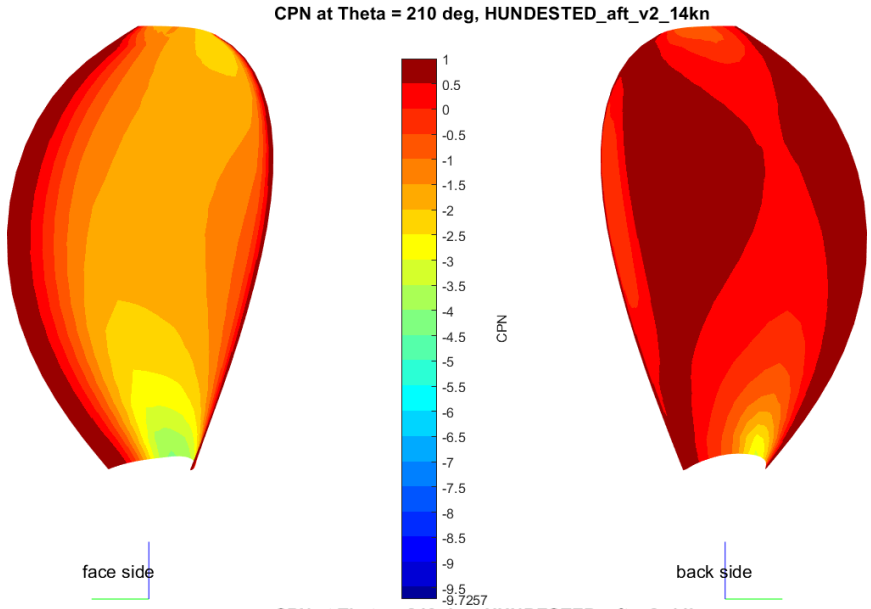
CPN at Theta = 210 deg, HUNDESTED_aft_v2_14kn
1
0.5
0
-0.5
-1
-1.5
-2
-2.5
-3
-3.5
-4
-4.5
-5
-5.5
-6
-6.5
-7
-7.5
-8
-8.5
-9
-9.5
-9.7257
CPN
face side
back side

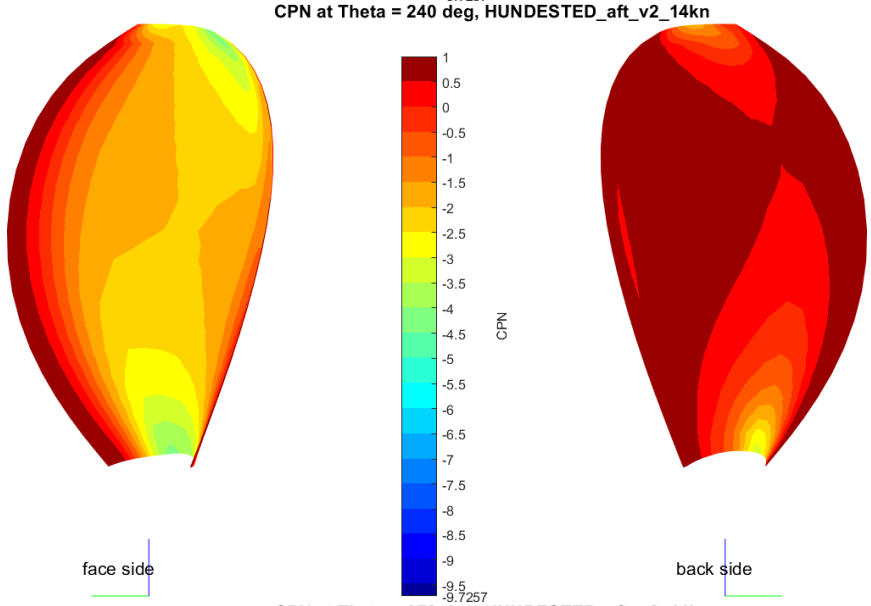
CPN at Theta = 240 deg, HUNDESTED_aft_v2_14kn
1
0.5
0
-0.5
-1
-1.5
-2
-2.5
-3
-3.5
-4
-4.5
-5
-5.5
-6
-6.5
-7
-7.5
-8
-8.5
-9
-9.5
-9.7257
CPN
face side
back side

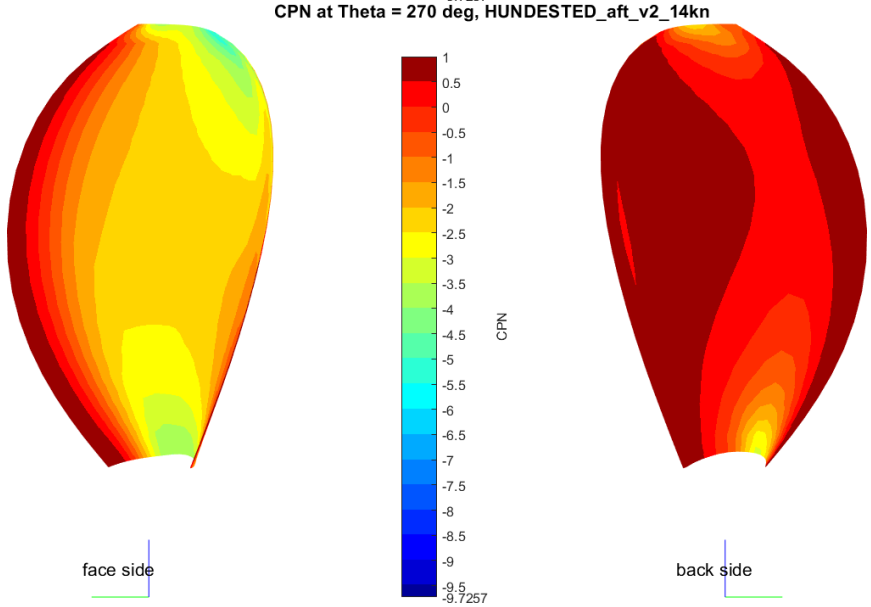
CPN at Theta = 270 deg, HUNDESTED_aft_v2_14kn
1
0.5
0
-0.5
-1
-1.5
-2
-2.5
-3
-3.5
-4
-4.5
-5
-5.5
-6
-6.5
-7
-7.5
-8
-8.5
-9
-9.5
-9.7257
CPN
face side
back side

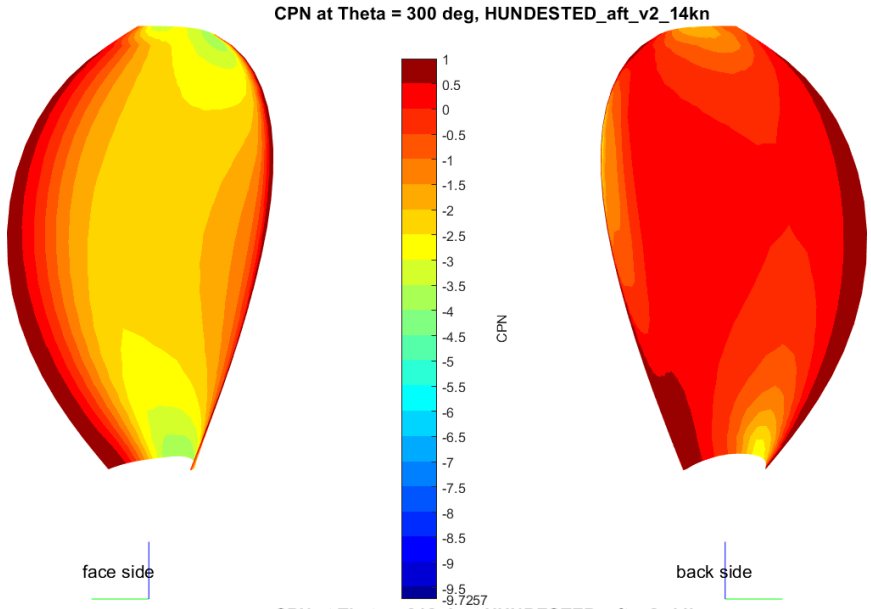
CPN at Theta = 300 deg, HUNDESTED_aft_v2_14kn
1
0.5
0
-0.5
-1
-1.5
-2
-2.5
-3
-3.5
-4
-4.5
-5
-5.5
-6
-6.5
-7
-7.5
-8
-8.5
-9
-9.5
-9.7257
CPN
face side
back side

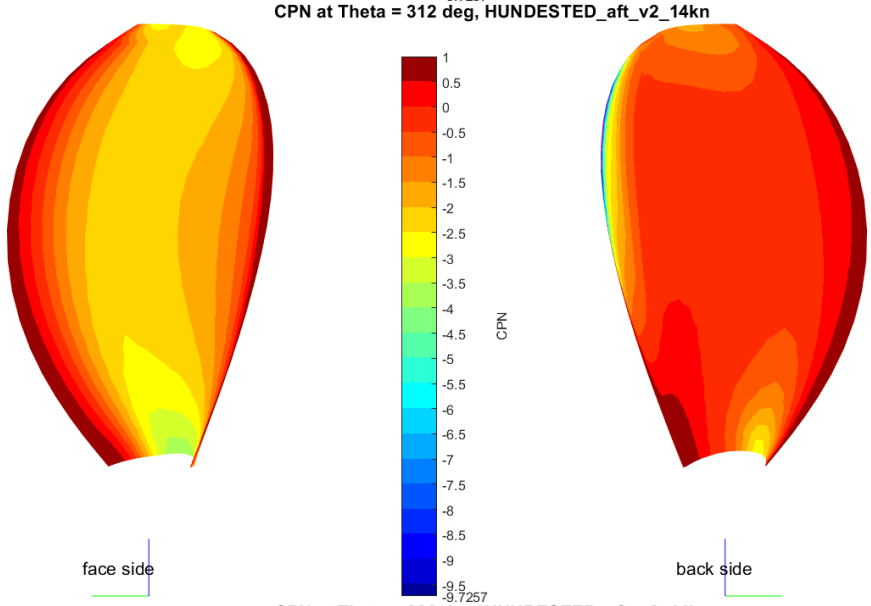
CPN at Theta = 312 deg, HUNDESTED_aft_v2_14kn
1
0.5
0
-0.5
-1
-1.5
-2
-2.5
-3
-3.5
-4
-4.5
-5
-5.5
-6
-6.5
-7
-7.5
-8
-8.5
-9
-9.5
-9.7257
CPN
face side
back side

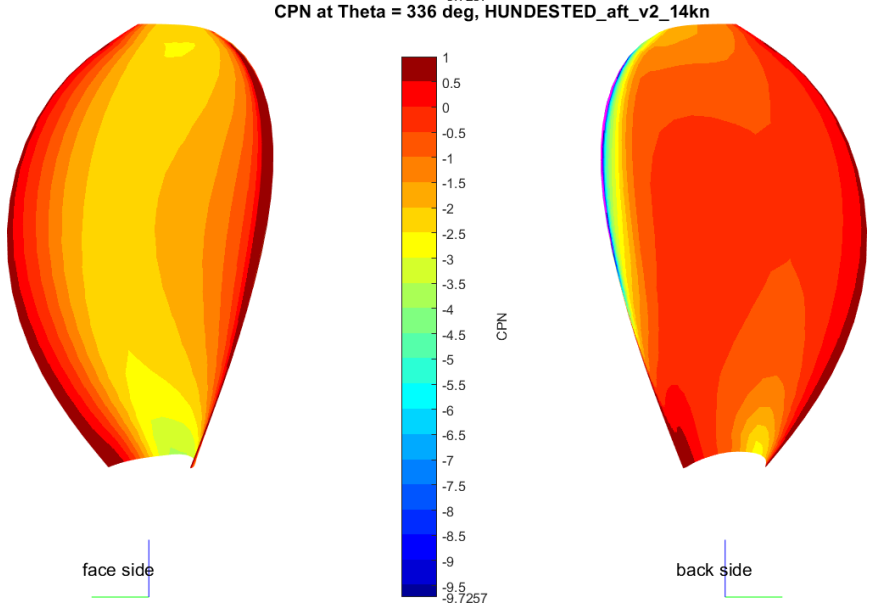
CPN at Theta = 336 deg, HUNDESTED_aft_v2_14kn
1
0.5
0
-0.5
-1
-1.5
-2
-2.5
-3
-3.5
-4
-4.5
-5
-5.5
-6
-6.5
-7
-7.5
-8
-8.5
-9
-9.5
-9.7257
CPN
face side
back side

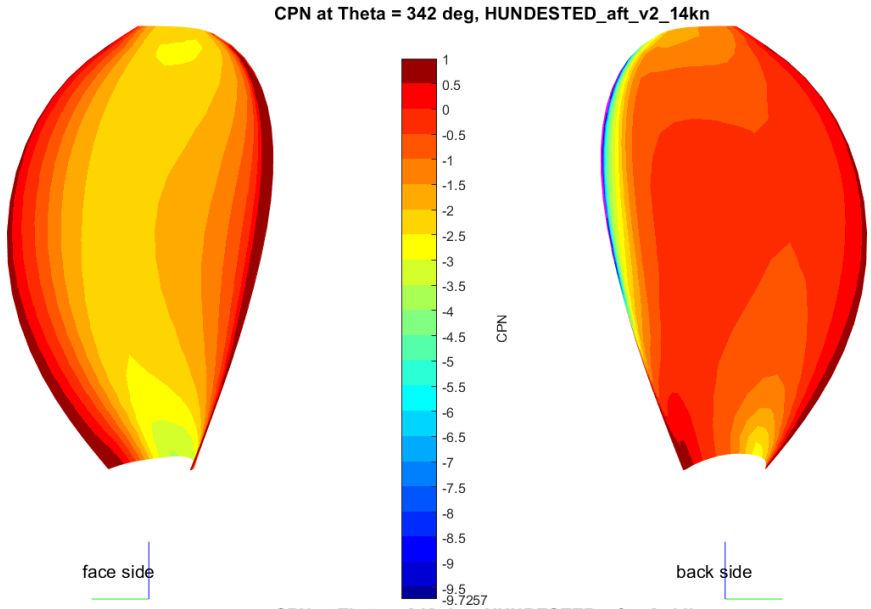

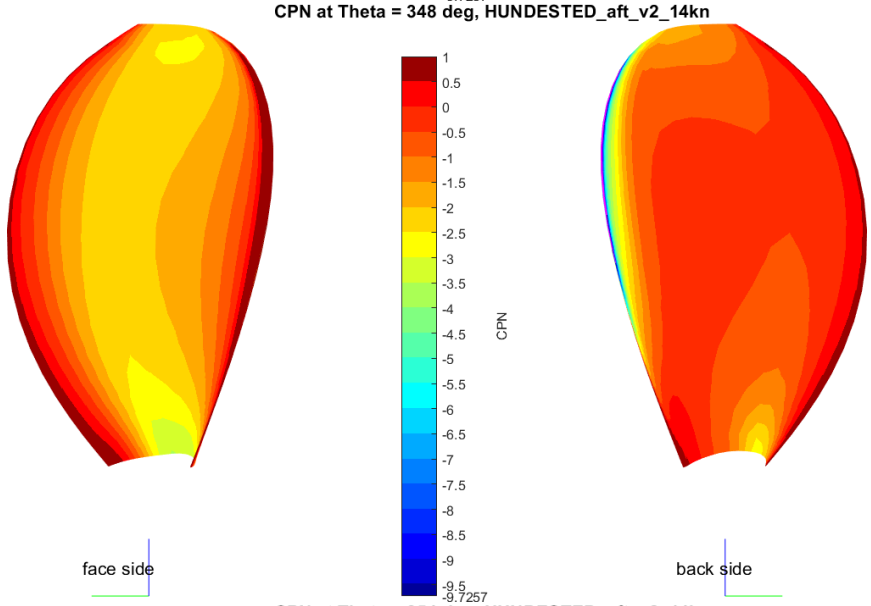

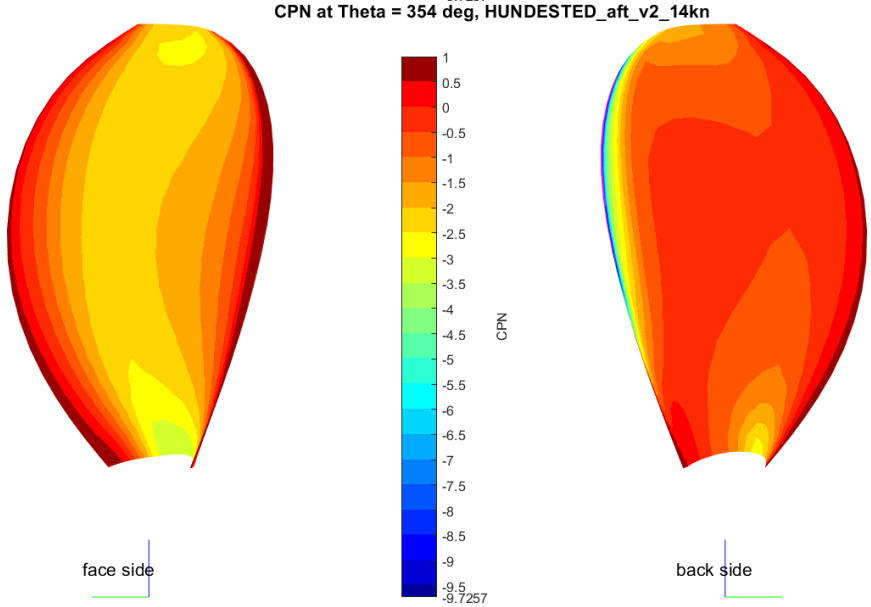

PRESSURE CONTOURS ON THE AFT PROPELLER AT 14 KNOTS, REGENERATING 125 KW MODE

PRESSURE CONTOURS ON THE FRONT PROPELLER AT 16 KNOTS, REGENERATING 250 KW MODE

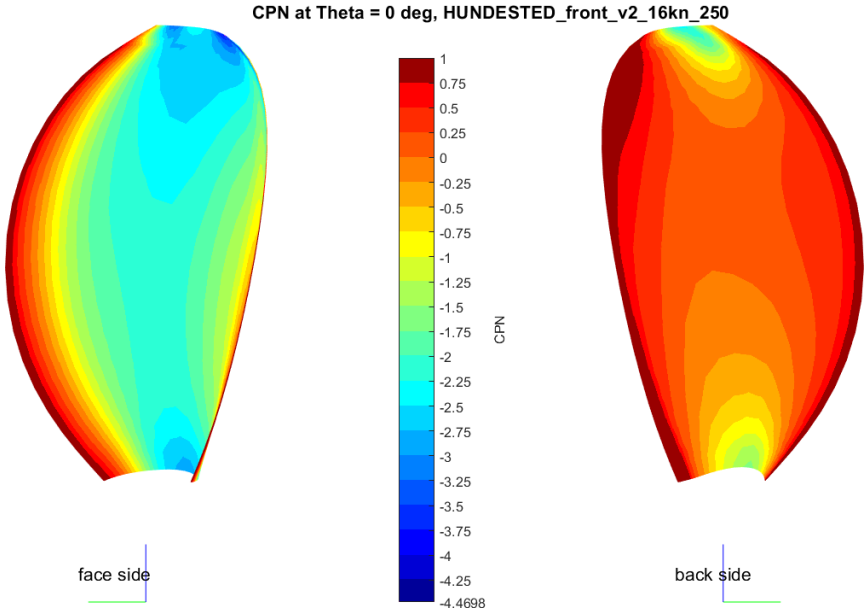

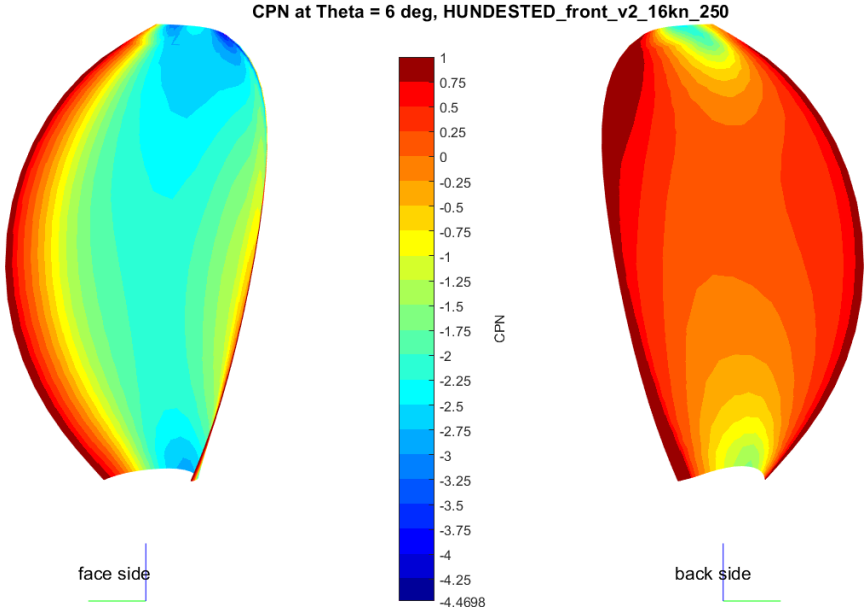

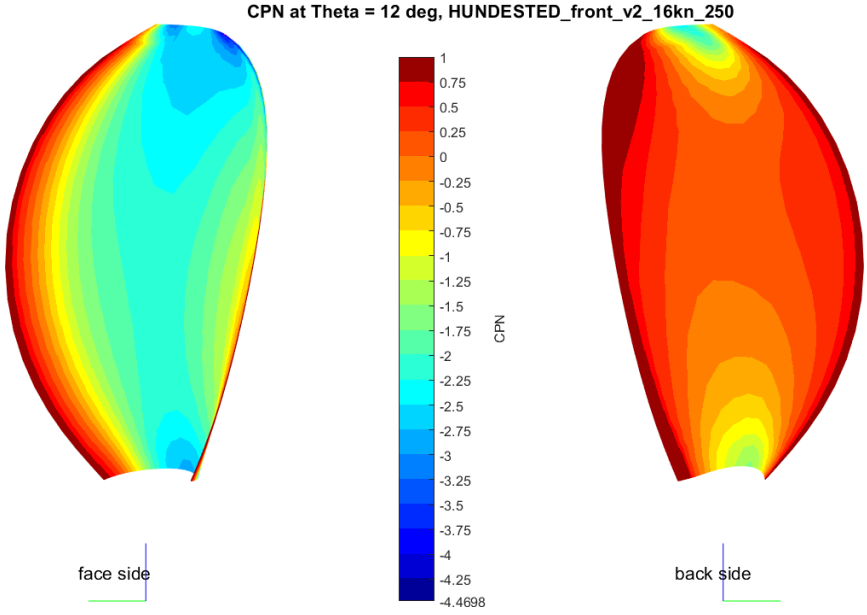

CPN at Theta = 30 deg, HUNDESTED_front_v2_16kn_250

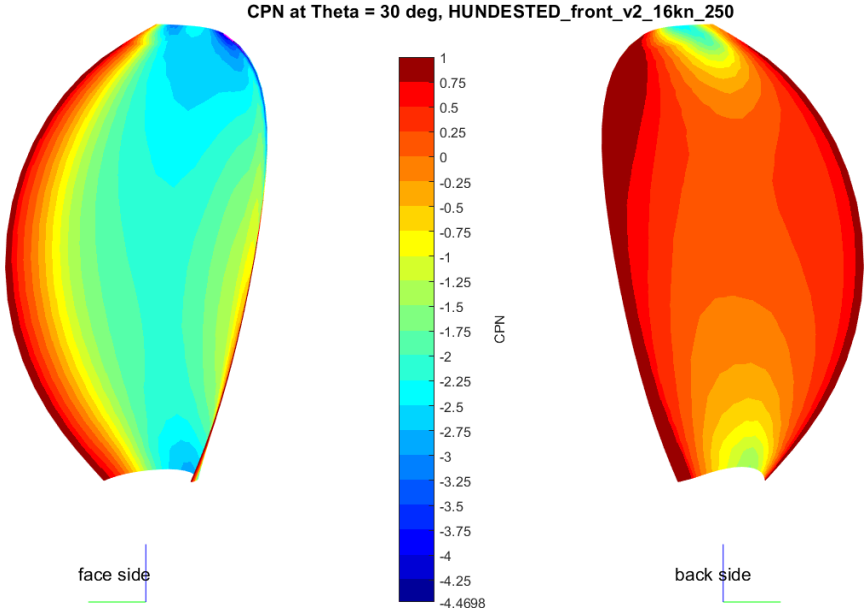

CPN at Theta = 60 deg, HUNDESTED_front_v2_16kn_250

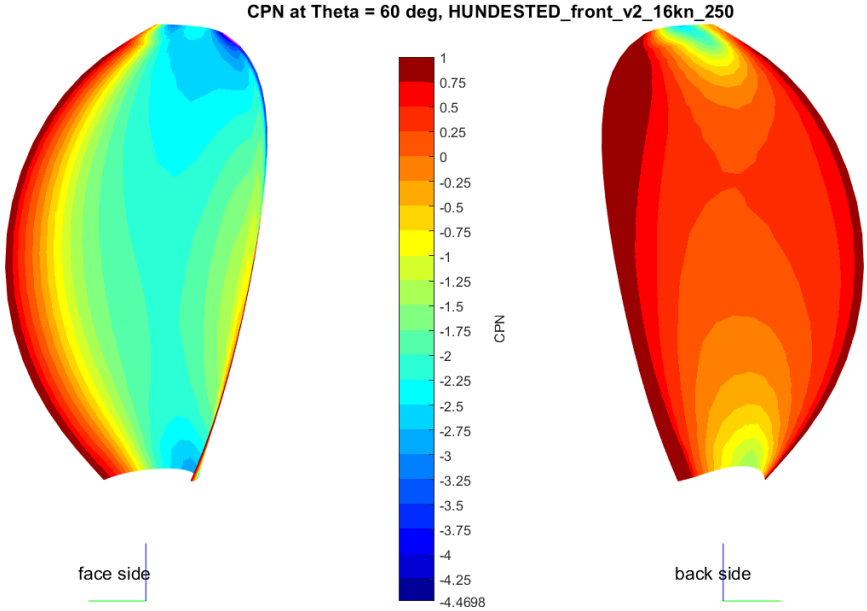

CPN at Theta = 90 deg, HUNDESTED_front_v2_16kn_250

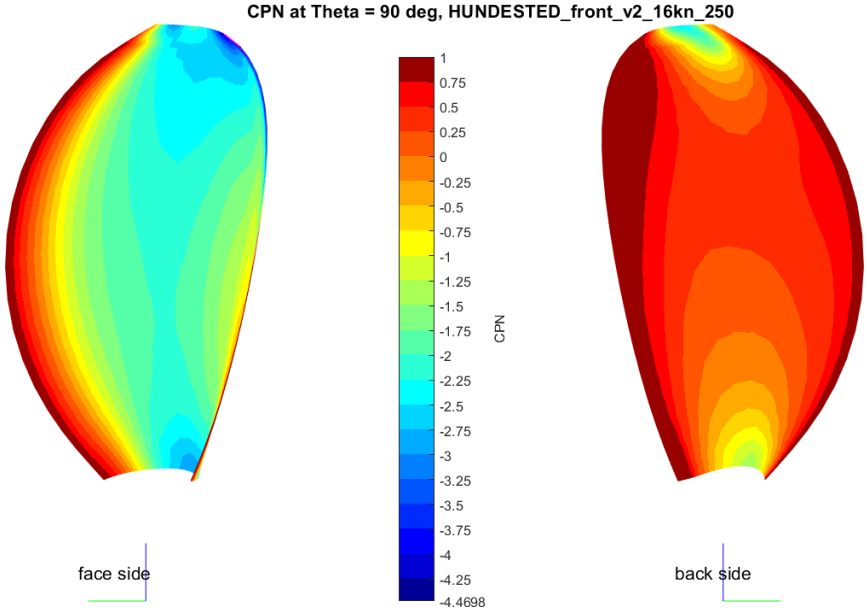

CPN at Theta = 120 deg, HUNDESTED_front_v2_16kn_250

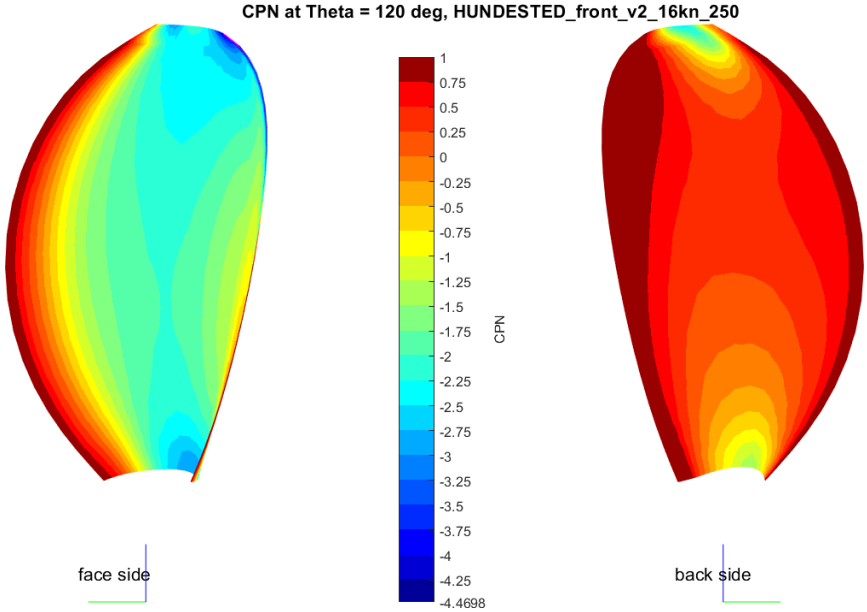

CPN at Theta = 150 deg, HUNDESTED_front_v2_16kn_250

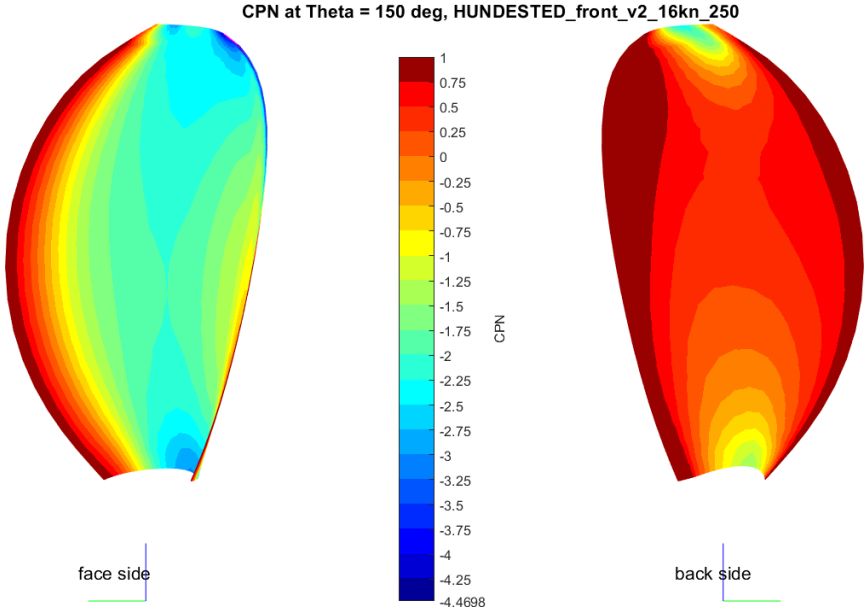

CPN at Theta = 180 deg, HUNDESTED_front_v2_16kn_250

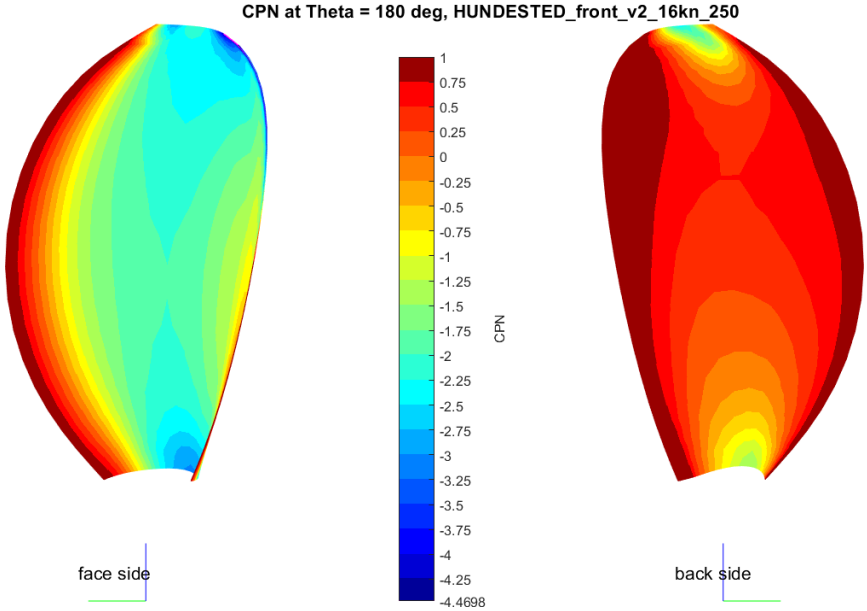

CPN at Theta = 210 deg, HUNDESTED_front_v2_16kn_250

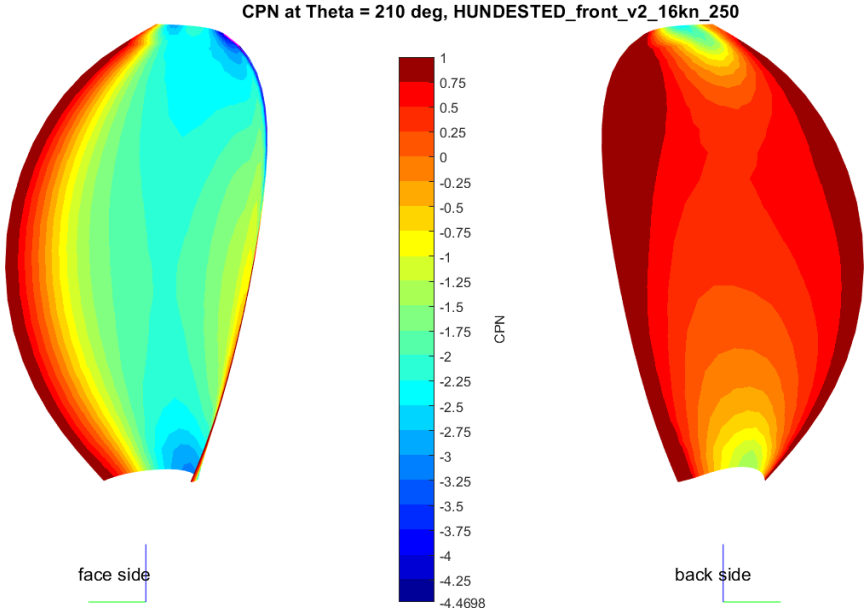

CPN at Theta = 240 deg, HUNDESTED_front_v2_16kn_250

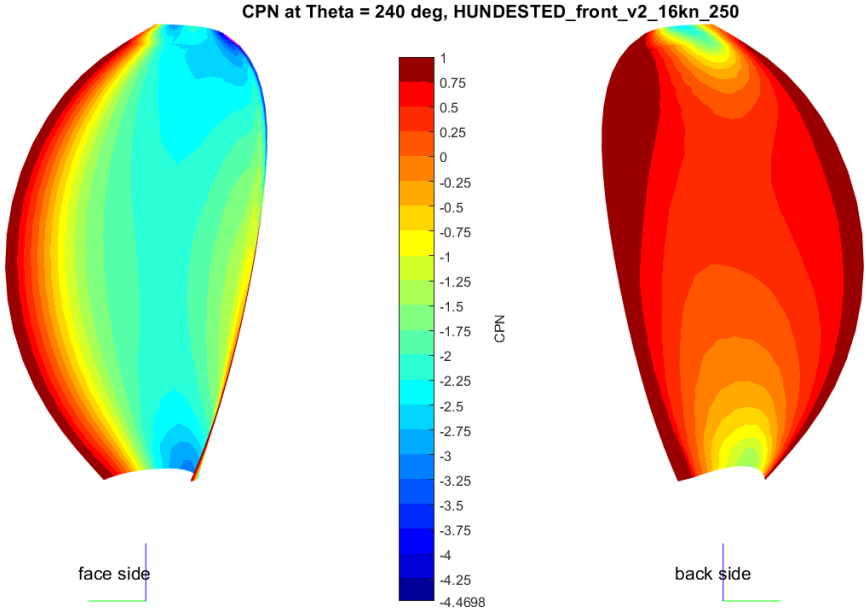

CPN at Theta = 270 deg, HUNDESTED_front_v2_16kn_250

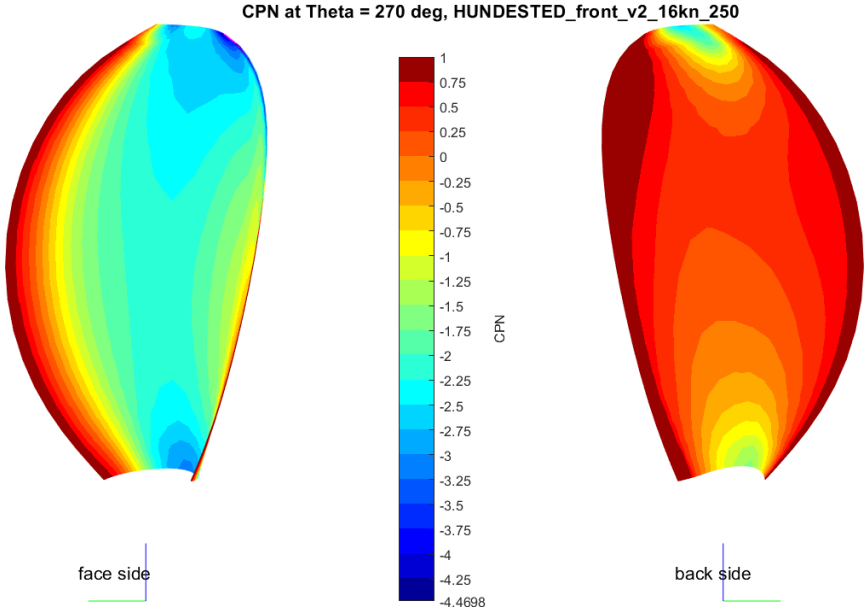

CPN at Theta = 300 deg, HUNDESTED_front_v2_16kn_250

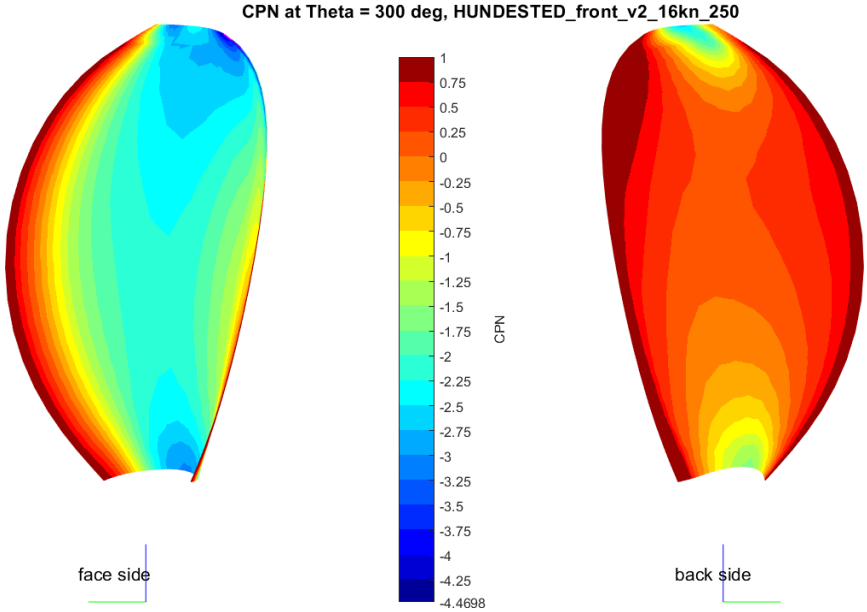

CPN at Theta = 312 deg, HUNDESTED_front_v2_16kn_250

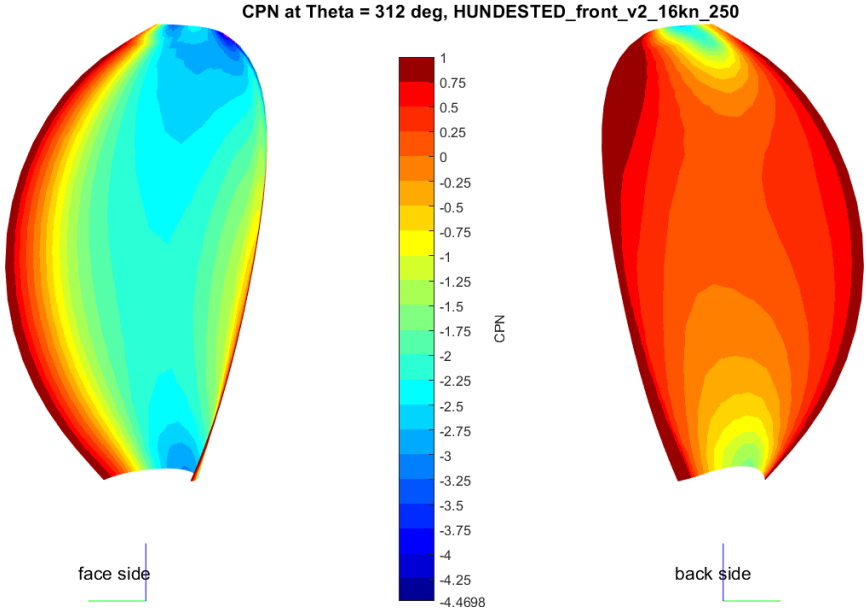

CPN at Theta = 336 deg, HUNDESTED_front_v2_16kn_250

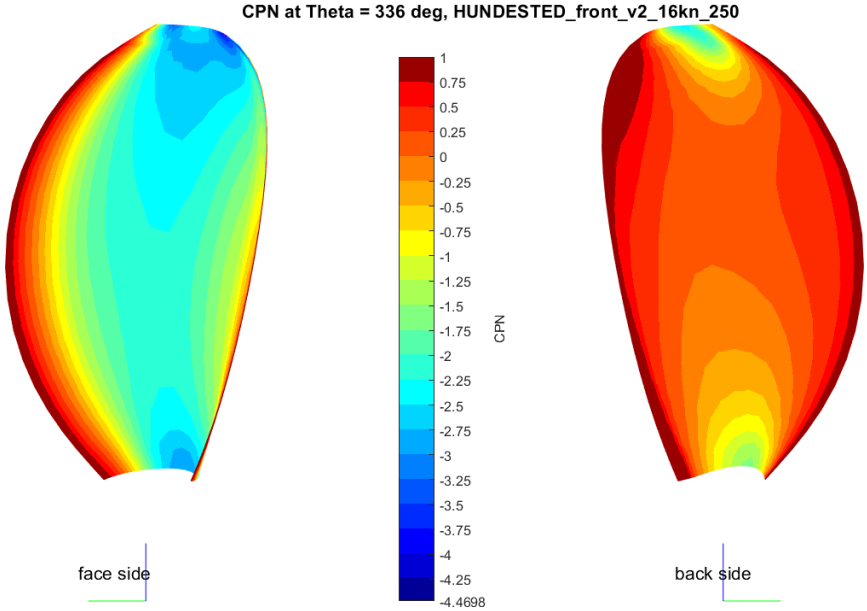

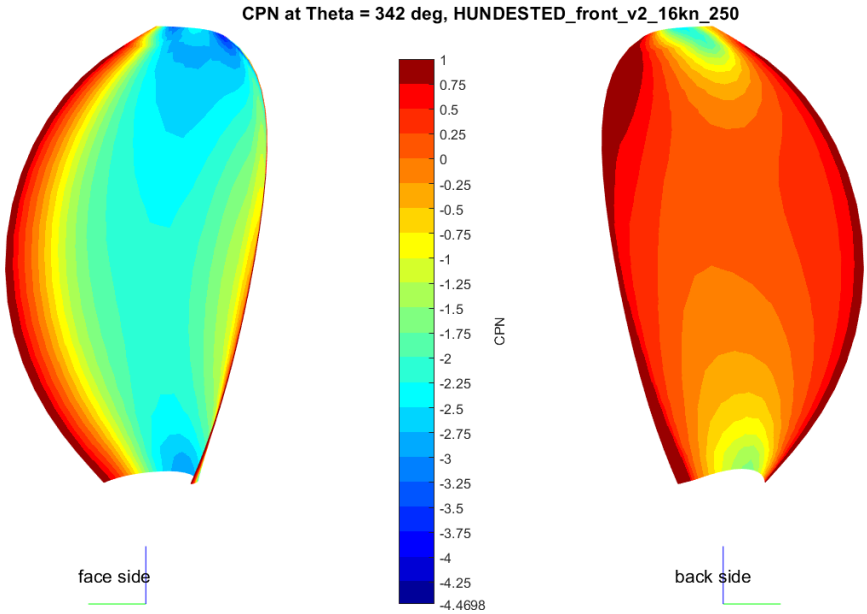

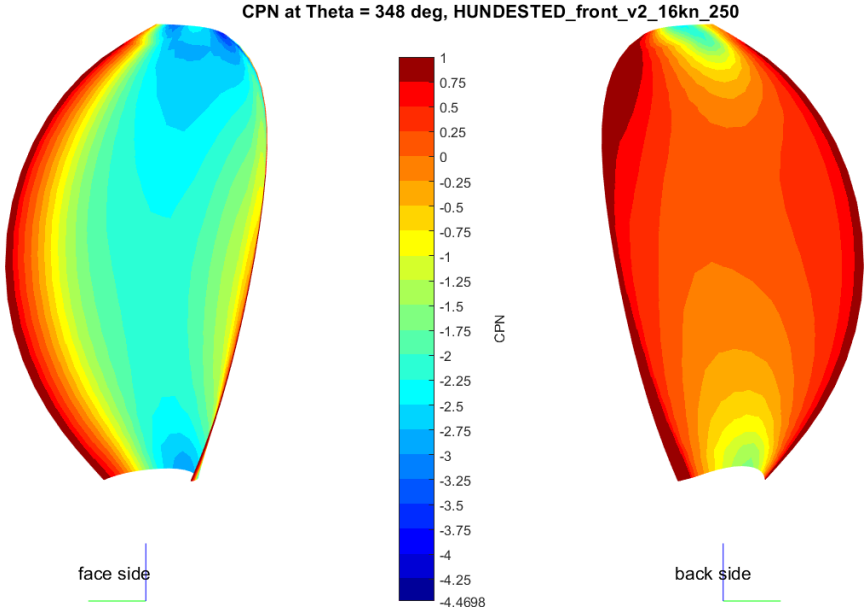

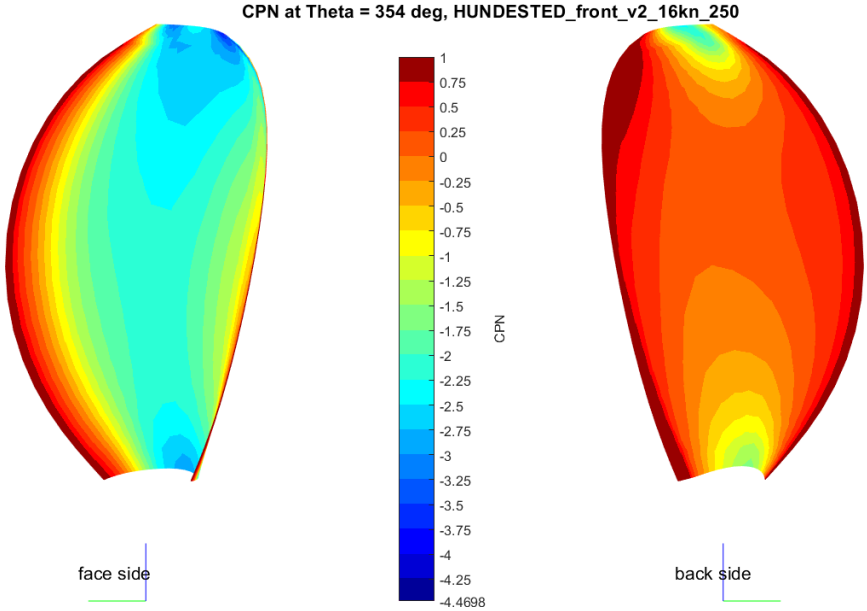

PRESSURE CONTOURS ON THE FRONT PROPELLER AT 16 KNOTS, REGENERATING 250 KW MODE

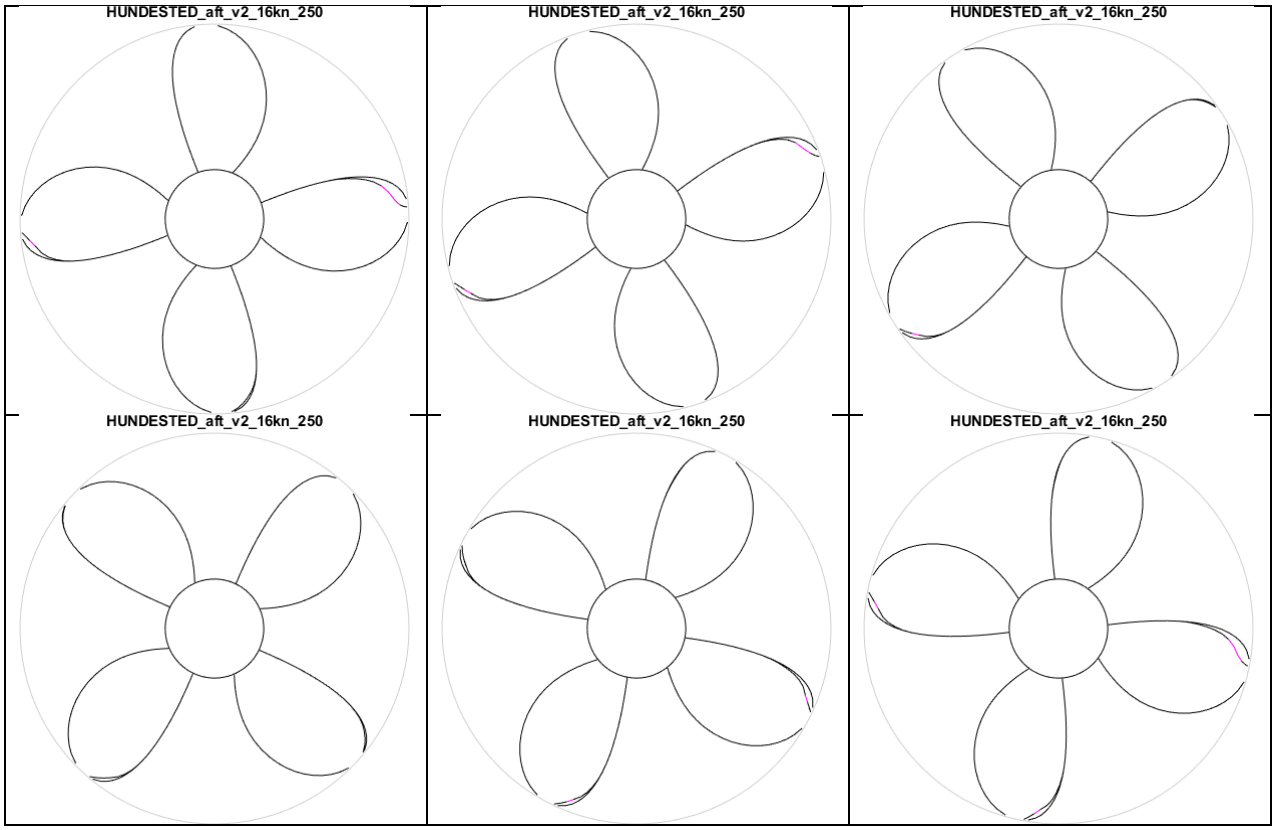

CAVITATING BEHAVIOUR AFT PROPELLER, REGENERATING, 250 KW TOTAL

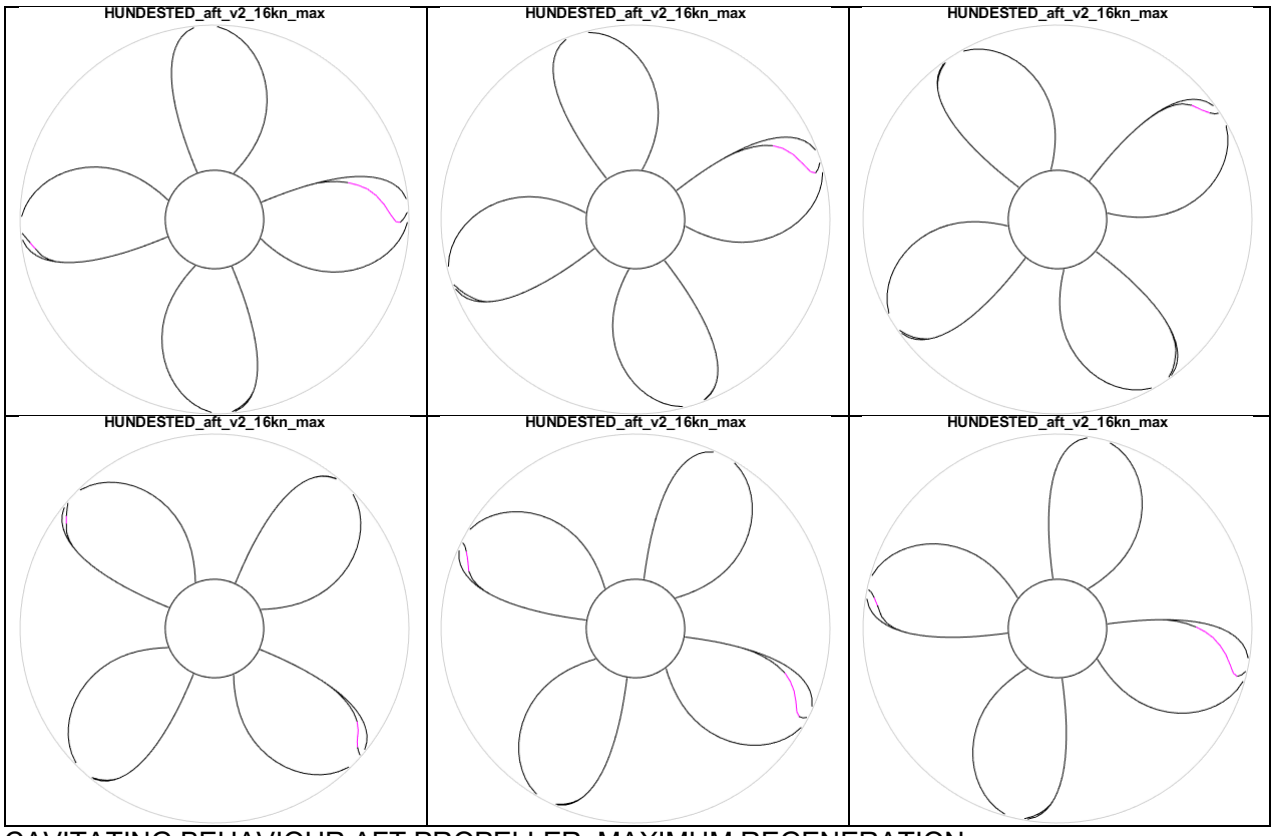

CAVITATING BEHAVIOUR AFT PROPELLER, MAXIMUM REGENERATION

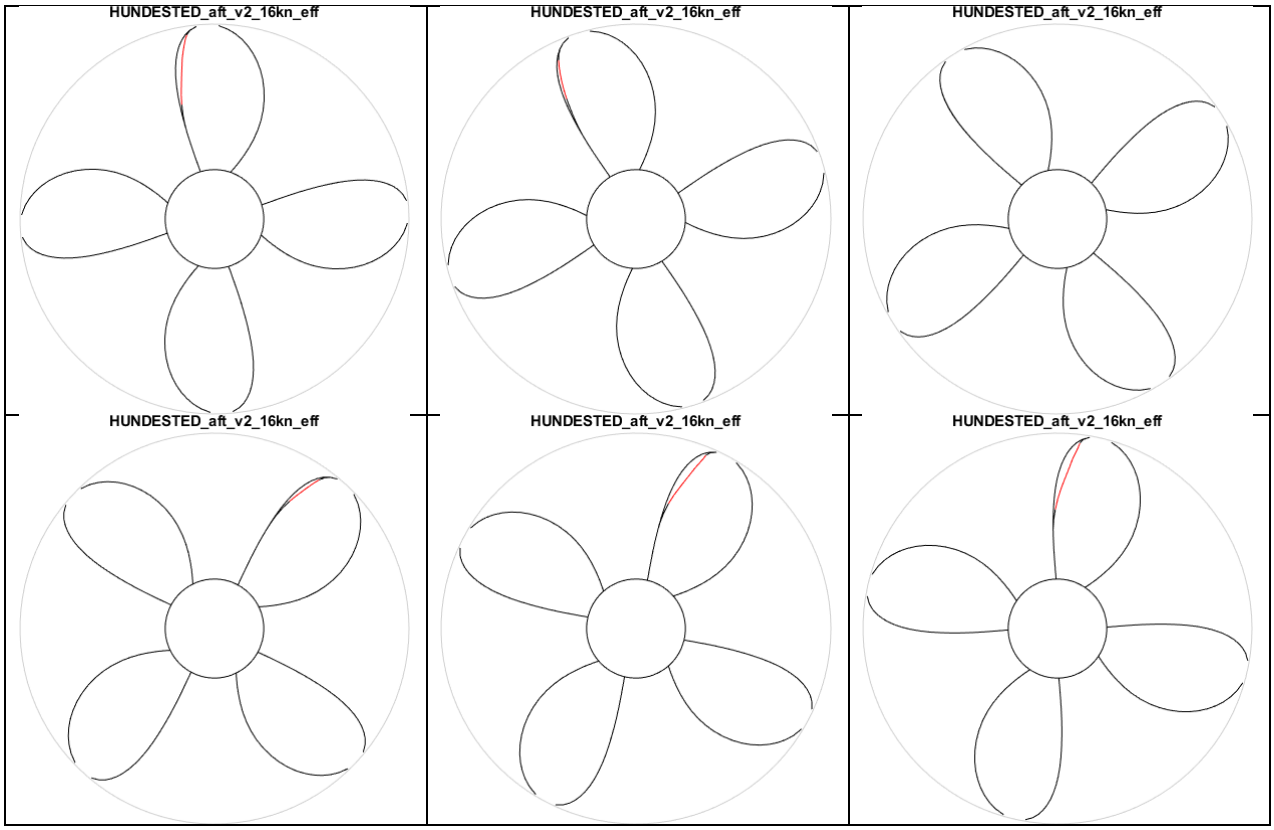

CAVITATING BEHAVIOUR AFT PROPELLER, MOST EFFICIENT REGENERATION

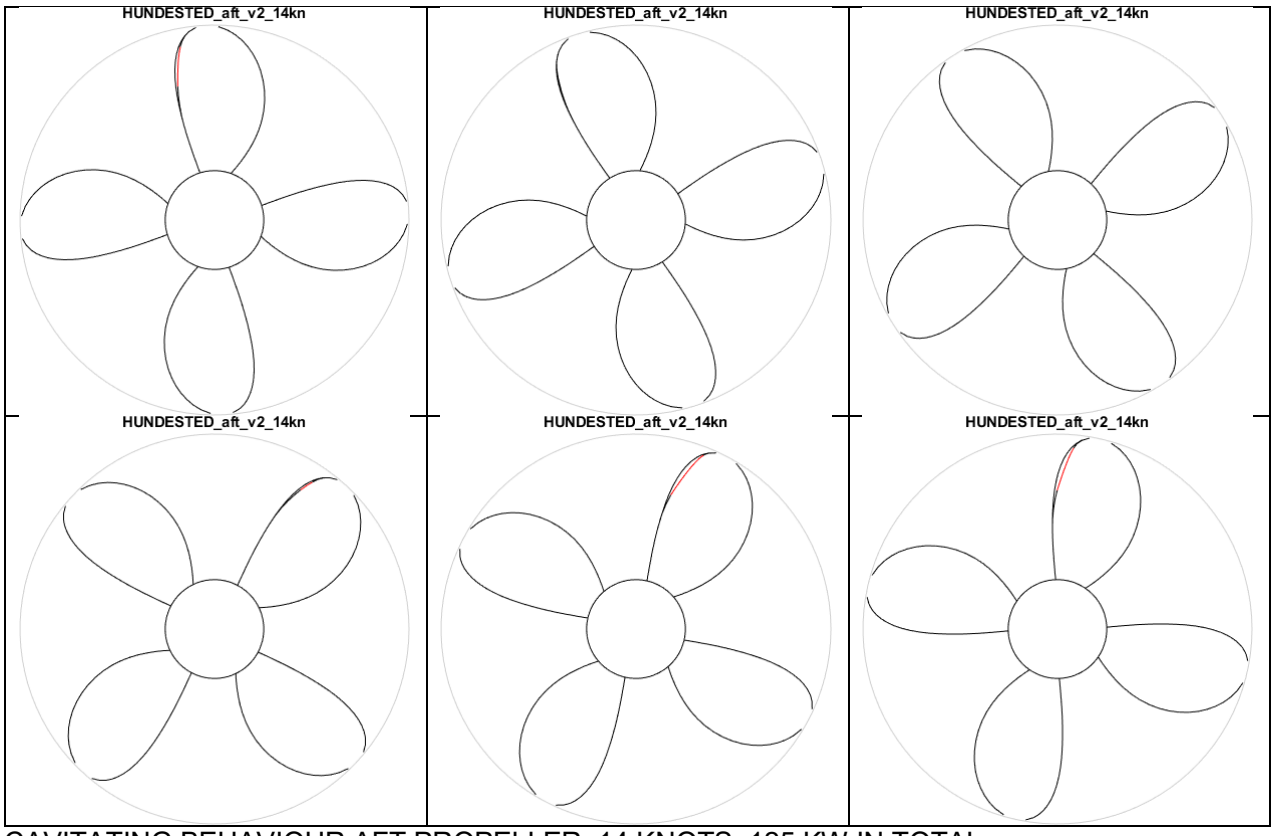

CAVITATING BEHAVIOUR AFT PROPELLER, 14 KNOTS, 125 KW IN TOTAL

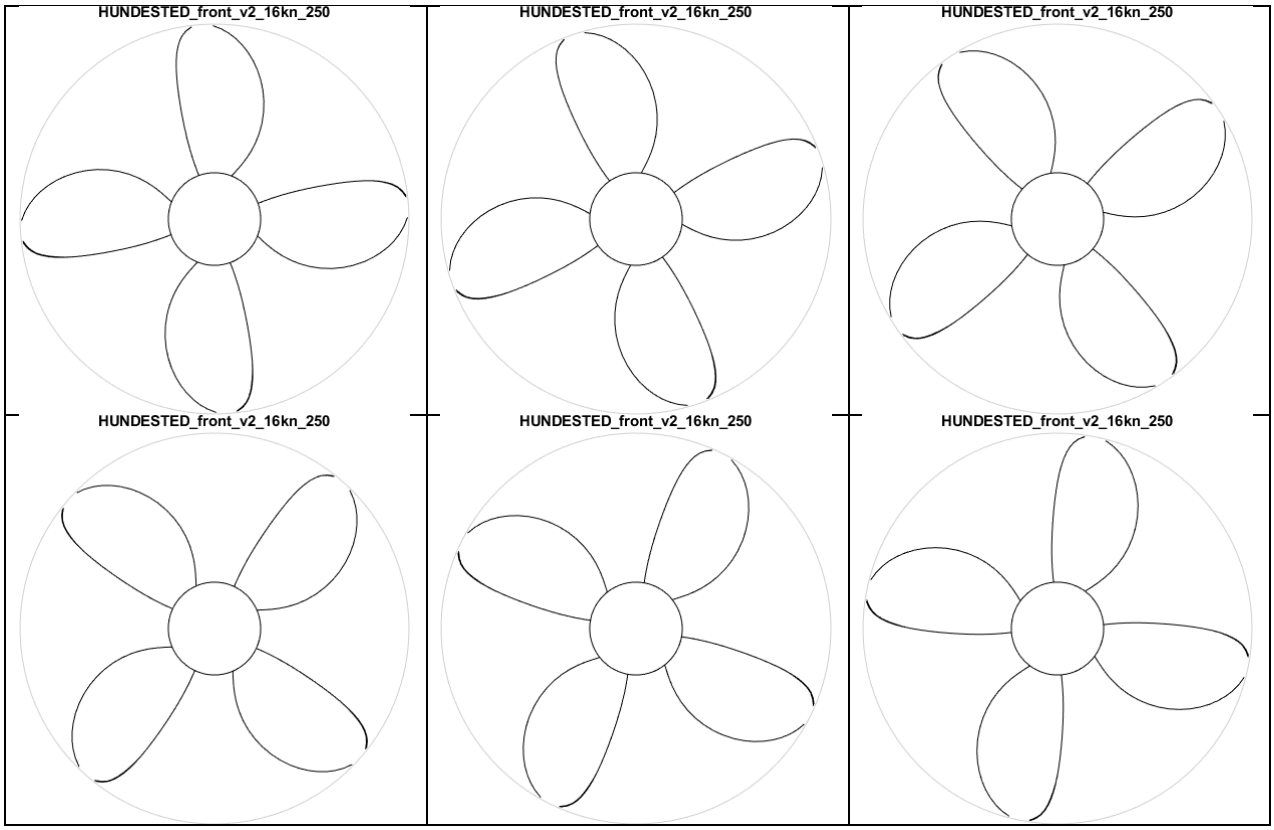

CAVITATING BEHAVIOUR FRONT PROPELLER, REGENERATING, 250 KW TOTAL

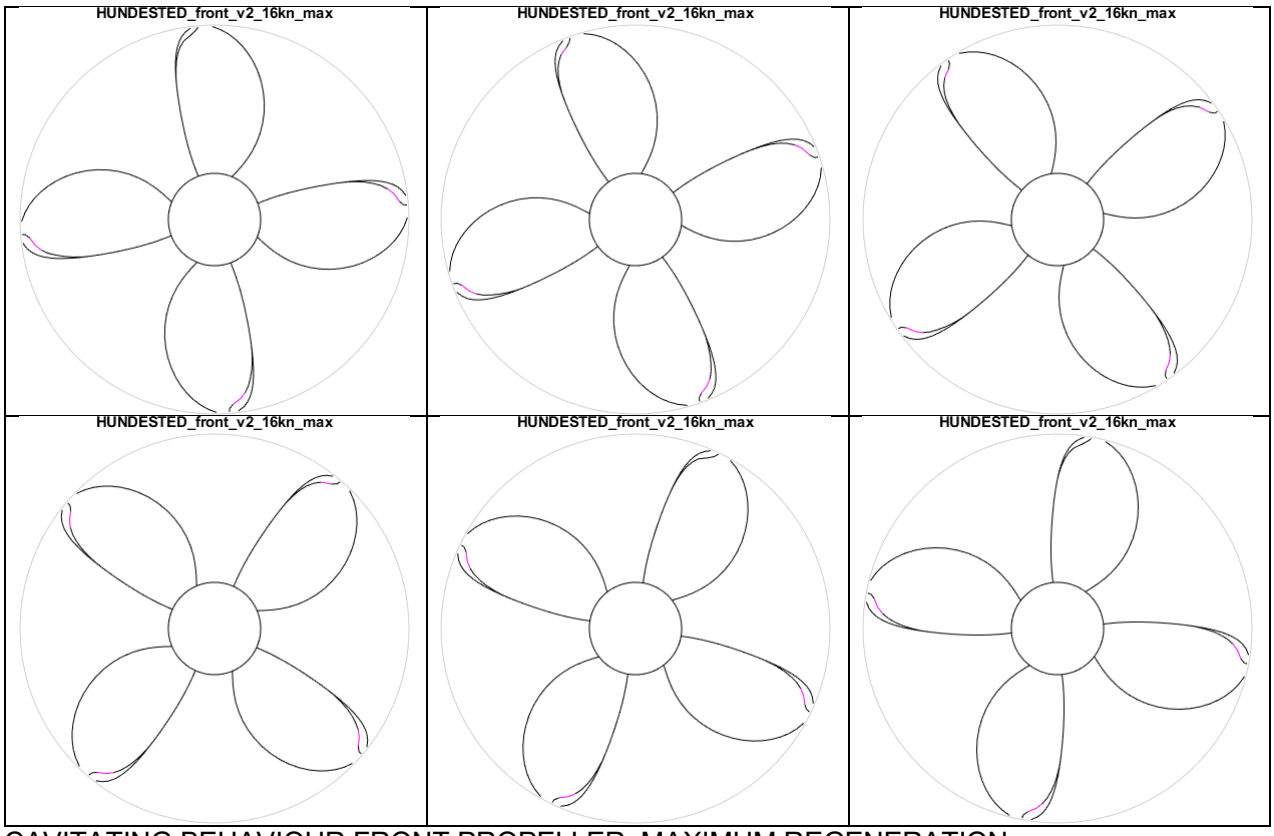

CAVITATING BEHAVIOUR FRONT PROPELLER, MAXIMUM REGENERATION

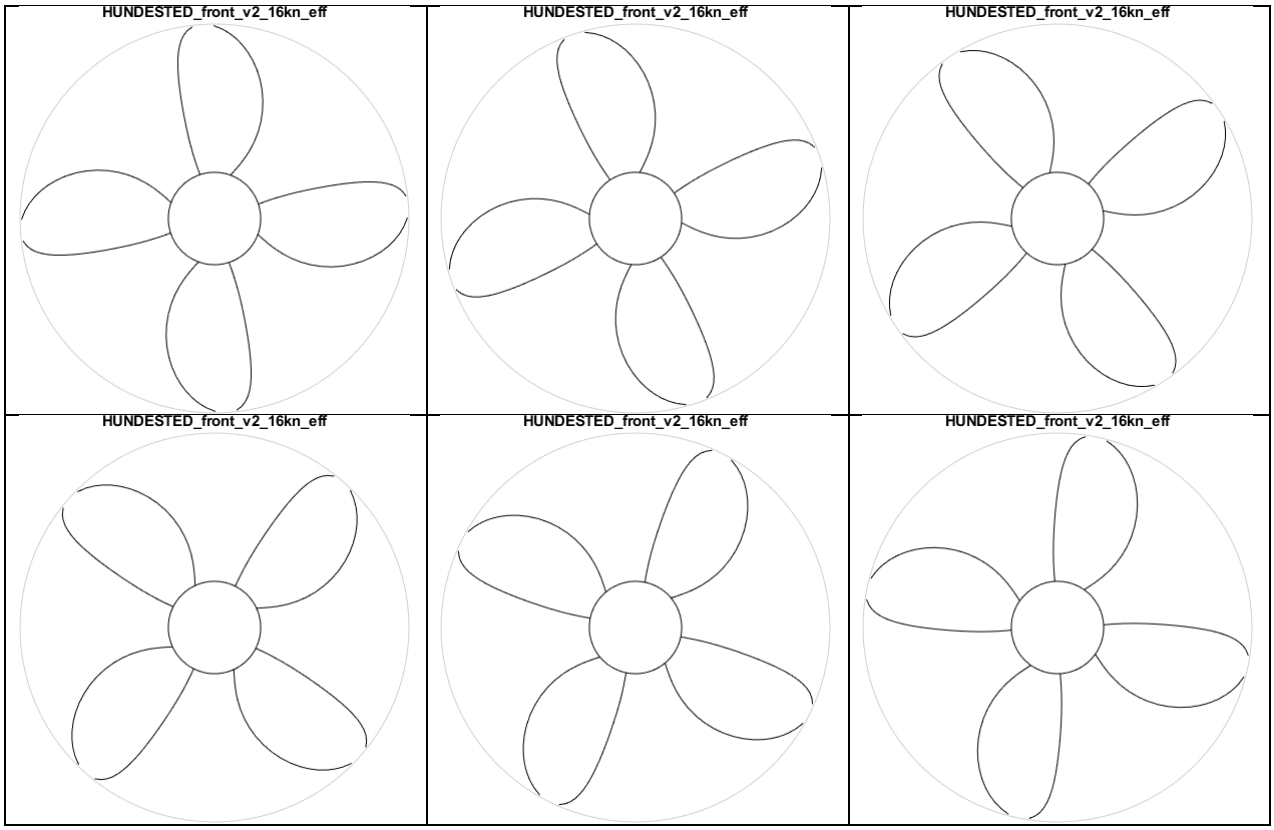

CAVITATING BEHAVIOUR FRONT PROPELLER, MOST EFFICIENT REGENERATION

APPENDICES

APPENDIX I

LIST OF SYMBOLS

Symbol	Symbol in computer print	Title
GEOMETRY OF SHIP AND PROPELLER		
A_{BT}		Transverse cross-section area of bulbous bow
A_E		Expanded propeller blade area
A_E/A_O		Expanded propeller blade area ratio
A_M		Midship sectional area below still waterline
A_O		Propeller disc area
A_T		Transom area below still waterline
A_T/A_M		Transom area ratio
A_W		Waterplane area
A_X		Maximum transverse sectional area below still waterline
A_V	AV	Area of portion of ship above waterline projected normally to the direction of relative wind
B		Maximum breadth moulded at or below still waterline
B_M		Maximum breadth moulded at midship
B_{WL}		Maximum breadth moulded at still waterline
c		Chord length of propeller blade section
c/D		Chord length-diameter ratio
c_{REF}		Chord length between reference line and leading edge
c_t		Chord length between maximum thickness point and leading edge
C_B		Block coefficient
C_M		Midship section coefficient
C_P		Longitudinal prismatic coefficient
C_{WP}		Waterplane area coefficient
d		Hub diameter
d/D		Hub-diameter ratio
D		Propeller diameter
FB		Position of centre of buoyancy aft of FP
f		Camber of propeller blade section
h_o		Submergence of propeller shaft axis measured from still water-plane
h_B		Height of centroid of A_{BT} above keel
i_E		Half angle of entrance
L_{OA}		Length overall
L_{OS}		Length overall submerged
L_{PP}		Length between perpendiculars
L_{WL}		Length on still waterline
LCB		Longitudinal position of centre of buoyancy

Symbol	Symbol in computer print	Title
P		Propeller pitch
P/D		Pitch-diameter ratio
r		Radius of propeller blade section
R		Radius of propeller
S,S_{HULL}		Projected wetted surface bare hull
S_{APP}		Wetted surface area appendages
S_1,S_{TOT}		Total wetted surface area
t		Maximum thickness of propeller blade section
t/c		Maximum thickness-chord length ratio
T		Mean draught moulded
T_A		Moulded draught at aft perpendicular
T_F		Moulded draught at forward perpendicular
dTA	dTA	Dynamic draught change at aft perpendicular
dTF	dTF	Dynamic draught change at forward perpendicular
Z		Number of blades
λ		Scale ratio
Φ		Pitch angle of propeller section
∇	DISV	Displacement volume moulded
$-_m$	$-_M$	Subscript for model
$-_s$	$-_S$	Subscript for ship

Symbol	Symbol in computer print	Title
RESISTANCE, OPEN WATER AND PROPULSION		
AC_{Res}		Ship resistance admiralty coefficient
AC_{Prop}		Ship propulsive power admiralty coefficient
C_A	CA	Total Incremental resistance coefficient for model-ship correlation
C_{A0}	CA_0	C_A basic
C_{Arough}	Crough	C_A roughness
C_{Aas}	Caas	C_A air resistance
C_{Abk}	Cbk	C_A bilge keels
$C_{Aballast}$	Cballast	C_A small draught
C_{AD}	CAD	Admiralty coefficient for propulsion
C_D		Drag coefficient
$C_{D\nabla}$		Power-displacement coefficient
C_E	CE	Admiralty coefficient for resistance
C_F	CF	Specific frictional resistance coefficient
ΔC_F		Roughness allowance coefficient
C_L	CL	Lift coefficient
C_P		Power loading coefficient
C_Q	C_Q	Propeller torque coefficient
C_{QBL}	C_{QBL}	Propeller blade spindle torque coefficient
C_R	CRES	Specific residual resistance coefficient
C_T	CT	Specific total resistance coefficient
C_{Th}		Thrust loading coefficient
C_{TP}	C_{TP}	Propeller thrust coefficient
C_{TD}	C_{TD}	Duct thrust coefficient
C_V	CV	Specific total viscous resistance coefficient
C_W	CW	Specific wavemaking resistance coefficient
C_X	CX	Specific air resistance coefficient
Ⓒ	CIRCC	R.E. Froude's resistance coefficient
F	F	Towing force in propulsion test
F_D	FD	Viscous scale effect on resistance
F_n	FN	Froude number
F_P	PULL	Pull of ship
F_{PO}	PULL	Pull of ship in bollard condition
Ⓕ	CIRCF	R.E. Froude's frictional resistance coefficient
g		Acceleration due to gravity
J	J	Advance coefficient
J_V	JV	Apparent advance coefficient
1+k	1+K	Three-dimensional form factor on flat plate friction

Symbol	Symbol in computer print	Title
k_p		Equivalent sandroughness of propeller blade surface
k_s		Roughness height of hull surface
k_{siP}	k_{siP}	Dependency of propulsive efficiency with resistance increase
k_{siN}	k_{siN}	Dependency of propeller shaft speed with power increase
k_{siV}	k_{siV}	Dependency of propeller shaft speed with speed change
K_Q	KQ	Torque coefficient
K_T	KT	Thrust coefficient
K_{TD}	KT-D	Duct thrust coefficient
K_{TP}	KT-P	Propeller thrust coefficient
K_{TS}	KT-S	Stator thrust coefficient
Ⓚ	CIRCK	R.E. Froude's speed-displacement coefficient
MCR		Maximum continuous rating
SMCR		Specified maximum continuous rating
NCR		Normal continuous rating
n	N	Rate of revolutions
P_B		Brake power
P_D	PD	Power delivered to the propeller(s)
P_E	PE	Effective power
P_I		Indicated power
P_S	PS	Shaft power
Q	Q	Torque
R	R	Resistance in general
R_n	RN	Reynolds number
R_A		Model-ship correlation resistance
R_F	RF	Frictional resistance
R_V	RV	Total viscous resistance
R_W	RW	Wavemaking resistance
s_A		Apparent slip ratio
s_R		Real slip ratio
t	THDF	Thrust deduction fraction
t*		Thrust deduction fraction from load variation test
T	TH	Thrust
T_D	TH-D	Duct thrust
T_P	TH-P	Propeller thrust
T_S	TH-S	Stator thrust
T_U	TH-U	Azimuthing thruster unit thrust
t_V	TV	Running trim

Symbol	Symbol in computer print	Title
V	V	Speed of ship or ship model
V_r	Vr	Radial flow velocity component in the direction of the z-axis of the Pitot tube, and is positive if directed down for strut orientation tests or outward in a wake survey
V_t	Vt	Tangential flow velocity component in the direction of the y-axis of the Pitot tube, and is positive if directed to port for strut orientation tests or in clockwise direction in a wake survey
V_x	Vx	Longitudinal flow velocity component in the direction of the x-axis of the Pitot tube, and is positive if directed aft
V_A	VA	Advance speed of propeller relative to water flow
w_T	WT	Effective wake fraction on thrust identity
w_Q	WQ	Effective wake fraction on torque identity
β		Advance angle of propeller blade section
β_h		Angle of the flow in the x-y plane of the Pitot tube co-ordinate system, and is positive if the flow is directed to port for strut orientation tests
β_v		Angle of the flow in the x-z plane of the Pitot tube co-ordinate system, and is positive if the flow is directed to the hub for strut orientation tests
η_B		Propeller efficiency behind ship
η_D	ETA-D	Propulsive efficiency
η_ε	ETA-ε	Merit coefficient
η_G		Gearing efficiency
η_H	ETA-H	Hull efficiency
η_M		Mechanical efficiency
η_o	ETA-O	Propeller efficiency in open water
η_R	ETA-R	Relative-rotative efficiency on thrust or torque identity
η_S		Shafting efficiency

Symbol	Symbol in computer print	Title
ν		Coefficient of kinematic viscosity
ρ		Mass density
τ		Ratio propeller thrust and total thrust of ducted propeller system
τ_w		Wall shear stress
$-_m$	-M	Subscript for model
$-_o$	-O	Subscript for open water
$-_s$	-S	Subscript for ship

Symbol	Symbol in computer print	Title
CAVITATION, HULL PRESSURES, SHAFT FORCES AND NOISE		
$a_{X\,0.8}$		Longitudinal clearance from propeller clearance curve to stern frame at a height of 0.8 R above propeller shaft axis
a_z		Vertical clearance of propeller tip in top position to the hull
A_i		Single amplitude of i-th harmonic component of periodic pressure signal
B_S		Waterline beam at station at most forward point of screw aperture
c		Speed of sound
C		Empirical constant
Cp		Pressure coefficient
D_M		Depth moulded
$E_{H,V}$		Thrust eccentricity
f		Frequency in general
f_1		Blade passage frequency
$f(\Theta)$		Function of mean periodic pressure signal
$F_{H,V}$		Propeller induced dynamic force acting on the shaft
$F_{x,y,z}$	FX,FY,FZ	Propeller induced dynamic force acting on the hull
$F_{z\,eq}$		Equivalent vertical excitation force
g		Acceleration due to gravity
h		Immersion in general
J	J	Advance coefficient
$M_{H,V}$		Propeller induced dynamic moment acting on the shaft
$M_{x,y,z}$	MX,MY,MZ	Propeller induced dynamic moment acting on the hull
n	N	Rate of revolutions
p		Sound pressure
p_o		Ambient pressure
p_v		Vapour pressure of water
r		Distance to cavitating propeller
R_n	RN	Reynolds number
V	V	Speed of ship or model
V_A	VA	Advance speed of propeller relative to water flow
α_i		Phase angle of i-th component in harmonic function
Θ		Angular propeller blade position
ρ		Mass density of water

Symbol	Symbol in computer print	Title
σ_f		Non-dimensional parameter for frequency
σ_n		Cavitation number related to rotation rate
σ_p		Non-dimensional parameter for sound pressure
σ_v		Cavitation number related to flow velocity
$_H$	$_H$	Subscript for horizontal
$_m$	$_M$	Subscript for model
$_s$	$_S$	Subscript for ship
$_V$	$_V$	Subscript for vertical

APPENDIX II

PROCEDURES OF MODEL TESTS

Procedure of open water tests

Single propeller

The propeller model is fitted on a horizontal driving shaft, and is moved through the water at an immersion of the shaft axis of at least the diameter of the propeller. The thrust and torque are measured in the hub of the propeller model.

In the test the loading of the propeller is normally varied by varying the speed of advance and keeping the rate of revolutions constant. When limitations in the measuring range (for J-values close to zero) and/or carriage speed (for high J-values) are reached, the rate of revolutions is varied too.

The measured thrust values are corrected for the resistance of the hub and streamlined cap experienced in the test. This correction is determined experimentally in a test with the hub only.

The torque and (corrected) thrust are expressed in non-dimensional coefficients K_{To} and K_{Qo}. Together with the open water efficiency η_o they are presented as a function of the advance coefficient J.

The non-dimensional thrust and torque coefficients are defined as:

$K_{To} = T/(\rho n^2 D^4)$ and $K_{Qo} = Q/(\rho n^2 D^5)$

The open water efficiency and advance coefficient are defined as:

$\eta_o = J\, K_{To}/(2\pi K_{Qo})$ and $J = V/(nD)$

The open water characteristics are not corrected for scale effects, unless stated otherwise.

Propeller with nozzle

In the case a nozzle is used in the propulsion system the nozzle thrust can be measured as well. In this case the non-dimensional nozzle thrust is defined as:

$K_{TDo} = T_D/(\rho n^2 D^4)$

in which the rotation rate n and diameter D are those from the propeller.

Complex propulsor

In the case of an azimuthing thruster or pod unit the thrust of the complete unit can be measured as well. Also in this case the non-dimensional unit thrust is defined as:

$K_{TUo} = T_U/(\rho n^2 D^4)$

In this case the propeller cap is not replaced by a special streamlined cap as for open or ducted propellers and no correction is applied to the propeller thrust.

On the measured results of pod or thruster open water tests, scale effect corrections are made which are explained in a separate appendix to this report.

Procedure of propulsion tests

In the model propulsion tests the same turbulence tripping on the hull and appendages is applied as in the resistance tests. The propulsion tests are carried out in two parts:

a) The first part consists of a load-variation test at one or sometimes more than one constant speed.
b) The second part consists of a speed-variation test at constant apparent advance coefficient J_V (= constant propeller load) or at the self-propulsion point of ship ($F = F_D$).

In the propulsion test the propeller thrust T_m, the propeller torque Q_m and the longitudinal towing force F acting on the model is recorded for each tested combination of model speed V_m and propeller rotation rate n_m. Thrust and torque are measured inside the propeller hub.
During the propulsion test the ship model is free to heave and pitch.

The results of the propulsion tests are analysed in the following way.
The required thrust at the self-propulsion point of ship is determined from:

$$T_s = \left(T_m + (F_D - F)\frac{\partial T_m}{\partial F} \right) \lambda^3 \frac{\rho_s}{\rho_m}$$

in which:

T_m = measured propeller thrust
F = measured longitudinal model towing force
F_D = scale effect correction on viscous resistance

The quantity $\partial T_m/\partial F$ is determined from the load-variation test.
In a similar manner, by interpolation in the measured data using the results of the load-variation test, the required torque and propeller rotation rate at self-propulsion point of ship are determined.

In the extrapolation to full-scale values scale effects are considered:

- On the resistance (F_D).
- On the propulsor entrance velocity (wake).
- On the propeller blade friction.

Procedure of cavitation observation tests

The test conditions for cavitation tests are chosen such that the average propeller thrust loading (expressed by K_T and J-identity) is equal on model and full scale.
In addition the pressure is lowered to such a level that model and full-size cavitation numbers are equal at corresponding points in the propeller disc.
For an arbitrary point at an immersion h_m the propeller cavitation number is:

$$\sigma_{nm} = \frac{p_{om} - p_{vm} + \rho_m g h_m}{0.5\, \rho_m n_m^2 D_m^2}$$

in which p_{om} is the surface pressure on model scale and p_{vm} is the vapour pressure of the water. For the ship, which is geometrically similar at a length scale λ, the cavitation number is:

$$\sigma_{ns} = \frac{p_{os} - p_{vs} + \rho_s g \lambda h_m}{0.5\, \rho_s n_s^2 \lambda^2 D_m^2}$$

The cavitation numbers for model and ship are equal, provided:

$$p_{om} - p_{vm} = \frac{(p_{os} - p_{vs})(\rho_m n_m^2)}{(\rho_s \lambda^2 n_s^2) + \rho_m g h_m (n_m^2 / (\lambda n_s^2) - 1)}$$

This condition is fulfilled for all values of h_m if $n_m = n_s \lambda^{0.5}$ and p_{om} - p_{vm} = $(\rho_m/\rho_s)(p_{os}$ - $p_{vs})/\lambda$ (Froude scaling for propeller revolutions and pressure). Substitution of ρ_s/ρ_m = 1.025 and p_{os} - p_{vs} = 99.05 kPa gives:

p_{om} - p_{vm} = 96.64 / λ [kPa]

This, in fact, can only be realised in a depressurised towing tank or a tunnel with free surface. For a cavitation tunnel without a free surface a rate of rotation for model scale is chosen within practical limits related to the tunnel capacity, the particular test set-up and the ranges of static pressure to be adjusted. Requiring equal cavitation numbers on model and full scale then leads to the pressure to be adjusted in the tunnel. Obviously, at only one horizontal level the condition of equal cavitation numbers can be fulfilled.

Apart from equal cavitation numbers in the model test facility and on the full scale the propeller loadings have to correspond.

As a measure for the propeller load the advance coefficient of the full-scale propeller is used with:

$J = V_A / (nD)$

With Froude scaling of the rotation rate of the propeller and the pressure in a depressurised towing tank the model speed then becomes:

$V_m = (V_s/\lambda^{0.5})(V_A/V)_s / (V_A/V)_m$

in which $(V_A/V)_s / (V_A/V)_m$ is the scale effect on the entrance velocity of the propeller.

In the cavitation tunnel it is common practice to acquire the correct propeller load by adjusting the water velocity to arrive at K_T-identity. At K_T-identity the J-identity is almost fulfilled. It should be noticed that the dynamometer is adjusted for the pressure difference inside and outside the cavitation tunnel.

In addition to the adjustment of the correct propeller load and cavitation numbers additional measures are taken to minimise the scale effect on the inception of propeller cavitation. To compensate for the difference in number of cavitation nuclei on model scale (in general only necessary in the Depressurised Wave Basin), a cloud of tiny gas bubbles is generated upstream of the propeller by means of electrolysis of the tank water. To this purpose a cathode and an anode are glued to the ship model in the form of metal strips of 0.5 mm thickness and 3.5 mm wide. In addition to electrolysis, leading edge roughness is used in the test for tripping the flow over the propeller blades to turbulence, because in laminar flow cavitation inception is subject to severe scale effects. The roughness consists of carborundum grains glued in a distributed form in a strip at the leading edges of the blades. Not only the effect on transition from a laminar to a turbulent boundary layer is considered important, also the generation of additional small nuclei at the roughness elements in the direct vicinity of the blade surface is regarded an important factor in suppressing the scale effects on cavitation inception.

The Reynolds number and number of nuclei on model scale determine the required grain size. In the Depressurised Wave Basin mostly a grain size of 60 μm is used. In the cavitation tunnels sandblasting of the leading edges is sometimes applied to achieve the required roughness, and due to testing at higher Reynolds numbers smaller roughness elements are needed in general.

In addition to the observation of the propeller cavitation in predefined conditions the margin against pressure side cavitation is established in the cavitation experiment. In the cavitation tunnel the water velocity is varied and at the point of inception the thrust coefficient is measured.
In the Depressurised Wave Basin the rotation rate is varied during a few measuring runs at constant speed of the ship model. The thrust coefficient K_T is established from the load variation test in the propulsion experiment. From the relationship between K_T and σ_n for the inception of pressure side cavitation the margin expressed in K_T of the predicted full-scale operation point is then found.

Procedure of propeller cavitation inception tests in the Depressurised Wave Basin

A complete propeller cavitation inception diagram is established in the Depressurised Wave Basin by means of visual detection.

During the tests electrolysis of the tank water ahead of the propeller(s) is applied in order to supply the flow through the propeller disc(s) with a sufficiently large number of cavitation nuclei. Moreover, carborundum grains of 60 μm are applied to the leading edges of the blades of the observed propeller model in order to reduce the scale effect on cavitation inception to a minimum by inducing turbulent flow over the blades and by generating additional nuclei close to the blade surface.
In addition, a strip of carborundum grains is applied at the forward end of the propeller hub in order to generate locally additional nuclei to stimulate inception of blade-root cavitation and hub-vortex cavitation.

The visual determination of cavitation inception is done by means of a video camera. First, the camera is installed forward of the propeller inside or outside the ship model. With the camera in this position the back of the propeller can be observed. Secondly, the camera is installed behind the ship model, where it is used to observe the face of the propeller. The propeller is illuminated by a stroboscopic light source, which is located above the propeller model behind a perspex window or outside the ship model.

For each type of cavitation the difference between the distinct propeller blades as regards their cavitation behaviour is investigated first. The blade, which shows the “average” cavitation behaviour for a certain type of cavitation, is selected for the eventual cavitation inception test. Prior to the actual test the radius and angular blade position are determined at which inception occurs for each distinct type of cavitation.

The inception conditions of a particular type of cavitation are then determined by a variation of the rotation rate of the propeller model at a constant speed of the ship model. Next, the rotation rate at which the cavitation disappears is established similarly during the same run. The average of these two rotation rates is called the inception rotation rate. This procedure is repeated for a number of speeds of the ship model and for each particular type of cavitation.

During the cavitation inception tests the air pressure in the towing tank is lowered to the Froude scaled level:

$p_{om} = p_{vm} + 96.64 / \lambda$ [kPa]

Model speeds are constant during the measuring run but the propeller rotation rates are slowly varied with an almost constant rotation rate at the inception point. From the measured inception conditions (p_o, V_m, n_m) the cavitation number σ_n and the thrust coefficient K_T are determined using the results of the load-variation test in the propulsion experiment and taking into account the influence of the leading edge roughness on the thrust coefficient as determined experimentally in a few supplementary measuring runs in the inception test.

In the inception diagram the model inception points are shown in combination with the predicted full-scale K_T-σ_n relationship (operation curve). If there would be no scale effects on cavitation inception the model inception curves are valid for the full scale as well. When effective leading edge roughness and nuclei seeding is applied in the model test, scale effects are supposed to be absent as far as sheet and bubbly types of cavitation are concerned. It is generally accepted that important viscous scale effects are present on the inception of free vortex cavitation.

According to McCormick: "On cavitation produced by a vortex trailing from a lifting surface", Journal of Basic Engineering, Trans. ASME, September 1962, there is a direct relation between the cavitation inception number and the Reynolds number. For equal angles of attack (equal loading) the cavitation inception number σ_{ni} scales with:

$$\frac{\sigma_{nis}}{\sigma_{nim}} = \left(\frac{R_{ns}}{R_{nm}} \right)^{0.35}$$

where R_n is the Reynolds number of the propeller, which is proportional to nD^2/ν, where n is rotation rate, ν is kinematic viscosity and D is diameter.

Hence,

$$\frac{\sigma_{nis}}{\sigma_{nim}} = \left(\frac{n_{is} D_s^2 \nu_m}{n_{im} D_m^2 \nu_s} \right)^{0.35}$$

Writing for the inception rotation rate:

$$n_i = \sqrt{\frac{p_o - p_v + \rho g h}{0.5 \rho \sigma_{ni} D^2}}$$

Because the tank pressure scales by Froude's law of similitude:

$$(p_o - p_v + \rho g h)_m = (p_o - p_v + \rho g h)_s \frac{\rho_m}{\rho_s} \frac{1}{\lambda}$$

we find by substitution:

$$\frac{\sigma_{nis}}{\sigma_{nim}} = \left(\frac{n_{nim}}{n_{nis}} \right)^{0.175} \left(\frac{\nu_m}{\nu_s} \right)^{0.35} \lambda^{0.525}$$

Hence,

$$\frac{\sigma_{nis}}{\sigma_{nim}} = \left(\frac{\nu_m}{\nu_s} \right)^{0.298} \lambda^{0.447}$$

Tip-vortex cavitation inception is assumed to follow McCormick's scaling rule.
Regarding hub-vortex cavitation it is noted that there are some indications that the scaling rule of McCormick is not the proper rule to be applied. Data from ships on which viewing trials were carried out indicate that the scale effect on hub-vortex cavitation inception is probably smaller than according to McCormick's rule.

Since no proper alternative rule has been formulated yet, the method of McCormick is still applied to the cavitation numbers of hub-vortex cavitation inception determined in the present tests.

Procedure for hull pressure fluctuation measurements

Conditions for the pressure fluctuation measurements are determined using the results of the propulsion test and applying Froude scaling. Similarity of the thrust coefficient K_T and the cavitation number σ_n between model scale and full scale are adopted. This determines the required ambient pressure in the Depressurized Wave Basin. In the following, the subscript s indicates the full-scale value and the subscript m indicates the model-scale value. From Froude similarity:

$$n_m = n_s \sqrt{\lambda}$$

resulting in:

$$p_{0m} - p_{vm} = (\rho_m / \rho_s)(p_{0s} - p_{vs}) / \lambda = 96640 / \lambda$$

where n is the rotation rate in Hz, p_0 and p_v are the ambient and vapour pressures respectively in Pa, ρ the density of water in kg/m^3 and λ the geometric scale ratio of the ship model.

Model speed is also determined based on Froude scaling, although a correction is needed for the scale effect on the ship's wake. The propeller is, on average, too heavily loaded on model scale. In order to correct for this, the model speed is increased slightly. Some ship types (mostly slender vessels such as container ships) exhibit a stronger scale effect on the wake peak in the upper part of the propeller disk. In this area the velocity deficit on model scale is larger than on full scale. Since this is typically also the area where most of the cavitation occurs, the model speed is further increased in order to have the correct propeller loading and thus cavitation pattern in this part of the propeller disk.

To reduce scale effects on cavitation inception, a strip of carborundum grains is applied to the leading edges of the propeller blades on both suction and pressure side. This roughness helps to increase the extent of turbulent flow over the propeller blades such that the flow is more similar to full scale. Electrolysis is used to generate small bubbles to ensure that there are sufficient nuclei for proper cavitation inception.

The hull pressure fluctuations are measured by, typically, 21 charge mode pressure transducers. They are mounted flush in the hull of the ship model above the propeller as shown in the figure below.

The signals from the pressure transducers are sampled and digitised. In order to remove the influence of small changes in the propeller rotation rate, the measurements are resampled to 360 samples per revolution, based on the measured blade angular position. These resampled signals are equidistant with respect to blade position, but not necessarily with respect to time. In order to ensure that the blade passage frequency (BPF) is well captured, only complete revolutions are considered.

This means that only the signal between the first and the last time that blade number 1 is in the top position (blade angular position 0°) is selected. The measured signals are then transformed to the frequency domain as a harmonic series according to:

$$f(\theta) = A_0 + \sum_{i=1}^{\infty} A_i \sin(iZ\theta + \alpha_i),$$

where:

$f(\theta)$	=	function of the mean periodic pressure signal
A_0	=	static value of the function
A_i	=	amplitude of i-th harmonic component
α_i	=	phase angle of i-th harmonic component
θ	=	angular propeller position with θ = 0° corresponding with blade number 1 in top position
Z	=	number of blades

In this expression the frequency for i = 1 is equal to the blade passage frequency (BPF), which is the fundamental frequency of the pressure fluctuations. A_i and α_i are calculated for i = 1, 2, 3 and 4. The amplitudes are given as zero-to-peak values.

Correction for vibrations of the ship model

Additionally, acceleration transducers are fitted in the aft body of the model to measure the vibrations of the ship model. The ship model vibrates due to the pressure fluctuations from the propeller as well as vibrations from the drivetrain. Because of these vibrations, the hull of the ship also radiates pressure fluctuations, which are also measured by the pressure sensors. Since this influence is not representative of the full-scale ship, it should be corrected for. This is done by processing the measured vibration signals and using them to compute the part of the radiated pressure fluctuations due to hull vibration. These are then subtracted from the measured pressures (taking both the amplitude and the phase into account) to obtain the pressure fluctuations for an infinitely rigid ship.

Converting the results to full scale

The corrected model-scale pressure amplitudes (in Pa) are converted to full-scale values according to:

$$(A_i)_s = (A_i)_m \frac{\rho_s}{\rho_m} \lambda,$$

where the subscript s denotes full scale, m denotes model scale.

Only the amplitudes of the pressure fluctuations are scaled. The full-scale phase angles are taken equal to the model values, thus ignoring the small effect of the finite propagation velocity of the radiated pressure waves.

The results of the hull pressure fluctuation measurements are also presented graphically in a narrowband spectrum. These graphs are currently only presented on model scale (both the frequency and the amplitude values). They can therefore not be directly compared to the values in the table or to graphs of other vessels. However, the spectral plots can be used to determine whether broadband excitation occurs, which would indicate a risk of resonance.

Computation of excitation forces

In order to judge the risk of onboard vibrations, the pressure distribution over the hull is integrated to obtain excitation forces. This integration is done by defining triangles between the pressure sensors as illustrated in the figure below, which shows a top view of typical pressure sensor locations (orange dots) in a ship model. The blue dots indicate the so-called 'zero points' at which the pressure fluctuations are assumed to have decayed to zero, and which are included for interpolation purposes.

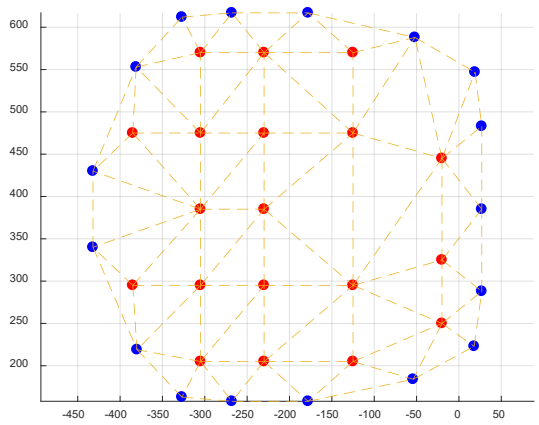

Note that this figure is a top view; the positions of the sensors and zero points are defined in three dimensions, thus taking the shape of the ship's hull into account. The pressure amplitude of the three corner points is interpolated to the centroid of each triangle while taking the phase information into account. This pressure value at the centroid is then multiplied by the surface area of the triangle to obtain the force per triangle. This is then decomposed into the components x, y and z using the normal of the triangle. Thereafter the contributions of all triangles are summed (taking the phase into account) to obtain the total excitation forces. This is done for each of the four harmonics of the BPF. The amplitude and phase of the corresponding moments with respect to a given point (usually the propeller centre) are also computed.

The resulting forces and moments are related to the co-ordinate system shown below.

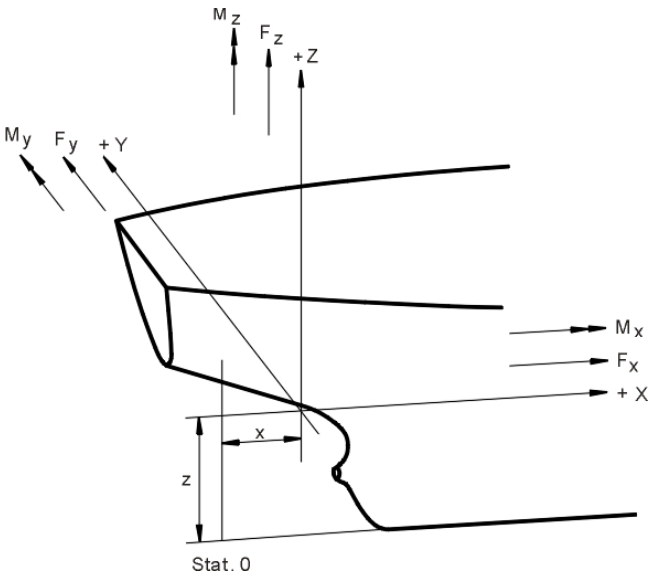

in which:

x	=	longitudinal distance from station 0
z	=	vertical distance from baseline
F_x	=	longitudinal force, positive in forward direction
F_y	=	transverse force, positive in port direction
F_z	=	vertical force, positive in upward direction
M_x	=	longitudinal moment, vector positive in forward direction
M_y	=	transverse moment, vector positive in port direction
M_z	=	vertical moment, vector positive in upward direction

The input for the integration of the forces (i.e. the pressure amplitudes and phases and the location of the pressure sensors) is on full scale. This means that the computed forces are also given as full-scale values without the need for further scaling.

If the measurements are carried out on a ship fitted with two propellers, both propellers will be operating during the measurement. Therefore, the pressure fluctuations take the contribution of both propellers into account. The integration, however, is only carried out for the area above one single propeller. For a ship equipped with two propellers, the forces will be given for a combination of two propellers rotating in phase with each other. The force amplitudes can then be added directly without an influence of the phase but mirrored around the ship centre line. As a result, the vertical excitation force F_z and the longitudinal force F_x double while the transverse force F_Y is zero. This is a worst case scenario; if the actual propellers do not rotate in phase, the combined F_z and F_x will be lower.

Assessment of excitation forces

In order to give a first estimate of the risk of vibrations, the results are compared to the `van der Kooij criterion'. An equivalent vertical excitation force (F_{Zeq}) is determined based on the four harmonics of F_Z (in kN):

$$F_{Zeq} = \sqrt{\sum_{i=1}^{4} i * F_{z,i}^2}$$

The number of the harmonic, i, is also used as a weighting factor, which accounts for the fact that vibrations at higher harmonics contribute more strongly in the perception of vibration nuisance. This equivalent force should be smaller than the van der Kooij criterion:

$$F_{Zeq} < c \nabla \left(0.75 + 75 / L\right)$$

where:

∇	=	displacement of the vessel in m^3
L	=	length between perpendiculars in m
c	=	constant, dependent on ship type

Typical values for the constant c are:

c	=	7 for VLCCs and container ships with the bridge forward
c	=	5 for product tankers and container ships with the bridge aft
c	=	3 for ferries, cruise ships and yachts

Should the equivalent force F_{Zeq} be above the criterion a strong risk of vibration-related nuisance aboard the vessel is expected. This is, however, also dependent on the structural response of the vessel. If resonance occurs, vibration nuisance may be a problem even when the force is below the criterion.

DOCUMENTATION SHEETS

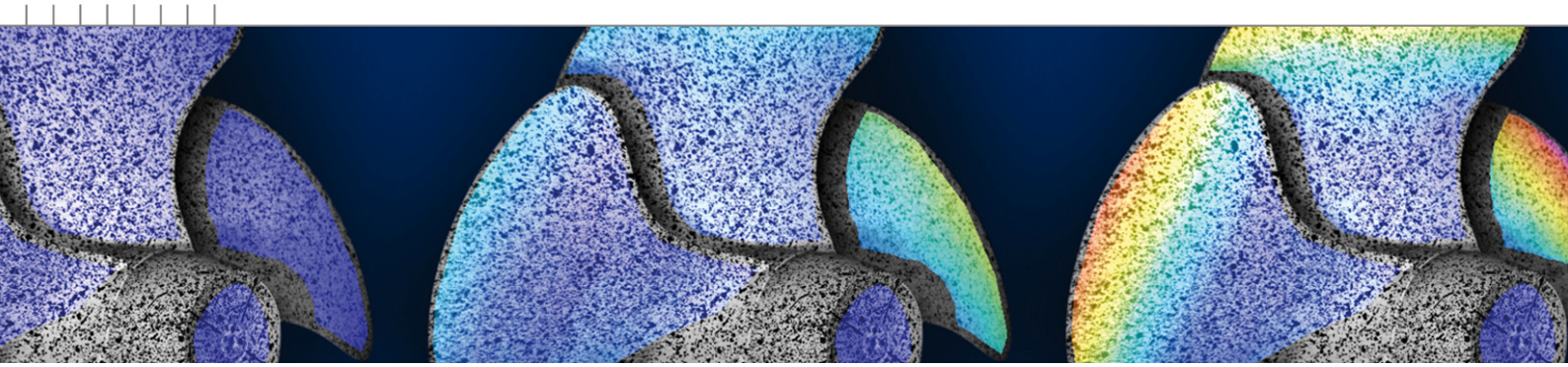

PROCAL

Calculating propeller performance in potential flow

MARIN internal use only

The computer program PROCAL calculates the unsteady inviscid flow including sheet cavitation around a propeller geometry using a boundary element method. It is used for the analysis of the propeller performance operating in open water or in a wake field of a ship hull. For the analysis of the hull pressure fluctuations of the non-cavitating and cavitating propeller, a coupling is made with the boundary element method EXCALIBUR, which solves the acoustic wave equation and takes the diffraction of the ship hull and the free surface into account. PROCAL has been developed in the period 2003-2008 within the Cooperative Research Ships organisation (CRS). Extensive use has been made of MARIN's experience in the implementation and application of boundary element methods for propeller analysis.

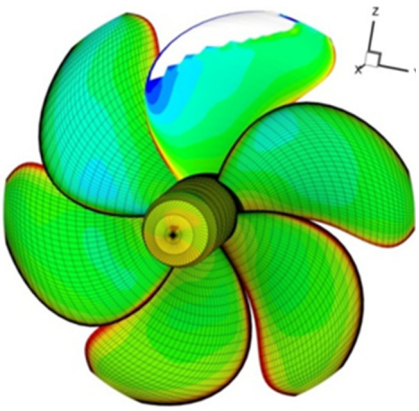

Applications

The PROCAL code has been applied to a wide variety of propeller geometries to analyse:

- Open water performance (shaft thrust and torque)
- Behind-hull performance (blade and shaft forces and moments)
- Sheet cavitation inception, extent and volume
- Field velocities and propeller-induced pressure fluctuations

The code is capable of analysing multi-component propulsors and its application for podded propellers, propeller-rudder combinations and ducted propellers is currently being investigated. The code has also been applied for the analysis of wings at varying angles of attack.

Accuracy

The code has been validated for a large number of different propeller geometries and it gives, in general, good results. The accuracy depends somewhat on the propeller geometry and the operating point, but PROCAL results are very consistent making it a reliable propeller analysis tool for a wide range of propeller geometries. The sheet cavitation model shows very realistic patterns and good correlation with model scale and full-scale observations while predicting only a small phase lead in the growth of the cavity compared to experiments. An acceptable prediction of the pressure pulses on the hull for the first blade passage frequency is obtained.

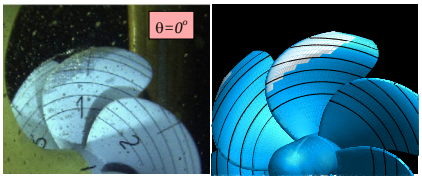

Comparison between cavitation extents observed during experiments in the Depressurised Towing Tank (DTT) and computed by PROCAL.

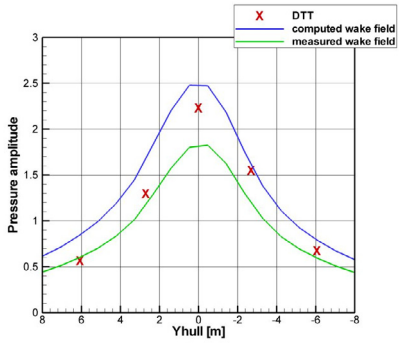

Variation of pressure fluctuations on the hull in the propeller plane. PROCAL results are shown using a measured wake field and a PARNASSOS computed ship wake and compared with model scale measurements in the DTT.

References

- Vaz, G. and Bosschers, J.; "Modelling Three-dimensional Sheet Cavitation on Marine Propellers Using a Boundary Element Method", Sixth international symposium on Cavitation, CAV2006, Wageningen, 2006.
- Bosschers, J., Vaz, G., Starke, A.R., Wijngaarden, E. van; "Computational Analysis of Propeller Sheet Cavitation and Propeller-ship interaction", RINA conference MARINE CFD2008, Southampton, 2008.

For more information contact MARIN:
SOSC
T + 31 317 49 32 37
E sosc@marin.nl

Input

The graphical user interface PROVISE, developed by DRDC Atlantic within the CRS, helps to generate and visualise the panel distribution for the propeller and the hub, to generate the other input files and to analyse the results. The propeller geometry needs to be described by a propeller description file using tabular offset data for the foil sections and radial distribution data of pitch, chord, skew and rake. A hub geometry of arbitrary shape can be generated in PROVISE. The propeller inflow velocity field, representing the effective wake field of the hull, is specified in a ship wake file. Finally, the coordinates where field point velocities and pressures are to be calculated need to be selected. The wake field of the ship hull can be obtained from model tests or from computations using MARIN's RANS solvers PARNASSOS and REFRESCO. These computations can be made for model scale and full-scale conditions. Several methods are available for obtaining effective wake fields from nominal or total wake fields.

Output

A large variety of output files are generated, showing pressure, cavity thickness and velocity distributions on the propeller and hub geometry, pressure and velocities in field points and hull points, radial distribution of loading, cavity length and volume on the propeller blade, and the integrated forces and moments for each blade and as transmitted to the propeller shaft. All results can easily be visualised using PROVISE.

Computational approach

PROCAL uses the Morino formulation to solve for the velocity potential. The geometry of the propeller wake is modelled by either an empirical formulation or by an iterative approach computing the wake pitch and tip vortex roll-up. An iterative procedure is applied to satisfy the pressure Kutta condition at the propeller blade trailing edge. The cavitation model iteratively solves the non-linear boundary conditions assuming that the cavity thickness remains small. The analysis of the propeller in a wake field is performed in the time domain for a number of shaft revolutions until the change in propeller wake strength and blade loading between subsequent revolutions is sufficiently small.

Restrictions

As the code is based on inviscid flow theory, the influence of boundary layers, flow separation and vortex formation is not included. These effects may become important for the analysis of high skew propellers and propellers operating in off-design conditions. The cavitation model is restricted to sheet cavitation and therefore does not include vortex cavitation and cloud cavitation that can be generated from the aft end of the sheet.

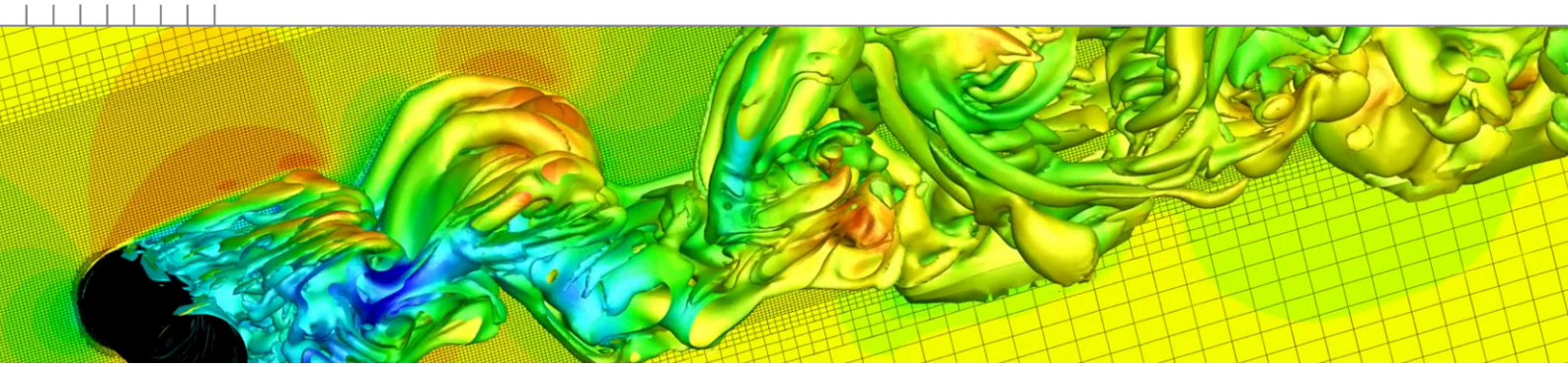

ReFRESCO

A community-based open-usage and open-source CFD code for the Maritime World

The CFD code ReFRESCO has been under development since 2005. It is based on state-of-the-art numerical algorithms and software features, and on the long-standing experience of MARIN in CFD. ReFRESCO stands for Reliable&Fast Rans Equations (code for) Ships (and) Constructions Offshore. In several respects it resembles a general-purpose CFD commercial code, although it has been verified, validated and optimised specifically for numerous maritime industry applications.

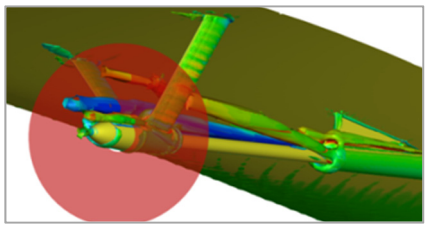

Fully-appended ships

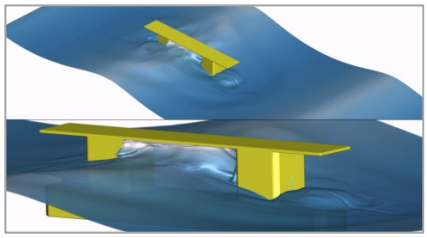

Impacts

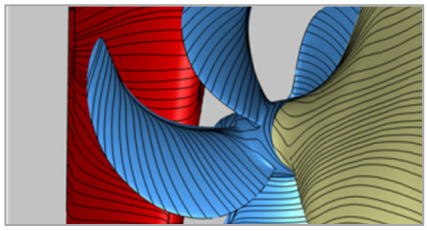

Cavitation

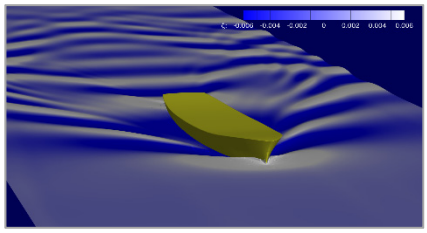

Free surface & waves

Computational method

ReFRESCO is a viscous-flow CFD code that solves multiphase (unsteady) flows using the incompressible Navier-Stokes equations, complemented with turbulence and cavitation models [1]. The equations are discretised using a finite-volume approach and in strong-conservation form. A pressure-correction equation based on the SIMPLE algorithm is used to ensure mass conservation [2]. At each implicit time step, the non-linear system for velocity and pressure is linearised using Picard's method. A segregated or coupled approach may be used. The code is parallelised using MPI and runs on Linux workstations and HPC clusters.

CFD features

Due to specific numerical schemes, ReFRESCO can deal robustly with low up to high (full-scale) Reynolds numbers, permitting the accurate estimation of scale effects. The face-based implementation permits the handling of grids from several different grid-generation packages. State-of-the-art CFD features such as moving, sliding and deforming grids, as well automatic grid adaptation (refinement and/or coarsening) are also available. Both 6DOF rigid-body, and flexible-body (fluid-structure interaction) simulations, can be performed. For turbulence modelling, both traditional RANS and Scale-Resolving Simulations (SRS) models such as SAS/DDES/IDDES/XLES, PANS and LES can be used. Noise predictions can be made using an acoustic analogy module. Couplings with propeller models (RANS-BEM coupling), fast-time simulation tools (XMF) and wave generation potential flow codes (OceanWave3D, SWASH) are implemented.

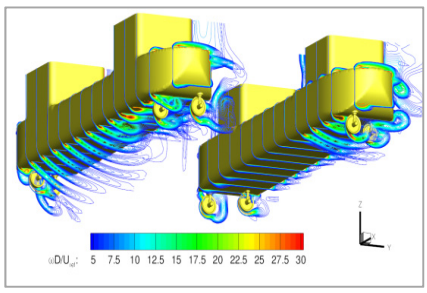

Current loads

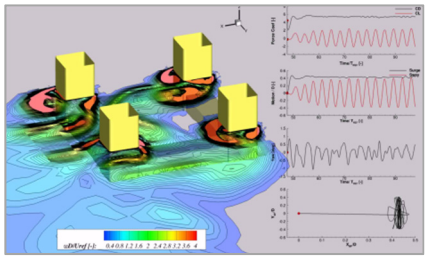

VIV & VIM

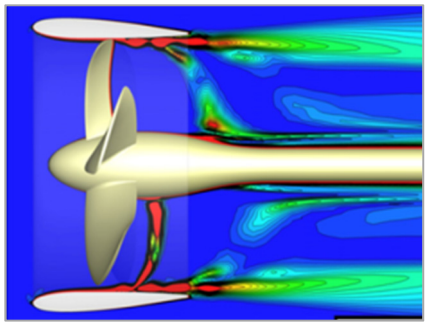

Propellers

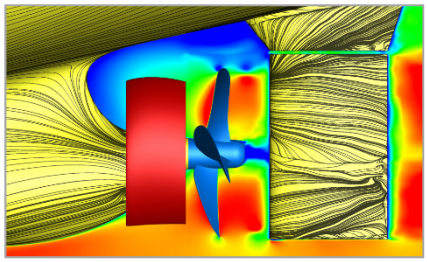

Energy Saving Devices (ESDs)

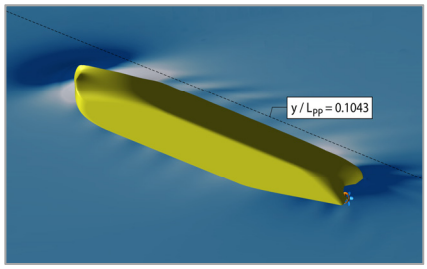

Propulsion

For more information contact MARIN: the ReFRESCO YouTube channel or contact the MARIN CFD group

T + 31 317 49 39 11

E refresco@marin.nl

W www.refresco.org

Development and applications

ReFRESCO is currently being developed, verified and validated at MARIN in collaboration with several other worldwide non-profit organisations (universities and research institutes). Modern verification & validation (V&V) techniques and tools are used in the development and application of ReFRESCO. ReFRESCO has been applied, verified and validated for the following range of applications:

- Resistance and propulsion of fully-appended ship hull forms;
- Submarines, including manoeuvres and geometry optimisation;
- Propeller and complex propulsor flows, including cavitation;
- Energy-saving devices;
- Marine current and floating wind turbines;
- Current and wind loads on offshore structures;
- VIV and VIM of offshore structures and renewable energy devices;
- Thruster-hull and thruster-thruster interaction problems;
- Free-surface flows, wave loads and wave impacts;
- Seakeeping problems such as loads and motions for free-floating structures.

ReFRESCO-Operation and ReFRESCO-ReSearch

Two types of partnership are available to companies and institutes wishing to use ReFRESCO. The ReFRESCO-ReSearch partnership focuses on sharing the code for collaborative research, without any fees but common open development, testing, verification and validation. Tight quality control is enforced by MARIN and there is only one ReFRESCO source repository for all partners. ReFRESCO-Operation extends the ReFRESCO-ReSearch partnership by allowing commercial application of ReFRESCO (a membership fee is required). In addition, the user gains access to ReFRESCO support services, as well as MARIN's CFD best practice guidelines.

Bibliography

[1] Vaz, G., Jaouen, F. and Hoekstra, M.; "Free-Surface Viscous Flow Computations. Validation of URANS code FreSCo", OMAE2009, Hawaii, Honolulu, USA. 2009.

[2] Klaij, C. M., and Vuik, C.; "Simple-type Preconditioners for Cell-centered, Colocated Finite Volume Discretization of Incompressible Reynolds-averaged Navier-stokes Equations", International Journal for Numerical Methods in Fluids, 71(7), pp. 830–849. 2013.

ReFRESCO

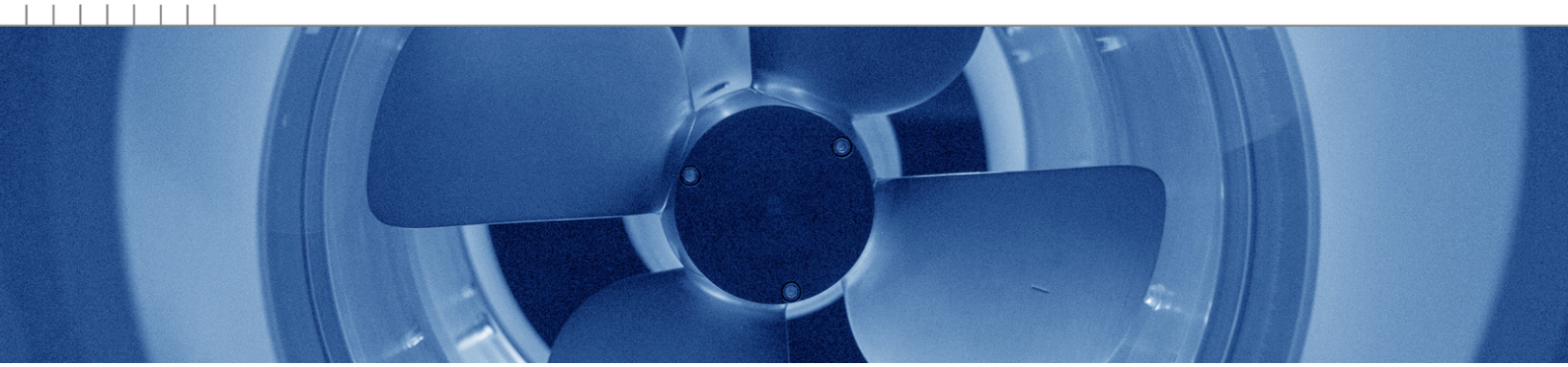

Propeller Design Support & Evaluation

MARIN offers its propulsor services to ship yards, operators, propeller manufacturers and suppliers of marine propulsion components. These services include an independent prediction of the performance of propellers and design support. Propeller design involves finding the right balance between conflicting objectives, for instance between propulsive efficiency and cavitation related nuisances like propeller induced pressure pulses on the ship hull and underwater noise. The hydrodynamic performance is evaluated by computational methods, often followed by model experiments or full scale observations.

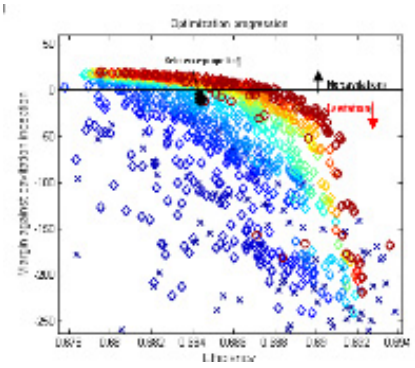

Example of optimization case with final Pareto front in red. Both the margin against cavitation and efficiency should be maximized.

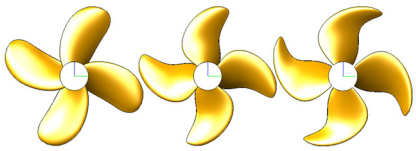

Example of propeller candidates within an optimization study

MARIN focuses on a wide-range of propeller designs, e.g. high-end “low-noise” propellers for yachts, naval, research and cruise ships with delayed cavitation inception, propellers with low vibration-excitation and ducted propellers for special purpose vessels such as dredgers, tugs and fishing vessels. Also for merchant ships, MARIN can for instance provide insight into whether the best possible compromise between the propulsive efficiency and cavitation related pressure pulses is achieved or further improvements can be made.

Throughout the years, MARIN developed substantial knowledge of propulsors by means of calculations, model tests and full scale tests. This experience is virtually indispensable for a good propeller design.

Evaluation

An independent second opinion on a propeller design may for instance be required:

- to provide good understanding of the best possible efficiency within given boundaries;
- before proceeding to more expensive model test experiments or propeller manufacturing;
- after the vessel’s commissioning as trouble shooting, when there are, for example, problems including cavitation erosion or onboard vibrations and noise.

A propeller evaluation will always be tuned to the specific project at hand. MARIN will give expert advice on the performance and draw recommendations to solve possible issues.

Design

By using the latest design techniques and experience within the whole chain of design, model tests and full scale observations, MARIN is able to make a best suited independent propeller design based on the specifications provided by the customer. The MARIN propeller blade design often acts as a reference or counter design for third parties.

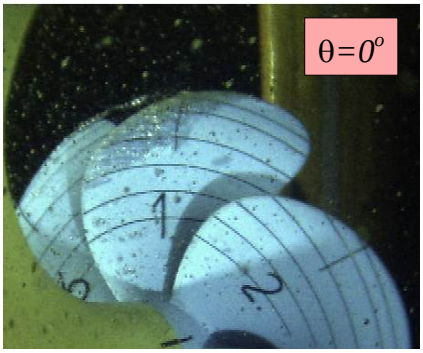

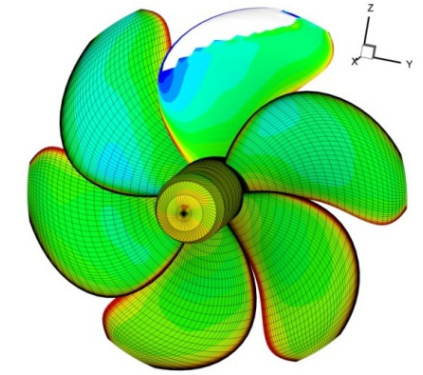

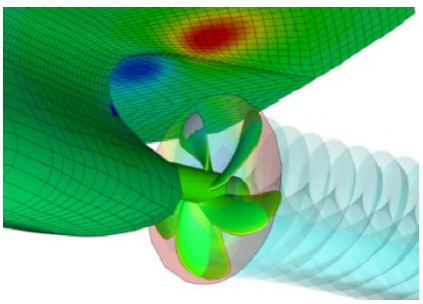

Optimization

Multi-objective optimisation techniques allow propeller designers to perform design studies. An optimization gives insight in the different trade-offs between conflicting objectives and indicates the influence of design constraints on the attainable objectives. Possible objectives or constraints are for instance efficiency, avoidance of pressure side cavitation, cavitation volume, pressure pulses, tip vortex nuisance, material stress or weight. The propeller is fully parameterized to allow large design freedom. The optimization either serves as a preliminary investigation of feasible objectives in conceptual design studies or as a choice support tool for the best possible compromise which serves as starting point for further detailed design.

Model experiments

Verification of propulsive performance and cavitation behaviour by model experiments is often desired by ship owners to check whether the design fulfils the expectations and is likely to reach its targets at full scale. Cavitation observations, pressure pulse measurements and noise recordings are performed daily in MARIN's Depressurised Wave Basin (DWB).

Full scale observations

Full scale cavitation observations are indispensable as feedback for propeller design and interpretation and correlation of model tests. MARIN offers a full scale consulting and monitoring service, and has gained considerable experience in a broad field of ship types over the years. Each time, MARIN carefully analyses the propulsor performance which is used to further improve propeller design methodology and model experiments.

Design conditions

For each propeller design study the design conditions such as shaft power, thrust, RPM and ship speed are necessary. Either model tests with stock propellers, CFD studies or empirical methods could be used to determine the design conditions, all of which are offered by MARIN. Furthermore, the wake field in which the propeller operates should be known, preferably the effective wake field at full scale.

Tools

Throughout the years, several systematic series such as the Wageningen B, C & D series were generated and computational tools were developed. Detailed propeller design and prediction of pressure distributions and cavitation patterns are possible with the Boundary Element Method (BEM) PROCAL. Pressure pulses on the hull due to cavitation will be analysed with the BEM code EXCALIBUR. Optimization can be performed using a genetic algorithm which is coupled to a geometry generator and PROCAL. Effective wake fields could be computed with MARIN's RANS codes PARNASSOS or REFRESCO on either model or full scale by coupling them to PROCAL. Nowadays, state of the art full RANS propeller computations are becoming more and more the standard.

For more information contact MARIN:
department Ships
T +31 317 49 34 72
E ships@marin.nl

M A R I N
P.O. Box 28

6700 AA Wageningen
The Netherlands

T +31 317 49 39 11
E info@marin.nl

I www.marin.nl